
The Northeast Pacific Ocean and Northwest Coast of North America within the global climate system, 29,000 to 11,700 years ago

Mann Daniel H. ^{1,*}, Gaglioti Benjamin V. ²

¹ Institute of Arctic Biology, University of Alaska, Fairbanks, AK 99705, United States of America

² Water and Environmental Research Center, University of Alaska, Fairbanks, AK 99775, United States of America

* Corresponding author : Daniel H. Mann, email address : dhmann@alaska.edu

Abstract :

The Northwest Coast of North America stretches 4000 km from Bering Strait to Washington State. Here we review the history of glaciation, sea level, oceanography, and climate along the Northwest Coast and in the subarctic Pacific Ocean during the Last Glacial Maximum and deglaciation. The period of interest is Marine Isotope Stage 2 between ca. 29,000 calendar years ago (29 ka) and 11,700 calendar years ago (11.7 ka). The glacial history of the Northwest Coast involved multiple glacial systems responding independently to latitudinal variations in climate caused by changes in the North American ice sheets and in the tropical ocean-atmosphere system. Glaciers reached their maximum extents 1–5 kyrs later along the Northwest Coast than did large sectors of the Laurentide and Fennoscandian Ice Sheets. Local, Last Glacial Maxima were reached in a time-transgressive, north to south sequence between southwestern Alaska and Puget Sound. The history of relative sea level along the Northwest Coast during Marine Isotope Stage 2 was complex because of rapid isostatic adjustments by a thin lithosphere to these time-transgressive glacial fluctuations. Multiple lines of evidence suggest Bering Strait was first flooded by the sea after 11 ka and that it probably did not assume its present-day oceanographic functions until after 9 ka. The coldest intervals occurred during Heinrich Event 2 (ca. 26–23.5 ka), again between ca. 23 and 21.5 ka, and during Heinrich Event 1 (ca. 18–15 ka). At these times, mean annual sea surface temperatures cooled by 50 to 80 C in the Gulf of Alaska, and glacial equilibrium-line altitudes fell below present sea level in southern Alaska and along the Aleutian Island chain. Sea ice episodically expanded across the subarctic Pacific in winter. Oceanographic changes in the Gulf of Alaska tracked variations in the vigor of the Asian Summer Monsoon. The deglaciation of the Northwest Coast may have served as the trigger for global climate changes during deglaciation. Starting ca. 21 ka, marine-based glaciers there were increasingly destabilized by rising eustatic sea level and influxes of freshwater and heat associated with the rejuvenation of the Asian Summer Monsoon. Rapid retreat of marine-based glaciers began ca. 19 ka and released vast numbers of ice bergs and large amounts of freshwater into the Northeast Pacific. Resultant cooling of the North Pacific may have been teleconnected to the North Atlantic through the atmosphere, where it slowed Atlantic Meridional Overturning Circulation and initiated the global effects of Heinrich Event 1, ca. 18–15 ka. During the Younger Dryas, ca. 12.8–11.7 ka, mean annual sea surface temperatures were 40 to 60 C cooler than today in the Gulf of Alaska, and sea ice again expanded across the subarctic Pacific in winter. Conditions of extreme seasonality characterized by cold, dry winters and

warm, steadily ameliorating summers caused by the southward diversion of the Aleutian Low in winter may explain the previously enigmatic records of Younger Dryas climate along the Northwest Coast.

Keywords : Paleoenvironments, Marine Isotope Stage 2, Last Glacial Maximum, last global deglaciation, Northwest Coast of North America, Northeast Pacific Ocean

1. INTRODUCTION

The energy gradient between low and high latitudes which fuels the general circulation in the atmosphere and ocean implies that the dynamics of glacial-interglacial cycles cannot be understood without the tropics. Berger et al. (2006)

The ice-age history of the Northwest Coast of North America (Fig. 1) is important because this 4000-km coastline is the interface between North America and the North Pacific Ocean. As a result, its climate is largely a function of the ocean/atmosphere system of the North Pacific. Because the Northwest Coast lies upwind from much of North America, its paleoenvironmental history strongly influenced that of the rest of the continent. Our purpose here is to update and expand an early review of Northwest Coast paleoenvironments (Mann and Hamilton 1995) with the wealth of new information that has emerged from multiple fields of inquiry over the intervening thirty years.

The focus here is on the last glacial cycle, which corresponds roughly to Marine Isotope Stage 2 (MIS 2), the Last Glacial Maximum and deglaciation, considered here as the interval 29,000 to 11,700 calendar years Before Present (hereafter 29 ka to 11.7 ka). This was a period of repeated, global changes in glaciers, sea ice, ocean circulation, and storm tracks (Clark et al. 2012; Shakun et al. 2012). These changes afford an opportunity to understand how the planet's ocean/atmosphere/cryosphere systems respond to forcing from a variety of external drivers and internal interactions, some of which are either absent or of minor importance in the present-day system. MIS 2 also saw dramatic shifts in the distributions of plants and animals, including the earliest dispersal of people from Eurasia into North America. Although still debated, the route taken by the First Americans may have followed the Northwest Coast (Fladmark, 1979; Willerslev and Meltzer, 2021). Because of space limitations, this review concentrates on the physical aspects of the Northwest Coast's paleoenvironments.

Today, the ocean/atmosphere system of the subarctic Pacific and the Northwest Coast is linked to tropical systems through a complex system of teleconnections. These teleconnections operate through both oceanic tunnels (e.g., the Kuroshio Current) and atmospheric bridges (e.g., the Aleutian Low). Understanding how these connections worked in the past may help

predict their future behaviors. The tropics are the heat engine of the global ocean/atmosphere system, and the underlying premise of this review is that changes at high latitudes can only be understood through their connections with the tropics.

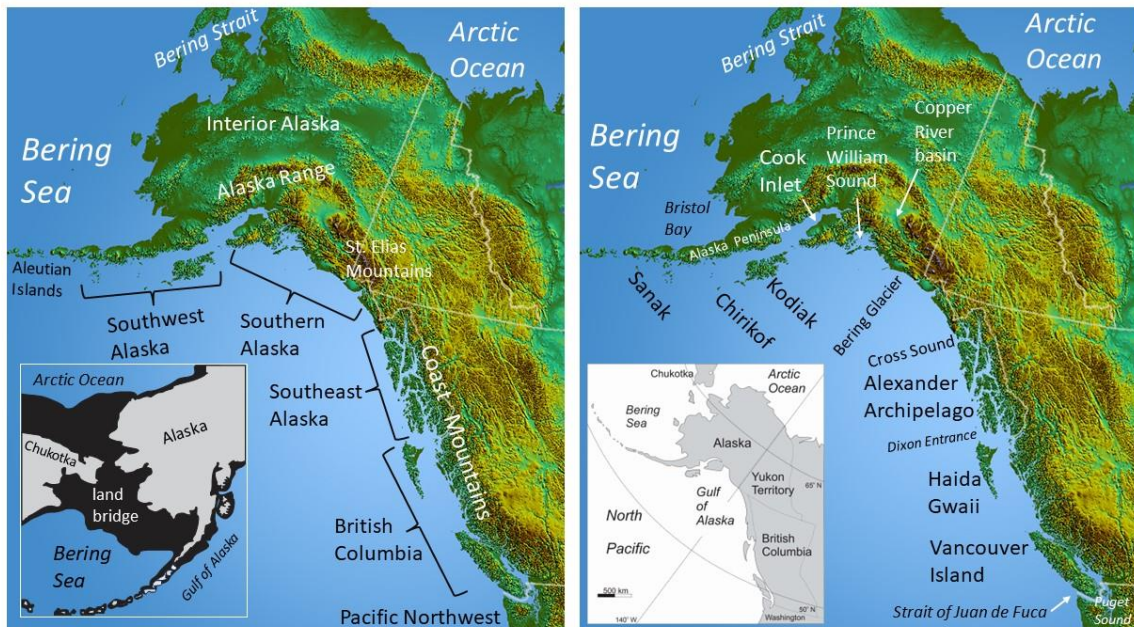


Figure 1. The Northwest Coast of North America. The Bering Land Bridge (**lower left**) is shown as it existed at the height of the last ice age.

2. PALEOENVIRONMENTAL RECORDS FROM THE NORTHWEST COAST AND SUBARCTIC PACIFIC

2.1. Glacial history

2.1.1. “Cordilleran Ice Sheet” or “Cordilleran Glacier Complex”?

It is useful to define some terminology before reviewing the extent and timing of glaciation along the Northwest Coast. During the global Last Glacial Maximum (hereafter, LGM), the Northwest Coast was lined by marine-based glaciers that drained ice masses accumulated over the western Cordillera of North America (Fig. 2). Chamberlin (1895) referred to this assortment of ice caps, valley glaciers, and piedmont glaciers as the “Cordilleran Ice Sheet”. Although often depicted as a single, confluent body of ice extending from Washington State to

southwestern Alaska, in fact this accumulation of ice consisted of a myriad of glaciologically independent glaciers. This was particularly true in the high ranges of the southwest Yukon and southern Alaska, where the dynamics of different glaciers were coordinated only in the sense of responding to shared climate drivers, and, in the case of glaciers reaching tidewater, by changes in relative sea level that affected how much ice was lost by calving icebergs into the sea. Only in south-central sector of the Cordilleran Glacier Complex in British Columbia (Fig. 3) where bedrock plateaux allowed the formation of coalescent ice domes during the local LGM was there a degree of glaciological integration comparable to that occurring in the Laurentide Ice Sheet (Clague 1989; Clague and Ward 2011; Perkins and Brennand 2015; Seguinot et al. 2016; Menounos et al. 2017; Eyles et al. 2018).



Figure 2. Distribution of glaciers and ice sheets (blue) during the Last Glacial Maximum at high latitudes in the northern hemisphere. Redrawn from Ehlers et al. (2011) and Simms et al. (2019). The numbers are estimates of the meters of eustatic sea-level draw-down contained in different ice sheets. Estimates of sea-level drawdown are from Simms et al (2019) and Stokes et al. (2012). "CGC" = Cordilleran Glacier Complex, "LIS" = Laurentide Ice Sheet, "FIS" = Fennoscandian Ice Sheet.

The assortment of glaciers present over northwestern North America during Marine Isotope Stage 2 is more appropriately called the Cordilleran Glacier Complex than the Cordilleran Ice Sheet. The term "complex" is more appropriate because an ice sheet is glaciologically integrated (Bates and Jackson 1987), while a glacier complex is not. The Laurentide Ice Sheet (LIS), for example, at its maximum extent flowed radially from a 3 km-high ice dome centered over the lowlands of the Canadian Shield (Marshall et al. 2000; Dyke et al. 2002; Dalton et al. 2020). The different sectors of the LIS were dynamically integrated at a continental scale (Winsborrow et al. 2004; Stokes et al. 2016). In contrast, large sectors of the Cordilleran Glacier Complex (CGC) consisted of relatively thin ice whose flow was topographically segregated into independent ice bodies (Clague 1989; Clague et al. 2011; Eyles et al. 2018). This was particularly true during deglaciation as mountain ridges emerged from the down-wasting ice (Fulton 1991; Margold et al. 2013; Menounos et al. 2017). An immediate benefit of recognizing the CGC as a "complex" rather than an "ice sheet" is to recognize the high potential for asynchronous glacier fluctuations (Darvill et al. 2018). This tendency that was accentuated further along the Pacific coast by the presence of numerous marine-based glaciers whose dynamics were susceptible to non-climatic drivers (Benn et al., 2007; Stokes et al. 2014).

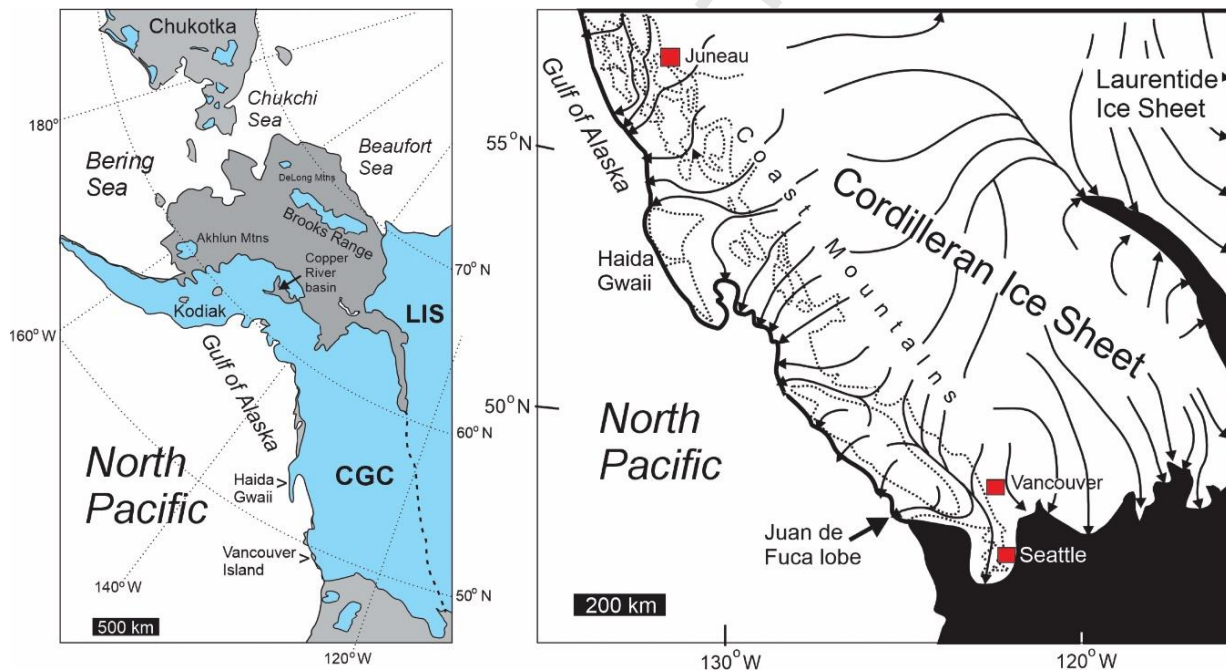


Figure 3. **LEFT** The Cordilleran Glacier Complex (CGC) consisted of numerous, glaciologically independent glacier systems. The extent of glacial ice in northwestern North America ca. 21 ka is from Dalton et al. (2020). Ice extent in Chukotka is from Barr and Clark (2012), and ice extent in the DeLong Mountains is from Hamilton (2010), and in the Brooks Range from Kaufman et al. (2011). "LIS" = Laurentide Ice Sheet. **RIGHT** The only fully integrated, ice-sheet portion of the CGC occupied the interior highlands of British Columbia and Alberta, and this was only for brief

intervals during Marine Isotope Stage 2. Generalized flow patterns shown as arrows. Redrawn from Clague and James (2002).

2.1.2. Major features of the Cordilleran Glacier Complex

The Cordilleran Glacier Complex (CGC) developed when alpine glaciers expanded and coalesced (Kerr 1934). Infrequently during the most glaciogenic phases of the late Pleistocene, glaciers thickened enough to form one or more ice domes over the interior of British Columbia (Clague and James 2002) (Fig. 4), and the formation of these domes caused the flow axis to shift eastward of the Coast Mountains (Stumpf et al. 2000). Even in this southern, ice-sheet portion of the CGC, deglaciation was geographically complex compared to much of the Laurentide Ice Sheet because of the alpine topography (Clague 1989; Clague and Ward 2011; Margold et al. 2013; Perkins and Brennand 2015).

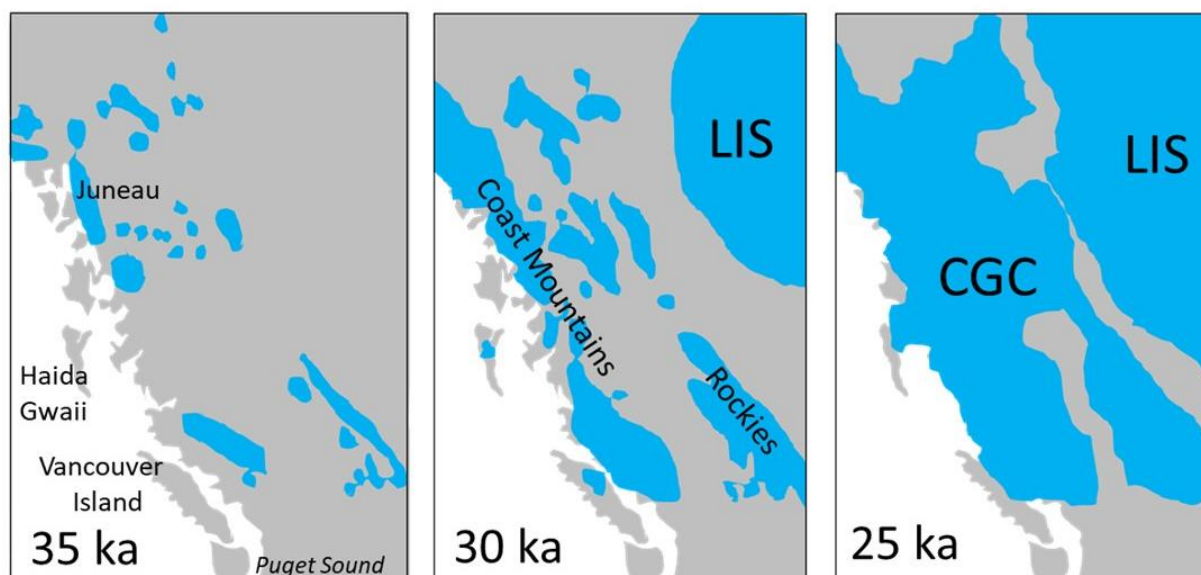


Figure 4. The expansion of the Laurentide Ice Sheet (LIS) and the Cordilleran Glacial Complex (CGC) during the onset of Marine Isotope Stage 2 as inferred by Clague and Ward (2011). Note that by 30 ka the LIS was expanding westward as an integrated ice sheet, while the CGC was still coalescing from multiple alpine ice caps.

Salient features of the Cordilleran Glacier Complex (CGC) include: 1) Its wide latitudinal range. Its northernmost glaciers terminated in the subarctic landscapes of Interior Alaska, while its southernmost glaciers overrode forests in Washington, Idaho, and western Montana. 2) Its 4000-km long marine margin. Many of the CGC's outlet glaciers and ice streams flowed onto the continental shelf where they were marine-based, which meant their beds were positioned at or

below contemporary sea level. 3) Its North Pacific moisture source. Unlike the Laurentide Ice Sheet (LIS), the CGC was nourished almost entirely by North Pacific moisture. 5) Its numerous warm-based glaciers. Because of its maritime position and relatively low altitudes and latitudes, significant portions of the CGC were at the pressure-melting point (Booth and Hallet 1993; Clague and James 2002). 6) Its complexity of flow. In contrast to much of the LIS, the CGC developed over mountainous terrain (Clague and James 2002). 7) Its dynamism. The relatively small sizes and warm basal temperatures of the glaciers comprising the CGC made them respond rapidly to changing climate.

2.1.3. Timing and extent of the Marine Isotope Stage 2 glaciation along the Northwest Coast

2.1.3.1. *Puget Sound and southwestern British Columbia*

Following a prolonged interstadial during Marine Isotope Stage 3 (ca. 57-29 ka), glaciers coalesced and advanced out of the southern Coast Mountains and the highlands of Vancouver Island beginning ca. 30 ka (Clague 1981; Clague and James 2002; Clague and Ward 2011) (Fig. 5). Ice first reached the Fraser Lowland and northern Puget Sound during the Coquitlam Stade, accompanied by an advance of alpine glaciers in the Cascade Mountains (Booth et al. 2003; Porter and Swanson 2008). After a standstill or a minor retreat between 23 and 21 ka, the Puget Lobe advanced rapidly into Puget Sound, crossing the site of Seattle ca. 17.6 ka and reaching its maximum extent near present-day Olympia, Washington ca. 17 ka (Porter and Swanson 1998). The maximum extent of the Puget Lobe lasted < 500 years (Menounos et al. 2009). Meanwhile, another ice lobe flowed westward down the Strait of Juan de Fuca to terminate on the continental shelf (Hendy and Cosma 2008; Taylor et al. 2014). During this Vashon Stade, alpine glaciers descending from the Cascade and Olympic Mountains coalesced with the main flow of ice originating in Canada (Riedel et al. 2010), while east of the Cascade Mountains, ice lobes advanced down the Okanagan valley and the valleys further east (Porter 1976; Booth et al. 2003; Balbas et al. 2017). Some of these ice lobes, including the Purcell Lobe near the present Idaho/Montana border, dammed lakes whose repeated outburst floods may have affected the oceanography and climate of the entire North Pacific (Section 4.1.9).

The Vashon Stade ended with the rapid retreat of ice out of Puget Sound beginning before 16 ka (Fig. 5). This rapid retreat probably began when the Juan de Fuca Lobe was dislodged from its terminal moraine shoal by rising sea level (Clague and Ward 2011; Taylor et al. 2014). By 15.5 ka, Puget Sound was ice free, and a large calving embayment had formed in the Strait of Georgia near the International Border (Menounos et al. 2009; Clague and Ward 2011). Abrupt warming at the onset of the Bølling ca. 14.7 ka reduced the ice volume of the Cordilleran Glacier Complex (CGC) in western Canada by approximately half in < 500 years (Menounos et al. 2017). In inland regions where the CGC existed as an integrated ice sheet, rapid melting gave rise to an assortment of independent alpine glaciers and ice caps by the end of the Younger Dryas, ca. 11.7 ka (Menounos et al. 2017).

As the ice withdrew into the Coast Mountains and the North Cascades, marine waters invaded the isostatically depressed landscapes of Puget Sound and the Fraser Lowlands (Thorson 1989; Dethier et al. 1995; Clague and James 2002; Mosher and Hewitt 2004). In southern Puget Sound, short-lived proglacial lakes formed and then drained as their outlets were progressively uncovered as the ice margin retreated northward and down-wasted.

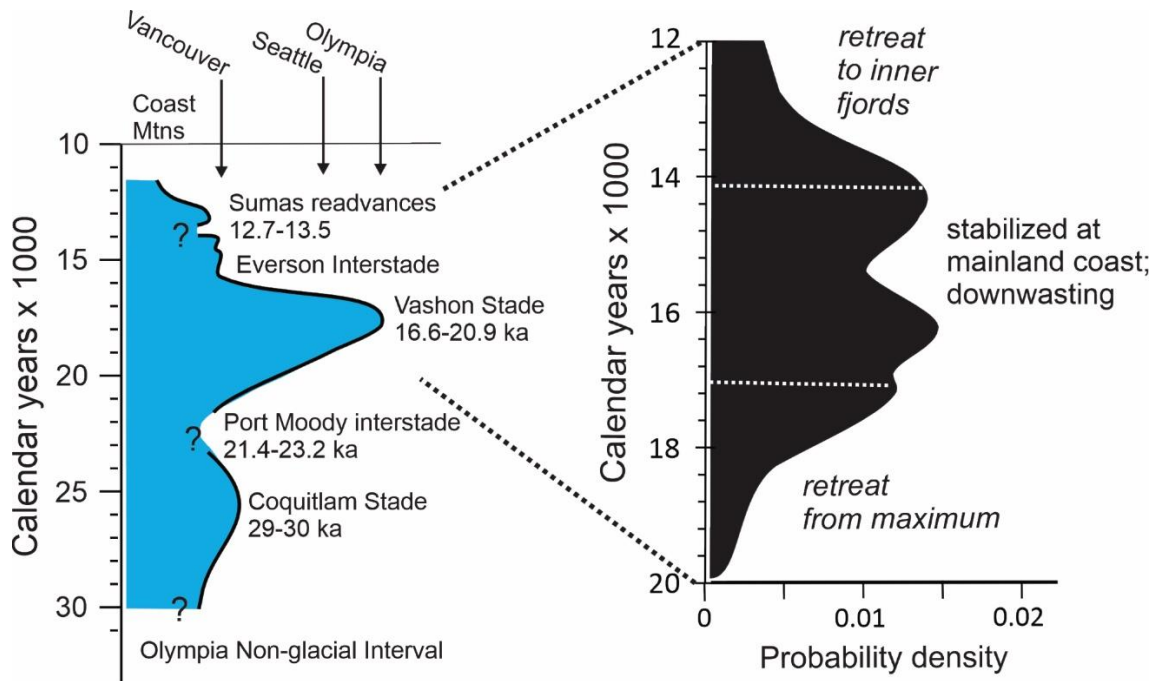


Figure 5. **LEFT** Time/distance diagram for southwest British Columbia and Puget Sound during Fraser Glaciation (Porter and Swanson 1998; Booth et al. 2003; Darvill et al. 2018) modified from Cosma and Hendy (2008). **RIGHT** The timing of glacial retreat along the central British Columbia coastline between Vancouver Island and Southeast Alaska expressed as the probability density of exposure ages (Darvill et al. 2018; Darvill et al. 2022).

2.1.3.2 Western coast of Vancouver Island

Alpine glaciers advanced from the mountainous interior of Vancouver Island ca. 30 ka, prior to the island being overtopped by mainland ice flowing west out of the Coast Mountains (Clague and Ward 2011). The local Last Glacial Maximum (ILGM) on Vancouver Island occurred between 20 and 15 ka (Darvill et al. 2018). The outer, western coast of the island was glaciated last and deglaciated first, which resulted in relatively brief periods of glacial cover (Hebda et al. 2022). Grounded ice reached the outer coast at different times in different places. For example, Topknot Lake on the northwestern outer coast was overrun by ice before 17.1 (Hebda et al. 2022), while Port Eliza on the central, outer coast was not overrun until after 16.3 ka (Al-Suwaidi et al. 2006). The seaward extent of glaciation remains unclear (Darvill et al. 2018), and

some locations on the northwest coast of Vancouver Island may have escaped glaciation (Hebda 1997; Hebda et al. 1997; Hebda et al. 2022). Areas further south along the western coast of Vancouver Island that were covered by ice were deglaciated prior to 16 ka (Al-Suwaidi et al. 2006).

Marine records off the western coast of Vancouver Island add valuable details to the record of glaciation (Fig. 6). Glaciomarine sedimentation began ca. 29.5 ka (Cosma and Hendy 2008). Episodes of iceberg rafting became increasingly frequent after ca. 19.5 ka, with a major peak in the deposition of ice-berg rafted debris (IRD) occurring ca. 17-16, which was coeval with the Vashon Stade maximum in Puget Sound and its initial retreat. A later spike in IRD deposition occurred off the western coast of Vancouver Island ca. 14.8 ka at the beginning of the Bølling interstadial (Cosma and Hendy 2008; Taylor et al. 2014) (Fig. 6).

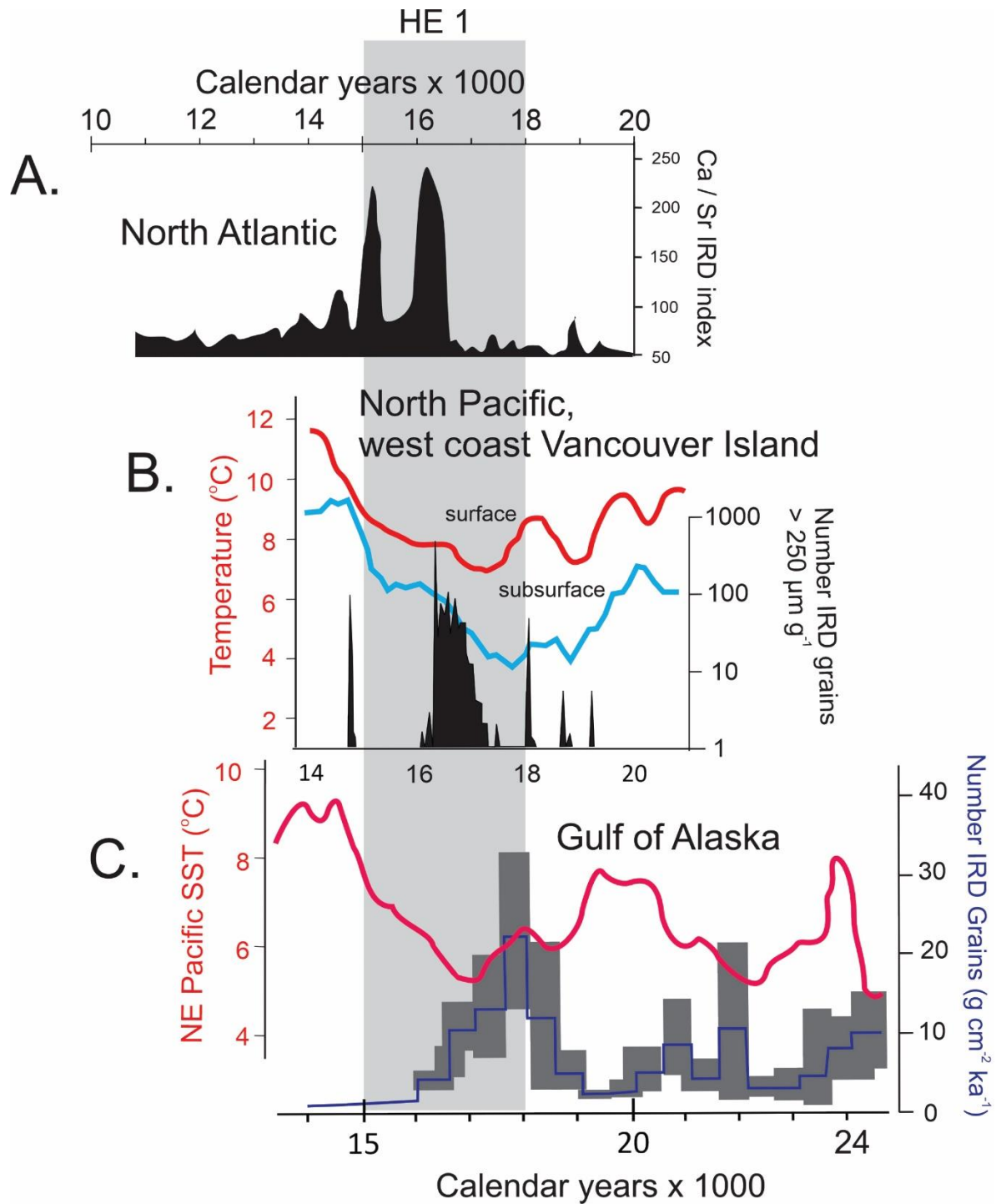


Figure 6. Marine records of deglaciation inferred from ice-rafted debris (IRD) and sea surface temperature (SST). **A.** The IRD record from Site U1308 in the North Atlantic (Hodell et al. 2017). **B.** IRD concentrations and ocean temperatures inferred from planktonic foraminiferal Mg/Ca records in Core MD02-2496 from the continental slope of Vancouver Island, British Columbia (Taylor et al. 2014). **C.** IRD accumulation rates in Core U1419 from the northeastern the Gulf of

Alaska (Walczak et al. 2020). The red line shows the mean annual SST in the Gulf of Alaska as estimated by Praetorius et al. (2023).

2.1.3.3. *Central British Columbia coast and Haida Gwaii*

The central British Columbian coast extends from Vancouver Island to Dixon Entrance (Fig. 3). Haida Gwaii (Queen Charlotte Islands) has been a focus of research concerning glaciation and relative sea level because of its unique geography and biogeography. The archipelago lies on the outer edge of the continental shelf and is separated from the mainland by 50-150 km of shallow marine waters (Hecate Strait and Queen Charlotte Sound) (Fig. 7). Its biogeography is considered unusual because of the occurrence of endemic, genetically unique, and disjunct species (Heusser 1989; Godbout et al. 2008; Shafer et al. 2010; Pruett et al. 2013; Mathewes et al. 2015; Fedje et al. 2021). The occurrence of some of these unique taxa may relate to the presence of ice-free areas that afforded biological refugia during Marine Isotope Stage 2. Reconstructions of glacier extent and timing are necessary to identify where and when these ice-free areas and biological refugia might have existed (Heusser 1960; Clague 1981; Mathewes and Clague 2017; Shaw et al. 2020; Fedje et al. 2021).

During an extended period of interstadial climate between 50 and 31 ka, temperate rainforest vegetation grew in the lowlands of Haida Gwaii under a climate that was only slightly cooler than today (Warner et al. 1984; Mathewes et al. 2015). The western edge of the Cordilleran Glacier Complex advanced into Hecate Strait ca. 30 ka, and after ca. 24 ka merged with alpine glaciers flowing eastwards from the uplands of Haida Gwaii (Blaise et al. 1990; Barrie and Conway 1999; Mathewes and Clague 2017). This coalescence was probably short-lived because of the relatively small size of glacier catchments on Haida Gwaii and because the proximity of the open Pacific Ocean prevented the buildup of thick glacial ice over the islands. As a result, areas on the western coast of Haida Gwaii, which borders the outer shelf edge, possibly remained ice-free and subaerial during the local LGM (Barrie et al. 2021).

During the local Last Glacial Maximum (LGM) ca. 24 to 18 ka, multiple ice streams flowed onto the continental shelf north and south of Haida Gwaii through Dixon Entrance and eastern Hecate Strait (Eyles et al. 2018). Ice reached thicknesses of ~ 400 m in Queen Charlotte Sound (Barrie and Conway 1999) and ~ 700 m in northern Hecate Strait and Dixon Entrance (Hetherington et al. 2004). These ice streams calved into the open Pacific along the outer shelf edge (Fig. 7), leaving only thin and transient glacier margins to advance westward across Hecate Strait to merge with the glaciers flowing eastwards from Haida Gwaii (Barrie et al. 2021). The steep gradient in ice thickness between the inner fjord zone of the mainland and the outer shelf generated an isostatic forebulge that caused relative sea level to fall below -150 m along the eastern coastline of Haida Gwaii prior to 14 ka (Hetherington et al. 2004) (Section 2.2). This resulted in large areas of Queen Charlotte Sound lying above sea level until this forebulge

collapsed and eustatic sea level flooded the area ca. 10 ka (Fedje and Josenhans 2000; Fedje et al. 2005; Shaw et al. 2020).

Lowland areas on Haida Gwaii and the adjacent continental shelf may have become ice-free before ca. 19.4 ka (Blaise et al. 1990; Mathewes and Clague 2017; Darvill et al. 2018), although alpine glaciers persisted in the uplands. Minimum-limiting ages from cosmogenic exposure dating indicate that ice derived from the Coast Mountains had retreated eastward to the mainland coast by 17 ka (Barrie and Conway 1999), and perhaps as early as 18 ka (Darvill et al. 2018; Barrie et al. 2021). Upon reaching the mainland coast, the ice margin paused and possibly readvanced between ca. 17 and 14 ka (Fig. 5) (Darvill et al. 2018; Darvill et al. 2022). During this 17-14 ka readvance or standstill along the central British Columbia coast, the interior portions of the Cordilleran Glacier Complex continued to downwaste and thin (Darvill et al. 2022). Glaciers underwent a final, fluctuating retreat into the inner, mainland fjords between 14 and 13 ka (Hetherington et al. 2004; Eamer et al. 2017; Barrie et al. 2021; Darvill et al. 2022).

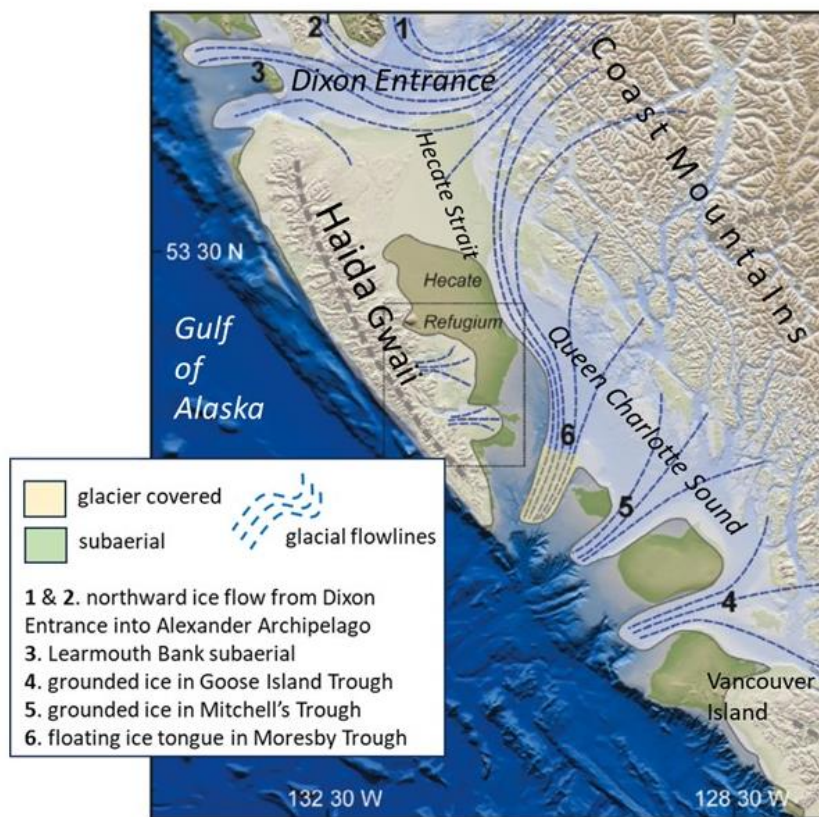


Figure 7. Glacier extent and locations of possible ice-free areas around Haida Gwaii and in Queen Charlotte Sound during the local Last Glacial Maximum between ca. 24 and 18 ka. Modified slightly from Shaw et al. (2020).

2.1.3.4. *An ice-free area / refugium on Haida Gwaii?*

Building on the studies of Barrie and Conway (1999, 2002), Barrie et al. (2009), Hetherington et al. (2004), and Josenhans et al. (1994; 1997), Shaw et al. (2020) and Barrie et al. (2021) have reconstructed the paleogeographies of Dixon Entrance, Hecate Strait, and Queen Charlotte Sound during the local Last Glacial Maximum (ILGM) and subsequent deglaciation (Fig. 7). Their reconstructions suggest that grounded ice from the mainland flowed southwards in the coast-parallel trough along the eastern (mainland) side of Hecate Strait. Upon reaching Queen Charlotte Sound, this ice stream split and flowed through three, cross-shelf troughs to empty into the open Pacific. In a pattern familiar from glaciated continental shelves elsewhere (Wellner et al. 2001; Nielsen et al. 2005; Batchelor and Dowdeswell 2014), the cross-shelf troughs in Queen Charlotte Sound were separated by low-relief banks, which Shaw et al. (2020) suggest remained unglaciated and subaerial. With relative sea level lowered by > 150 m (Josenhans et al. 1997; Shugar et al. 2014) (Section 2.2), an ice-free, subaerial area measuring roughly 150 km long and 10-50 km wide may have existed along the eastern side of Moresby Island, the southern major island of the Haida Gwaii group. This potentially ice-free area, which Shaw et al. (2020) relate to the “Hecate refugium” inferred to exist by Mathewes and Clague (2017) based on paleoecological evidence, would have consisted of an outwash plain criss-crossed by proglacial rivers. During the ILGM, the borders of this ice-free area would have repeatedly shifted in response to changes in glacier positions and sea level (Josenhans et al. 1997). It remains to be demonstrated whether this ice-free area provided a biological refugium. If it did, the biota it sheltered were probably limited to arctic-alpine species.

More certain is the existence of extensive ice-free and subaerial surfaces in Hecate Strait and Queen Charlotte Sound between ca. 18 and 10 ka. When by 17.6-16.6 ka, mainland ice had retreated to the present coastline (Darvill et al. 2018; 2022), and the ice cap over Haida Gwaii had retreated into the island highlands, some 40×10^3 km² of present-day Queen Charlotte Sound and Hecate Strait were ice-free and subaerial (Shaw et al. 2020). This extensive lowland remained subaerial until ca. 10 ka when the sea transgressed the area (Josenhans et al. 1997; Shugar et al. 2014) (Section 2.2).

2.1.3.5. *Southeast Alaska (Alexander Archipelago)*

The Alexander Archipelago (Fig. 1) extends 500 km north from Dixon Entrance to Cross Sound and 200 km west from the Coast Mountains to the Gulf of Alaska. The archipelago consists of island massifs bordered by strandflats along the outer Gulf of Alaska coastline (Fig. 8). During the local Last Glacial Maximum (ILGM), island ice caps coalesced with glaciers originating in the Coast Mountains and sent ice streams seaward through fjords to calve on the continental shelf (Capps 1931; Holtedahl 1958; Carrara et al. 2007; Lesnek et al. 2018; Lesnek et al. 2020; Barrie et al. 2021). Since the 1930s, biologists have speculated that ice-free areas were

present in the Alexander Archipelago and sheltered biota during the last ice age (Hultén 1937; Heusser 1960; Klein 1965; Heusser 1989; Heaton et al. 1996; Cook et al. 2001; Carrara et al. 2007; Ager 2019); however, the existence of biological refugia in Southeast Alaska remains controversial (Walcott et al. 2022), much as it is on Vancouver Island (Hebda et al. 2022) and Haida Gwaii (Mathewes and Clague 2017; Fedje et al. 2021).

A major advance in the glacial geology of the Alexander Archipelago occurred when Lesnek et al. (2018) demonstrated that cosmogenic dating was feasible in this temperate-rainforest setting by using ice-scoured bedrock surfaces and glacially transported boulders above present tree line. These exposure ages show that regional deglaciation was underway by 17.7 ± 0.7 ka (Lesnek et al. 2018). Additional exposure-age dating has narrowed the timing of ice retreat from the outer coastline to between 17 and 15 ka and showed that ice had retreated eastward to the coast of the mainland before 14 ka (Lesnek et al. 2020).

Mountainous, fjord-land topography complicates interpretation of the chronology of glacial dynamics in the Alexander Archipelago. The fjords may have been deglaciated first through the calving retreats of marine-based glaciers, leaving island ice caps perched on the intervening uplands (Baichtal et al. 2021). On the other hand, in similar terrain along the outer coast of Norway, high-altitude surfaces were deglaciated early and remained subaerial for millennia before adjacent fjord became ice free (Regnéll et al. 2021). Deciphering the pattern of deglaciation in Southeast Alaska will require cosmogenic dating of surfaces ranging in elevation from sea level to mountain ridges.

Additional cosmogenic dating by Walcott et al. (2022) suggests that ice retreated from the outer coast of the northern Alexander Archipelago (Chichagof and Baranof Islands) ca. 15.1 ± 0.9 ka, and from the outer coast of the southern archipelago ca. 16.3 ± 0.8 ka. The cessation of ice-rafted debris deposition in the Gulf of Alaska ca. 14.8 ka suggests that most marine-based glaciers had retreated onto land by then (Davies et al. 2011; Praetorius and Mix 2014). These estimates for deglaciation timing are consistent with the basal ages of freshwater lakes (Engstrom et al. 1990; Ager and Rosenbaum 2009; Ager et al. 2010; Ager 2019) and with the ages of marine shells associated with glacio-marine deposits at various locations in the Alexander Archipelago (Mann and Streveler 2008; Baichtal et al. 2021).

More closely limiting ages on the local Last Glacial Maximum (ILGM) in the southern Alexander Archipelago come from the ^{14}C ages of bones recovered from On Your Knees Cave (in the Tlingit language: *Shuka Káa*) (Heaton et al. 1996; Heaton and Grady 2003; Lesnek et al. 2018). This cave is located at 56° N on northern Prince of Wales Island approximately 125 m above present sea level, 40 km east of Chatham Strait, 60 km inland from the outer coastline, and approximately 140 km from the outer edge of the continental shelf. *Shuka Káa* was the den of Arctic foxes (*Vulpes lagopus*) and contains the abundant bones of ringed seal (*Pusa (Phoca) hispida*), an ice-dependent seal species now restricted to the northwest Pacific, the Arctic Ocean, and parts of the North Atlantic. Twenty-six ring seal bones from the cave range in age from 30 to 14 ka. The only time interval when the error terms of consecutive ^{14}C ages do not

overlap is between 19.8 and 17.2 ka, suggesting this was the only time when the cave was sealed off from the ocean, presumably by overriding glacial ice (Lesnek et al. 2018). This unique chronostratigraphic evidence suggests the ILGM was brief and of limited extent in the southern Alexander Archipelago. The *Shuka Káa* record constrains the ILGM in Southeast Alaska to at most a 2.6-kyr interval that occurred 3 to 4 kyr after the Laurentide Ice Sheet reached its maximum in the Great Lakes region (Heath et al. 2018), 0.5 to 1 kyr after the time of maximum glaciation in the northwestern Alaska Range (Tulenko et al. 2022) (Section 2.1.3.12), and 0.5-1.5 kyr prior to the ILGM in Puget Sound (Porter and Swanson 1998) (Section 2.1.3.1).

It remains unclear how complete ice cover was over the Alexander Archipelago. Prior to the advent of exposure-age dating, it was thought that ice buried all but the highest summits of the Alexander Archipelago and terminated in a continuous, calving margin along the outer continental shelf (Mann and Hamilton 1995). Carrara et al. (2007) and Lesnek (2020) suggested that certain areas along the outer coast remained ice-free throughout the Last Glacial Maximum. The ring-seal chronology from *Shuka Káa* is consistent with limited, short-lived ice cover; however, Walcott et al. (2022) suggest that even outer coast areas were glaciated until ca. 16.3 to 15.1 ka. These authors imply that ice extended onto the continental shelf along the entire seaward margin of the archipelago, an interpretation that is consistent with the reconstruction of ice flowing to the shelf break in Queen Charlotte Sound and Dixon Entrance (Shaw et al. 2020; Barrie et al. 2021).

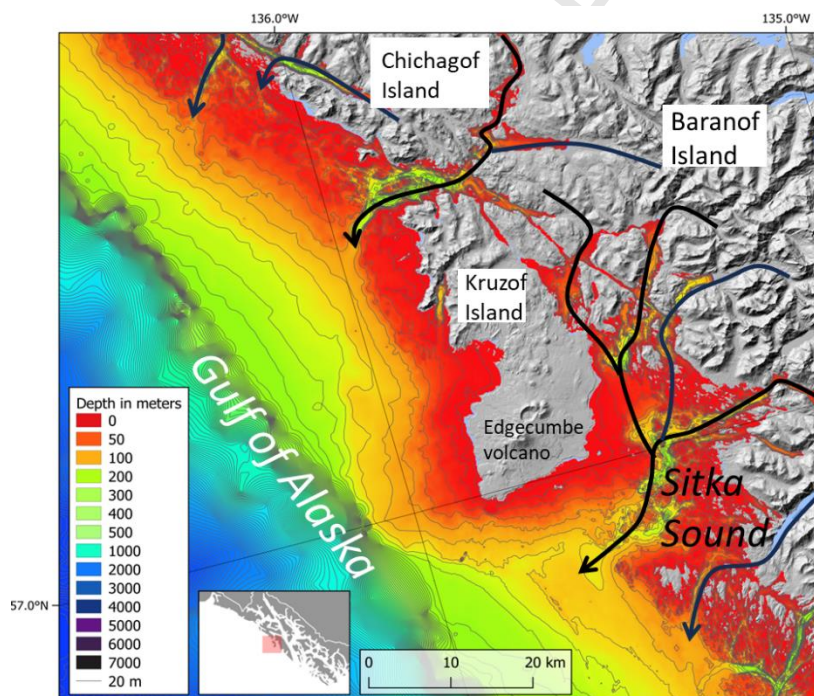


Figure 8. A representative area of the outer coast of the Alexander Archipelago showing the narrow (20-40 km) continental shelf and the well-developed strandflat (< 50 m water depth). This strandflat was incised by glaciers issuing from the fjord systems that crisscross the

archipelago. The strandflat is less-developed near southern Kruzof Island because of the Quaternary volcanic deposits of Mount Edgecumbe. Arrows show the inferred flow patterns of major outlet glaciers. The geomorphic imprint of glaciation is relatively light along this coastline compared to farther northwest along the Gulf of Alaska. Bathymetric data are from Zimmermann and Prescott (2015); the map is generated in QGIS v3.26.2. The onshore digital elevation model is from Zabihi et al. (2021).

In summary, the local Last Glacial Maximum (ILGM) occurred in Southeast Alaska between 19.8 and 17.2 ka, which is later than the southern margins of the Laurentide and Fennoscandian Ice Sheets, but prior to the ILGM in Puget Sound. Because the ILGM occurred in Southeast Alaska after 20 ka when eustatic relative sea level was rising, marine-based ice streams draining the Alexander Archipelago would have been increasingly destabilized, even in the absence of major shifts in climate. Deglaciation proceeded quickly and involved rapid calving retreats beginning ca. 17 ka and intensifying after 16 ka. As in the calving retreat of other marine-based ice complexes (Small et al. 2018), fjord topography/geometry in some cases superseded climate in determining the spatial and temporal pattern of ice retreat in the Alexander Archipelago. The western margin of the Cordilleran Glacier Complex had retreated to the inner fjords of the Coast Mountains by 14 ka. If ice-free areas did exist in Southeast Alaska during the ILGM, they were located on outer coast mountainsides and/or near the outer edge of the continental shelf where the presence of an isostatic forebulge (Hetherington et al. 2004; Shaw et al. 2020; Baichtal et al. 2021; Barrie et al. 2021) allowed them to persist during deglaciation despite rising sea level. Striking progress has been made in deciphering the extent and timing of the LGM in Southeast Alaska; however, a critical next step is to sample exposure ages along topographic gradients in order to reconstruct glacier flowlines, trimline altitudes, equilibrium-line altitudes, and the seaward extent of ice on the continental shelf.

2.1.3.6. *Southern Alaska: Cross Sound to the Copper River delta*

The coastline between Cross Sound and the Copper River delta (Fig. 9) is backed by glaciated peaks rising to 6000 m asl. Rapid tectonic uplift since the Oligocene (Lease et al. 2021) has outstripped topographical lowering by glacial erosion (Merrand and Hallet 2001). Embayments are widely separated and consist of fjord mouths, some still occupied by glaciers, including the piedmont lobes of the Malaspina and Bering Glaciers. Repeated glaciations have left widespread evidence of glacial erosion and glaciomarine sedimentation on the continental shelf (Carlson et al. 1982; Molnia 1986; Eyles and Lago 1990; James et al. 2009a; Gulick et al. 2015). These glacial features include moraines, mega-scale glacial lineations, drumlins, trough-marginal moraines, cross-shelf troughs, inter-trough banks, trough-mouth fans, grounding-zone wedges, ice-proximal fans, and thick accumulations of glaciomarine sediment (Swartz et al. 2015; Zimmermann and Prescott 2015; Montelli et al. 2017; Clary et al. 2021). The

accumulation of these glaciogenic features over a 23-million year history of marine-based glaciation makes it challenging to identify glacial limits reached during Marine Isotope Stage 2.

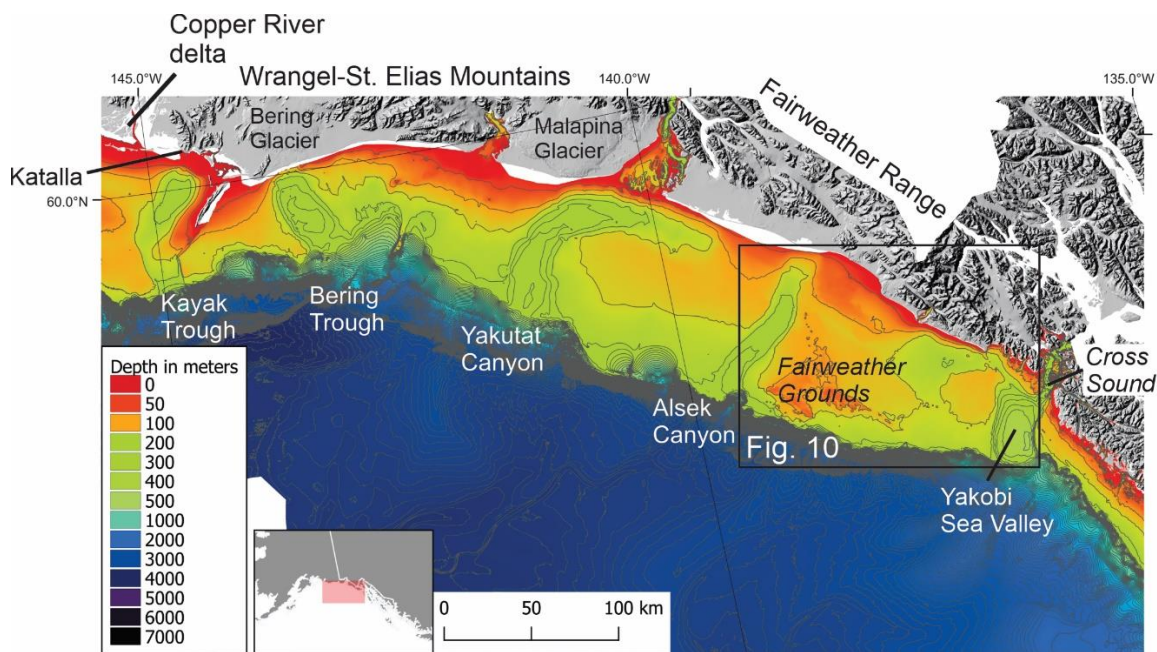


Figure 9. Cross-shelf troughs attest to prolonged, intense glaciation of the continental shelf between the Yakobi Sea Valley and the Copper River delta. Bathymetric data are from Zimmermann and Prescott (2015); the map is generated in QGIS v3.26.2. The onshore digital elevation model is from Zabihi et al. (2021).

The extent of glaciers on the continental shelf of the northern Gulf of Alaska during the Last Glacial Maximum (LGM) has been the topic of continued speculation (Capps 1931; Karlstrom 1964; Coulter et al. 1965; Péwé 1975; Molnia 1986; Hamilton 1994; Manley and Kaufman 2002; Dyke 2004; Kaufman et al. 2011; Dalton et al. 2020; Haeussler et al. 2022). Based solely on the geomorphology of the continental shelf, which remains largely undated, LGM ice probably flowed to the outer shelf edge throughout the region. Previous reconstructions show glacier tongues extending seaward through the cross-shelf troughs, with the inter-trough banks remaining ice free (Molnia 1986; Kaufman et al. 2011; Dalton et al. 2020); however, based on what is known from glaciated continental shelves in Iceland (Geirsdóttir et al. 2009) and western Norway (Laberg et al. 2000; Ottesen et al. 2005; Batchelor and Dowdeswell 2014; Montelli et al. 2022), these inter-trough banks were probably also ice covered, albeit by thinner and less-dynamic ice than the ice streams in the troughs.

Recent compilations of the bathymetry of the continental shelf (Zimmermann and Prescott 2015), together with the mapping of fish habitats (Greene et al. 2011), reveal moraines and possible glacial trimlines on the inter-trough banks between the Yakobi Sea Valley and the

Alsek Canyon (Fig. 10). The presence of multiple moraines there suggest a complex glacial history during Marine Isotope Stage 2 (MIS 2). Of particular interest are the Fairweather Grounds, a 540-km² area of exposed bedrock that protrudes as much as 80 m above the surrounding continental shelf and shoals at a depth ~ 24-m (Greene et al. 2011). Acoustic mapping suggests the presence of an erosional trimline (Greene et al. 2007) that could delineate the seaward extent of inter-trough, glacial ice during MIS 2. If this interpretation is correct, then glaciers did not reach the outer shelf edge here during the local Last Glacial Maximum.

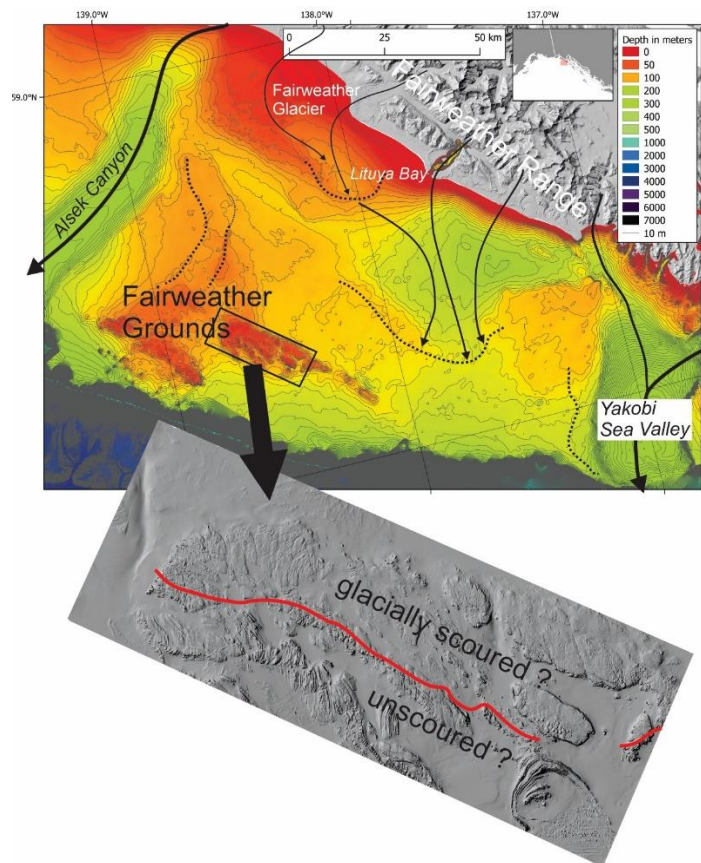


Figure 10. The Fairweather Grounds on the outer continental shelf between the Yakobi Sea Valley and the Alsek Canyon may have escaped glaciation during Marine Isotope Stage 2. Hypothetical glacial flowlines are shown as solid arrows. Dashed lines show possible moraines. Ice streams probably flowed to the outer shelf edge through the cross-shelf troughs; however, moraines on the intervening banks suggest limited ice cover there. Mapping of fish habitats revealed a possible glacial trimline on the Fairweather Grounds (Greene et al. 2007; Greene et al. 2011). Age control over these submerged features is presently lacking. Bathymetric data are from Zimmermann and Prescott (2015); the map generated in QGIS v3.26.2. Onshore digital elevation model is from Zabihi et al. (2021).

Much of what is known about the glacial history of this sector of the Gulf of Alaska coastline during Marine Isotope Stage 2 comes from marine cores. Basal organics in a core from the Yakobi Sea Valley date to ca. 15 ka, suggesting deglaciation occurred around that time (Barron et al. 2009). Multiple peaks in ice-rafted debris in the northeastern Gulf of Alaska indicate a complex pattern of glacier retreat interrupted by either stillstands or readvances of marine-based ice. Bouts of iceberg-rafted debris (IRD) deposition occurred offshore of the Bering Glacier ca. 25-23, 22, and 21 ka, followed by a peak in deposition between 18.5 and 16.5 ka, which was immediately before or possibly during the early stages of Heinrich Event 1 (HE 1) (Walczak et al. 2020) (Fig. 6). In a sediment core taken closer to the Bering Glacier, Cowan et al. (2020) found broad peaks in IRD deposition between 26.5 and 24 ka and again between 18.5 and 17 ka. Freshening of ocean surface waters occurred ca. 16.7 ka, probably in response to widespread melting of ice during regional glacial retreat (Davies et al. 2011). A transition to hemipelagic, laminated sediment in the same cores ca. 14.8 ka indicates that most of the formerly marine-based glaciers retreated onto land by that time, causing iceberg calving to cease (Davies et al. 2011; Praetorius and Mix 2014).

Onshore, Sirkin and Tuthill (1987) dated basal peat near Katalla near the eastern edge of the Copper River delta to 15.8-17.9 ka. Chapman et al. (2009) dated a basal peat on Wingham Island, also near Katalla, to 13.8-14 ka, while Peteet (2007) obtained basal peat dates from the Bering Glacier foreland as old as ca. 16 ka. Taken together, these minimum-limiting ^{14}C dates indicate the Bering Glacier had retreated from the present coastline between 16 and 14 ka. The Bering Glacier had retreated even further inland than its present terminal position before 12 ka, possibly as early as 14 ka (Molnia and Post 1995).

2.1.3.7. Prince William Sound

During the Last Glacial Maximum (LGM), glaciers from the Chugach and Kenai Mountains converged in Prince William Sound (PWS) and buried island massifs under ~ 700 m of ice (Fig. 11). Two ice streams flowed out of PWS into the Gulf of Alaska, one on either side of Montague Island, and then crossed the continental shelf to terminate at the shelf break (Haeussler et al. 2015; Haeussler et al. 2022). Information about the chronology of glaciation in PWS is fragmentary. A minimum-limiting date of 14.1-15.0 ka on ice retreat comes from Upper Whitshed Lake near the western edge of the Copper River delta (Garrett et al. 2015). Another limiting date on deglaciation comes from the town of Valdez where Reger (1991) dated terrestrial plant remains to 15.6-12.7 ka. Exposure-age dating suggests ice had retreated from northwestern Prince William Sound before 14.3 ± 1.6 ka and from sites near sea level in west-central Prince William Sound before 12.9 ± 1.1 ka (Haeussler et al. 2022).

Farther west, the fjord-indented coastline of the Kenai Peninsula attests to a long history of erosion by marine-based glaciers (Fig. 11). Glacial troughs, inter-trough banks, and

well-preserved end moraines suggest glaciers flowed to the outer shelf edge there during the local Last Glacial Maximum (Haeussler et al. 2022); however, these features remain undated. The presence of drowned cirques along this coastline suggests that glacier equilibrium-line altitudes fell below present-day sea level during the local Last Glacial Maximum (P  w   1975).

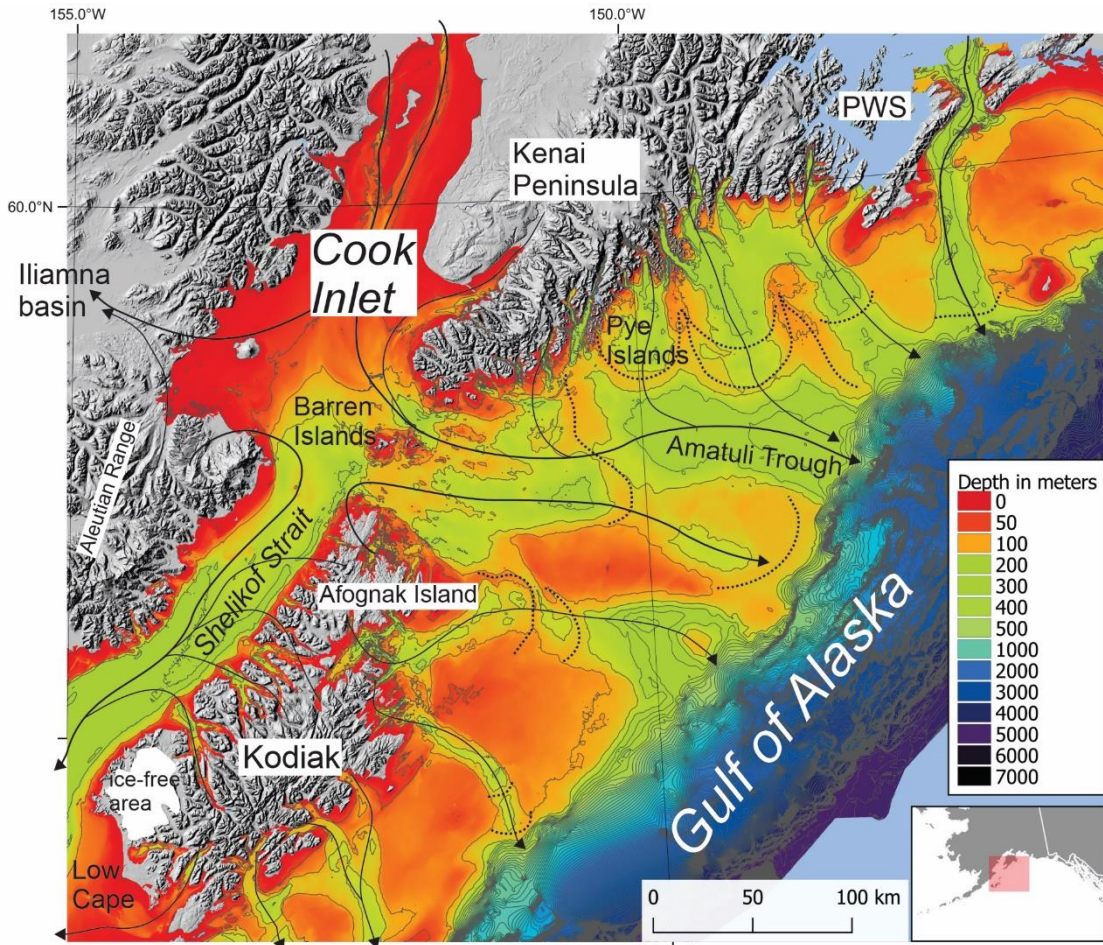


Figure 11. Seafloor geomorphology suggests glaciers terminated at the outer edge of the continental shelf between Prince William Sound (PWS) and the Kodiak Archipelago during the Last Glacial Maximum. Prominent moraines are shown as dashed lines, and hypothetical glacial flowlines down troughs are shown as solid arrows. In the eastern part of the map, geomorphic interpretations are modified from Haeussler et al. (2015; 2022). Bathymetric data are from Zimmermann and Prescott (2015); the map is generated in QGIS v3.26.2. The onshore digital elevation model is from Zabihi et al. (2021).

2.1.3.8. Cook Inlet Lowland

The glacial history of the Cook Inlet Lowland during Marine Isotope Stage 2 (MIS 2) was spatially and temporally complex and remains poorly understood (Briner et al. 2017). Much of what is known about the Quaternary history of this region comes from the work of Richard Reger and his colleagues (Reger et al. 1995; Reger and Pinney 1997; Reger et al. 2008b), who in turn built on the exploratory work of Karlstrom (1964). The Cook Inlet Lowland occupies a structural trough surrounded by mountain ranges (Fig. 11). Its watershed drains some 100,000 km² from the southern flank of the Alaska Range to the Gulf of Alaska. During the local Last Glacial Maximum (ILGM), multiple piedmont lobes expanded into the Cook Inlet Lowland from all sides. Because precipitation declined and equilibrium altitudes rose towards the north/inland (Péwé 1975), glaciation was most intense at the seaward end of Cook Inlet (Fig. 11). Based on trimline altitudes and estimates of equilibrium-line altitudes, Mann and Peteet (1994) suggested that ice reached a thickness of at least 300 m at the mouth of Cook Inlet during the ILGM. The presence of high-level (410 m) glacial scouring on the Barren Islands in the mouth of Cook Inlet, together with the presence there of volcanic erratics transported from the Alaska Peninsula suggest that Cook Inlet ice flowed through the Amatuli Trough to reach the outer shelf edge (Fig. 11). Ice also overflowed low passes in the Aleutian Range to feed the ice lobe that filled the Iliamna Basin in the headwaters of Bristol Bay (Stilwell and Kaufman 1996). During MIS 2, marine-based ice masses in lower Cook Inlet and on the inner continental shelf repeatedly dammed lakes in upper Cook Inlet (Karlstrom 1964; Schmoll and Yehle 1986).

Reger et al. (2008b) inferred that glaciers began to advance into the Cook Inlet Lowland from the surrounding ranges ca. 30 ka. The buildup of glacial ice at the mouth of Cook Inlet eventually formed an ice dam behind which a lake > 100 m in depth formed in the upper inlet. Glaciers flowing from the western ranges crossed this lake to override the Kenai lowlands east of the inlet. Reger et al. (2008a) estimate that the local Last Glacial Maximum occurred between 24.2 and 22.8 ka during the Moosehorn Stade. Minimum-limiting dates on the Moosehorn Stade come from nine cosmogenic dates on erratic boulders that yielded an average age of 20.1 ± 1.4 ka (Tulenko et al. 2022). These exposure-age dates are consistent with the ¹⁴C ages of barnacle plates in glaciomarine sediments within the Moosehorn Stade's terminal moraine that range in age from 19.5 to 18.6 ka (Reger et al. 2008b).

Deglaciation triggered complex interactions between isostatic rebound, episodic seismic displacements, and rising eustatic sea levels (Schmoll and Yehle 1986). A marine transgression began ca. 19.2-19.0 ka when rising marine waters breached the ice dam at the mouth of Cook Inlet and invaded the isostatically-depressed lowlands (Reger et al. 1995; Reger et al. 2008b). By 19 ka, marine waters extended some 200 km into Cook Inlet (Reger et al. 2008b) and by 17.6 ka reached upper Cook Inlet. By ca. 16.5 ka, marine waters extended > 60 km north of present tidewater (Reger et al. 1995).

Three or more glacial standstills or readvances interrupted the course of the deglaciation of Cook Inlet (Karlstrom, 1964). The last of these deposited the 100-km long Elmendorf Moraine in the upper inlet ca. 16.8 ka (Kopczynski et al. 2017), although Reger (pers.

comm., 2021) places the building of the Elmendorf moraine slightly later, between 16.8 and 16.0 ka. Retreat from the Elmendorf moraine was underway by 16.8, or possibly by 16.0 ka, and retreat accelerated at the onset of the Bølling/Allerød ca. 14.7 ka (Kopczynski et al. 2017). Ice had retreated from upper reaches of the Cook Inlet Lowland by 13.7 ka (Kopczynski et al. 2017) and from the eastern Kenai Lowland by 13.1 ka (Broadman et al. 2022).

In summary, the Cook Inlet Lowland remains a key, understudied region of the Northwest Coast. Preliminary studies have primed the area for detailed work in the future. For example, cosmogenic dating of the rich moraine record on both sides of Cook Inlet has just begun (Tulenko et al. 2022). The marine depositional settings in Cook Inlet provide numerous opportunities for reconstructing detailed ^{14}C chronologies of glacial history once the marine reservoir effect is better quantified. The mountainous topography surrounding the lowland and the high topography of islands near its mouth make it an ideal setting for glaciological modelling. To fully understand the glacial record of the Cook Inlet Lowland, detailed bathymetric surveys, marine coring, and onshore stratigraphic work are needed that are comparable to what has been done around Haida Gwaii (Section 2.1.3.4).

2.1.3.9. Kodiak Archipelago

Multiple ice caps developed over Kodiak and Afognak Islands during Marine Isotope Stage 2. Outlet glaciers radiating from Afognak Island flowed northward into Shelikof Strait and eastward into the Amatuli Trough (Fig. 11). Ice caps in the uplands of Kodiak Island sent outlet glaciers southwards to the outer edge of the continental shelf (Greene et al. 2016) as well as northwards into Shelikof Strait. During the local Last Glacial Maximum (ILGM), ice from the Kodiak Archipelago and the Alaska Peninsula converged in Shelikof Strait and flowed southwestward (Fig. 12). A suite of geomorphic features characteristic of fast flow within ice streams are preserved on the floor of the Shelikof Trough (Zimmermann et al. 2019). These include mega-scale glacial lineations, drumlins, and trough-marginal moraines (Batchelor and Dowdeswell 2014). The detailed bathymetry compiled by (Zimmermann et al. 2019) and the very preliminary ice-flow modelling of Mann and Peteet (1994) suggest that the Shelikof Ice Stream terminated at the outer edge of the continental shelf during the ILGM.

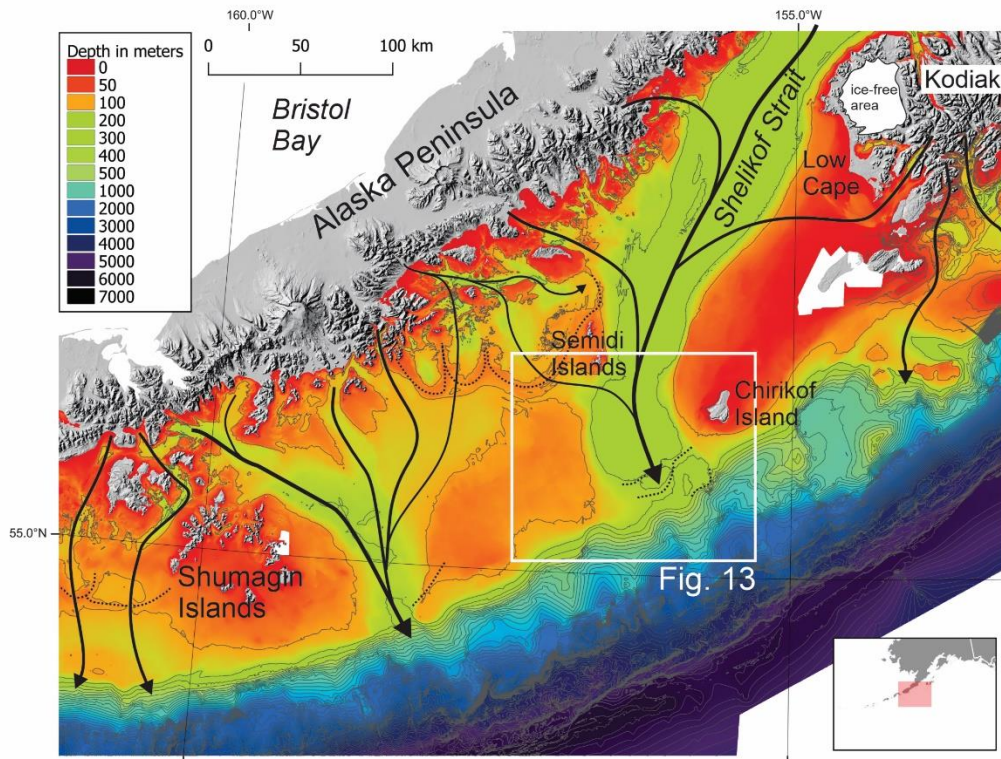


Figure 12. Bathymetry of the continental shelf between the Kodiak Island and the Shumagin Islands. The interpretation of the seafloor geomorphology is based on Zimmermann et al. (2019). Hypothetical glacial flowlines (solid arrows) depict multiple ice streams originating on the Alaska Peninsula and Kodiak Archipelago and terminating along the outer continental shelf. Small ice caps were centered over the Semidi and Shumagin Islands. Multiple moraines located inboard of the shelf edge suggest a complex history of glacial stillstands and readvances during deglaciation. Bathymetric data are from Zimmermann and Prescott (2015); the map generated in QGIS v3.26.2. Onshore digital elevation model is from Zabihi et al. (2021). White box shows location of Fig. 13.

Karlstrom (1964) suggested that an ice-free area existed on southwestern Kodiak Island during the Last Glacial Maximum. This was later confirmed by mapping moraines (Karlstrom 1969) and ^{14}C -dating glacial stratigraphy (Mann and Peteet 1994). Much of this ice-free area consisted of interconnected proglacial lakes fed by ice-marginal streams whose courses and outlets shifted frequently. The subaerial, ice-free terrain on southwestern Kodiak Island during the local Last Glacial Maximum was probably restricted to several 100 km^2 of alpine ridgelines that protruded above the level of these lakes and yet were below local snowlines. Because of its limited area, changeable nature, and the prevailing periglacial climate, this ice-free area on

southwest Kodiak area probably provided a biological refugium for only a limited number of arctic-alpine biota.

¹⁴C-dated stratigraphy along the margin of the ice-free area on southwestern Kodiak indicates that ice advanced down Shelikof Strait between 27.4 and 26.4 ka (Mann and Peteet 1994). Deglaciation occurred prior to 18.2-17.4 ka at Low Cape (Beta-3958), which indicates the outer continental shelf was ice free prior to that time. A readvance of unknown extent occurred at Low Cape between 16.5 and 15.4 ka (Mann and Peteet 1994).

Glacial equilibrium-line altitudes (ELAs) on the northwestern (leeward) side of Kodiak Island were probably 300-400 m above present sea level during the local Last Glacial Maximum (ILGM) (Mann and Peteet 1994), but probably fell to present sea level or below on Afognak Island and in lower Cook Inlet. The presence of drowned cirques in the Shumagin Islands suggests the ELA there was below present sea level. By analogy with the Antarctic Peninsula today (Ferrigno et al. 2002; Davies et al. 2012), an ice cap whose ELA lay within 100 m sea level was sensitive to slight changes in ocean temperature, not to mention in relative sea level itself. As discussed in Section 2.3, sea ice was seasonally present in this region during the coldest intervals of Marine Isotope Stage 2.

Based on glacial features preserved on the seafloor between Kodiak and Sanak Island, Zimmermann et al. (2019) inferred that glaciers flowed to the outer shelf edge during the local Last Glacial Maximum (ILGM). The occurrence of multiple moraine loops on the seafloor south of the Shumagin and Semidi Islands (Fig. 12, 13) suggests a complex history of standstills and readvances during deglaciation, and the presence of iceberg scours on the adjacent seafloor indicates these post-ILGM moraines were deposited by calving glaciers (Greene et al. 2016; Zimmermann et al. 2019).

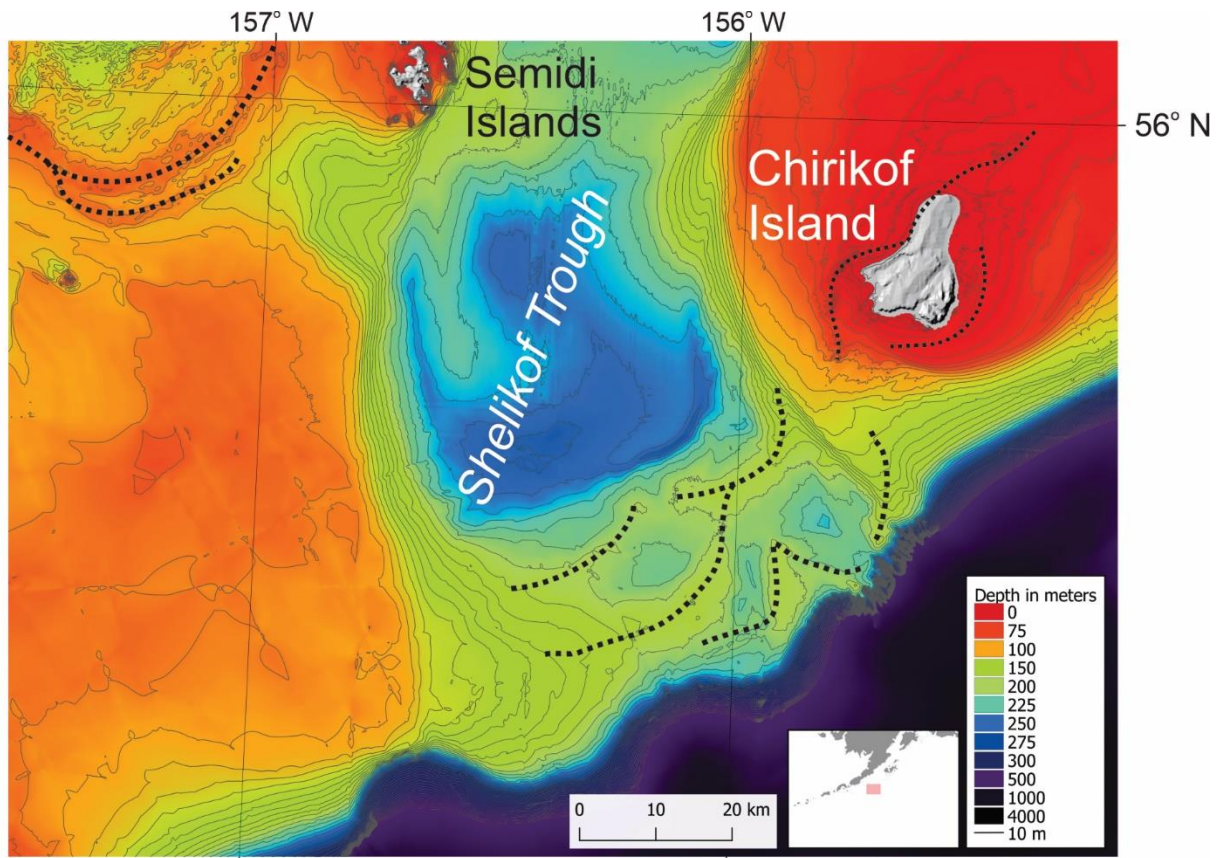


Figure 13. Bathymetry of the seaward end of the Shelikof Trough. Dashed lines show moraines. Seafloor geomorphology is modified slightly from Zimmermann et al. (2019). Bathymetric data are from Zimmermann and Prescott (2015); the map is generated in QGIS v3.26.2. Onshore digital elevation model is from Zabihi et al. (2021).

2.1.3.10. Sanak Island

Sanak Island (54.41°N, 162.64°W) lies 60 km offshore of the Alaska Peninsula and 30 km inboard of the continental shelf's outer edge (Fig. 14). Raised beaches and wave-planed, lowland surfaces attest to a postglacial marine transgression. Mann and Peteet (1994) inferred from trends in reconstructed snowlines that 100-300 m of ice covered Sanak during the local Last Glacial Maximum; however, Misarti et al. (2012) suggested that maximum ice thickness over Sanak was thin, < 70 m, although it is unclear what evidence this was based on. The oldest basal ^{14}C date from three lakes on Sanak Island indicates deglaciation occurred before 15.2-16.2 ka (Misarti et al. 2012). These authors extrapolated their lacustrine age/depth curve below the oldest ^{14}C date and asserted deglaciation occurred at "nearly 17 ka BP". This conclusion is problematic because of the variability typical in sedimentation rates in proglacial areas. Because Sanak Peak rises to 530 m asl and consists of granodiorite (Moore 1974), it may

provide an excellent site for using exposure-age dating to reveal the extent and timing of glaciation on the continental shelf here.

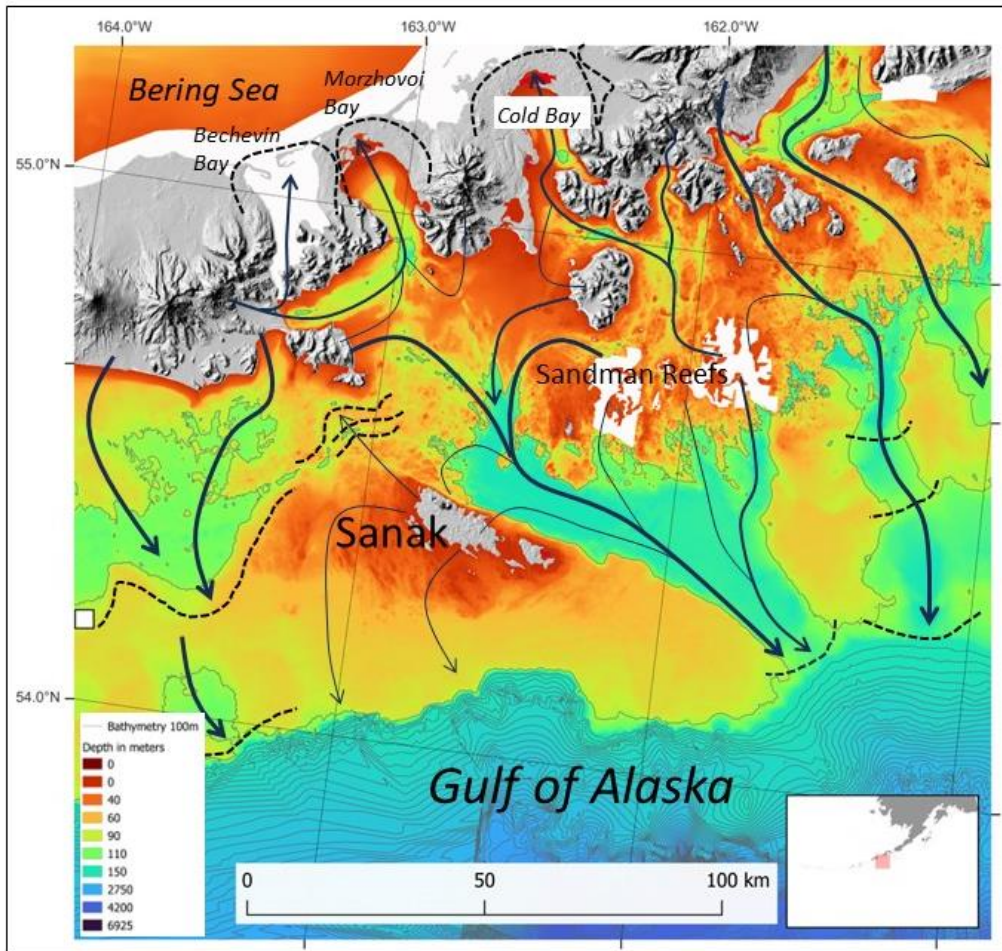


Figure 14. Bathymetry on the continental shelf south of the outer Alaskan Peninsula near Sanak Island. Prominent terminal moraines were left by outlet glaciers that crossed the peninsula and terminated in the southern Bering Sea. Dashed lines show probable moraines on the sea floor. Black arrows are hypothetical glacier flow lines. Bathymetric data are from Zimmermann and Prescott (2015); the map is generated in QGIS v3.26.2. Onshore digital elevation model is from Zabihi et al. (2021).

Glaciers emanating from one or more ice caps centered over the inner shelf near Sanak Island flowed northward across the Alaskan Peninsula to terminate in the Bering Sea, where they left moraine complexes at the heads of Cold Bay and Morzhovoi Bay (Fig. 14). For a shelf-based ice cap to exist at this location, the equilibrium-line altitude must have been at or below

present sea level. By analogy with similarly positioned ice caps on the Antarctic Peninsula today (Ferrigno et al. 2002; Davies et al. 2012), sea ice was probably present in the adjacent ocean, at least in winter.

2.1.3.11. *Alaska Peninsula (Bristol Bay)*

The glacial history of the Alaska Peninsula (Fig. 12) is of particular interest because during Marine Isotope Stage 2 it separated the unglaciated, subaerial portions of the Bering Land Bridge from the Northwest Coast Route along which the first people may have dispersed into lower latitude North America. Unfortunately, the glacial history of the Alaska Peninsula is understood only in general terms (Muller 1952; Péwé 1975; Detterman 1986). A ^{14}C date on organics incorporated in outwash graded to an end moraine in the Kvichak River drainage suggest a glacial advance occurred upstream in the Iliamna Basin sometime after 31-30 ka (Stilwell and Kaufman 1996). In the Naknek valley, ^{14}C dates suggest moraine construction between 42 and 31.7 ka (Mann and Peteet 1994). These limiting dates from the Kvichak and Naknek valleys suggest a major ice advance occurred late in Marine Isotope Stage 3 (MIS 3) and that advances during MIS 2 were less extensive. In the case of the Kvichak valley, the local Last Glacial Maximum probably corresponds to the undated, prominent moraine system that encloses Iliamna Lake.

During Marine Isotope Stage 2 (MIS 2), multiple ice lobes flowed into the Bristol Bay lowland from ranges to the south, east, and north (Kaufman et al. 2011). Equilibrium-line altitudes were lowered by approximately 600 m on Kodiak Island and by 400 m along the northern flank of the Alaska Peninsula (Mann and Peteet 1994). Snowlines assigned to the local Last Glacial Maximum (ILGM) parallel modern ones in the region, supporting previous suggestions that the geography of winter precipitation and summer temperature during the ILGM generally paralleled those of present (Péwé 1975; Hamilton and Thorson 1983).

2.1.3.12. *Alaska Range*

The Alaska Range arcs 650 km from the Yukon border to southwestern Alaska and contains some of the highest peaks in North America. The glaciated Alaska Range creates a barrier to the moisture carried by storms from the Gulf of Alaska and maintains the strongly continental climate of Interior Alaska. This rain-shadow effect was also prominent during Marine Isotope Stage 2 when glaciers south of the range flowed hundreds of kilometres onto the continental shelf of the Gulf of Alaska, while glaciers north of the range extended mere tens of kilometres into the lowlands of the Interior (Péwé 1975; Hamilton and Thorson 1983; Kaufman et al. 2011).

Beginning in the east in the Delta River watershed, an exposure age from the Fish Lake valley (63° 31' N, 144° 29' W, informal name) suggested the local Last Glacial Maximum (ILGM)

occurred at 22.4 ± 0.6 ka (Young et al. 2009). Briner (2017) reinterpreted a cluster of ca. 16.5-ka ages obtained by Young et al. (2009) as representing the true ILGM and revised these ages to 18.7 ± 0.2 ka using an updated ^{10}Be -production rate (Fig. 15). A readvance or standstill occurred in the Fish Lake valley at 11.6 ± 0.3 ka during the Younger Dryas chronozone (Young et al. 2009). Matmon et al. (2010) obtained several cosmogenic dates on boulders from a moraine previously identified as the ILGM limit (Péwé 1975; Péwé and Reger 1983) and suggested the ILGM occurred ca. 17 ka. Despite being the most accessible area in the Alaska Range, the glacial chronology of the Delta River area remains somewhat uncertain.

Scattered, maximum-limiting ^{14}C dates constrain the local Last Glacial Maximum (ILGM) in the central Alaska Range as occurring after 27 ka (Porter 1983; Thorson 1986). On the northern side of the range in Denali National Park, limiting ^{14}C dates constrain the ILGM between 22.2 and 21.1 ka (Ten Brink and Waythomas 1985; Briner and Kaufman 2008; Briner et al. 2017). Two readvances or standstills occurred there, one between 21.1 and 17.6 ka and another between 15.8 and 15.1 ka (Briner et al. 2017) (Fig. 15).

The most closely dated moraine sequence in the Alaska Range comes from the Revelation Mountains in the western Alaska Range where extensive cosmogenic dating of boulders in an iconic moraine sequence in the Swift River valley indicate the local Last Glacial Maximum (ILGM) occurred at 21.3 ± 0.8 ka (Fig. 15). Three readvances or standstills followed at 20.2 ± 1.0 ka, 19.6 ± 1.0 ka, and 17.7 ± 0.8 ka (Tulenko et al. 2018) (Fig. 15).

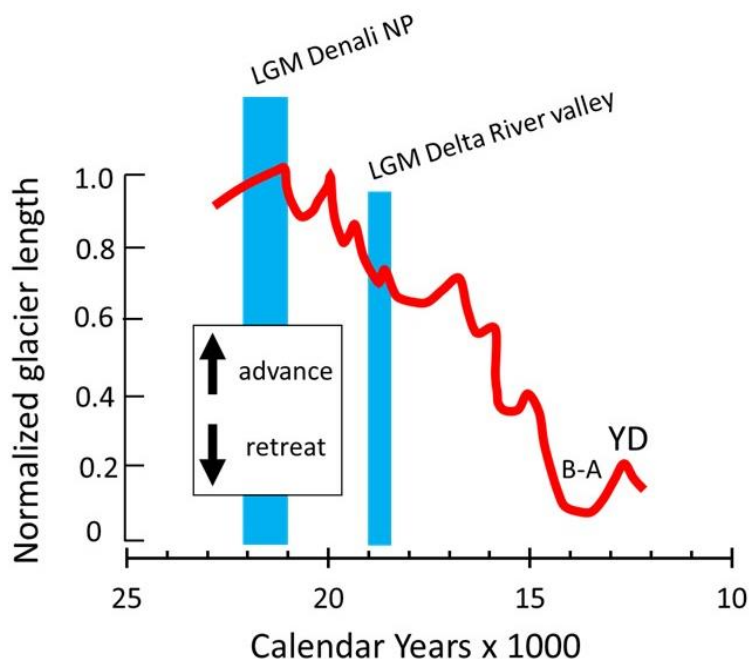


Figure 15. Timing of the Last Glacial Maximum (LGM) in the Alaska Range. The red line depicts deglaciation of the Revelation Mountains. “Normalized glacier length” depicts the present-day glacier-terminus position as “0” and the LGM terminus position as “1”. Redrawn from Tulenko et

al. (2018, 2022). The timing of the LGM in the Delta River valley and Denali National Park is from Briner (2017). “B-A” is the Bølling-Allerød. “YD” is the Younger Dryas.

2.1.4. Glacier fluctuations during the Younger Dryas, 12.8 to 11.7 ka

In southwestern British Columbia and western Washington, several readvances of ice occurred between 14.5 and 11 ka, interrupting overall glacial retreat (Friele and Clague 2002; Menounos et al. 2009). These included a readvance in the Fraser Lowland that may have coincided with the Younger Dryas (YD) (Kovanen 2002; Kovanen and Easterbrook 2002). Evidence is currently lacking for glacial advances along the Gulf of Alaska margin during the YD (Kaufman et al. 2010); however, glacial advances (or standstills) are documented during the YD chronozone in southwestern British Columbia and in the western Canadian Cordilleran (Lakeman et al. 2008; Menounos et al. 2009, 2017), as well as in the continental interior of southern Alaska (Young et al. 2019; Tulenko et al. 2022). The absence of YD glacial advances along the Gulf of Alaska coastline is reminiscent of their absence in coastal East Greenland (Levy et al. 2016) and Arctic Norway (Wittmeier et al. 2020). Like glaciers in coastal Greenland (Funder et al. 2021), maritime glaciers along the Gulf of Alaska margin may actually have been retreating during the YD. Limited evidence exists for an early-cold, late-warm pattern of climate changes during the YD in southern Alaska in the form of a moraine deposited ca. 12.5 ka in the Ahklun Mountains (Young et al. 2019) (Section 3.3). We return to the enigmatic nature of climate during the YD chronozone in Section 3.3.

2.1.5. Summary of glacial history along the Northwest Coast during Marine Isotope Stage 2

Glaciers in most sectors of the Cordilleran Glacier Complex reached their maximum extents relatively late during the Last Glacial Maximum (LGM), which is usually placed between 26.6 and 19 ka (Clark et al. 2009) (Fig. 16). Many glacial systems along the Northwest Coast reached maxima after major sectors of the Laurentide and Fennoscandian Ice sheets. The local Last Glacial Maximum (ILGM) occurred earliest in northern sectors of the Northwest Coast. In the Swift River valley of the Alaska Range (Fig. 15) the ILGM occurred at 21.3 ± 0.8 ka, while the ILGMs in Puget Sound, the Strait of Juan de Fuca, Vancouver Island, and in Eastern Washington/Idaho all occurred between 18 and 15 ka (Fig. 5). These ILGMs in the southern sector of the Northwest Coast coincided with Heinrich Event 1 (HE 1) and were roughly in synchrony with a widespread episode of the period of recessional moraine deposition occurring in the western, conterminous USA (Laabs et al. 2020) (Fig. 16). In Southeast Alaska, the ILGM occurred at an intermediate time between 19.8 and 17.2 ka.

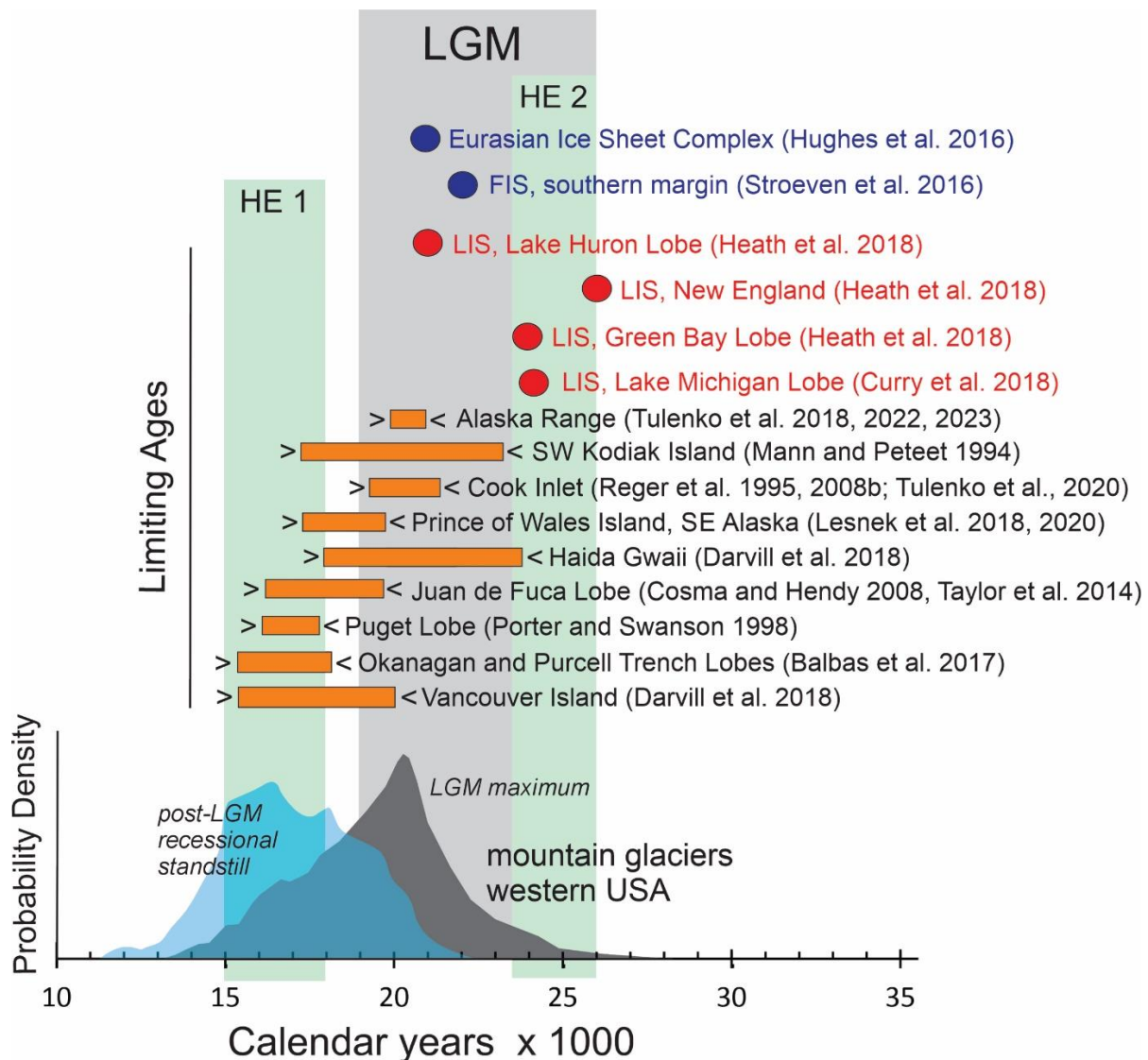


Figure 16. **ABOVE** Limiting dates on the Cordilleran Glacier Complex (CGC) (orange bars), the Laurentide Ice Sheet (LIS, red balls), and the Fennoscandian Ice Sheet (FIS, blue balls). "LGM" = global Last Glacial Maximum. "HE 1" = Heinrich Event 1. "HE 2" = Heinrich Event 2. **BELOW** Probability density distributions of the minimum-limiting exposure ages of the moraines deposited by alpine glaciers in the western, conterminous United States (Redrawn from Laabs et al., 2020). In the western USA, "post-LGM recessional moraines" were deposited during a region-wide glacier standstill or readvance centered at 17.0 ± 1.8 ka during Heinrich Event 1.

Like the timing of local Last Glacial Maxima (ILGM), the retreats of marine-based glaciers were time transgressive along the Northwest Coast. Rapid calving retreats began in the Strait of Juan de Fuca and off the western coast of Vancouver Island ca. 17.5 ka, but earlier, ca. 19 ka, in the northeastern Gulf of Alaska (Fig. 6) (though see Section 4.1.10). The timing of deglaciation

of the continental shelf between Haida Gwaii and the Aleutian Chain remains largely unknown, although early work from southwestern Kodiak indicates that the outer shelf was ice free by 18.3-17.5 ka, although a readvance of unknown extent then occurred between 16.5 and 15.4 ka. In southern sectors of the Northwest Coast, glaciers had retreated to the inner-fjord zone by 13-14 ka. The timing of glacial advances during the Younger Dryas (YD) chronozone remains obscure, probably because they were rare. What records do exist suggest advances occurred early in the YD, followed by retreats. The climatic regime responsible for this pattern is explored further in Section 3.3.

Along the Alaskan coast, newly available bathymetric data reveal numerous terminal moraines located at the mouths of cross-shelf troughs between Cross Sound and the inner Aleutians (Fig. 8-14). Although the troughs are composite features carved during multiple glaciations, the presence of well-preserved glacial features suggests they were probably reoccupied by ice streams during the local Last Glacial Maximum (ILGM). Bathymetric data also reveal complex sequences of recessional moraines bordering former island ice caps located south of the Alaska Peninsula. This is consistent with earlier inferences that equilibrium-line altitudes fell to near or below present sea level along the Gulf of Alaska coast between Prince William Sound and the Aleutians during the ILGM.

2.2. Relative sea level (RSL)

2.2.1. The Northwest Coast between Puget Sound and Kodiak Island

The Northwest Coast of North America experienced a history of changes in relative sea level (RSL) that was markedly complex in space and time (Fig. 17) (Mosher and Hewitt 2004; Mann and Streveler 2008; Roe et al. 2013; McLaren et al. 2014; Shugar et al. 2014; Letham et al. 2016; Baichtal et al. 2021). This complexity stemmed from the effects of time-transgressive glacier fluctuations combined with the region's relatively thin lithosphere and low-viscosity asthenosphere, which made RSLs respond rapidly and sensitively to glacier loading (Larsen et al. 2005; James et al. 2009b; Hu and Freymueller 2019). Further complexity arose from the region's ongoing tectonism (Mann and Crowell 1996; Shennan et al. 2014). The following overview of RSL history along the Northwest Coast is based largely on the review of Shugar et al. (2014).

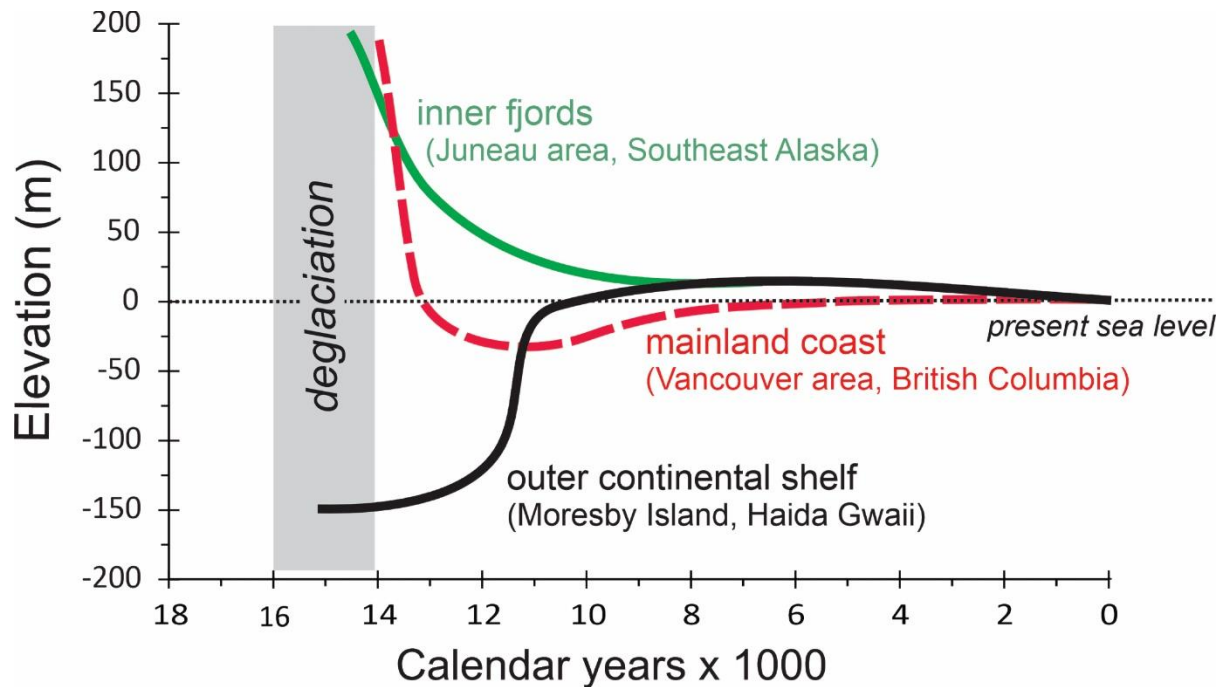


Figure 17. Relative sea level (RSL) varied widely according to location. Shown here are representative RSL curves from positions along a coast-perpendicular transect spanning ~ 100 km from the outer continental shelf to the inner fjord zone. The curves for Haida Gwaii and Vancouver areas are from Shugar et al. (2014). The Juneau area curve is from Baichtal et al., (2021).

During the deglaciation, marine waters transgressed as high as 220 m across the isostatically depressed, western flank of the Coast Mountains in coastal British Columbia and Southeast Alaska (Miller 1972, 1973, 1975; Clague and James 2002). Areas within the zone of maximum ice loading (e.g., the inner-fjord zone) experienced steadily falling sea levels because recovery from large amounts of isostatic depression continuously exceeded the rate of eustatic sea-level rise (Fig. 17). Seaward of the zone of maximum ice loading, isostatic rebound initially surpassed rising eustatic sea level, but was later exceeded by it rise as uplift slowed. Between 14 and 12 ka in southwestern British Columbia, this pattern of relative sea level change resulted in lowstands of -11 m near Vancouver, B.C.; -30 m near Victoria, B.C.; and -46 m on western Vancouver Island (Shugar et al., 2014).

Offshore islands like Haida Gwaii experienced quite different relative sea level (RSL) histories because relatively little isostatic depression occurred near the seaward ice limits of the glacier coverage (Fig. 17). At its lowest point, RSL fell below the typical, eustatic drawdown of around -120 m as the result of crustal forebulges developing in response to thick ice loads to the east. Deep accumulations of glacial ice over the western flank of the Coast Mountains squeezed the mantle seaward, where it elevated the crust of the outer continental shelf by

some 20-30 m. This resulted in RSL in Haida Gwaii falling to around 150 m below present RSL just prior to deglaciation (Fig. 17). Then, as the forebulge migrated eastwards, RSL rose 5-10 m higher than present in the early and mid-Holocene, before falling back to its present level ca. 2 ka. This same pattern of post-glacial RSL change also occurred on the continental shelf bordering the Alexander Archipelago (Baichtal et al. 2021), and possibly along much of the coastline of the northern Gulf of Alaska. Records of RSL become increasingly fragmentary north of Cross Sound (Shugar et al. 2014) with the exception of Bering Strait.

2.2.2. Relative sea level history of Bering Strait

2.2.2.1. Existing data and inferences

Whether Bering Strait is a land bridge or a seaway has important consequences for the climate of Eastern Beringia (Mann et al. 2001; Bartlein et al. 2015), for the functioning of the global ocean/atmosphere system (Section 4.1.6), and for a diverse set of biogeographical concerns (Hopkins 1967; Hoffecker et al. 2023). Multiple approaches have been used to reconstruct the history of the Bering Land Bridge. Comparisons between bathymetry and eustatic sea levels over the last 140 ka (Lambeck and Chappell 2001; Siddall et al. 2003) suggest Bering Strait was subaerial between 140 and 130 ka, submerged between ca. 130 and 110 ka, intermittently submerged between 110 and 70 ka, and subaerial again between 70 and 11 ka (Fig. 18). Such comparisons ignore the possibility that the bathymetry of the strait has changed over the last 140 kyr (Section 2.2.2.2). Furthermore, comparing estimates of relative sea level to bathymetry is an inherently fuzzy process because the elevation errors in eustatic sea level curves are generally between 2 and 10 m (Chappell et al. 1996; Keigwin et al. 2006; Abdul et al. 2016).

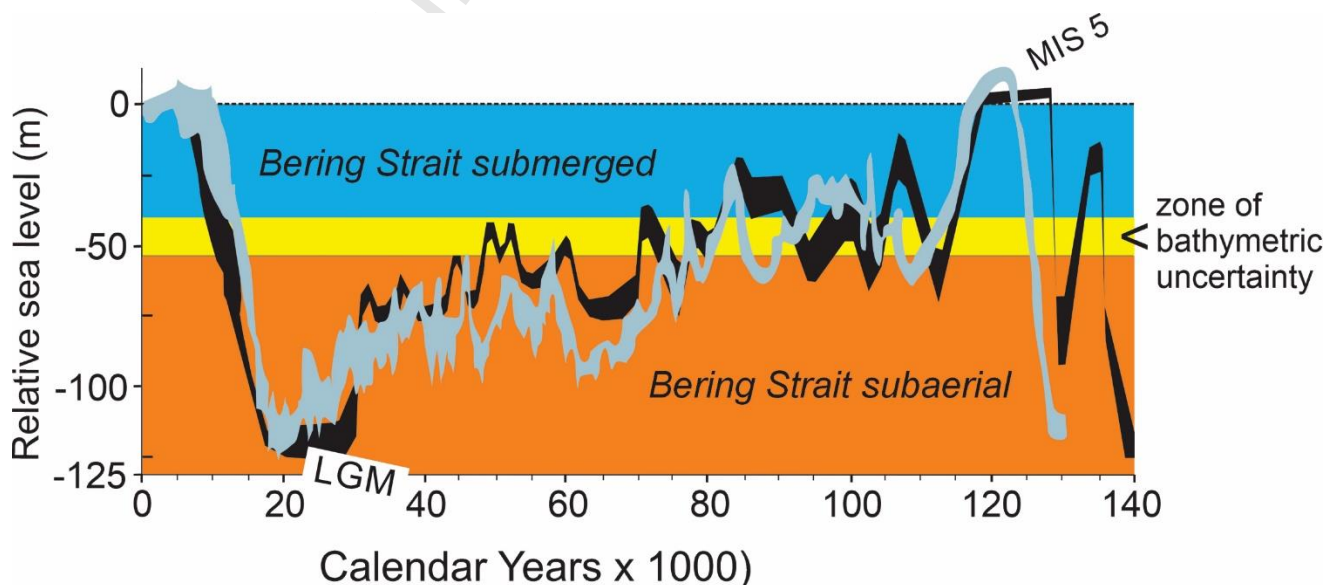


Figure 18. The bathymetry of Bering Strait compared with eustatic sea level over the last 140,000 years based on far-field data of Lambeck and Chapelle (2001) (**black**) and Sidall et al. (2003) (**grey**). Today, the shallowest sill in the strait lies around -53 m. "LGM" = global Last Glacial Maximum. "MIS 5" = Marine Isotope Stage 5, the last interglacial.

Based on the ^{14}C ages of terrestrial organic matter recovered in cores from the Chukchi Sea continental shelf, McManus and colleagues (McManus et al. 1983; McManus and Creager 1984) estimated that Bering Strait was last flooded ca. 14,400 ^{14}C years, or roughly 17 to 18 ka (Fig. 19). As Elias et al. (1996) pointed out, this was a widely limiting, maximum-age estimate because ^{14}C -dead carbon was probably contained in the samples dated and because younger organic deposits were probably eroded away as marine waters rose. Working with sediment cores from the Bering Sea inner shelf, Elias et al. (1996) dated terrestrial peats to 16.1-12.8 ka at depths of 42 to 48 m below present sea level. Based on these ages, they suggested the initial flooding of Bering Strait occurred after 12.8 ka.

Keigwin et al. (2006) analyzed a marine core taken north of Bering Strait at a depth of -53 m and inferred that a major transition from estuarine to open-sea conditions occurred ca. 12 ka (Fig. 19). Also working on the Chukchi shelf north of the strait, Hill and Driscoll (2008) obtained an age of 10.9 ± 0.2 ka on a marine shell recovered one meter above what they interpreted to be a transgressive surface in -59 m water depth, suggesting that sea level neared the -53 m level on the northern side of Bering Strait about that time.

The dates when North Pacific whale and mollusk species first arrived in the Arctic Ocean have also been used to infer when Bering Strait first opened. Dyke and Savelle (2001) found the remains of bowhead whales (*Balaena mysticetus*) in the Canadian Arctic Archipelago as old as $10,850 \pm 140$ ka, which is consistent with Bering Strait opening ca. 11 ka (Fig. 19). Also consistent with a ca. 11 ka opening of the strait is the striking diversification of the molluscan fauna that occurred in the western Arctic Archipelago after 10.3 ka (Dyke and Savelle 2001).

More puzzling is the appearance of possible Pacific-endemic mollusk species in the western Arctic Archipelago prior to 12.5 ka. On Banks Island, Dyke et al. (1996) found *Macoma (Limecola) balthica* shells dating to 12.6 ka, while England and Furze (2008) discovered shells of *Cyrtodaria kurriana* dating to 13.5 ka (Fig. 19). Both these ages take into account an estimated marine-reservoir effect. One possibility is that both these species survived the Last Glacial Maximum in marine refugia somewhere in the North Pacific, and then reinvaded the Arctic Basin when their larvae/veligers drifted northward through the newly inundated and still shallow strait. These dispersal events could have occurred when water levels in Bering Strait were still quite shallow (Pico et al., 2020). If this were the case, the strait must have initially opened before 13.5 ka (England and Furze 2008).

An alternative explanation is that the 13-ka *Macoma* and *Cyrtodaria* specimens from the western Arctic Archipelago in fact date to 10-11 ka, but the 0.5 ka correction for the marine-

reservoir effect used by Dyke et al. (1996) and England and Furze (2008) is an underestimate. While some authors think that marine-reservoir effects (MARs) > 1 kyr are unlikely in the Arctic Ocean (England and Furze 2008; Pico et al. 2020), MARs in polar seas are influenced by variations in sea-ice cover, ocean upwelling, and air-sea gas exchange, all of which can affect marine radiocarbon concentrations (Butzin et al. 2017, Heaton et al. 2020) (Section 4.1.10.2). Uncertainty surrounding the Arctic's marine reservoir effect during the deglacial continues to hamper sea-level reconstructions in Bering Strait.

A third explanation for 13-ka *Macoma* and *Cyrtodaria* from the western Arctic Archipelago is that the dispersal capabilities of these two, purportedly Pacific-endemic species have been underestimated, and that in fact they reached the Beaufort Sea from the North Atlantic early in postglacial times via the Northeast Passage prior to the opening of Bering Strait. Although England and Furze (2008) think this unlikely, both *Macoma balthica* and *Cyrtodaria kurriana* have circumboreal distributions today. Moreover, *C. kurriana*'s distribution is strikingly discontinuous, so its absence from sediment cores along the Siberian continental shelf early in postglacial times (England and Furze 2008) is not a convincing argument that their pelagic larvae were not carried into the Beaufort Sea by the same coastal currents that today carry Atlantic waters eastward along the Siberian continental shelf (Weingartner et al. 1999).

By modelling temporal patterns of crustal responses to transient loadings and un-loadings by glacial ice and ocean water, Peltier et al. (2015) suggested that Bering Strait flooded ca. 11 ka (Fig. 19). Elaborating on this approach, Pico et al. (2020) used varying scenarios of deglaciation timing over western North America to model relative sea level (RSL) history in Bering Strait, taking into account the complex interactions between eustatic sea-level history, distant isostatic effects, and the changing gravitational effects of the CGC on RSL in the Bering and Chukchi Seas. Their modelling results suggest Bering Strait was initially flooded beginning ca. 13 ka, followed by a RSL standstill that lasted until ca. 11.5 ka. Prior to ca. 13 ka, Pico et al. (2020) think that RSL in Bering Strait was significantly higher (by ~10 m) than at far-field locations in tropical seas due to isostatic and gravitational effects from the Cordilleran Ice Sheet (Section 2.2.2.2) (Fig. 19, 20). Only after ca. 13 ka do Pico et al.'s (2020) models show RSL in Bering Strait converging with the global, eustatic sea-level curve of Lambeck and Chappell (2010) (Fig. 19).

Jakobsson et al. (2017) inferred that Bering Strait was flooded by the sea ca. 11 ka BP based on a combination of sedimentology, changes in the concentration of biosilica, and shifts in the δC^{13} of organic matter in sediment cores from the Chukchi Sea (Fig. 19). Uncertainty about the local marine reservoir effect at this location during the late-glacial period (Hanslik et al. 2010; Butzin et al. 2017; Skinner et al. 2017) suggest 11 ka BP is a maximum-limiting age estimate.

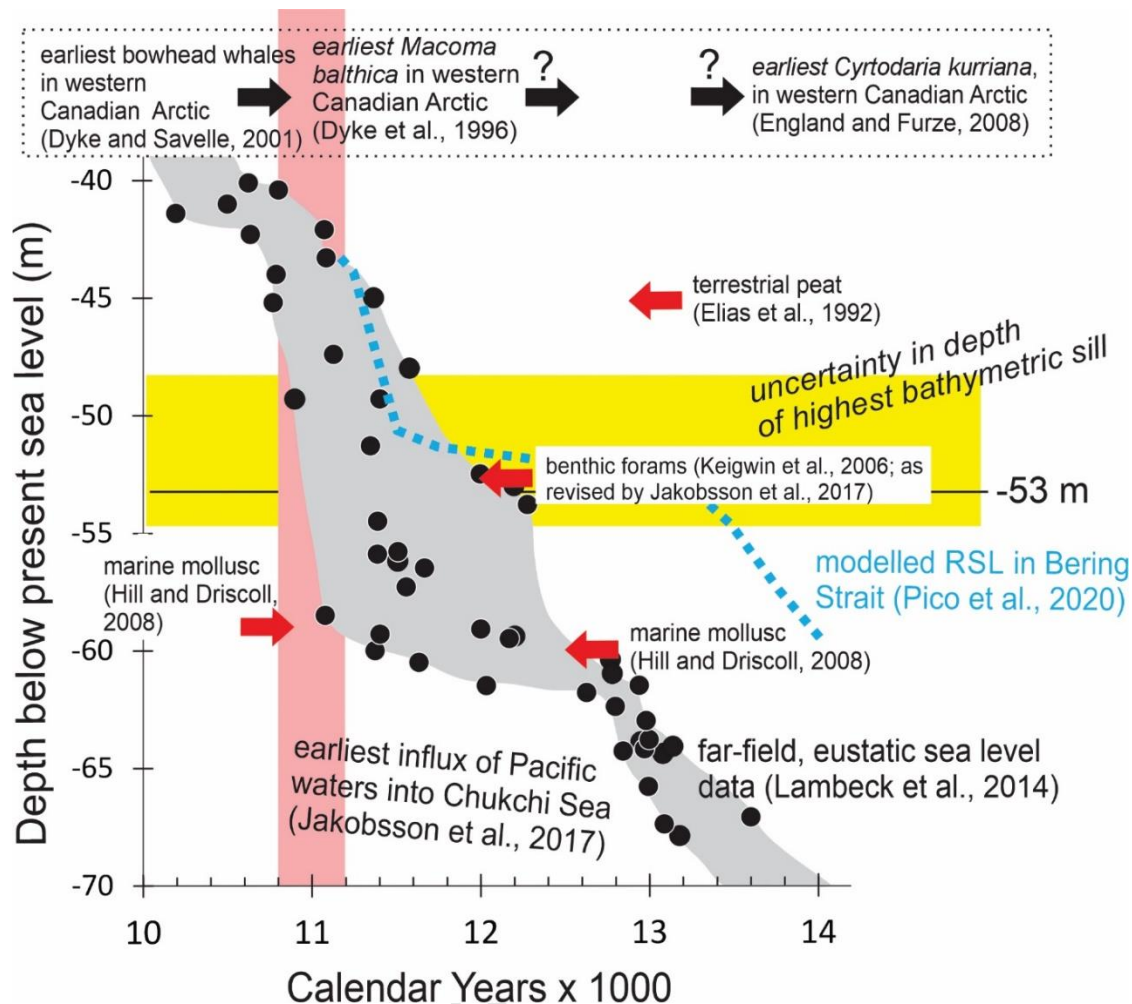


Figure 19. Age constraints on the most recent flooding of Bering Land Bridge. Black dots are far-field, eustatic sea-level data (Lambeck et al. 2014). The grey shading encloses these data and their approximate errors. Arrows indicate whether a ^{14}C date is a maximum- or minimum-limiting age estimate, with the tips of arrow lying on the approximate calendar age of each sample. Samples marked by red arrows are plotted according to depth. The shallowest (highest) sill in Bering Strait today is around -53 m. The yellow band depicts an estimated 10-m band of uncertainty in the altitude of the lowest sill in Bering Strait at the time of initial flooding (Section 2.2.2.2). The pink, vertical bar marks the earliest influx of North Pacific waters into the Chukchi Sea according to Jakobsson et al. (2017). Black arrows in the upper panel show when marine species that are thought to have been restricted to the North Pacific prior to Bering Strait opening first appeared in the Arctic Basin. As discussed in the text, the arrival dates of these mollusk species may be red herrings.

Farmer et al. (2021; 2023) analyzed sediment cores taken north of Bering Strait for $\delta^{15}\text{N}$ in planktonic foraminifera (Fig. 20). Because $\delta^{15}\text{N}$ is higher in the North Pacific than the Arctic

Ocean, it provides a geochemical proxy for the presence of an open (flooded) Bering Strait. Their data suggest that relative sea level (RSL) dropped below the lowest sill in the strait sometime between 40 and 35 ka, and that North Pacific water again flooded the strait starting ca. 11 ka. Because of uncertainties surrounding the marine reservoir effect during the Late Pleistocene, Farmer et al. (2021; 2023) refrain from calibrating their ^{14}C dates and instead interpret their data at millennial timescales.

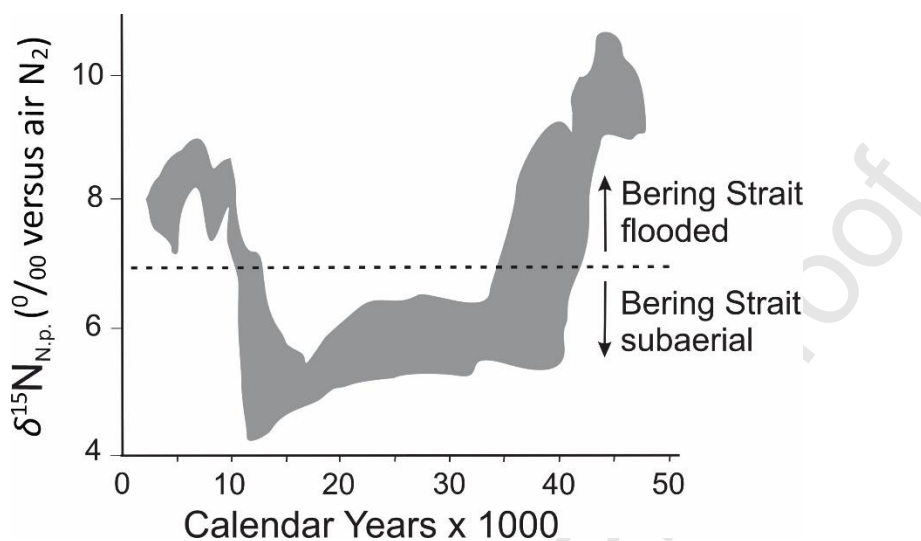


Figure 20. Opening and closing of Bering Strait inferred from nitrogen isotopes in

foraminifera in sediment cores from the western Arctic Ocean (Farmer et al. 2021; Farmer et al. 2023). The grey polygon encompasses the error-ranges of $\delta^{15}\text{N}$ values in three cores. The dashed line shows the maximum $\delta^{15}\text{N}$ value expected when the strait is closed to the ingress of North Pacific water.

Other proxy data that are consistent with initial flooding of Bering Strait ca. 11 ka include anoxic episodes on the Bering Sea shelf that ended ca. 11 ka, possibly as a result of enhanced circulation after Bering Strait first opened (Küehn et al. 2014). Deposition of sand-rich layers began on the Bering Slope ca. 11 ka, suggesting that the present-day ocean current regime was established then (Wang et al., 2021).

2.2.2.2. Bathymetric uncertainties

Inferences about when Bering Strait was open/closed that are based on eustatic sea-level records are complicated by uncertainty surrounding the altitude of the lowest bathymetric sills in Bering Strait when it was first inundated. This uncertainty comes from five sources, none of which are well-constrained. Based mainly on the effects of thermokarst deflation and erosion

by currents, we speculate that the altitude of the shallowest sills in Bering Strait may have been as much as 5 m higher than today; however, factors including tectonism and far-field glacial effects could mean that the sill altitudes were actually several meters lower than today.

1) Thermokarst deflation. When they were dry land during the Last Glacial Maximum, the surfaces of the Bering and Chukchi continental shelves were inflated by excess ice in the underlying permafrost. Excess ice is the volume of ice in frozen ground that exceeds the pore volume present under thawed conditions (Harris et al. 1988). Today in the unconsolidated deposits underlying coastal landscapes in northern Alaska and Yakutia, excess ice frequently comprises 40-80% of the uppermost 5 to 20 m of the ground by volume (Kanevskiy 2003; Shestakova et al. 2021). Much of this ice takes the form of syngenetic ice wedges within deposits of ice-age loess (Kanevskiy et al. 2011; Murton et al. 2015; Gaglioti et al. 2018). Thick loess deposits accumulated in the Bering Strait region during Marine Isotope Stage 2 and 3 (Péwé 1975; Muhs et al. 2003; Ager and Phillips 2008). When excess ice comprises 50% of the uppermost 10 m of the ground, the overall ground surface can be elevated by approximately 5 m. When the sea transgresses across such a surface, it thaws the upper layers of permafrost causing subsea thermokarsting (Shakhova et al. 2017; Shakhova et al. 2019; Angelopoulos et al. 2020). Features consistent with such thermokarsting are visible in some of the seismic profiles from Bering Strait illustrated in Hill and Driscoll (2008).

2) Erosion by bottom currents. Strong currents run through Bering Strait today (Clement Kinney et al. 2022), and these currents have removed an unknown amount of sediment since the strait was initially flooded. Erosion was probably most intense when the transgressing sea first flooded the strait (Keigwin et al. 2006).

3) Diastrophism. The Bering Strait region is tectonically active in a spatially complex manner (Marlow et al., 1994). The Bering plate is now rotating clockwise at $4-8 \text{ mm a}^{-1}$ (Cross and Freymuller, 2008). Along much of the coastline of western Alaska, the marine limit established ca. 100 ka during Marine Isotope Stage 5 now lies 6-10 m above sea level, but in certain places has subsided below sea level (Brigham-Grette and Hopkins, 1995). Ten meters of subsidence over 100 kyr suggests that the rate of vertical displacement due to tectonism has been $> 1 \text{ m}$ over the last 11 kyrs in certain areas of the Bering Strait region. Pico et al. (2020) estimate that $< 3-4 \text{ m}$ of vertical movement has occurred in the Bering Strait since 20 ka.

4) Far-field glacial effects. Although few glaciers existed in the immediate vicinity of Bering Strait during the Last Glacial Maximum (Brigham-Grette 2001), relative sea level (RSL) in the Bering and Chukchi Seas was affected by the isostatic effects of distant ice loads over northwestern North America and by the gravitational effects of these ice masses (Pico et al., 2020). Uncertainties surrounding the chronology of the Cordilleran Glacier Complex (Section 2.1.3) limit the accuracy of modeling these far-field effects; however, they might have caused 5-10 m of local variation in RSL changes across in Bering Strait region during the deglacial period (Pico et al., 2020).

5) Mantle Dynamics (Dynamic Topography). The flow dynamics of the mantle affect relative sea level (RSL) and complicate the effects of glacial isostasy and eustatic changes (Moucha et al. 2008). These mantle-induced changes can be significant at millennial time scales during the late Pleistocene (Austermann and Forte 2019). The presence of multiple volcanic fields of Late Pleistocene age in western Alaska and on Bering Sea islands (Liang et al. 2024) attest to a non-quiet mantle, and the dynamic topography of the Bering Strait region may still be adjusting to the southward jump of the subduction zone from the northern Bering Sea to the Aleutian Trench that occurred after 55 Mya (Akinin et al, 2020).

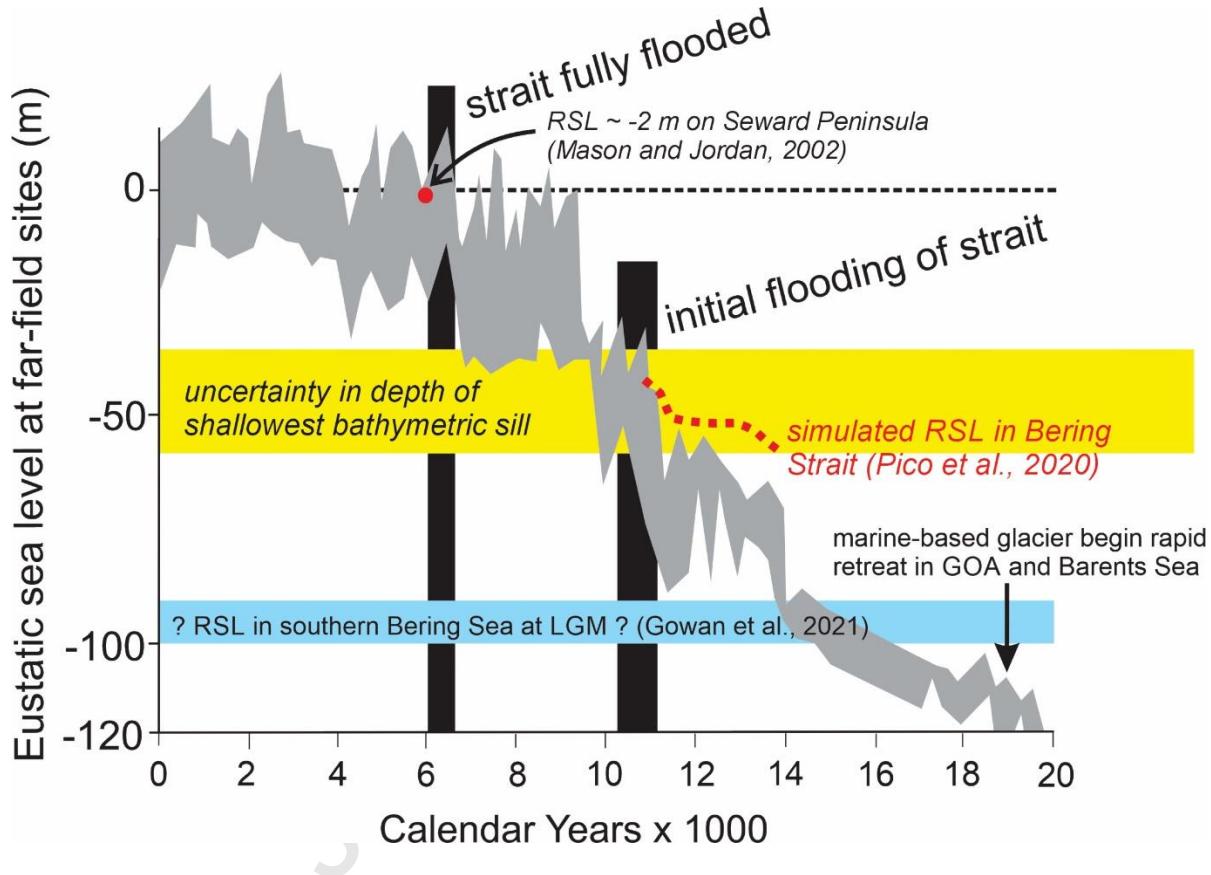


Figure 21. Timing of the most recent flooding of Bering Strait based on the last 30 kyr of eustatic sea level recorded at far-field sites (Sidall et al. 2003, Lambeck et al. 2014). The grey area encloses these eustatic data and their approximate error terms. "GOA" = Gulf of Alaska. "LGM" = Last Glacial Maximum.

In summary, North Pacific water probably first penetrated Bering Strait ca. 11.5 ka. The analyses of Pico et al. (2020) and Farmer et al. (2021, 2023) suggest the rate of relative sea level (RSL) rise slowed prior to this during the Younger Dryas chronozone, 12.9 - 11.7 ka. Multiple, unquantified factors make it uncertain how deep Bering Strait was at the time when it initially flooded, which complicates assigning an exact date to this event. Here we assign a ± 5 m

uncertainty to the shallowest sill depth. The key question for oceanography and climatology is not when sea water first flowed through Bering Strait but when the strait became deep enough to assume its present-day oceanographic functions (Section 4.1.6). Only after ca. 9 ka did Bering Strait become deep enough to transmit significant amounts of ocean water from the North Pacific to the Arctic/Atlantic Oceans, and not until after 7 ka did Bering Strait reach its present depth (Fig. 21).

2.3. History of sea ice in the subarctic Pacific during Marine Isotope Stage 2

Sea ice forms when sea surface temperature (SST) cools below -2° C. Glacial ice can also be widespread in the sea in the form of icebergs, and these two forms of ice mingle where marine-based glaciers border polar seas. Today in the Gulf of Alaska, sea ice is present only in winter and is restricted to inner fjords where surface waters are relatively fresh and cold air masses cross the coastal ranges from the continental interior. Even in the inner fjords, sea ice is ephemeral and thin today.

Current understanding of the timing and extent of sea ice in the high-latitude North Pacific during Marine Isotope Stage 2 (MIS 2) is sparsely distributed. In contrast to the North Atlantic, only a handful of deep-sea cores dating to the last 20 ka have been analyzed for sea ice proxies between Kamchatka and Southeast Alaska. A core from the Yakobi Sea Valley off of Southeast Alaska noted an increase in the abundance of sea ice diatoms during the Younger Dryas chronozone (Barron et al., 2009). Further north on the Gulf of Alaska continental shelf near the Bering Glacier, the sea ice diatoms in Core U1421 (Cowan et al. 2020; Praetorius et al. 2023) may record the presence of glacial ice in addition to sea ice (Fig. 26), at least prior to ca. 16.5 when intense iceberg calving was underway in the Bering Trough. This record suggests that ice of any kind was scarce on the continental shelf between 23 and 19 ka, increased during Heinrich Event 1 (HE 1), and declined abruptly after ca. 14 ka. Throughout MIS 2 and 3, sea ice in the northeast Pacific was probably most abundant and seasonally persistent near the coast (Praetorius et al. 2023) and adjacent to calving glaciers (Taylor et al. 2014; Barrie et al. 2021).

Analysis of Core PAR87-A10 (de Vernal and Pedersen, 1997) from the Patton Sea Mount in the southwestern Gulf of Alaska ($54^{\circ} 21.8' N$, $148^{\circ} 28' W$) indicates that the Last Glacial Maximum (LGM) was a time of prolonged, seasonal ice cover, but counter-intuitively suggests that Heinrich Event 1 (HE 1) was a period of reduced sea ice cover (Fig. 22). These results are partly contradicted by another core from the Patton Sea Mount (Core SO202-27-6; Méheust et al. (2018) that suggests sea ice cover was sparse during the LGM, increased to “variable” ice cover during HE 1, declined during the Bølling/Allerød, and then increased slightly during the Younger Dryas chronozone.

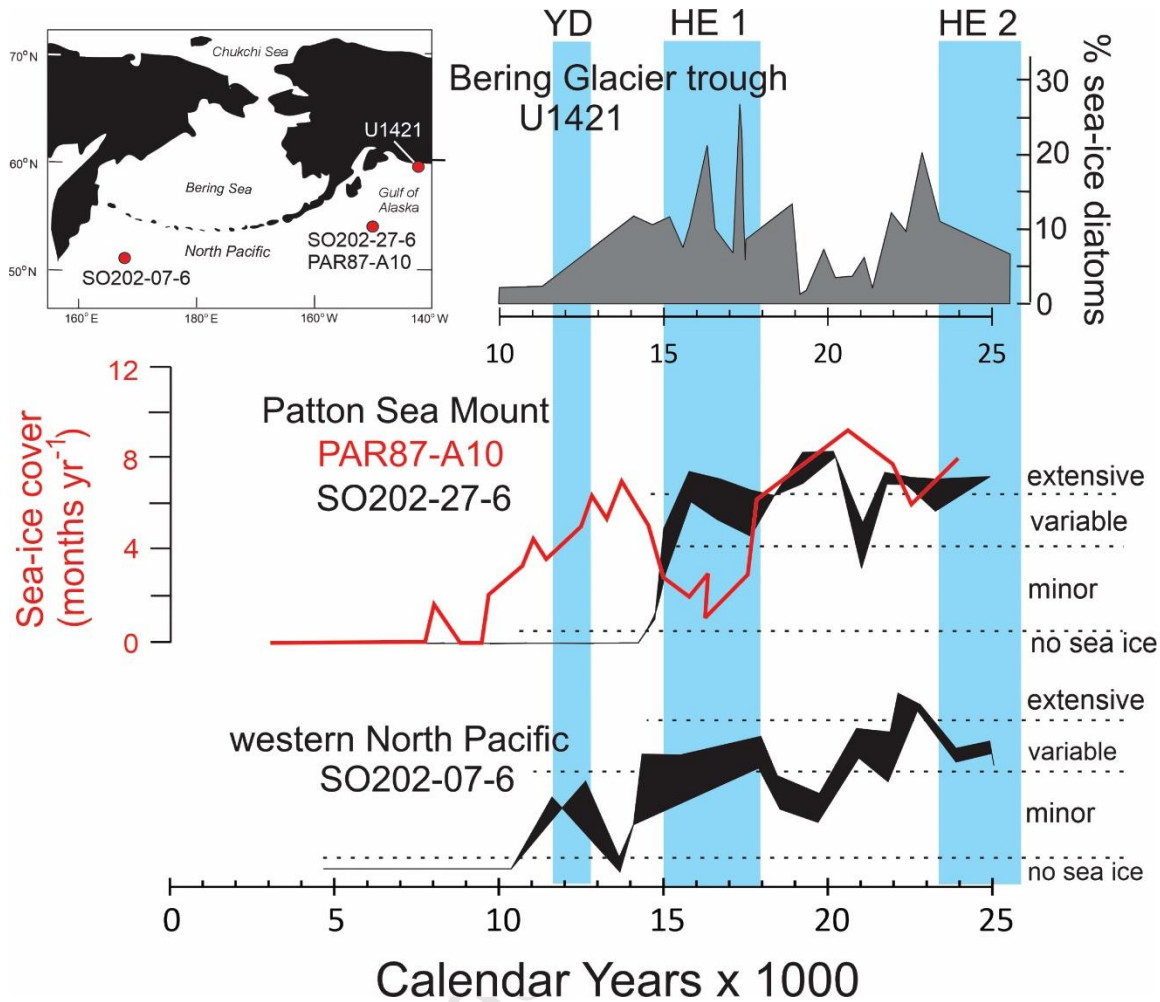


Figure 22. Four records of sea ice from the subarctic Pacific. Core U1421 (Cowan 2022) is from the continental slope near the Bering Glacier trough and may record iceberg-derived glacial ice in addition to sea ice. Core PAR87-A10 from the Patton Sea Mount was analyzed by de Vernal and Pedersen (1997). Core SO202-27-6 is also from the Patton Sea Mount (Méheust et al. 2018), and Core 202-07-06 is from the northwestern North Pacific (Méheust et al. 2018). "YD" = Younger Dryas. "HE 1" = Heinrich Event 1. "HE 2" = Heinrich Event 2.

Core 202-07-06 from the Detroit Sea Mount in the northwestern Pacific (51° 16.29' N, 167° 41.98' E) suggests an extensive sea ice cover at 23-22 ka followed by reduced coverage until ca. 20 ka and then an increase in ice cover that peaked early during Heinrich Event 1 (Fig. 22) (Méheust et al. 2018). Sea ice disappeared from the area during the Bølling/Allerød but then reappeared during the Younger Dryas chronozone.

Sediment cores from the western Bering Sea and near southeastern Kamchatka suggest that between 20 and 10 ka the extent of sea ice repeatedly shifted across hundreds of kilometers (Max et al. 2012). Core SO202-18-6 was taken near the present southern edge of

winter sea ice (Fig. 22) (Méheust et al. 2018). It suggests extensive sea ice cover during the Younger Dryas chronozone, ice-free conditions from 11.7 -10 ka, followed by extensive ice cover thereafter. During the Last Glacial Maximum (LGM), perennial sea ice may have covered the Bering Sea (Sancetta 1983; Sancetta et al. 1984; Caissie et al. 2010; Pelto et al. 2018). In the southern Bering Sea, the period between 17 and 11.3 ka saw a transition to seasonally ice-free conditions, followed after ca. 11.3 ka by ice-free conditions that lasted year-round (Caissie et al. 2010).

Méheust et al. (2018) made a speculative reconstruction of maximum sea ice extent during the Last Glacial Maximum (LGM) (Fig. 23). At its maximum in spring, pack ice may have arced across the North Pacific from Kamchatka to North America, possibly reaching latitudes as low as 55° N along the Northwest Coast near the British Columbia-Alaska border. The sea ice regime in the North Pacific during the LGM probably resembled that of subantarctic seas today (Maksym 2019) rather than the present Arctic Ocean (Weeks 2010). As in the Southern Ocean, North Pacific sea ice was highly exposed to storm winds and waves across enormous fetches. In this setting, sea ice tends to drift and eventually enter warmer water where it melts. Because of the relatively low latitude and large wave fetch, most sea ice in the Gulf of Alaska was thin, first-year ice forming in autumn and melting by the following August. Thin, seasonally ephemeral ice like this tends to be highly unstable and undergo widespread deformation (Weeks, 2010). Fast ice would have existed along some shorelines, most likely in fjords not occupied by glaciers.

Potential insights into ice conditions near shore during Marine Isotope Stage 2 (MIS 2) come from faunal remains in On Your Knees Cave (*Shuka Káa*) on Prince of Wales Island (56° N) in Southeast Alaska (Heaton, 2003; Heaton and Grady, 2003). Among the bones recovered from this former fox lair are those of ring seal (*Pusa (Phoca) hispida*) and Arctic fox (*Vulpes lagopus*). Ring seals inhabit floating ice throughout the year, and Arctic foxes can live on both tundra and sea ice. In addition to these sea ice-indicating remains, the genes of polar bears (*Ursus maritimus*) occur in brown bear populations (*Ursus arctos*) on some islands in Southeast Alaska (Cahill et al. 2018), suggesting that they too inhabited the Northwest Coast during the local Last Glacial Maximum.

At first glance, the occurrence of ring seal, polar bear, and Arctic fox near On Your Knees Cave suggests that sea ice must have existed in the Alexander Archipelago and offshore in the Gulf of Alaska. On the other hand, polar bears and ice seals live today in southeastern Greenland in fjords where sea ice is present only seasonally (Laidre et al. 2022). Instead of pack ice, the ice seals and polar bears in these fjords utilize the mélange of glacial ice derived from icebergs. Similar iceberg-based habitats exist today at scattered locations along the Gulf of Alaska coastline, and they were probably extensive during deglacial phases of Marine Isotope Stage 2 (Shaw et al. 2020; Barrie et al. 2021). It follows that ice-dependent fauna from On Your Knees Cave does not provide conclusive evidence for sea ice as far south as Prince of Wales Island in Southeast Alaska. Interestingly, the bone fauna of the Port Eliza sea cave (49° 50'N)

contains abundant salt-water fish but no ice-dependent marine mammals (Al-Suwaidi et al. 2006).

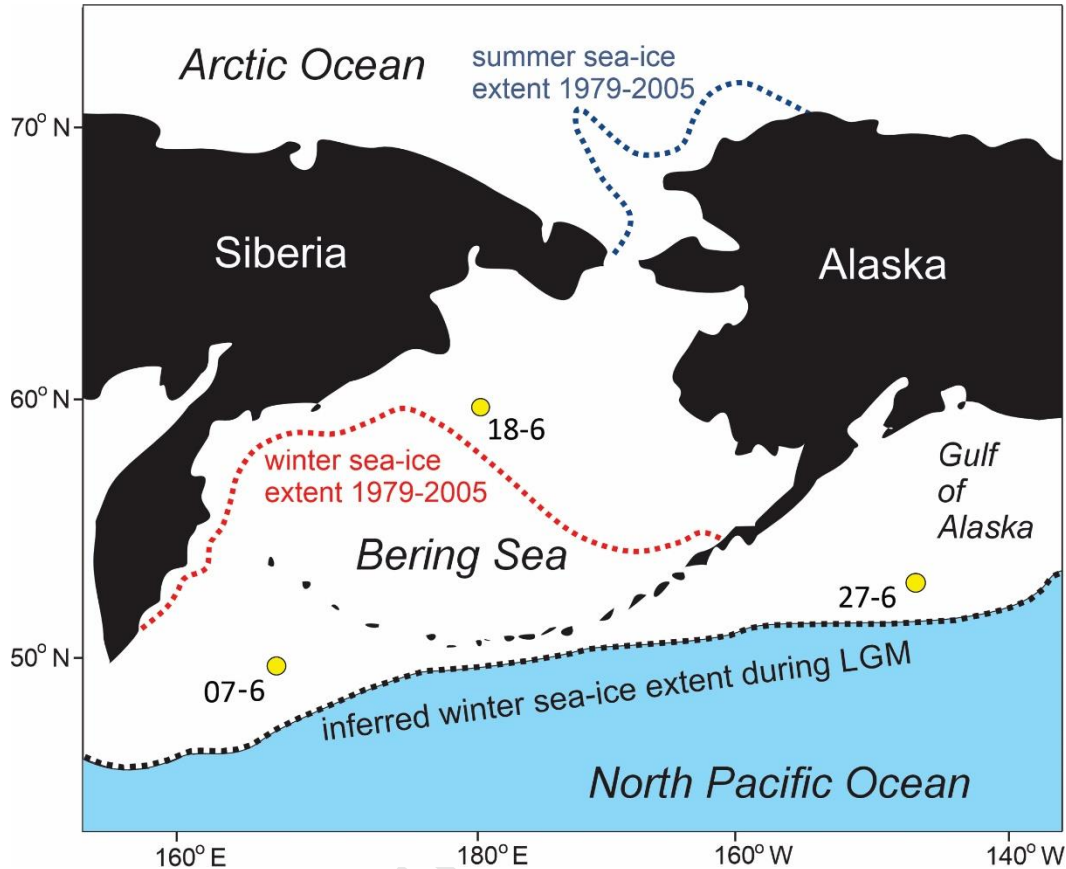


Figure 23. The extent of winter sea ice during the last glacial maximum inferred from sea ice proxy biomarkers in marine cores (yellow dots). Modified slightly from Méheust et al. (2018). In the eastern Gulf of Alaska, sea ice may have extended in winter to ca. 55° N during the coldest intervals of Marine Isotope Stage 2.

In summary, the history of sea ice in the North Pacific during MIS 2 remains poorly understood. When at its greatest extents ca. 24-22 ka and 18-15 ka, winter sea ice covered an area of the high latitude North Pacific and its marginal seas that was some $\sim 3 \times 10^6$ km² greater than today. Together with the 1×10^6 km² of land exposed on the Bering Sea continental shelf by lowered eustatic sea level, this seasonal expansion of sea ice added some 4×10^6 km² of "terrestrial" surface to the subarctic Pacific region during late winter and spring. As sea ice does in subantarctic seas today (Watson et al. 2015), sea ice in the North Pacific during the Last

Glacial Maximum undoubtedly had widespread impacts on overturning circulation and ocean ventilation.

3.0 SYNTHESIS: OF THE NORTHEAST PACIFIC REGION DURING MARINE ISOTOPE STAGE 2

3.1. Evidence from paleoceanography

Though still sparse compared to records from the North Atlantic, paleoceanographic data from the subarctic Pacific has accumulated rapidly over the last several decades. Oxygen isotope records from the continental slope near the Bering Trough in the northeastern Gulf of Alaska suggest sea surface temperatures (SSTs) there were 8° C cooler than today during Heinrich Event 2 (HE 2), ca. 23.5-26 ka (Fig. 24) (Praetorius et al. 2023). Three other cold periods followed, one at 23-21.5, another during Heinrich Event 1 (HE 1) between 18 and 16 ka, and the final one during the Younger Dryas chronozone. A record of planktonic foraminiferal Mg/Ca off the west coast of Vancouver Island suggests SSTs were 7° C cooler than today between 18 and 17 ka (Taylor et al. 2014) (Fig. 7). This is consistent with paleobotanical records from the coastline of the Olympic Peninsula in western Washington that suggest temperatures were $\geq 5^{\circ}$ C cooler than today and that precipitation was less than half of today's during the coldest part of Marine Isotope Stage 2 (Heusser et al. 1999).

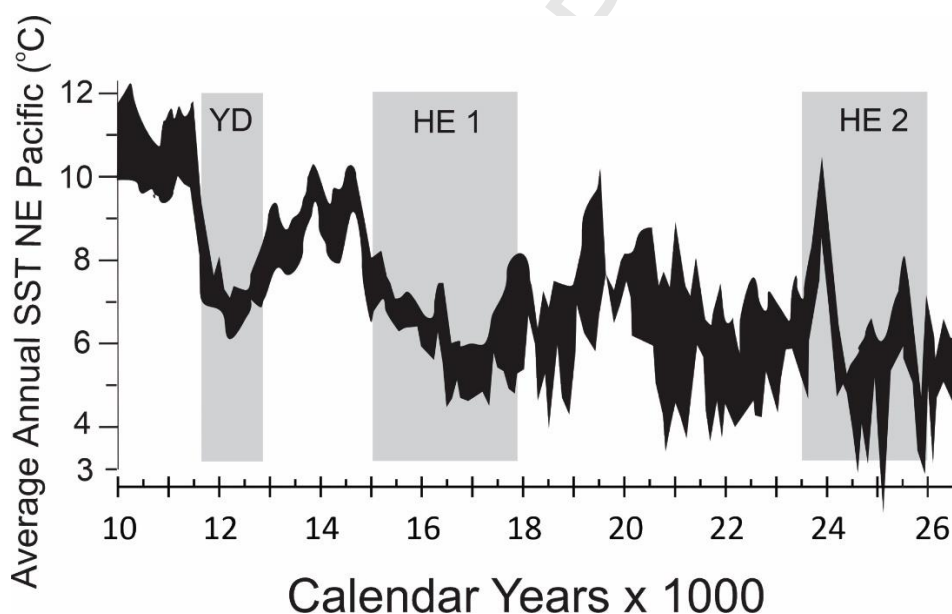


Figure 24. Sea surface temperatures in the Northeast Pacific between 42° and 60° N. Redrawn from Praetorius et al. (2023). "YD" = Younger Dryas. "HE 1" = Heinrich Event 1. "HE 2" = Heinrich Event 2.

A compilation of marine proxy data by Paul et al. (2021) suggests sea surface temperatures (SSTs) in the North Pacific cooled less than they did at similar latitudes in the North Atlantic (Fig. 25). Based on diverse proxy data, Margo Project Members (2009) inferred that summer SSTs were 2-4° C cooler in the southern and central Gulf of Alaska during the Last Glacial Maximum (LGM) than today. Tierney et al. (2020) estimated mean annual SSTs in the Gulf of Alaska during the LGM by combining data-based estimates of ocean temperature with integrative general circulation modeling. They concluded that nearshore SSTs were 5-15° C colder than today, with the coldest temperatures occurring nearest the coastlines of Southeast Alaska and British Columbia (Osman et al. 2021).

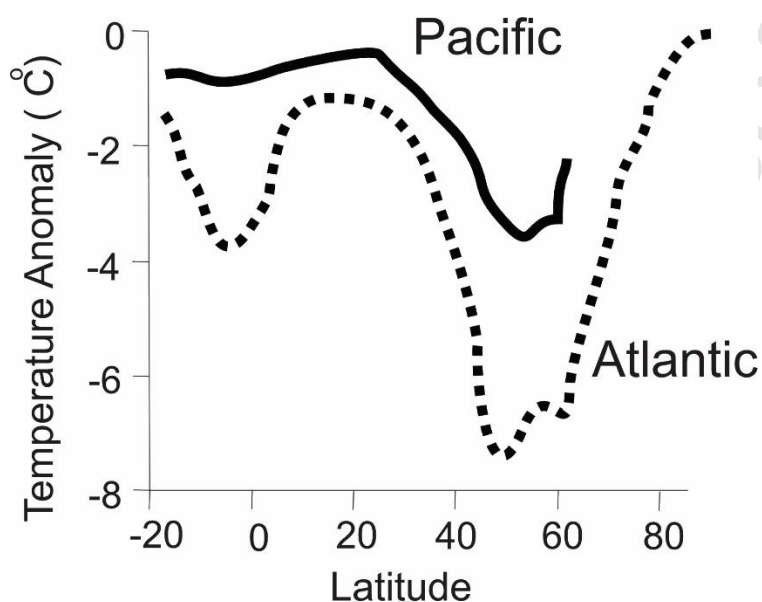


Figure 25. Zonally averaged, annual-mean sea surface temperature anomalies between the Last Glacial Maximum and today compiled from various sources by Paul et al. (2021).

3.2. Inferences from general circulation models

Much of what we know about the climate of the Northeast Pacific region during Marine Isotope Stage 2 comes from the outputs of general circulation models (GCMs). Only the most relevant ones are mentioned here. Bromwich et al. (2004) inferred that July surface temperatures along the Gulf of Alaska coastline were at most 5° C cooler during the Last Glacial Maximum (LGM) than today. In accordance with earlier (e.g., COHMAP Members (1988)) and later modelling studies (e.g., Löfverström et al. (2014)), Bromwich et al. (2004) found that during the Last Glacial Maximum, the polar jet split around the topographic barrier formed by the Cordilleran Glacier Complex and the Laurentide Ice Sheet (Fig. 26). The split jet stream caused storm tracks to be diverted away from Southeast Alaska and British Columbia, which then enhanced winter precipitation in northern (Prince William Sound) and northwestern

sectors (Kodiak, Alaska Peninsula) of the Northwest Coast (Bromwich et al. 2004). Splitting of the polar jet during the LGM is not duplicated in some other GCM experiments, which predict only a southward shift and strengthening of the polar jet (Bartlein et al. 1998; Ullman et al. 2014).

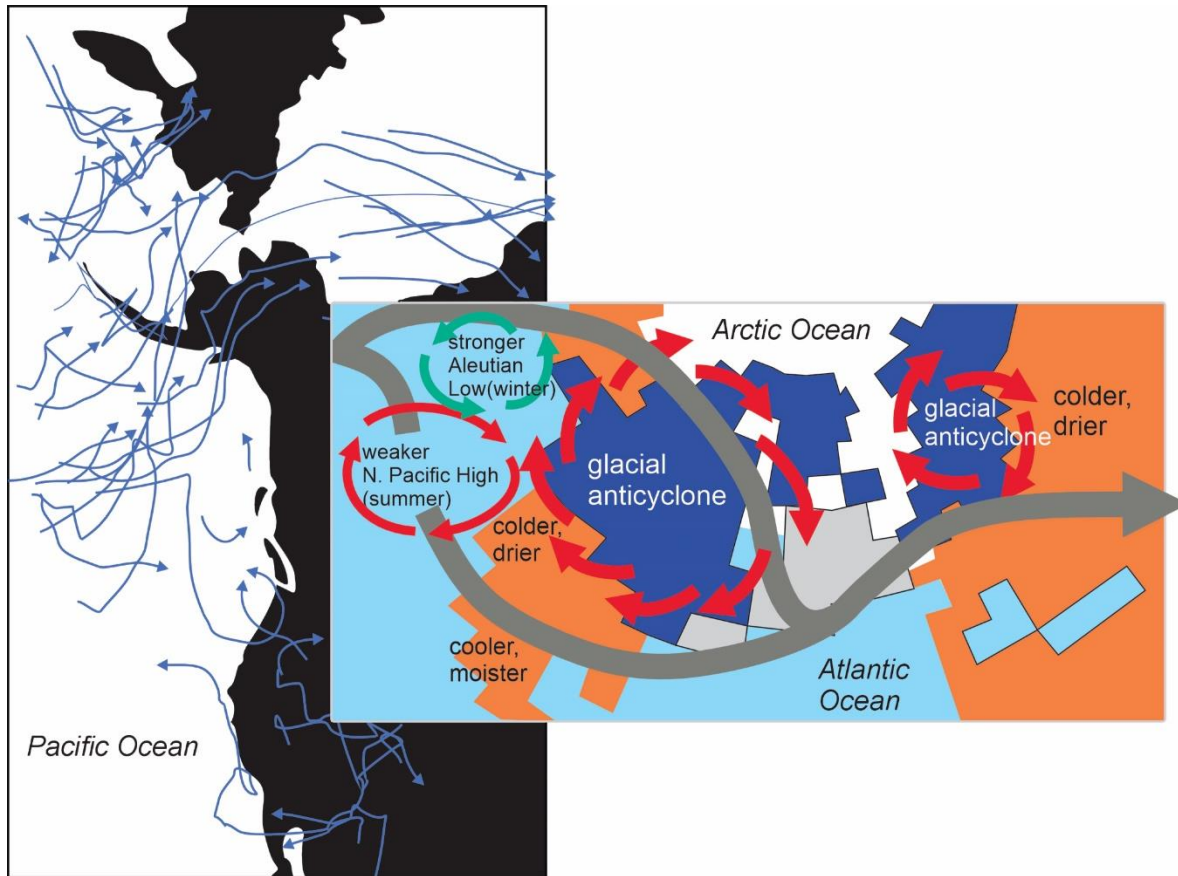


Figure 26. At times during the Last Glacial Maximum, the presence of 3-km high ice sheets over northern North America created persistent anticyclonic flow. This probably split the polar jet in winter and diverted storm tracks (blue lines) around it. **LEFT** Storm tracks predicted in the modelling experiments of Bromwich et al. (2004). **RIGHT** The classic split-jet scenario resulting from the modelling experiments by COHMAP Members (1988).

Morée and Schwinger (2020) interpret their modelling results as showing that mean annual temperatures were 2.5-5°C cooler along the eastern Gulf of Alaska coast during the Last Glacial Maximum (LGM), with precipitation similar to today in the central and southern gulf, but slightly greater in the northwestern gulf. The modelling experiments of Ullman et al. (2014) suggest that at 21 ka strong cooling occurred over the North Pacific, and that the amount of this cooling responded sensitively with the changing height of the Laurentide Ice Sheet. Their results also suggest significantly less precipitation along in the eastern Gulf of Alaska during the LGM.

In contrast to paleoceanographic and modelling studies indicating that significant cooling occurred in the Gulf of Alaska region during the Last Glacial Maximum (LGM), the modelling study of Otto-Bliesner et al. (2006) suggested that mean annual sea surface temperatures (SSTs) were 1-1.5° C warmer. Even more warming is suggested by the modelling studies of Löfverström et al. (2014), Liakka and Löfverström (2018), and Tulenko et al. (2020). An LGM warming of 2° to 6.5° C in mean annual surface temperatures over the Gulf of Alaska and over Alaska as a whole is suggested by the modelling results of Liakka and Löfverström's (2018) in response to anticyclonic circulation induced by the orographic effects of the North American ice sheets. As foreshadowed by earlier modelling experiments (Kutzbach and Guetter 1986; Broccoli and Manabe 1987; Bartlein et al. 2015), this warming was caused by the poleward transport of energy within atmospheric stationary waves that developed along the western flanks of the ice sheets. This northward transport of energy was enhanced by positive feedbacks involving reduced surface albedo, decreased cloud cover, and enhanced transport of latent heat poleward along the Northwest Coast. The warming caused by the highest reconstructed heights of the Laurentide Ice Sheet would have caused glacier equilibrium lines to rise in northern sectors of the Northwest Coast, which Liakka and Löfverström (2018) and Tulenko et al. (2020) suggest is the reason why large parts of Alaska remained unglaciated during the last ice age.

3.3. Climate during the Younger Dryas (YD)

Oceanographic proxy data suggest that sea surface temperatures (SSTs) in the Gulf of Alaska cooled nearly as much between 12.9 and 11.7 ka during the Younger Dryas (YD) chronozone as during the Last Glacial Maximum (Barron et al. 2009; Walczak et al. 2020; Praetorius et al. 2023) (Fig. 24). Onshore, biological records also suggest that the climate cooled significantly around the Gulf of Alaska margin (Peteet and Mann 1994; Hu et al. 1995; Hansen and Engstrom 1996); however, vegetational responses to the YD varied across the region and were typically subtle (Kokorowski et al. 2008; Kaufman et al. 2010; Ager 2019). For example, Mathewes et al. (1993) used palynology to infer that YD summers on Haida Gwaii were 2-3° C cooler than today and that the overall climate was wetter; however, reconstructions elsewhere in southern Alaska and British Columbia suggest a diversity of moisture regimes existed in different sectors of the Northwest Coast (Kokorowski et al. 2008; Jones et al. 2009; Fedje et al. 2011; Hebda et al. 2022).

Limited evidence from glacial geology in Southwest Alaska suggests the occurrence of an early-cold / late-warm pattern of climate change over the course of the Younger Dryas (YD) chronozone (Young et al. 2019). An early-cold / late-warm pattern is also suggested by changes in water chemistry and diatom abundance in Nimgun (Hu et al., 2002) and Arolik Lakes, also in Southwest Alaska, (Hu et al. 2007, Kaufman et al., 2010). This early-cold / warm-late pattern is absent from the Gulf of Alaska sea surface temperature record (Fig. 24), nor is it reflected in the vegetation record of YD cooling from southwestern Kodiak Island (Peteet and Mann 1994; Hajdas et al. 1998). Rising water levels in Discovery Pond on the Kenai Peninsula suggest

increasing effective moisture beginning at 12.2 ka, some 500 years before the end of the YD chronozone (Kaufman et al. 2010).

Some of the enigmatic aspects of Younger Dryas (YD) climate along the Northwest Coast could relate to accentuated seasonality. YD winters along the Northwest Coast may have been cold and dry, while summers may have been warm and steadily growing warmer. This interpretation of YD climate has gained increasing consensus in the North Atlantic region (Levy et al. 2016; Schenk et al. 2018; Young et al. 2019; Rea et al. 2020; Funder et al. 2021; Putnam et al., 2023). The cause of accentuated seasonality in the North Atlantic region during both Heinrich Event 1 and the YD (Fig. 27) may have been the expansion of winter sea ice, which made winters colder but had little effect on summer conditions (Denton et al. 2005, 2021). Despite the colder winters, summer conditions in Greenland remained relatively mild and continued to warm over the course of global deglaciation, including during the YD chronozone (Putnam et al., 2023; Bromley et al., 2023) (Fig. 27).

The occurrence of cold and dry winters could explain the rarity of glacier advances along the Northwest Coast during the Younger Dryas (YD) chronozone. Because glaciers existing within a maritime climatic regime are typically more sensitive to winter precipitation (accumulation) than to summer temperature (ablation) compared to continental glaciers (Ohmura et al. 1992), the apparent absence of YD advances by glaciers bordering the Gulf of Alaska could have been the result of winters that were colder and drier than the preceding Bølling/Allerød Interstadial. Extreme winter conditions might also explain the replacement of ferns by ericaceous shrubs on the windswept tundra of southwestern Kodiak during the YD (Petet and Mann 1994). The limited vegetation responses to the YD along the Northwest Coast (Hansen and Engstrom 1996; Ager et al. 2010, 2019) may reflect the fact that the most extreme climates of the YD occurred during the dormant season.

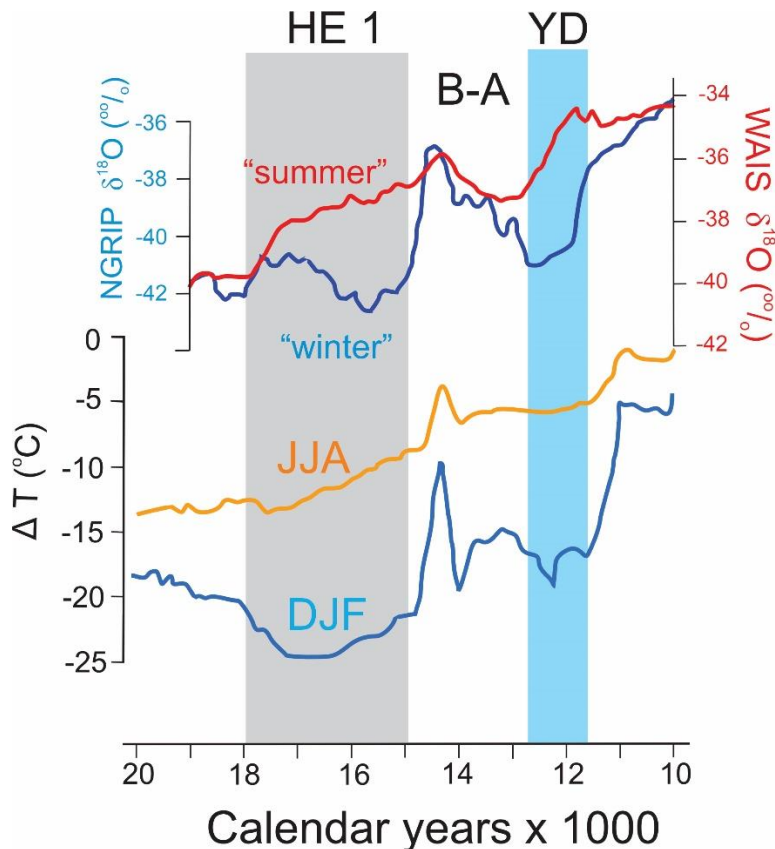


Figure 27. The Extreme Winters Hypothesis asserts that high, northern latitudes experienced accentuated seasonality during Heinrich Event 1 and the Younger Dryas (Denton et al., 2005; 2022). Starting at 19 ka, winter temperatures cooled in response to the increased extent of seasonal sea ice, even while summer temperatures progressively warmed. **ABOVE** The Greenland NGRIP ice core $\delta^{18}\text{O}$ record (NGRIP Members, 2004) and the West Antarctic Ice Sheet Divide Ice Core (WAIS) $\delta^{18}\text{O}$ record (WAIS Divide Project Members, 2015) redrawn from Putnam et al. (2023). These authors argue that the WAIS record is a proxy for global, summer temperatures and that the NGRIP record is a proxy for winter temperatures in the North Atlantic region. **BELOW** Simulated summer and winter temperatures relative to sites near sea level in East Greenland today. "JJA" = June, July, August. "DJF" = December, January, February. Redrawn from Buizert et al. (2015).

3.4. Evidence from paleo-glacier mass balances

Estimates of the paleo-equilibrium line altitudes (ELAs) of glaciers are consistent with 4-5° C cooling in summer across the Gulf of Alaska region during the Last Glacial Maximum (LGM). A glacier's mass balance is an equifinal state resulting from different combinations of temperature and precipitation. That said, temperature tends to be paramount because it influences both the amount of precipitation arriving as snow and the amount of snow melting

(Mackintosh et al. 2017). Summer temperatures are particularly important in controlling glacier mass balance through their effects on melt (Oerlemans 2005; Zemp et al. 2015). The greater the precipitation and the warmer the temperature at the equilibrium line, the more sensitive is the glacier's mass balance to changes in either variable (Oerlemans 1992, Anderson and Mackintosh 2012). When in climate-sensitive phases of their advance/retreat cycles, marine-based glaciers that lose mass via iceberg calving tend to respond faster to temperature changes than do land-terminating glaciers of similar lengths (Jóhannesson et al. 1989). It follows that marine-based glaciers along the Northwest Coast during Marine Isotope Stage 2 responded sensitively and quickly to changing climate compared to glaciers located in the interior of the continent.

Using the accumulation-area ratio method (Porter 2000) and reconstructions of paleo-equilibrium-line altitudes (ELAs), Tulenko et al. (2023) estimate that $\sim 4^\circ\text{C}$ of cooling occurred in summer in the western Alaska Range during the local Last Glacial Maximum (ILGM), which is consistent with other paleo-proxy data from Interior Alaska (Péwé 1975; Kurek et al. 2009). The presence of glacial cirques below sea level today on the coasts of the Kenai Peninsula and Alaska Peninsula suggests that ELAs there were $> 800\text{ m}$ lower than today (Mann and Peteet 1994). A similar estimate of ELA depression results after assuming a moist adiabatic lapse rate (Mackintosh et al. 2017) and an LGM marine-boundary layer 5°C cooler than today (Section 3.1). On the Shumagin Islands (Fig. 12, 28), where mean monthly summer temperature is now 10°C , the ELA probably fell $\sim 900\text{ m}$ during the ILGM. This amount of ELA lowering brought it below present sea level, which is consistent with the reconstructions of Mann and Peteet (1994) and agrees with what would happen within the present phase space of alpine glaciers in response to a 5°C cooling (Fig. 28). The fact that precipitation strongly modifies the effect of temperature within the glaciogenic phase space defined in Figure 28 indicates that changes in winter precipitation were important in controlling glacier dynamics along the Northwest Coast during the LGM.

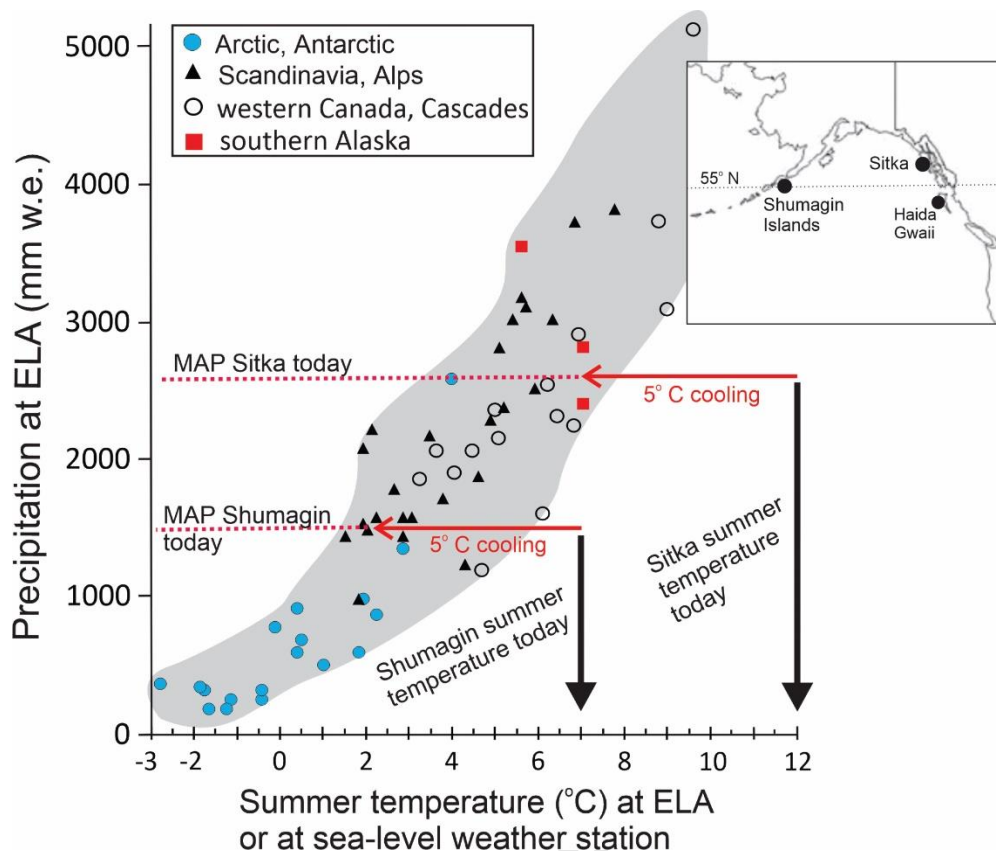


Figure 28. The precipitation and temperature phase space of 70 existing glaciers (Ohmura et al. 1992) can be used to infer how cooling over the Gulf of Alaska during the Marine Isotope Stage 2 affected glaciers there. In response to the $\sim 5^{\circ}\text{C}$ cooling suggested by records of sea surface temperature from marine cores and general circulation models, equilibrium line altitudes (ELAs) would have lowered to near modern sea levels on the Shumagin Islands and near Sitka, even without increases in precipitation. The modern climate data are from the Alaska Climate Research Center, <https://akclimate.org/data/air-temperature-normals/>. "MAP" = mean annual precipitation.

3.5. Insights from the history of pluvial lakes in the Southwest SA

Some of the precipitation diverted southwards to supply pluvial lakes in the western USA occurred at the expense of storm tracks that would otherwise have resulted in snow feeding glaciers in Alaska and British Columbia. For this reason, the chronology of these pluvial lakes provides insights into climate and glacier changes along the Northwest Coast. The western USA experienced higher effective moisture than today during the deglacial period, 21-11 ka (Reheis et al. 2014; Oviatt 2015; Hudson et al. 2019). Closed topographic basins filled with water brought by extratropical cyclonic storms traveling in the Aleutian Low and being diverted southward around the southern margins of the Cordilleran Glacier Complex and the Laurentide

Ice Sheet (Antevs 1948). Abundant precipitation probably also arrived more directly from the central Pacific via atmospheric rivers (Lyle et al. 2012; Lora et al. 2017; Löffverström 2020, Skinner et al. 2023).

Lakes began to fill in the Basin and Range region of the western USA at the beginning of Marine Isotope Stage 2 (Fig. 29). Most of these pluvial lakes reached high stands between 18 and 15 ka, which is 5 to 8 kyrs after most sectors of the Laurentide Ice Sheet reached their Last Glacial Maxima. Many of these lake high stands occurred during Heinrich Event 1 (Munroe and Laabs 2013) (Fig. 29), which was also when the Vashon Lobe reached its maximum extent in Puget Sound (Fig. 5). There are suggestions that northern basins like Lake Chewaucan in southeastern Oregon reached high stands later than southern basins (Hudson et al. 2019), possibly as a result of storm tracks shifting northward as the ice sheets down-wasted (Oster et al. 2015). Most pluvial lakes dried rapidly after ca. 15 ka during the Bølling-Allerød interval (Fig. 29).

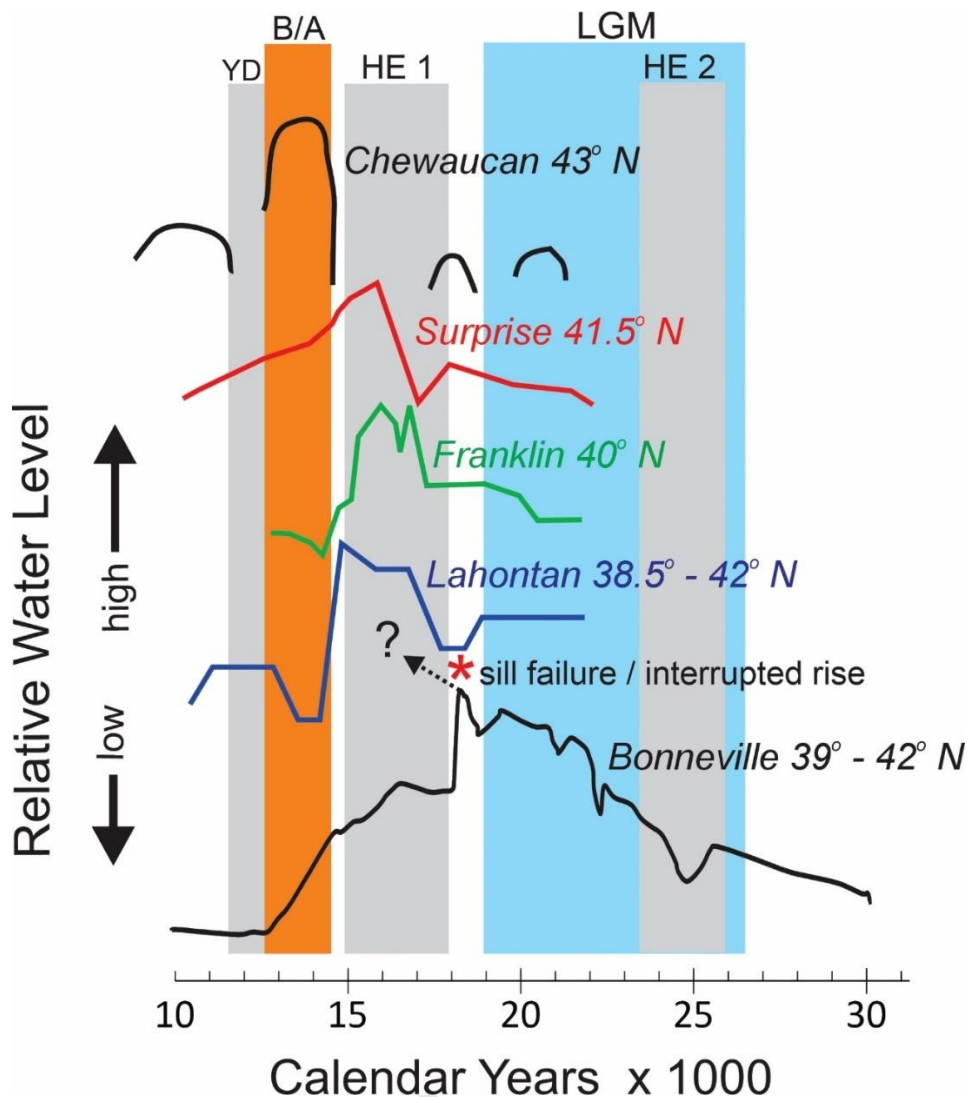


Figure 29. Lakes began to fill closed basins in the western USA early during Marine Isotope Stage 2, but they only reached peak levels during Heinrich Event 1. The water-level records for Lakes Chewaucan, Surprise, Franklin, and Lahontan are from Hudson et al. (2019). The Lake Bonneville curve is from Oviatt et al. (2015).

For decades, the cause of the pluvial interval in the western USA has been assigned to a southward shift of North Pacific cyclonic storms caused by the orographic effects of the North American ice sheets (Antevs 1945, 1948; Broccoli and Manabe 1987; Benson et al. 1995; Bromwich et al. 2004; Munroe and Laabs 2013; Lachniet et al. 2017; Liakka and Löffverström 2018). Recently, this “shift in the Westerlies hypothesis” has been challenged by more nuanced explanations, and these are relevant to what was happening at the same time further north along the Northwest Coast.

One variation on Antevs' (1945) idea is that rather than storm tracks uniformly shifting southwards, the polar jet stream along which these storms tracked was confined and steered into the western USA between an expanded subtropical high centered over Mexico and a semi-permanent high centered over the northern ice sheets (Oster et al. 2015). Another idea is that the deglacial wetting of the western USA resulted from a combination of the ice sheets' orographic effects and the global impacts of the southward shift of the thermal Equator that was caused by weakening of Atlantic Meridional Overturning Circulation (AMOC) (Broecker and Putnam 2013; Lora et al. 2017; Hudson et al. 2019). According to this hypothesis, a southward shift in the thermal Equator altered zonal-mean meridional circulation globally (Bradley and Diaz 2021) and locked storm tracks over western North America (Oster et al. 2015) into the north-dry, south-wet dipole pattern (Wise 2010) that exists over the western USA today under El Niño conditions (Hudson et al. 2019) (Section 8.1.3.1). Support for this "ice sheet + AMOC-slowdown hypothesis" comes from the fact that the lake high stands occurred during Heinrich Event 1 (HE 1) and (most notably for Lake Lahontan (Fig. 29)) during the Younger Dryas (Munroe et al. 2020), which were times when slowing of AMOC caused equatorward shifts in the thermal Equator. Furthermore, the presence of cold steppe vegetation in southern Washington throughout MIS 2 (Whitlock and Bartlein 1997) is consistent with a long-term persistence of the ENSO precipitation dipole (Wise 2010) during that interval. Lake basins in many parts of the western USA desiccated rapidly upon the rejuvenation of AMOC and the rapid down-wasting of the North American ice sheets during the Bølling-Allerød period (14.7-12.9 ka). The beginning of the Holocene saw a sweeping reorganization of atmospheric circulation over western North America in < 1000 years, which may have been accompanied by a decline in the frequency of atmospheric river events (Lora et al. 2017).

Morrill et al. (2018) assert there was an additional cause for the wetting of the western USA during the deglacial period. Their modelling experiments suggest that regional cooling caused by the proximity of the ice sheets reduced the processes of moisture convection and divergent circulation that today cause drying of the region's atmosphere. This explanation is consistent with the strong cooling effect that the ice sheets had in southeastern Washington (Lopez-Maldonado et al. 2023) and in the northern Rocky Mountains (Hostetler and Clark 1997; Laabs et al. 2020; Quirk et al. 2022). Whatever the correct explanation, resolving these long-standing questions about the drivers of pluvial periods in the western USA will improve our understanding of the ocean-atmosphere-cryosphere interactions that occurred along the Northwest Coast during Marine Isotope Stage 2.

3.6 Summary of climate changes along the Northwest Coast during Marine Isotope Stage 2

The surface of the subarctic Pacific cooled less than the subarctic Atlantic at similar latitudes during Marine Isotope Stage 2 (MIS 2). Paleoceanographic data suggest the coldest intervals of MIS 2 occurred in the Northeast Pacific at 26-23.5 ka (Heinrich Event 2), 23-21.5, 18-15 ka (Heinrich Event 1), and 12.8-11.7 ka (Younger Dryas chronozone). Minimum sea surface

temperatures (SSTs) were probably 7° C colder than today off the western coast of Vancouver Island and 5-6° C colder in the northeastern Gulf of Alaska. Reconstructions of paleo-glacier equilibrium lines around the Gulf of Alaska during the Last Glacial Maximum are consistent with these estimates. Some modelling experiments suggest similar amounts of cooling; others suggest that SSTs in the Gulf of Alaska were actually warmer at times than today (Otto-Bliesner et al. 2006, Tulenko et al. 2020). The predictions of warmer SSTs come from general circulation models (GCMs) that incorporate the topographic effects of the North American ice sheets on atmospheric circulation. When ice cover was thickest over northwestern North America, a semi-permanent blocking high may have diverted air masses and cyclonic storms to its north and south. The presence of this blocking high would have diverted warmer air masses northward along the Northwest Coast into southern Alaska and reduced both snowfall and cloudiness there. At the same time, the southward diversion of cyclonic storms and atmospheric rivers would have brought more precipitation into the western USA (Löfverström 2020). Ice-topographic modulation of atmospheric circulation over the region may help explain the time-transgressive behavior of glaciers along the Northwest Coast.

During the Younger Dryas (YD) chronozone, sea surface temperatures (SSTs) in the northeastern Gulf of Alaska cooled by as much as 5° C. Paleoceanographic data do not resolve seasonal differences in SST, nor is seasonality clearly distinguished by any of the terrestrial proxies for temperature now available. As a result, it is unclear what the millennial- and seasonal-scale timings of YD climate were along the Northwest Coast. The Extreme Winter Hypothesis that has emerged from studies in the North Atlantic region (Denton et al. 2005, 2022) may help explain the so-far enigmatic records of the YD along the Northwest Coast.

4. THE ICE-AGE NORTHWEST COAST AND NORTHEAST PACIFIC IN A GLOBAL CONTEXT

4.1. Key processes; global impacts

The ocean/atmosphere/cryosphere systems of the Northeast Pacific and Northwest Coast participated in the rapid, global changes that characterized Marine Isotope Stage 2 (MIS 2). Based on the preceding review and on their importance today (Section 7.0), the following ten processes were probably also of key importance along the Northwest Coast during MIS 2. This section describes how these processes may have affected the Northwest Coast and Northeast Pacific and linked them to the rest of the planet.

1. Orbital variations in insolation
2. Aleutian Low
3. Asian Summer Monsoon
4. Oceanic heat transport in the Kuroshio Current system
5. El Niño-Southern Oscillation

6. Opening and closing of Bering Strait
7. Extent and timing of sea ice in the North Pacific
8. Variations in overturning ocean circulation in the North Pacific
9. Glacial outburst floods entering the North Pacific
10. Sea surface cooling in the Gulf of Alaska possibly triggering Heinrich Event 1

4.1.1. Orbital variations in insolation

4.1.1.1. *Were changes in low-latitude insolation important in the subarctic Pacific?*

The canonical Milankovitch view is that orbital variations drove the Pleistocene ice ages by reducing / increasing solar insolation at high northern latitudes (Fig. 30); however, the mechanisms involved remain unclear (Ruddiman 2003; Raymo et al. 2006; Tabor et al. 2014). The fact that glaciers in the southern hemisphere fluctuated synchronously with those in the north, despite out-of-phase forcing by summer insolation in the two hemispheres, suggests that boreal, summer insolation was not the sole driver of the northern ice sheets (Broecker and Denton 1989; Denton et al. 2021). The fact that summer insolation at low and high, northern latitudes varied in parallel (Fig. 31) suggests that low-latitudes processes could have played key roles. This is consistent with the low correlation between $\delta^{18}\text{O}$ records from southeast Asian speleothems and global ice volumes/eustatic sea level, which suggests that the chain of climate-change causation actually began in the tropics and went poleward rather than the other way around (Beck et al. 2018). Furthermore, an important role for low-latitude solar insolation in driving late Pleistocene events at higher latitudes is consistent with the planetary geography of energy receipt and dissipation (Pierrehumbert 2000; Rodgers et al. 2003; Chiang 2009).

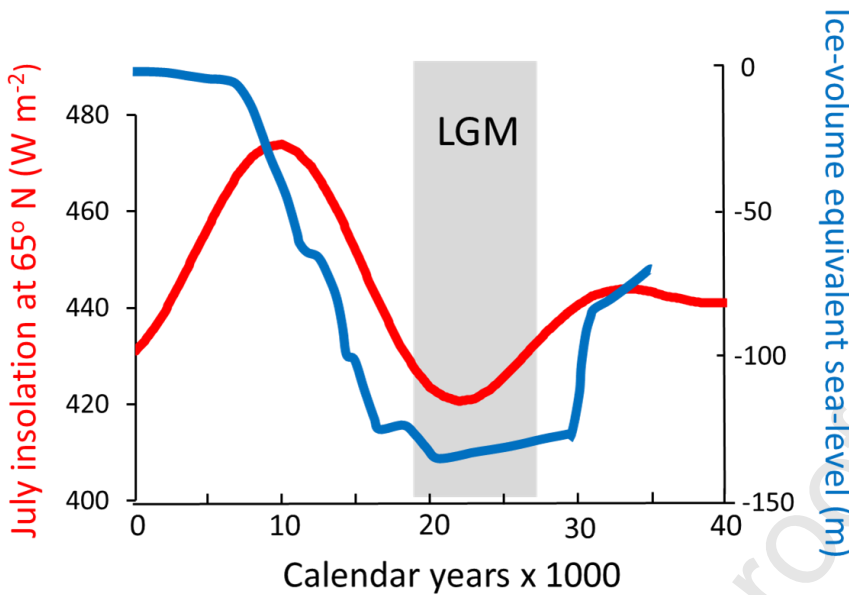


Figure 30. Global ice volumes generally tracked Milankovitch orbital forcing at high, northern latitudes (red). Eustatic sea level (blue) is a proxy for the amount of ice present on land. At first glance, the synchrony between insolation and eustatic sea level suggests that boreal summer insolation was the ultimate driver of glaciation and deglaciation (Shakun and Carlson 2010). “LGM” is the global Last Glacial Maximum. The sea level curve is from Lambeck et al. (2014). Milankovitch insolation data are from Laskar et al. (2011).

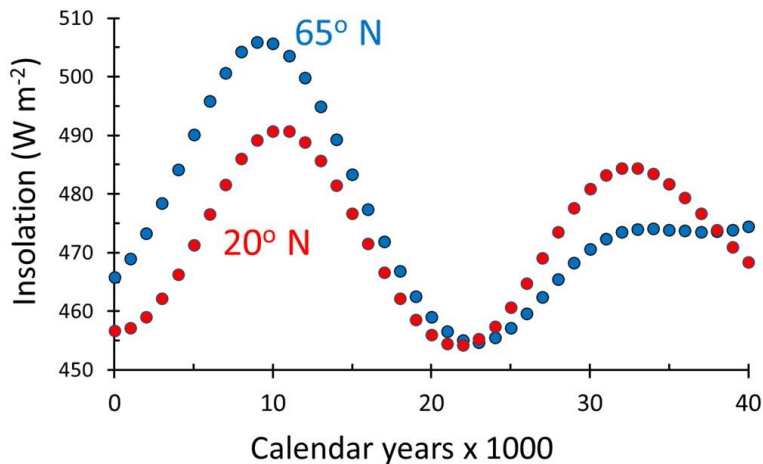


Figure 31. Solar insolation at 65° N in summer varied in parallel with insolation at low, northern latitudes, suggesting that high-latitude insolation may not have been the sole driver of the boreal ice sheets. Insolation data from Laskar et al. (2011).

4.1.1.2. *A role for meridional insolation gradients?*

Raymo and Nisancioglu (2003) proposed that meridional insolation gradients modulated Milankovitch effects on ice-sheet volume to such an extent that during the early Pleistocene they caused a 41-ka rhythm in sea surface temperatures (SSTs), despite the predominance of a 21-ka cycle in insolation during that interval in Earth's history. The 41-ka periodicity of obliquity may have overwhelmed precession's effects on ice-sheet growth and decay by altering latitudinal gradients in insolation, which then changed the poleward flux of heat and moisture. In a similar way during Marine Isotope Stage 2 (MIS2) latitudinal gradients in seasonal solar insolation may have played a key role in the dynamics of high-latitude ice sheets. The occurrence of the Last Glacial Maximum during a peak in the insolation differences between 10° N and 60° N (Fig. 32) is consistent with this meridional-gradient mechanism contributing to the inception, growth, and demise of the Cordilleran Glacier Complex.

How might insolation changes at low latitudes have affected the environments of the Northwest Coast through changes in the latitudinal gradient in solar insolation? Today, the most important atmospheric bridges (Section 7.1.3) between the tropics and the Northwest Coast are the Asian Summer Monsoon (ASM) and the Aleutian Low (AL), both of which are strongly influenced by conditions in the Equatorial Pacific. Today, steepening of meridional temperature gradients intensifies the jet streams, the mid-latitude Westerlies, and the subtropical ocean gyres (Lee and Poulsen 2005; Molnos et al. 2017; Lutsko and Popp 2018; Trenberth 2022). In response, the ASM also tends to penetrate further north (Deininger et al., 2020). The net result is increased storminess over the North Pacific, particularly in winter (Liu et al. 2021), and it is these winter storms that provide the snow that nourishes glaciers along the Northwest Coast (McCabe et al. 2000; Meier et al. 2003; Malcomb and Wiles 2013). The next two sections describe the effects that insolation-caused changes in latitudinal insolation gradients may have had on the ocean/atmosphere/cryosphere system of the Northeast Pacific and Northwest Coast via the atmospheric bridges afforded by the Asian Monsoon and the Aleutian Low.

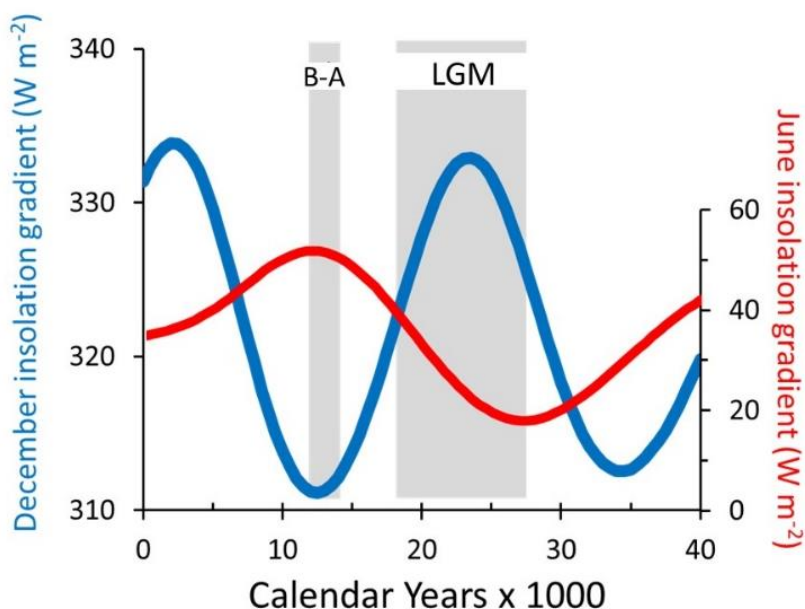


Figure 32. Orbital variations caused changes in the gradient of solar insolation at high and low northern latitudes. The steepness of this gradient probably affected the position of the Intertropical Convergence Zone (ITCZ), modulated the strength of the trade winds, and modified the pressure gradients responsible for generating extratropical cyclones. The onset of the Last Glacial Maximum (LGM) occurred when the winter gradient in insolation (blue line) between the northern tropics and the high, northern latitudes was steep and growing steeper, while the summer gradient (red line) was shallow and growing more so. Deglaciation accompanied a reverse in these seasonal gradients. The Bølling-Allerød (B-A) interstadial accompanied a minimum in the winter gradient. Insolation values are from Laskar et al. (2011).

4.1.2. Aleutian Low

The glacial history of the Northwest Coast (Fig. 16) and the chronology of pluvial lakes in the western USA (Fig. 29), reflect shifting latitudinal gradients in climate over the North Pacific. In response to steepened latitudinal temperature gradients and the accompanying increase in the zonality of atmospheric circulation (Löfverström et al. 2014; Skinner et al. 2023), the Aleutian Low (AL) shifted southward during the coldest intervals of Marine Isotope Stage 2 (COHMAP Members 1988; Munroe and Laabs 2013). As they do today (Section 7.1.2.3), the AL's tropical teleconnections influenced the tracks these storms took, along with their seasonality and intensity. Changes in the strength and position of the AL affected glaciers by changing summer temperatures and winter precipitation. Under glacial conditions, atmospheric rivers probably increased in frequency and contributed larger proportions of annual precipitation along the Northwest Coast than today (Löfverström 2020). Modelling output hints that atmospheric rivers may have been particularly important in sustaining glaciers' mass balances

in the Alaska Peninsula sector of the Cordilleran Glacier Complex (CGC) (Skinner et al. 2023). In response to the AL's southerly shift during Heinrich Event 1, the CGC advanced into western Washington between 16 and 17 ka. At that same time, pluvial lakes in the western USA reached their highest levels (Section 3.5), probably in response to a combination of increased winter precipitation and cooler, cloudier, less evaporative summer conditions.

Also during Heinrich Event 1, marine-based glaciers around Haida Gwaii (Section 2.1.3.4) and in the northern Gulf of Alaska and Alaska Range (Section 2.1.3) were retreating, possibly in response to declining precipitation. If the dipole pattern in winter precipitation that occurs today over the western USA during El Niño years also occurred at that time (Section 7.1.3.1), then glacial advances in southwestern British Columbia and in the western USA may have been responses to cooler summer temperatures rather than to increased winter precipitation.

Although changes in storm tracks within the Aleutian Low (AL) were probably instrumental in determining regional differences in the timing of glaciation between Alaska and the southwestern USA, how exactly teleconnection patterns (Section 7.1.2) such as the Pacific Decadal Oscillation (PDO), Pacific North American Pattern (PNA), and the Arctic Oscillation (AO) expressed themselves during Marine Isotope Stage 2 remains unclear. The presence of the North American ice sheets, combined with what were probably persistent Eastern Pacific Warm-El Niño (EPW-El Niño) conditions (Section 4.1.5), may have increased the frequency of the AO- and PNA+ patterns (Section 7.1.3). Because of these persistent EPW-El Niño conditions, PDO+ phases were probably also more frequent. Today, the conjunction of an EPW-El Niño with a PDO+ phase and winter PNA+ conditions tends to increase snowfall in southern and Southeast Alaska, while causing less snowfall in southern British Columbia and the Pacific Northwest, and bringing wetter conditions to the western USA. In contrast, the winter conditions that today are most favorable for glacier growth in the Pacific Northwest (and least favorable in southern Alaska) occur when PNA- patterns coincide with a PDO- phase and La Niña (Section 7.1.3). During the last ice age, similar anti-phase relationships in winter precipitation between southern/southeast Alaska and the Pacific Northwest may have caused time-transgressive glaciations in these different sectors of the Northwest Coast. That said, how exactly the AL's tropical teleconnections behaved when it shifted to its southernmost extreme along the Northwest Coast during Heinrich Event 1 remains to be deciphered.

4.1.3. Asian Summer Monsoon

Today, the Asian Summer Monsoon (ASM) transports large amounts of sensible and latent heat from the tropics into the subarctic Pacific (Wang et al. 2013) (Section 7.1.1). During Marine Isotope Stage 2 (MIS 2), the strength of the ASM generally tracked summer solar insolation (Fig. 33); however, several notable divergences occurred. After declining at the onset of MIS 2, monsoon vigor stabilized at a low level between ca, 25 and 20 ka, despite the continuing decline in summer insolation that occurred at 20° N. Even more radical divergences

occurred during Heinrich Event 1 (HE 1) (ca. 18 to 15 ka) and the Younger Dryas chronozone (YD) chronozone (12.9-11.7 ka) when the ASM weakened despite increasing insolation. Sharp declines in ASM vigor during HE 1 and the YD were probably related to summer cooling over Asia (Chiang et al. 2014) and over the western tropical Pacific, which was probably a response to the combination of weakened Atlantic Meridional Overturning Circulation (Section 4.2) and persistent Eastern Pacific Warm-El Niño conditions (Section 4.1.5). The position of the Intertropical Convergence Zone (ITCZ) is a key factor in monsoon climatology today (Broecker and Putnam 2013; Walker et al. 2015; Beck et al. 2018; Geen et al. 2020; Clemens et al. 2021), and southward shifts occurred in the ITCZ during both HE 1 and the YD (Chiang and Bitz 2005; Bradley and Diaz 2021) (Section 4.1.5).

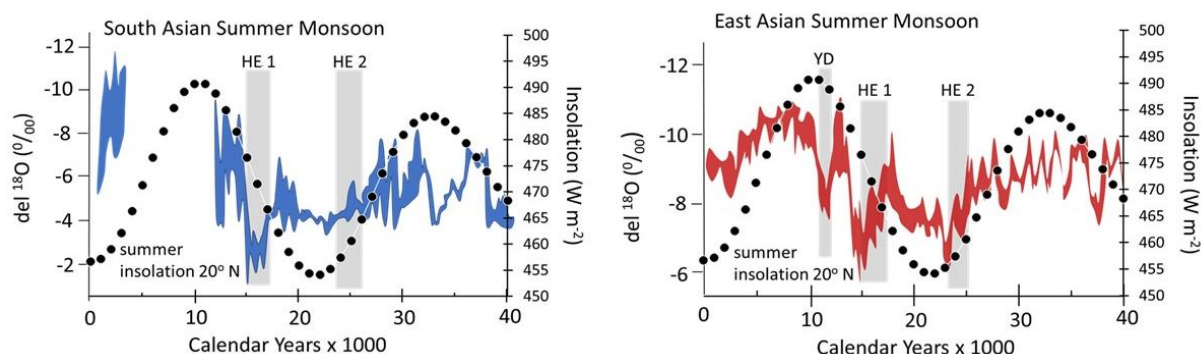


Figure 33. Speleothem $\delta^{18}\text{O}$ records the changing vigor of two components of the Asian Summer Monsoon in northern India (**RIGHT**) (Kathayat et al. 2016) and in southeastern China (**LEFT**) (Cheng et al. 2016). The dotted line is Milankovitch insolation from Laskar et al. (2011). "YD" = Younger Dryas. "HE 1" = Heinrich Event 1. "HE 2" = Heinrich Event 2.

Evidence for the changing influence of the Asian Summer Monsoon (ASM) on conditions in the subarctic Pacific during Marine Isotope Stage 2 (MIS 2) comes from records of sea surface temperatures (SSTs) (Walczak et al., 2020). SSTs in the Gulf of Alaska appear to have paralleled rainfall on the loess plateau in northern China (Fig. 34). Heinrich Events 1 and 2 (HE 1, 2) are clearly evident in both records, though a divergence occurred between 23.5 and 20 ka when the Gulf of Alaska's SSTs continued to cool while rainfall plateaued in northern China. The vigor of overturning circulation (ventilation) in the northeastern Gulf of Alaska also changed in parallel with the ASM, the latter recorded by $\delta^{18}\text{O}$ in speleothems in China and India, and by monsoon-fed lake levels in Tibet (Fig. 35). This correlation was especially pronounced during HE 1 and 2.

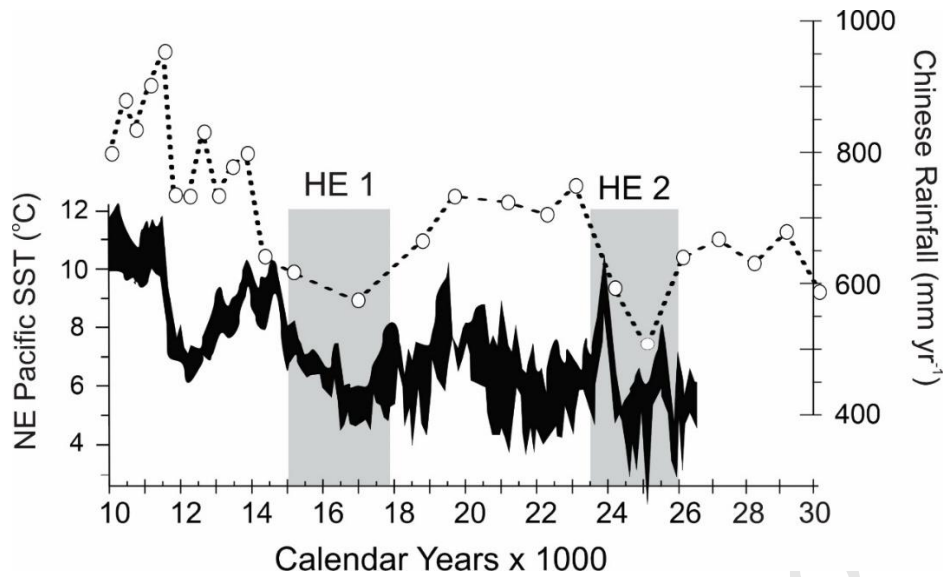


Figure 34. During much of Marine Isotope Stage 2, changes in sea surface temperature (SST) in the Gulf of Alaska roughly paralleled trends in summer rainfall in northern China. The SST record is from Praetorius et al. (2023), and the Chinese rainfall data are from Beck et al. (2018).

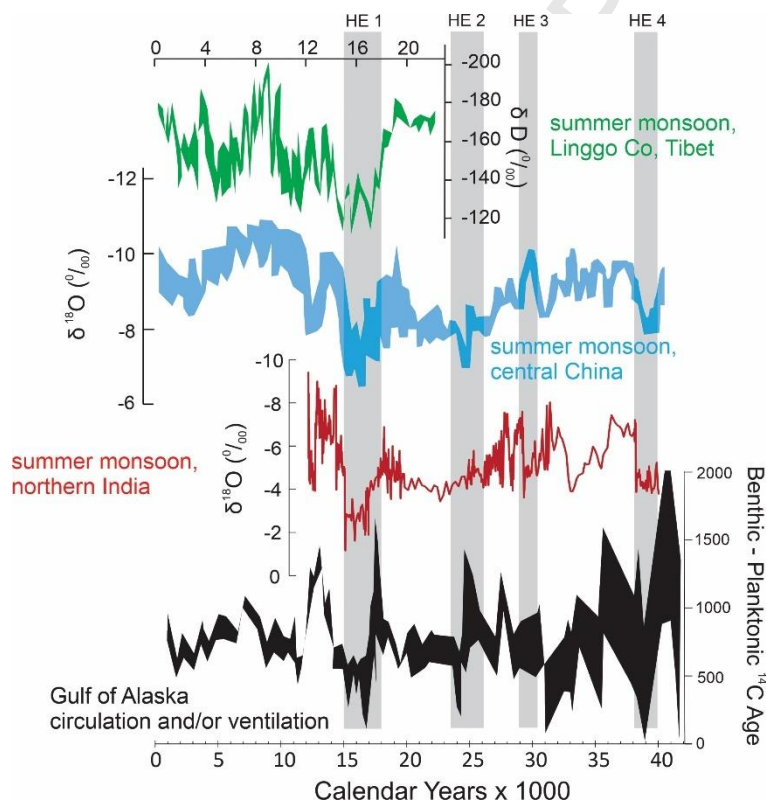


Figure 35. A record of vertical mixing in the Gulf of Alaska (Walczak et al., 2020) (**BOTTOM**) compared to three records of the Asian Summer Monsoon (ASM). The Indian speleothem record is from Kathayat et al. (2016), the Chinese speleothem record is from Cheng et al. 2016), and the Tibetan lake-level record is from Hou et al. (2017). The slowdown of vertical mixing in the Gulf of Alaska was accompanied by a peak in ice-rafted debris deposition there (Fig. 6). "HE 1-4" = Heinrich Events 1-4.

4.1.4. Oceanic heat transport

The Kuroshio current system transports tropical heat from Western Pacific Warm Pool (WPWP) to the high-latitude North Pacific (Section 7.1.1). The WPWP also exports heat to the Indian Ocean via the Indonesian Throughflow (ITF). ENSO affects the dynamics of the Kuroshio, the WPWP, and the ITF. What follows is an overview of how this system might have functioned during Marine Isotope Stage 2 and affected the Northwest Coast via the Asian Summer Monsoon and the Aleutian Low.

4.1.4.1. *Western Pacific Warm Pool and Indonesian Throughflow*

Because it threads its way across the Maritime Continent of the Indonesian Archipelago, the Indonesian Throughflow (ITF) is sensitive to changes in sea level (Fan et al. 2018). Thus Kuhnt et al. (2004) estimated that the ITF was reduced by 31% when eustatic sea level reached its low point during the Last Glacial Maximum. This would have reduced oceanic heat transport from the Western Pacific Warm Pool (WPWP) into the Indian Ocean by some 23%. The oceanic heat not exported to the Indian Ocean via the ITF probably exited the WPWP into the eastern Pacific via the Equatorial Under Current (Rodgers et al. 1999).

Despite a significant decrease in how much warm water was transported into the Indian Ocean by the Indonesian Throughflow (ITF), sea surface temperatures (SSTs) in the Western Pacific Warm Pool (WPWP) cooled by 4° to 5° C during the Last Glacial Maximum (LGM). This was accompanied by an eastward shift in the center of convective activity over the tropical Pacific (Xu et al. 2010; De Deckker 2016) (Fig. 36). In response, the Asian Summer Monsoon (ASM) weakened. Also in response to reduced convective activity over the western tropical Pacific, surface salinity increased there, while lowered eustatic sea level exposed large areas of the continental shelf (Voris 2000), both of which contributed to a decline in convection and rainfall over the region (Di Nezio et al. 2016). The coolest interval in the WPWP occurred between 20 and 17.5 ka, which coincided with the maximum extent of glaciers bordering the northern Gulf of Alaska (Fig. 16). After ca. 17.5 ka, sea surface temperatures warmed in the WPWP by 3-5° C, and temperatures peaked during the early Holocene (Linsley et al. 2010). By 15 ka, rising sea level had re-submerged large parts of the Maritime Continent, and by 14-15 ka a vigorous ASM was reestablished over the region (Kuhnt et al. 2015). Along the Gulf of Alaska

margin, reinvigoration of the ASM coincided with the majority of glaciers retreating out of tidewater (Fig. 16).

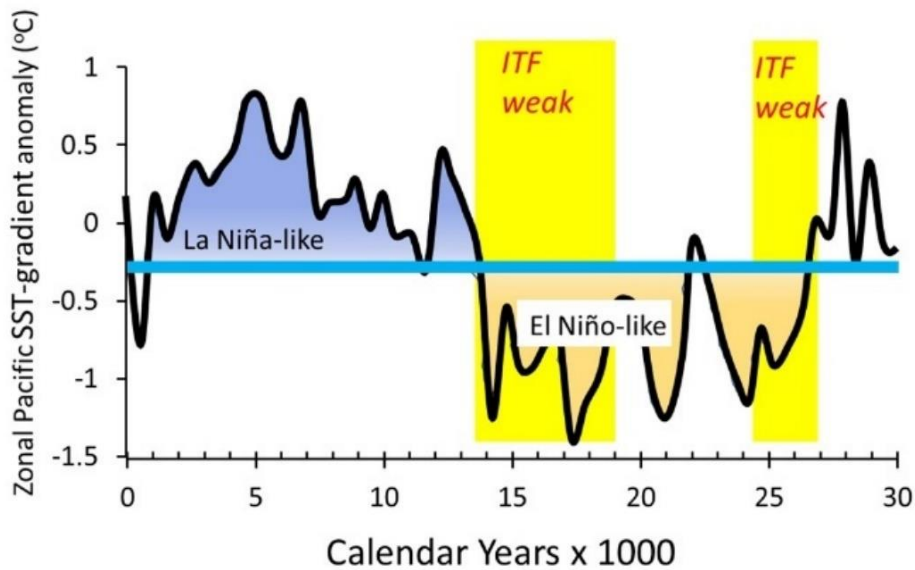


Figure 36. Changes in the vigor of the Indonesian Throughflow (ITF) and the phases of the paleo-ENSO inferred from changes in the zonal sea surface temperature gradient across the tropical Pacific (Fan et al. 2018).

4.1.4.2. Kuroshio Current system

Surprisingly little is known about the ice-age history of the Kuroshio Current despite the key roles that it now plays in regional and global climates (Section 7.1.1). The coldest intervals along the southern coast of Japan occurred between 30 and 28 ka and again between 17 and 15 ka when sea surface temperatures (SST) off the southern coast of Japan were $\sim 3^\circ\text{C}$ cooler than today (Ujiié et al. 2003). During these coldest times, the Kuroshio and Kuroshio Extension carried less water and probably turned eastward at lower latitudes than today (Gallagher et al. 2015; Kubota et al., 2021). Lower eustatic sea level during the Last Glacial Maximum (LGM) excluded the Kuroshio Current from the East China Sea (Ujiié et al. 2003). Based on the recent dynamics of the Kuroshio-Oyashio convergence (Qiu 2019), its southward shifts during ice-age stadials were probably in response to stronger winter monsoons associated with stronger Aleutian Lows, weaker summer monsoons, and increased flows of the Oyashio Current. By analogy with recent El Niño events (Hu et al. 2015), the Kuroshio and Kuroshio Extension probably experienced reduced flows during the coldest intervals of the LGM because of persistent Eastern Pacific Warm-El Niño conditions. Consistent with the positive correlation seen today between SST in the subarctic Pacific and the strength of the Kuroshio Current (Section 8.1.3), cold intervals near Japan accompanied cooler SSTs in the Gulf of Alaska (Fig. 24).

4.1.5. The El Niño-Southern Oscillation

Today, teleconnections between ENSO and the Aleutian Low (AL) link the oceanography and meteorology of the tropical Pacific with those of the high latitude North Pacific (Koboth-Bahr et al. 2021) (Section 7.1.3). Multiple studies suggest that El Niño-like conditions prevailed in the tropical Pacific during the Last Glacial Maximum (LGM). These include the work of Koutavas et al. (2002) who inferred that cooling of just 1.2°C occurred in the eastern equatorial Pacific during the LGM. This slight amount of cooling implies a weak zonal temperature gradient across the equatorial Pacific, weak Hadley and Walker circulations, and a southward shift of the Intertropical Convergence Zone (ITCZ), all of which are suggestive of persistent Eastern Pacific Warm-El Niño conditions. Koutavas et al., (2002) inferred that the regime of most frequent El Niño conditions ended at 15 ka, while La Niña-like conditions prevailed between ca. 9 and 4 ka.

Additional evidence for a persistent El Niño-like state in the equatorial Pacific during the Last Glacial Maximum (LGM) comes from the modelling results of Han et al. (2020) that suggest the zonal gradient in sea surface temperature (SST) across the tropical Pacific declined during the LGM and thereby caused a weakening and eastward shift of Walker Circulation. Both the above studies are consistent with Ford et al.'s (2018) conclusion based on $\delta^{18}\text{O}$ in foraminifera from cores in the eastern equatorial Pacific that the zonal SST gradient was lower and that the thermocline was deeper there, both of which are consistent with a persistent El Niño-like state existing during the LGM. Fan et al. (2013; 2018) reached a similar conclusion by reconstructing the zonal SST gradient across the tropical Pacific between 30 ka and today (Fig. 36). Based on this they inferred that El Niño-like conditions existed from ca. 26 to 14 ka, whereas La Niña-like conditions dominated during the mid-Holocene. Finally, SST records from across the tropical Pacific compiled by Zhang et al. (2022) also suggest a flattening of the zonal SST gradient from 30 to 19 ka consistent with El Niño-like conditions. The zonal gradient steepened between 19 and 16 ka, reached a peak at 11 ka, and then declined towards the present (Fig. 37).

In summary, the coldest times of Marine Isotope Stage 2 were probably spent under persistent Eastern Pacific Warm-El Niño (EPW-El Niño) conditions. By analogy with the present day (Section 7.1.3.2), the Northwest Coast probably experienced prolonged, positive phases of the Pacific Decadal Oscillation (PDO+) during the Last Glacial Maximum (LGM), although it is unclear how these PDO+ conditions were manifested when the polar jet was split and atmospheric flow was generally stronger and more zonal. By analogy with EPW-El Niño conditions today, cyclogenesis was probably increased in the North Pacific when EPW-El Niño conditions were strongest and most persistent during the LGM, which would have deepened the Aleutian Low, increased the occurrence of atmospheric rivers, and generally increased the amount of moisture transported into mid-latitude North America. Opposing this trend were reductions in the amounts of moisture and heat being transported poleward by the Asian Summer Monsoon and by the Kuroshio Current. Obviously, there is much to learn about how

ENSO, the Western Pacific Warm Pool, the Indonesian Throughflow, the Kuroshio system, and the Aleutian Low interacted during the rapidly changing phases of MIS 2 climate.

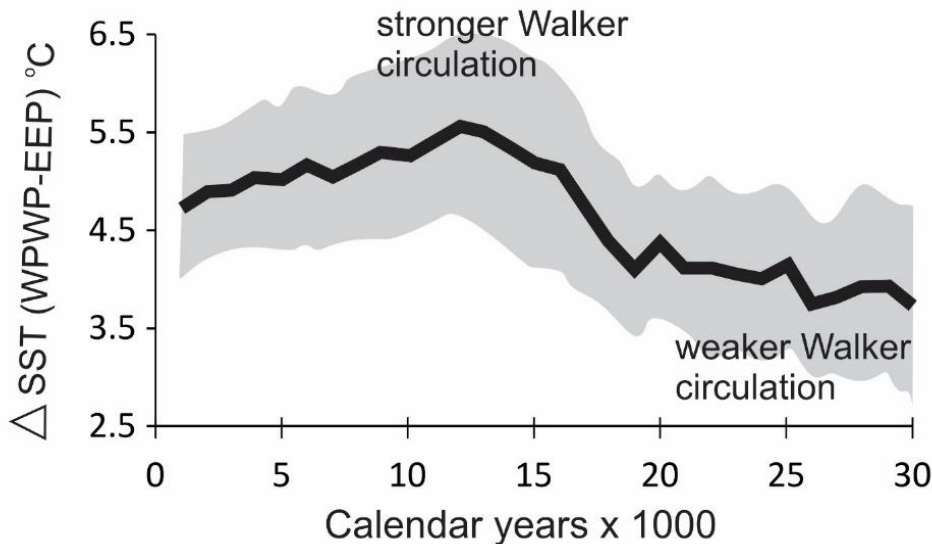


Figure 37. Annual, zonal sea surface temperature differences between the Western Pacific Warm Pool and the eastern equatorial Pacific based on a compilation of deep-sea sediment records by Zhang et al. (2022). The grey-shaded area shows one standard deviation around the estimates of differences in east-to-west sea surface temperatures. Walker Circulation is strongest during La Niña conditions and weakest during El Niño conditions. El Niño conditions were more frequent during the Last Glacial Maximum. Redrawn from Zhang et al. (2022).

4.1.6. Opening / closing of Bering Strait

As noted in Section 2.2.2, the key question about the role of Bering Strait in global systems is not when the strait was first flooded at the end of the ice age, but when it became deep enough to assume its modern oceanographic functions. Without significant amounts of oceanic heat transport (OHT) through the strait, the sea ice regime in the western Arctic Ocean probably remained in its full-glacial mode (Bradley and England, 2008), and without extensive open water in the Chukchi and Bering Sea, storm tracks probably remained farther south and followed more zonal tracks than today, which would have deprived the Arctic Basin of a large amount of the atmospheric heat it receives today (Section 7.1.2.1). Even if the initial flooding of Bering Strait occurred prior to 13 ka (Section 2.2.2), there would be little effect on the ocean-atmosphere system until near-modern sea levels were reached (Fig. 21). This point has been largely ignored in assessments of the paleoceanographic significance of Bering Strait (Hu et al. 2012; Praetorius et al. 2020).

Insights into the impacts of varying water depths in Bering Strait come from the analysis of Cessi (2020) who calculated the geostrophically balanced throughflow in Bering Strait today using this equation:

$$T_{BS} = H_{BS} * g \Delta\eta / f_{BS}$$

Where H_{BS} is the average depth of Bering Strait (67 m today), g is gravity force, $\Delta\eta$ is the difference in sea surface height between the Arctic/North Atlantic Oceans and the North Pacific (~ 0.2 m), and f_{BS} is the Coriolis parameter at 66°N ($1.2 \times 10^{-4} \text{ s}^{-1}$). Solving for the throughflow yields an estimated throughflow of 1 Sv under present conditions, which is equivalent to the northward flow observed through the strait today (Woodgate 2018).

If Pico et al.'s (2020) modelled relative sea level (RSL) curve for Bering Strait is correct, and assuming the shallowest sill in Bering Strait was indeed at -53 m, and if this sill was first transgressed ca. 13.2 ka (Fig. 19), then according to their model it would have taken until ca. 11.2 ka for RSL to rise an additional 10 m. Assuming the strait is a rectangular trough, and assuming the same difference in sea level between the North Pacific and Atlantic existed at 11.2 ka as today, Eq. 1 predicts that only ~ 0.2 Sv of northward flow would have occurred when the strait was 10 m deep. Even this modest flow is unlikely because Atlantic Meridional Overturning Circulation (AMOC) was reduced during the Younger Dryas (YD) chronozone (Hogg et al. 2016) between 12.9 and 11.7 ka. When AMOC slows, the difference in sea-surface heights between the North Pacific and Arctic/North Atlantic decreases, which removes a major cause of northward flow through Bering Strait (Cessi 2020)

In summary, when Bering Strait initially flooded did not coincide with the initiation of its present-day oceanographic functions. Bering Strait is unlikely to have carried sufficient North Pacific surface water (Hu et al. 2007; Hu et al. 2010; Hu et al. 2012) or freshwater from glacial outburst floods (Praetorius et al. 2020) into the North Atlantic via the Arctic Ocean to have influenced Atlantic Meridional Overturning Circulation until after eustatic sea level reached near-modern levels sometime after 10 ka (Fig. 21).

4.1.7. Sea ice

Sea ice affects the atmosphere and ocean in diverse ways (Polyak et al. 2010, Bhatt et al. 2014, Watson et al. 2015). It acts as a barrier to heat exchange between the colder atmosphere and the warmer ocean (Landrum and Holland 2022), which means its presence lowers air temperatures. Sea ice also affects ocean-atmosphere gas exchanges, overturning ocean circulation, storm tracks, and the routes of ocean currents (Walsh 1983; Alexander et al. 2004; Ferrari et al. 2014). Because sea ice in subpolar seas forms and melts annually and is highly sensitive to changing patterns of heat transfer within both the ocean and atmosphere (Aylmer et al. 2022), its changing extent can act as a rapid, sensitive driver of hemisphere-scale climate changes (Holloway et al. 2016; Wunderling et al. 2020). Modelling studies suggest that changes

in the extent of Arctic sea ice affects the position of the Intertropical Convergence Zone (Chiang and Bitz 2005) and the vigor of Atlantic Meridional Overturning Circulation (Liu and Fedorov 2019). The responses of sea ice cover to changing climate are markedly non-linear because of the ice-albedo effect (Serreze and Barry 2011), which means that both the decline and expansion of sea ice can occur suddenly. This rapidity of response is especially true for seasonal (winter) sea ice, which was the type widespread in the subarctic Pacific during Marine Isotope Stage 2 (Section 2.3).

Based on its seasonal cycle in the Arctic Ocean today, sea ice in the subarctic Pacific during Marine Isotope Stage 2 (MIS 2) began forming in October and reached its maximum extent in March, which means its effects on regional climate were greatest in late winter and spring. Based on how reductions in sea ice cover are affecting the Arctic and Antarctic today (Bhatt et al. 2014; Zhang et al. 2023), expansion of sea ice during MIS 2 would probably have steepened north-south temperature gradients over the North Pacific region, and as a result, strengthened upper-level westerly winds and intensified zonal atmospheric flow. When sea ice was at its maximum extent, the Aleutian Low and the Polar Jet would probably have been displaced southward and directed more zonally, which would have reduced winter precipitation in Alaska and increase it in the Pacific Northwest and the western USA (Section 4.1.2).

Changes in the extent of sea ice in the subarctic Pacific may have been a key driver of climate changes at regional and global scales during Marine Isotope Stage 2. Widespread sea ice expansion during winter in the North Atlantic underlies the Extreme Seasonality Hypothesis proposed to explain some aspects of climate during Heinrich Event 1 and the Younger Dryas (Broecker and Denton 1989; Denton et al. 2022; Putnam et al. 2023) (Fig. 27). This same hypothesis can be applied to the high-latitude North Pacific. As explored in Section 4.1.10, the 3500 km marine-based margin of the Cordilleran Glacier Complex may have been a hair trigger for Heinrich Event 1 by virtue of the large masses of marine-based glacial ice that were located on the Northeast Pacific's continental shelf ca. 19 ka (Section 2.1.3). When these glaciers retreated, icebergs and meltwater probably fueled the expansion of winter sea ice across the subarctic Pacific. Reconstructions of the extent of sea ice during MIS 2 (Section 4.1.7) suggest it episodically expanded and contracted over a region approximately twice the size of the Gulf of Mexico and at its maximum extended as far south as 55° N (Fig. 22). In response, the Aleutian Low would have shifted southward and deepened, diverting storm tracks away from southern and Southeast Alaska and into the Pacific Northwest and western USA. By this means, changes in sea-ice extent may have contributed to the time transgressive nature of glacier fluctuations along the Northwest Coast (Fig. 16). Sea-ice generated cooling of the high-latitude North Pacific may then have teleconnected via the atmosphere to the North Atlantic region (Petet et al. 1997).

4.1.8 Overturning circulation in the North Pacific

Today, overturning circulation in the North Pacific is restricted to the production of North Pacific Intermediate Water (NPIW) in the northwestern Pacific (Section 7.1.1.3). This limited amount of deep circulation is one reason the abyssal North Pacific contains so much ^{14}C -depleted CO_2 (Shackleton et al. 1988; Lund et al. 2011; Du et al. 2018; Walczak et al. 2020). Degassing of this sequestered CO_2 caused by changes in the vertical circulation of the deep North Pacific could have had large impacts on global climate (Feely et al. 2001; Rae et al. 2014; de La Fuente et al. 2015; Alves et al. 2018). Variations in overturning circulation in the North Pacific could also have affected climate by changing the global pattern of oceanic heat transport (Section 7.1.1.6). Like Atlantic Meridional Overturning does today, vigorous deepwater formation in the North Pacific would have drawn warm, surface waters to high latitudes (Rae et al. 2020). For these reasons, understanding the prehistoric dynamics of overturning circulation in the North Pacific has been a topic of intense interest and continuing controversy.

The production of North Pacific Intermediate Water (NPIW) probably increased during the Last Glacial Maximum when sea ice was more extensive (Keigwin 1998; Horikawa et al. 2010; Okazaki et al. 2010; Gong et al. 2019; Rae et al. 2020). Formation of sea ice releases salt into surface waters, which causes a decrease in buoyancy, which can then facilitate downwelling (Ferrari et al., 2015). Additional influences on overturning circulation in the North Pacific have been proposed, including the opening / closing of Bering Strait (Davies-Walczak et al. 2014), changes in the vigor of the South Asian Monsoon system (Lembke-Jene et al. 2017), and fluctuating amounts of exchange between the subtropical and subpolar gyres (Rae et al. 2020). During the coldest intervals of the last ice age, origination of NPIW may have expanded from the Sea of Okhotsk into the southern Bering Sea (Zhong et al. 2023).

Overturning circulation in the North Pacific may not always have been limited to the production of North Pacific Intermediate Water (NPIW) (Matsumoto et al. 2002; Cook et al. 2016; Max et al. 2017). One view is that overturning circulation intensified in the subarctic Pacific during the Last Glacial Maximum (LGM), to the extent of causing significant amounts of tropical heat to be carried to high, northern latitudes (Matsumoto et al. 2002; Okazaki et al. 2010; Rae et al. 2014; Maier et al. 2018; Rae et al. 2020). Based on a combination of computer modelling and multi-proxy data from multiple marine cores located mostly in the western North Pacific, Okazaki et al. (2010) interpreted a reduction in the ^{14}C age differences between benthic and planktic foraminifers (B-P ages) during Heinrich Event 1 (HE 1) as indicating a significant increase and deepening of overturning circulation. Consistent with this interpretation, Maier et al. (2018) found on the basis of diatom $\delta^{18}\text{O}$ in a core from the subarctic Pacific that the advection of subtropical water increased during coldest periods of the LGM.

Okazaki et al. (2010) proposed the following sequence of events occurred during the global cooling that accompanied Heinrich Event 1. 1) Meltwater from retreating glaciers around the North Atlantic made surface waters less dense, which caused Atlantic Meridional

Overturing Circulation (AMOC) to stop. 2) This caused the entire Northern Hemisphere to cool. 3) In response, the Intertropical Convergence Zone shifted southwards, which caused 4), a reduction in Atlantic to Pacific moisture transport, which led to 5), an increase in the salinity of surface waters in the North Pacific. The closed state of Bering Strait facilitated the buildup of salinity in the surface waters of the subarctic Pacific. 6) Saltier, denser surface waters weakened the halocline, which then triggered 7), meridional overturning circulation to depths of ~ 2500 m. 8) This enhanced circulation drew more salty, subtropical water into the North Pacific, which further enhanced overturning circulation, possibly to depths of 3000 m (Okazaki et al. 2010). Building on Okazaki et al.'s (2010) conclusions, Menviel et al. (2012) used an Earth system model to suggest that deep-overturing circulation in the subarctic Pacific may have created a bipolar seesaw in sea surface temperature between the North Pacific and Southern Ocean. Assuming Okazaki et al. (2010) were correct about Atlantic Meridional Overturing Circulation being shut down by the cooling of the North Atlantic, the onset of deep overturning circulation in the subarctic Pacific would also have generated a North Pacific / North Atlantic SST seesaw (Menviel et al., 2012).

Max et al. (2014) arrived at different conclusions about overturning circulation in the North Pacific during cold intervals of the last deglaciation. They reconstructed changes in ocean ventilation based on multiple cores from the northwestern North Pacific, including from the Sea of Okhotsk and western Bering Sea. Their results suggested that the formation of North Pacific Intermediate Water (NPIW) increased and ventilation was enhanced at depths shallower than 2100 m during both Heinrich Event 1 (HE 1) and the Younger Dryas (YD) chronozone when Atlantic Meridional Overturing Circulation was reduced. In other words, NPIW formation did increase, but in contrast to the Okazaki et al. (2010) scenario, deep-water formation never occurred. In fact, Max et al. (2014) inferred that North Pacific deepwater actually became more isolated from the ocean surface during HE 1 than it is today. Reconstructions of sea surface temperature (SST) and sea ice coverage during HE 1 and the YD (Max et al. 2012) failed to detect the warming expected if overturning circulation had in fact triggered positive feedbacks capable of destabilizing the subarctic North Pacific's halocline in the ways Okazaki et al. (2010) suggested. Instead of deep, overturning circulation of regional extent, Max et al. (2014) and later Rippert et al. (2017) inferred that only a modest revving-up of NPIW formation occurred during the coldest intervals of the last 20 kyr. Because North Pacific deepwater was more isolated from exchange with the atmosphere, Max et al. (2014) inferred that enhanced NPIW production in the high latitude North Pacific increased CO₂ sequestration in the deep North Pacific during the coldest times of Marine Isotope Stage 2.

Rae et al. (2014) interpreted the history of overturning circulation in the high-latitude North Pacific in a somewhat similar way as Max et al. (2014). In a core from the Patton Sea Mount in the southwestern Gulf of Alaska, Rae et al. (2014) found a marked decline in the ¹⁴C age differences between benthic and planktic foraminifers (B-P ages) during Heinrich Event 1, which they attributed to the mixing of older, deepwater (> 2000 m) with younger, shallower water masses. They suggested this resulted from warming sea surface temperatures and

increasing surface salinity caused by reduced freshwater input from the Asian Summer Monsoon.

In a subsequent study, Rae et al. (2020) compiled proxy data describing ventilation, primary productivity, temperature, and salinity across the ice-age North Pacific and then modelled their regional and global impacts. Their conclusion was that deepwater (below 2000 m) was poorly ventilated during the Last Glacial Maximum (LGM), much as it is today. In contrast, waters above ca. 2000 m were relatively well-ventilated, suggesting more vigorous and widespread formation of North Pacific Intermediate Water (NPIW) during the LGM, which they estimate could have reached 8 Sv yr⁻¹. This is approximately 4x what it is today, but still significantly less than Atlantic Meridional Overturning Circulation, even at the latter's minima during the LGM (Rae et al., 2020). These authors note that most of the sites where salinity and sea surface temperature increased and where the ¹⁴C age differences between benthic and planktic foraminifers (B-P ages) declined during the LGM are located in the subarctic Pacific. Rae et al. (2020) follow Okazaki et al.'s (2010) reasoning that enhanced NPIW formation was driven by a weakened, regional hydrological cycle caused by cooler global temperatures.

A major focus of the Rae et al. (2020) study was the impact of changes in North Pacific overturning circulation on CO₂ in the atmosphere. Today, widespread upwelling of nutrient- and CO₂-rich subsurface waters occurs in the subarctic Pacific, and CO₂ outgasses from this upwelling water (Fig. 38). During the Last Glacial Maximum (LGM), in contrast, Rae et al. (2020) inferred that limited vertical mixing caused CO₂-rich water to be trapped below ~2000 m, which is consistent with the conclusions of Max et al. (2014) and also with time series of ¹⁴C age differences between benthic and planktic foraminifers (B-P ages) compiled by Praetorius et al. (2020) showing that the ¹⁴C ages of near-surface and abyssal (< 2000-m depth) waters diverged markedly between ca. 20 and 17 ka and again during the Younger Dryas chronozone. Rae et al. (2020) suggested that the release of this long-sequestered CO₂ between ca. 15 and 10 ka acted as an important driver of global climate changes in the course of the modern circulation regime becoming established in the North Pacific (Gray et al. 2018).

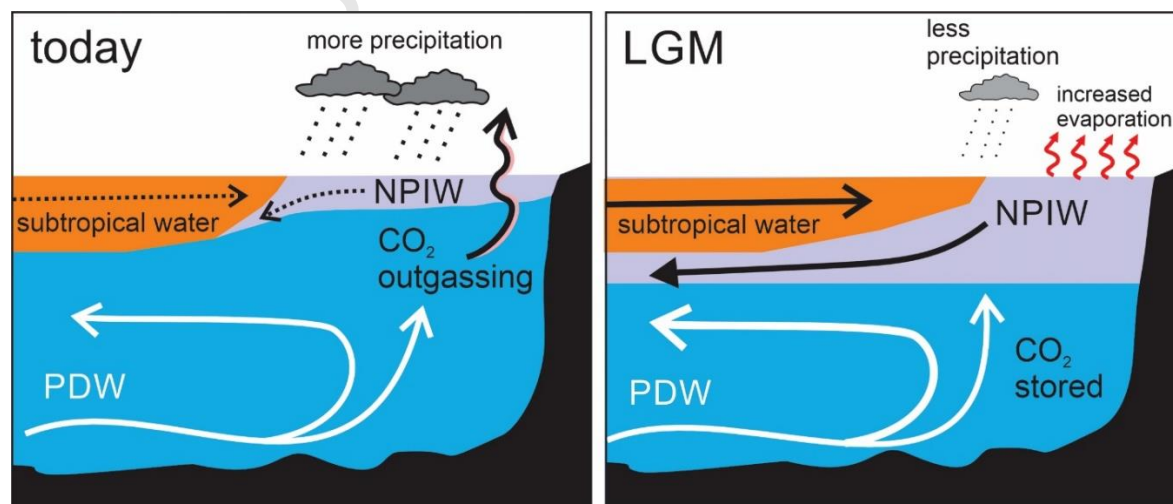


Figure 38. Differences in ocean circulation in the North Pacific between the Last Glacial Maximum (LGM) and today. Rae et al. (2020) inferred that during the LGM surface waters in the subarctic Pacific were saltier and warmer than during the Holocene because of the increased inflow of subtropical water, increased evaporation, and reduced precipitation. In response, the production of North Pacific Intermediate Water (NPIW) increased, which enhanced ventilation above ~2000 m but simultaneously isolated deeper water, causing large amounts of ^{14}C -depleted carbon to be sequestered there. This reconstruction does not hold for coastal waters in the Gulf of Alaska where a persistent halocline created by runoff from the coastal mountains probably suppressed overturning circulation throughout the LGM and during deglacial times. Redrawn from Rae et al. (2020). "PDW" = Pacific Deep Water.

In contrast to the conclusions of Okazaki et al. (2010; 2014) and Rae et al. (2020) that North Pacific overturning circulation intensified between 20 and 10 ka, Davies-Walczak et al. (2014) inferred that overturning circulation at intermediate depths near the glaciated, northeastern margin of the Gulf of Alaska was similar to or only slightly greater during the Last Glacial Maximum (LGM) than during the Holocene. Prior to ca. 14.5 ka, they found no evidence for a ^{14}C -depleted ("old"), intermediate-depth water mass indicating enhanced intermediate water formation. In the northeastern Gulf of Alaska, deep- and intermediate-level waters were most ventilated during the Bølling-Allerød (14.8-12.9 ka) and early Holocene, which parallels ventilation history in the North Atlantic and negates a seesaw relationship between the North Pacific and North Atlantic (Praetorius et al. 2020).

In summary, overturning circulation during the Last Glacial Maximum and Heinrich Event 1 (HE 1) in the North Pacific probably never approached the scale of Atlantic Overturning Circulation in terms of water volume, heat transport, and dissolved-carbon transfer. Overturning circulation probably never penetrated to depths below 2000 m; however, overturning circulation did increase during particularly cold periods like HE 1 and the Younger Dryas chronozone, which caused an increase in the production of North Pacific Intermediate Water (NPIW) in response to the combination of an expansion of sea ice, colder sea surface temperatures, and increased exchange between the subtropical and subpolar gyres. The expansion and invigoration of NPIW was most pronounced in the northwestern North Pacific where winter cooling was greatest bordering the Eurasian landmass. NPIW formation seems to have never expanded into the northeastern Gulf of Alaska where freshwater runoff from the coastal mountains and the Cordilleran Glacier Complex probably maintained a strong halocline. Despite never developing into deep, overturning circulation, changes in the vigor of NPIW probably did modulate the outgassing of CO_2 from the deepwater below it. In this way, it may have played an important, though still poorly understood role in modulating global climate during the last deglaciation.

4.1.9 Did outburst floods into the North Pacific trigger regional and global climate changes?

4.1.9.1 *Floods from the Columbia River Basin*

Today, the freshness of the North Pacific's surface waters influences the production of North Pacific Intermediate Water (NPIW) and the extent of sea ice (Section 7.1.1.3). Episodically during deglaciation, glacial outburst floods dumped large amounts of freshwater suddenly into the Northeast Pacific (Praetorius et al. 2020). Between ~ 19.3 and 14.9 ka, multiple floods occurred from lakes impounded behind glacial dams in the headwaters of the Columbia River (Atwater 1986, 1987; Blais-Stevens et al. 2003; Lopes and Mix 2009; Gombiner et al. 2016; Balbas et al. 2017). The largest of these floods occurred at 18.2 ± 1.2 ka (Balbas et al. 2017), about the time an even larger flood issued from pluvial Lake Bonneville when a sill leading into the Columbia River drainage collapsed (Oviatt 2015). The largest of these Columbia Basin floods released as much as 17 Sv of freshwater into the North Pacific via the Columbia River over the span of days to weeks (O'Conner and Costa 2004; Hendy 2009; Lopes and Mix 2009; Davies et al. 2011; Praetorius et al. 2020).

To detect the impacts of Columbia River outburst floods on the ocean / atmosphere system of the North Pacific, Praetorius et al. (2020) compiled records of sea surface temperature (SST), surface salinity, and ^{14}C -age offsets between near-surface and deepwater foraminifera between 20 and 10 ka. As did Maier et al. (2018) in an earlier study, Praetorius et al. (2020) found evidence for multiple episodes of cooling and freshening in the North Pacific accompanied by reductions in deep circulation that were probably related to megafloods (Fig. 39). The most significant episodes of freshening occurred in the intervals 19.5-18 ka and 13.4-11.8 ka. The earlier episode preceded Heinrich Event 1, though how closely depends on what limiting ages are assigned to that event. The latter freshening episode occurred during the Younger Dryas chronozone.

Given their large volumes, where they entered the North Pacific, and the subarctic Pacific's sensitivity to changes in its halocline, outburst floods from the Columbia River undoubtedly influenced climate along the Northwest Coast during Marine Isotope Stage 2. Computer modeling suggests that floodwaters released from the Columbia River would have circulated northward via the Alaska Coastal Current and reached the Gulf of Alaska and the eastern Bering Sea within five years (Praetorius et al. 2020). Another plume of freshwater would probably have spread westward to Japan within ten years. The effects of these floods on the climate and oceanography of the North Pacific may have been transmitted to the entire northern hemisphere (Maier et al. 2018). General circulation models also suggest that the cooling / freshening of the high latitude North Pacific resulting from Columbia River megafloods initiated cooling throughout the northern hemisphere, possibly enough cooling to tip the North Atlantic region into stadial conditions, which then might have triggered Heinrich Event 1 (Praetorius et al. 2020).

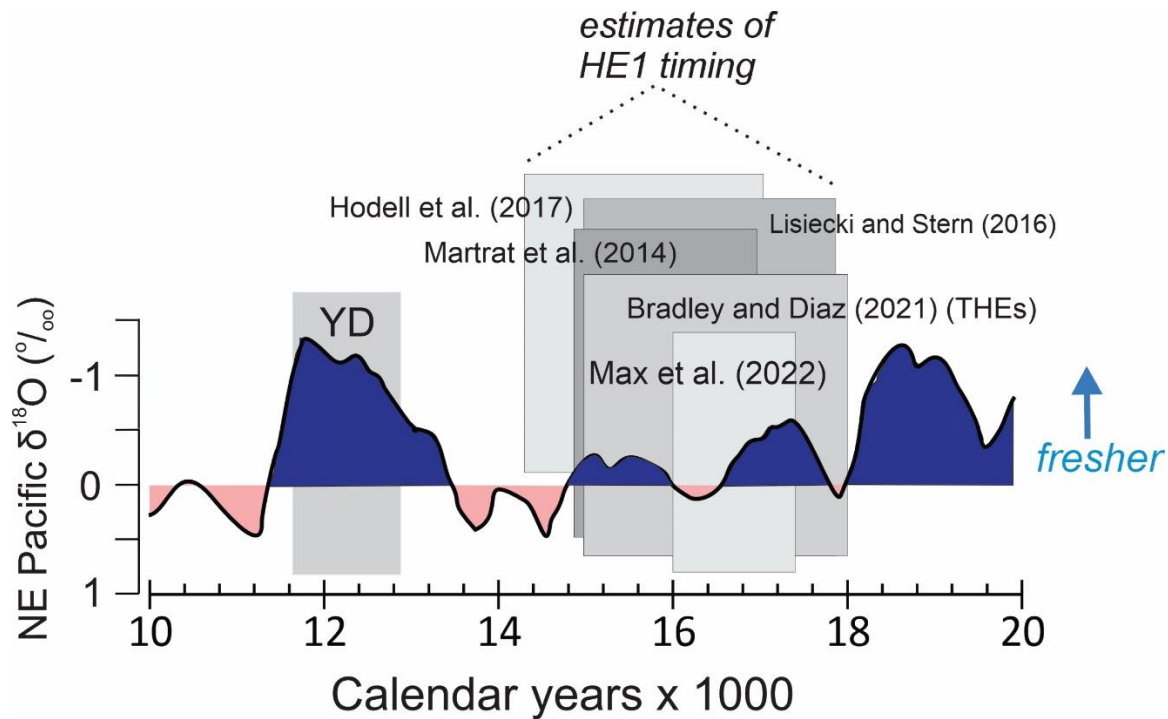


Figure 39. Changes in the relative freshness (blue) of surface water in the Northeast Pacific (redrawn from Praetorius et al. 2020). Differently shaded boxes show various authors' age estimates for the timing of Heinrich Event 1 (HE 1). "YD" = Younger Dryas. "THEs" = tropical hydrological events.

Uncertainties in when outburst floods actually issued from the Columbia River Basin make it difficult to test whether these floods triggered regional and global climate changes (Fig. 39). For instance, one of the largest floods occurred at 18.2 ka, but this date has a reported error of ± 1.5 kyr (Balbas et al. (2017). Similarly, the Lake Bonneville flood is only broadly constrained between 17.1 and 18.4 (Oviatt 2015), which means that it could have occurred after the beginning of Heinrich Event 1 (HE 1) and thus after the cooling of the subarctic Atlantic that preceded HE 1 (Max et al. 2022). Adding to the chronological challenges is the fact that the oceanographic time series used by Praetorius et al. (2023) has dating uncertainties caused by unknowns surrounding marine-reservoir ages (Section 4.1.10). The Columbia River flood-climate correlation is most convincing for the Younger Dryas (YD) chronozone; however, if it did trigger or contribute to the global YD (12.9-11.7 ka) through its effect on Atlantic Meridional Overturning Circulation, it did so via an atmospheric teleconnection (Petet et al., 1997) rather than an oceanic one because the Bering Strait was probably either closed or oceanographically insignificant at 12.9 ka (Section 4.1.6).

4.1.9.2. Alaskan outburst floods

The Columbia River Basin was not the only source of megafloods entering the North Pacific during Marine Isotope Stage 2. Large outburst floods also occurred from glacier-dammed lakes in southern Alaska, and while the timing of these floods remains obscure, their impacts on the oceanography and atmosphere of the North Pacific could have been significant because of where they entered the sea.

Of particular interest is Glacial Lake Atna in the Copper River Basin (Williams et al. 1989; Reger et al. 2008a; Wiedmer et al. 2010; Smith 2019) (Fig. 40). The Glacial Lake Atna-Susitna system episodically covered $> 9000 \text{ km}^2$ (Ferrians et al. 1989). Multiple outburst floods occurred through different outlets when local ice dams were breached (Smith 2019). Floods through Mentasta Pass traveled down the Tanana and Yukon Rivers into the Bering Sea (Reger et al. 2008a; Smith 2019). At least one flood entered upper Cook Inlet and the Gulf of Alaska via Tahnetta Pass (Fig. 40) (Wiedmer et al. 2010) (though see Reger et al. (2011)). Because it is the lowest point in the entire basin, the Copper River potentially carried the largest floods directly into the Gulf of Alaska (Nichols and Yehle 1969).

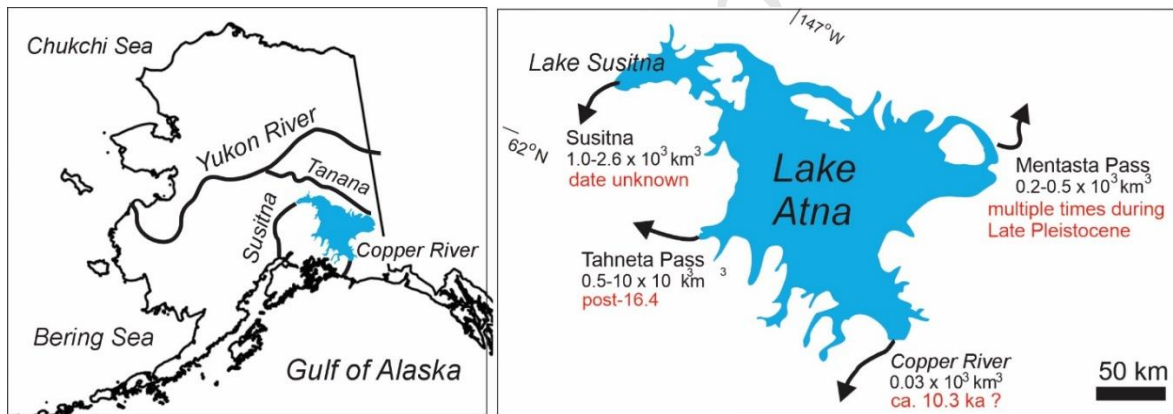


Figure 40. The largest glacier-dammed lake in Alaska during Marine Isotope Stage 2 was Glacial Lake Atna in the Copper River Basin. Multiple outburst floods from Lake Atna reached the Gulf of Alaska and the Bering Sea; however, the timings and magnitudes of these floods remain poorly known. Estimates of total flood volumes are from Wiedmer et al., (2010).

Wiedmer et al. (2010) estimated that some floods from Glacial Lake Atna were of similar size as megafloods from Glacial Lake Missoula in the Columbia River Basin (Zuffa et al. 2000, Lopes and Mix 2009). Some of the Lake Atna floods may have carried up to $2,600 \text{ km}^3$ of freshwater into either the Bering Sea (via Mentasta Pass) or the Gulf of Alaska (via the other three outlets) at rates as high as 11 Sv (Wiedmer et al. 2010). For comparison, an outburst flood from Glacial Lake Agassiz that reached the Arctic Ocean via the MacKenzie River valley around the time of the Younger Dryas had a larger total volume ($23,000 \text{ km}^3$), but may have occurred more slowly (1.8 to 2.5 Sv) (Norris et al. 2021).

The timings of megafloods from Glacial Lake Atna remain poorly constrained, but multiple floods are known to have occurred after 16 ka in the course of regional deglaciation (Reger et al. 2008a; Wiedmer et al. 2010; Smith 2019). If the megaflood over Tahnetta Pass (Wiedmer et al. 2010) did indeed occur, limiting dates on glacier retreat from the Matanuska valley (Williams et al. 1989; Kopczynski et al. 2017; R.D. Reger, pers. comm. 2021) suggest it took place after 16.4 ka. Some of the outburst floods happened after the earliest human occupation of the Copper River basin ca. 13 ka (Kari 2019; White et al. 2022). The final drainage of Glacial Lake Atna may have occurred down the Copper River shortly before 10.3 ka (Muhs et al. 2013; Smith 2019). Because of their direct inputs into the Gulf of Alaska and Bering Sea, outburst floods from Glacial Lake Atna could have had significant impacts on regional oceanography and climate.

4.1.10. Was the subarctic Pacific as a trigger point for global climate?

4.1.10.1. *The Walczak Hypothesis*

The North Pacific-centric hypothesis of Walczak et al. (2020) asserts that events in the ocean / atmosphere / cryosphere of the Gulf of Alaska preceded and triggered Heinrich Events in the North Atlantic region, which then had global effects. If true, this turns Atlantic-centric paleoclimatology on its head and generates a number of new questions. Here we consider the Walczak Hypothesis in the case of Heinrich Event 1 because it is the most recent and hence the best documented of the Heinrich events.

The scenario described in the Walczak hypothesis for Heinrich Event 1 (HE 1) starts in the tropics with the gradual strengthening of the Asian Summer Monsoon (ASM) beginning ca. 23 ka (Fig. 41). This strengthening of the ASM may have been in response to a northward shift in the Intertropical Convergence Zone (ITCZ) caused by an increase in summer insolation received at 10° north (Fig. 32). Based on how the ITCZ responded to similar latitudinal shifts during the Holocene (Deininger et al. 2020), a northern shift in June insolation near the Equator would have pushed the ITCZ further into the northern hemisphere, which, based on the monsoon's recent behavior (Wang et al. 2013; Walker et al. 2015), would have strengthened the ASM. A stronger and more extensive summer monsoon would then have increased the amounts of freshwater and latent heat transported into the North Pacific (Section 7.1.2.1). In response, sea surface temperature (SSTs), air temperature, and precipitation probably increased along the Northwest Coast, triggering rapid responses from the glaciers comprising the seaward flank of the Cordilleran Ice Sheet. At 20 ka, glaciers covered approximately $500 \times 10^3 \text{ km}^2$ of the continental shelf bordering the Northwest Coast. Many of these glaciers fed ice streams that were grounded below their contemporary sea level, and some were located as far south as 50° N. These calving-susceptible glaciers had been in extended positions for at least several millennia and so had reached isostatic equilibrium with the region's relatively thin lithosphere.

The situation was primed for rapid, iceberg-calving retreats at a time when eustatic sea level was beginning to rise.

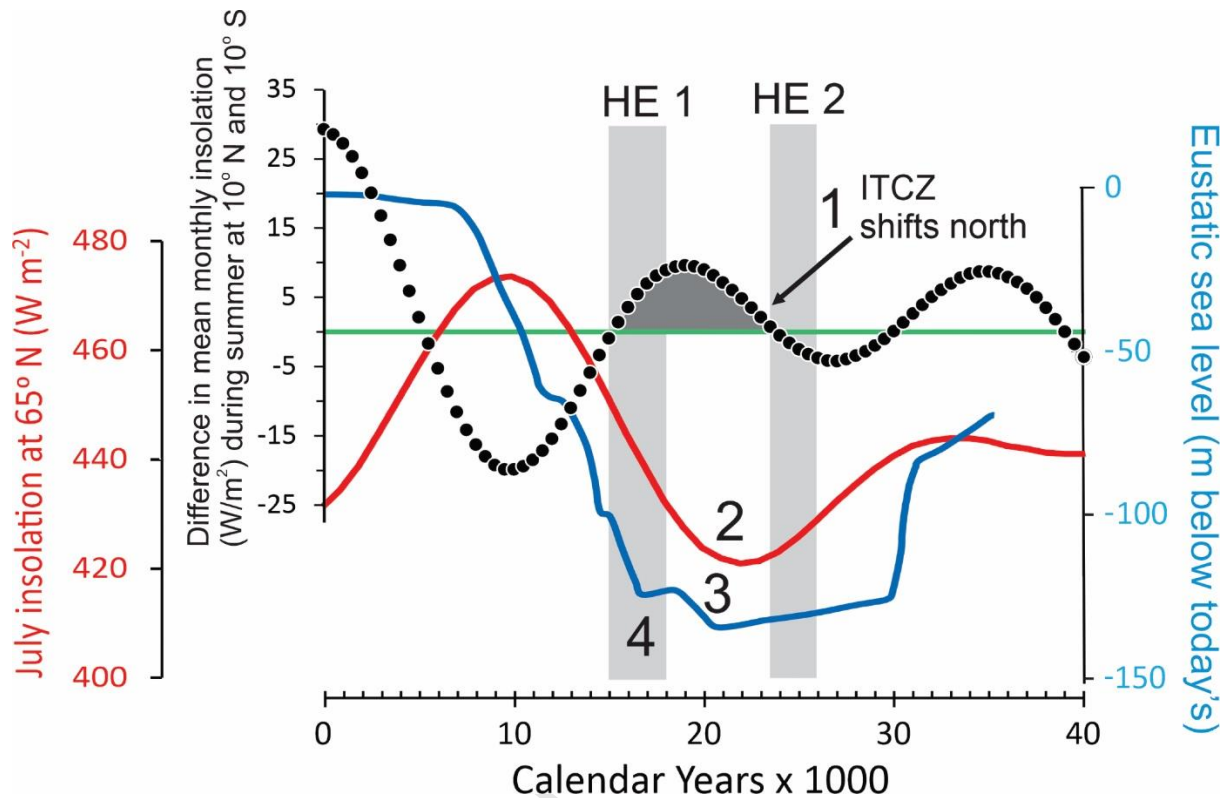


Figure 41. Setting the stage for Heinrich Event 1 (HE 1). **(1)** Beginning ca. 23 ka, Milankovitch orbital variations caused summer insolation to increase in the northern hemisphere tropics. In response, the Intertropical Convergence Zone (ITCZ) shifted northward, strengthening the Asian Summer Monsoon, which then transported more moisture and heat into the high-latitude North Pacific. **(2)** Ca. 22 ka, July insolation at 65°N began to increase and then ca. 21 ka, eustatic sea level started to rise **(3)** in response to ice-sheet melt. These phenomena combined to destabilize the marine-based glaciers fringing the Northwest Coast. According to the Walczak Hypothesis, meltwater and icebergs from these glaciers cooled the Gulf of Alaska and triggered Heinrich Event 1 **(4)**.

Continuing with the scenario described by the Walczak et al. (2020), the invigorated Asian Summer Monsoon freshened and warmed the surface waters of the subarctic Pacific, which steepened the halocline / thermocline there (Haug et al. 2005; Davies et al. 2011). This triggered widespread calving ablation of marine-based glaciers (Benn et al. 2007; Motyka et al. 2011) through the "Marcott Mechanism" (Fig. 43). The meltwater and icebergs from these retreating glaciers caused the expansion of sea ice in winter over some $3 \times 10^6 \text{ km}^2$ of the high-latitude North Pacific that today are perennially ice-free. The presence of this winter sea ice

displaced the Aleutian Low southwards and oriented it more zonally (Section 4.1.7). In response, winter temperatures and precipitation decreased across the northern sectors of the Northwest Coast and increased in the western USA.

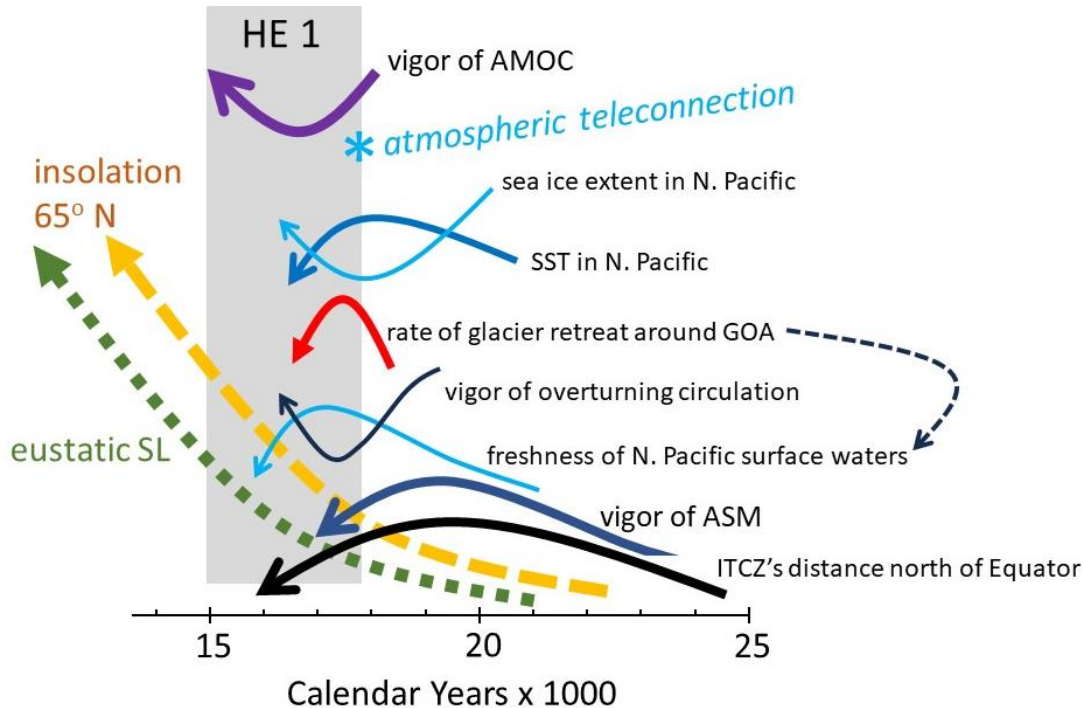


Figure 42. Heinrich Event 1 (HE 1) may have ultimately been triggered by changes in the tropical Pacific and the Gulf of Alaska. Strengthening of the Asian Summer Monsoon (ASM) beginning ca. 23 ka caused freshening of North Pacific surface waters, which reduced overturning circulation in the Gulf of Alaska (GOA). This triggered the rapid calving retreat of marine-based glaciers, which then added more freshwater, causing additional cooling and freshening accompanied by the spread of sea ice in winter. Cooling of the high latitude North Pacific was then communicated to the North Atlantic by an unidentified atmospheric teleconnection (though see Peteet et al., 1997), which cooled sea surface temperatures (SSTs) there and slowed Atlantic Meridional Overturning Circulation (AMOC). "SL" = sea level.

This idea that strengthening Asian Summer Monsoon (ASM) caused freshening of the subarctic Pacific is supported by Walczak et al.'s (2020) reconstruction of ocean circulation based on temporal patterns in the differences between the ^{14}C ages of benthic versus planktonic foraminifera (B-P) ages in a core located on the continental slope 75 km offshore of the Bering Glacier in the Gulf of Alaska (Fig. 35). Beginning ca. 18-19 ka, (B-P) ages diverged markedly, indicating a reduction in vertical mixing consistent with increased freshening of surface water. The rapid calving retreat of marine-based glaciers bordering the Gulf of Alaska is

recorded by widespread deposition of ice-rafted debris (IRD) between ca. 19 and 16 ka, with a peak of deposition ca. 17.5 ka (Fig. 6) (Walczak et al. 2020). These calving retreats were probably augmented by the gradual increase in solar insolation at high latitudes that began ca. 22 ka, and they were undoubtedly augmented by the progressive rise of eustatic sea level beginning ca. 21 ka (Fig. 41,42) (Section 2.2.2). The release of large amounts of meltwater from retreating, marine-based glaciers would have further accentuated the "Marcott Mechanism" (Fig. 43) and have contributed to enhanced sea ice cover across the subarctic Pacific during winter (Section 4.1.7), which would have contributed yet another positive feedback to the reduction of vertical mixing in winter and accentuation of glacier retreat (Chiang and Bitz 2005).

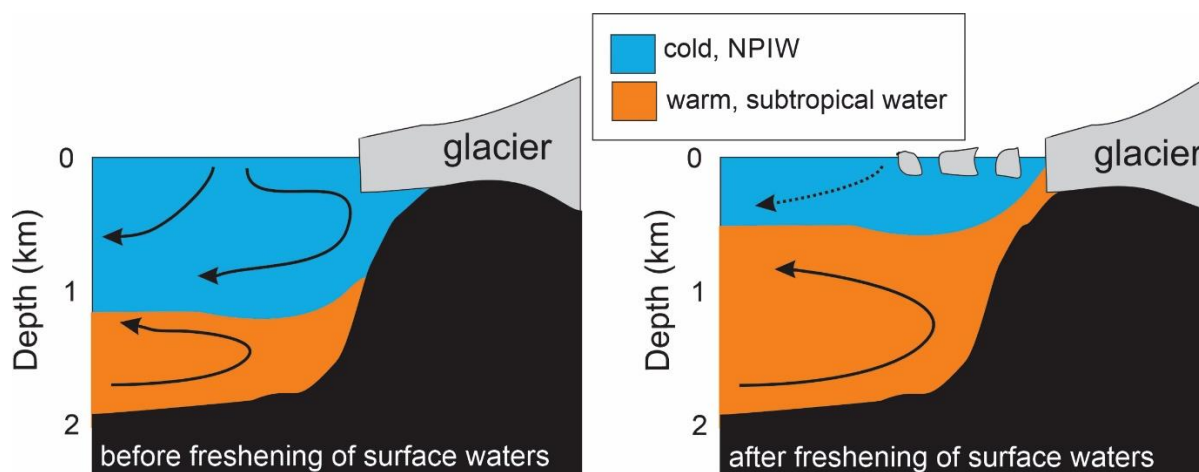


Figure 43. The "Marcott Mechanism". Reduction in overturning circulation can cause warmer ocean water to upwell along continental margins, where it can enhance the melting of marine-based glaciers. Once unseated from their terminal-moraine shoals, these glaciers may retreat rapidly through ice-berg calving without further stimulus from climate. Based on Benn et al. (2007), Marcott et al. (2011), Alvarez-Solas et al. (2013), Bassis et al. (2017). "NPIW" = North Pacific Intermediate Water.

4.1.10.2. Testing the Walczak Hypothesis

"...because of the limitations of age-model constraints in the North Pacific (related to poor knowledge of palaeo-reservoir ages), it is difficult to access the lead-lag relationship of North Pacific meltwater events with changes in the AMOC using proxy data." Maier et al (2018).

Dating accuracy is essential for testing the hypothesis that ocean/atmosphere changes in the Gulf of Alaska led the North Atlantic and triggered the global effects of Heinrich Events. Unfortunately, limited understanding of prehistoric marine reservoir ages makes it difficult to

assess lead-lag relationships between Atlantic Meridional Overturning Circulation, Heinrich Events, and meltwater events in the North Pacific (Maier et al. 2018).

A reservoir effect occurs when ^{14}C is depleted through radioactive decay while not being replaced by younger carbon (Stuiver and Braziunas 1993). Reservoir effects are often accentuated in the ocean because deepwater has only limited exchange with the new ^{14}C being formed in the upper atmosphere (Skinner et al., 2019). Water bodies differ in how isolated they are from the atmosphere (Matsumoto 2007), and so they vary in how depleted their ^{14}C contents are relative to the atmosphere (Alves et al. 2018). Today, marine-reservoir ages (MRAs) range from several centuries in low-latitude seas, to as much as several millennia in some polar seas (Butzin et al. 2017; Skinner et al. 2019). The larger the MRA is, the larger is ΔR , which is the difference between the local MRA and the modeled, global average MRA (Reimer 2012) (Fig. 44).

Anything that interferes with the vertical mixing of water between the ocean surface and the deep ocean can accentuate the reservoir effect (Alves et al. 2018). For example, a decline in how much C is fixed by photosynthesis in near-surface waters can increase the ΔR of the underlying water mass by reducing the amount of young, ^{14}C -rich organic matter being “pumped” downwards into deeper water in the form of dead organisms settling to the bottom. The shoaling or steepening of a halocline or thermocline can also increase the ΔR in deepwater by reducing overturning circulation. Covering the sea surface with sea ice is especially effective at increasing the ΔR of underlying water masses (Gordon and Harkness 1992; Butzin et al. 2017; Heaton et al. 2020). Also, glacial meltwater containing ancient, terrestrial organic matter can introduce ^{14}C -depleted water into ocean surface waters (Hutchinson et al. 2004; Cosma and Hendy 2008). All these phenomena are more frequent and widespread at high versus low latitudes, and, in the subarctic Pacific, all of them occurred more frequently during the ice age than during the Holocene (Hutchinson et al. 2004; Alves et al. 2018).

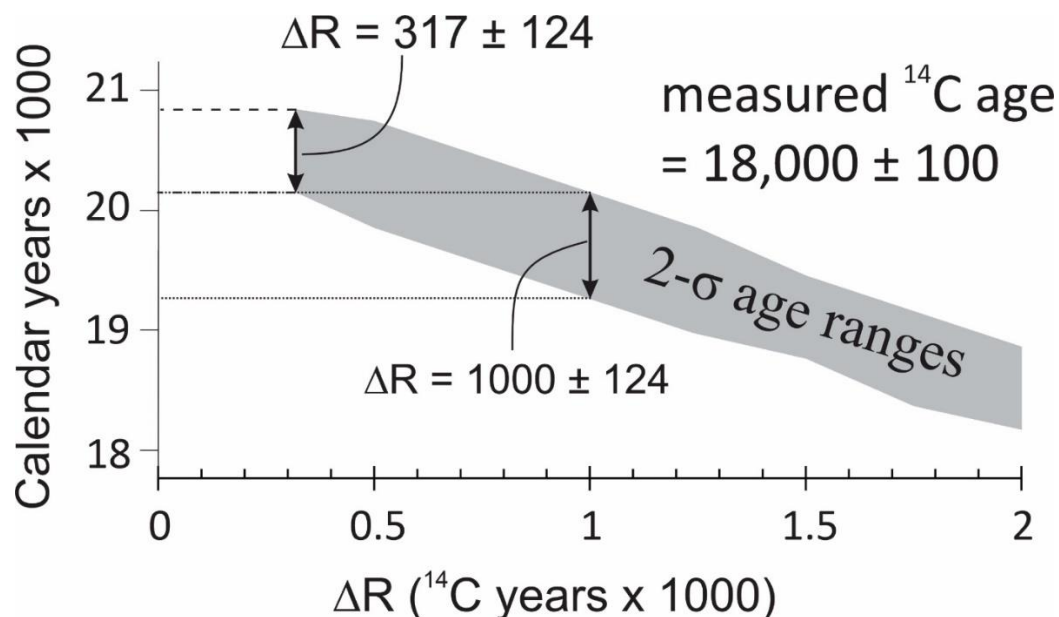


Figure 44. Marine-reservoir effects change ΔR , the difference in the ^{14}C contents of the marine-derived organic matter being radiocarbon dated and the contemporaneous ocean where it originated. The calendar age of a ^{14}C date becomes younger as ΔR increases. Shown here are the calibrated (calendar) age ranges of a hypothetical sample of marine carbon dated by ^{14}C to $18,000 \pm 100$ years. In this example, ΔR values vary between 317 years (the ΔR specified in the Calib 8.2 program's Marine20 database for the Southeast Alaska region) and 1000 years. Today, values of ΔR of 1000 years occur in some high-latitude oceans affected by sea ice and glacial meltwater (Stuiver et al. 1993; Hutchinson et al. 2004; Heaton et al. 2020).

Marine-reservoir effects complicate the calibration of ^{14}C dates obtained on organic carbon fixed by organisms in the sea (Reimer and Reimer 2017; Heaton et al. 2020). Two methods are typically used to estimate ΔR s and thereby correct for marine-reservoir effects. The first is by ^{14}C -dating marine samples of known age (e.g., museum collections of shells with precisely known dates of collection). The second is obtaining ^{14}C dates on paired terrestrial / marine samples found together at the same stratigraphic level (e.g., a pine needle and a bivalve shell within the same sedimentary unit) (Hutchinson et al. 2004; Alves et al. 2018; Hutchinson 2020). Based on the paired-sample approach, Schmuck et al. (2021) found that ΔR along the Northwest Coast declined from 575 ± 165 years during the Bølling/Allerød to -55 ± 110 years during the Younger Dryas, before increasing slightly over the course of the Holocene. To our knowledge, there are no published paired-sample records of ΔR from anywhere in the subarctic Pacific that pre-date $\sim 12,000$ ^{14}C yr BP (Schmuck et al. 2021).

Lacking the paired terrestrial-marine samples necessary to specify changes in marine reservoir ages (MRAs) prior to ca. 12 ka, Walczak et al. (2020) estimated ΔR values based on ocean-mixing models calibrated using modern mixing rates measured along pre-bomb depth

profiles of ^{14}C content in the subarctic Pacific. To assess the sensitivity of surface water ΔR s to changes in the MRA of pre-aged, deepwater entering the Gulf of Alaska as an underflow from the Southern Ocean, Walczak et al. (2020) varied the MRAs of this deepwater between 0 and 4000 yrs and then calculated the effect on the reservoir age of both benthic and surface waters. When ^{14}C -depleted deepwater increased in abyssal waters, benthic ages became older relative to planktic ages. This increased the ^{14}C age of the water that was upwelling in the subpolar gyre and advecting across the ocean surface, which caused planktic foraminifera ages to also become older. Modelling results suggested that changes in (benthic - planktic) ^{14}C ages (B-P ages) created surface reservoir ages 500 years older during the times in prehistory when the (B-P) age difference was largest, and 500 years younger when the age difference was least. Walczak et al. (2020) concluded that the planktic ΔR in the Gulf of Alaska has averaged 370 ± 350 years over the past 46 kyrs, which is within a decade of the last 200 years of surface-ocean ΔR in Southeast Alaska (Schmuck et al. 2021). Walczak et al. (2020) further concluded that the benthic ΔR in the Gulf of Alaska has averaged 1200 ± 600 over the past 46 kyrs.

Uncertainties in the marine-reservoir age (MRA) correction make it difficult to test the Walczak Hypothesis with the data at hand. Again, the oldest paired samples reported by Schmuck et al. (2012) date to only 12,000 ^{14}C yrs. In a companion study to the Walczak et al., (2020), Praetorius et al. (2020) attempted to validate the use of circa-modern values of ΔR by matching the timing of $\delta^{18}\text{O}$ records from foraminifera in the Gulf of Alaska with the calendar ages of the Bølling/Allerød and Younger Dryas. Both Walczak et al.'s (2020) modeling and Praetorius et al.'s (2020) wiggle-matching approaches for estimating paleo-MRAs and ΔR s assume stationarity in the pattern of vertical mixing in the North Pacific prior to ca. 14.7 ka, which is the onset of the Bølling-Allerød interstadial. Assuming stationarity in vertical mixing is problematic for several reasons. First, overturning circulation may have been more vigorous and widespread during the Last Glacial Maximum (LGM) in the North Pacific than it is today (Okazaki et al. 2010; Max et al. 2014; Rae et al. 2014; Rippert et al. 2017; Maier et al. 2018; Rae et al. 2020). Increased production of North Pacific Intermediate Water (NPIW) during the LGM implies a fundamentally different pattern of overturning circulation than what occurred during deglaciation and during the Holocene. Other complicating factors are that the (B-P) ages that Walczak et al. (2020) used come from relatively shallow water (670 m) on the upper continental shelf only 75 km offshore of the Bering Glacier. Major changes in circulation probably occurred as this and other glaciers retreated and as relative sea level rose 120+ m, which doubled the distance between the core site and the coastline.

Another reason why the assumption of stationarity in vertical mixing may be invalid prior to ca. 14.7 ka in the northeastern Gulf of Alaska is the presence of ice on the sea (Section 2.3). Extensive sea ice was present seasonally at this location during the coldest intervals of Marine Isotope Stage 2. It was probably a mixture of actual sea ice and icebergs; regardless, the presence of ice of either sort would have affected vertical mixing. Suppression of deep circulation by sea ice and by fresh surface water coming from melting glaciers would have

increased the marine reservoir ages of deepwater by reducing the exchange of ^{14}C across the sea surface and, possibly, by suppressing the biological pump.

Larger marine-reservoir ages (MRAs) mean that some parts of the chronology that the Walczak hypothesis is based upon may be too old by an undetermined amount. Based on the existing chronology, peak ice-rafted debris (IRD) deposition and minimum overturning circulation in the Gulf of Alaska led peak IRD deposition during Heinrich Event 1 (HE 1) in the North Atlantic by 1370 ± 550 years; however, some estimates of ice-age ΔR s in coastal waters of British Columbia and Washington range from 950-1200 yrs (Hutchinson et al. 2004) and possibly higher (Kovanen and Easterbrook 2002; Cosma and Hendy 2008). This magnitude of ΔR could reduce or even remove entirely the lead time of the North Pacific over the North Atlantic (Fig. 44). Compounding the problem is the uncertainty in the age of the HE 1 in the North Atlantic (Fig. 39), which makes it a moving target for comparisons with IRD deposition in the Gulf of Alaska.

In summary, if correct, the Walczak hypothesis fundamentally changes our understanding of how the ice-age planet functioned. It focuses attention on the tropic-subarctic teleconnections at work in the North Pacific that influenced the buildup and break-down of, the marine margin of the Cordilleran Glacier Complex, followed by the disintegration of the other boreal ice sheets. Testing this hypothesis requires an improved understanding of paleo-marine reservoir ages in the Gulf of Alaska.

4.2. Synthesis: The atmosphere/ocean/cryosphere system of the Northwest Coast and Northeast Pacific during Marine Isotope Stage 2 and its global interconnections

4.2.1. Overview

Many key processes that shaped the paleoenvironments of the Northwest Coast during Marine Isotope Stage 2 (MIS 2) are missing or diminished today. The Laurentide Ice Sheet and much of the Cordilleran Glacier Complex have vanished. Isostatic rebound is now mostly complete along the Northwest Coast (Section 2.2.1), leaving only localized responses to Little Ice Age deglaciation (Hu and Freymueller 2019). Along with the ice sheets went the glacial outburst floods and the flotillas of ice bergs, with the result that Atlantic Meridional Overturning Circulation is now relatively stable. The position of the Intertropical Convergence Zone, which during the Last Glacial Maximum was geographically fickle (Section 4.1.10), is also relatively stable, as is the rhythm of ENSO. Offshore, the absence of sea ice in the North Pacific, other than in the Bering Sea and Sea of Okhotsk, has reduced the capacity for the production of Intermediate Water (Section 4.1.8), which has stabilized the overall circulation of the North Pacific. Compared with MIS 2, the Holocene has been impoverished in terms of climate change. What was the sequence of events that brought the Northwest Coast out of its dynamic ice-age state into the more stable, Holocene one? What follows is a scenario of what might have happened from a global perspective, with the focus on the Northwest Coast.

4.2.2. The onset of Marine Isotope Stage 2 and the Last Glacial Maximum

Glacier cover increased in the northern hemisphere starting ca. 32 ka, probably in response to reduced summer insolation at both high and low, northern latitudes (Section 4.1.1). As ice sheets grew, eustatic sea levels fell, and blocking highs occurred more frequently over western Canada (Section 3.2). Once the Laurentide Ice Sheet had grown to its maximum extent between 24 and 21 ka, the polar jet tended to split north and south around it, which reduced the frequency of cyclonic storms reaching Southeast Alaska, Haida Gwaii, and the Pacific Northwest, causing a decline in snowfall there. This pattern of a blocking high over the western Cordillera accompanied by deep low in the Northeast Pacific corresponds to today's negative phase of the Arctic Oscillation (Section 7.1.3) and to the positive phase of the Pacific-North American Pattern, which tends to accompany drier winters in the Pacific Northwest and snowier winters in western Alaska.

Between ca. 24 and 21 ka, the northern branch of the polar jet probably looped across the exposed continental shelf of the Bering Sea, while the southern branch followed a southward-diverted path similar to the one it follows today when Eastern Pacific Warm-El Niños coincide with positive phases of the Pacific Decadal Oscillation (PDO+) (Section 7.1.3). A major difference was that during Marine Isotope Stage 2, this southern, precipitation-dipole pattern was probably a persistent feature lasting for millennia, rather than just for several years as it does today. The resulting increase in winter precipitation in the western USA, combined with cooling caused by proximity of the Cordilleran Glacier Complex and the Laurentide Ice Sheet, caused pluvial lakes to form (Section 3.5).

At the same time that chronic Eastern Pacific Warm-El Niño conditions (Section 4.1.5) caused a persistent positive phase of the Pacific Decadal Oscillation in the Northeast Pacific, the vigor of the Asian Summer Monsoon (ASM) declined (Section 4.1.3). The ASM experienced several major reductions, and these coincided with reduced overturning circulation in the Gulf of Alaska as revealed by minima in (Benthic-Planktic) ^{14}C ages (B-P) (Fig. 35). These (B-P) minima reflect weakening of the halocline in response to less freshwater being carried into the high-latitude North Pacific by the extratropical cyclonic storms usually fueled by the ASM (Section 4.1.2 and 8.1.2.2). This reduction of ASM-related moisture import, in conjunction with the diversion of storm tracks away from the eastern Gulf of Alaska, was probably why local Last Glacial Maxima along the Northwest Coast lagged most sectors of the Laurentide Ice Sheet (Section 2.1.5). This lag was most pronounced from Southeast Alaska southward, perhaps because colder temperatures further north in the Alaska Range compensated for drier conditions there and allowed glacier growth despite the reduced snowfall (Section 3.4).

Cooler sea surface temperatures (SSTs) in the Gulf of Alaska between 24 and 21 ka (Fig. 34) were accompanied by an expansion of sea ice north of $\sim 55^\circ\text{N}$ (Section 2.3). Sea ice was most widespread in the northwestern subarctic Pacific and the Bering Sea. Colder sea surfaces,

reduced precipitation, and the presence of perennial sea ice would have augmented the production of North Pacific Intermediate Water (NPIW). This increase in overturning circulation, albeit always much less than Atlantic Meridional Overturning Circulation even during the latter's minima, probably drew significant amounts of subtropical water into the subarctic Pacific at intermediate depths (Section 4.1.8). This influx of heat was probably responsible for warming SSTs in the Gulf of Alaska between ca. 22 and 20 ka (Fig. 34) (Section 3.1).

The onset of the Last Glacial Maximum after 30 ka accompanied a steepening of the insolation gradient between the tropics and the Arctic during winter months (Section 4.1.1). Steepening of this gradient intensified the transport of oceanic heat and atmospheric moisture from the tropical North Pacific to the subarctic Pacific. The gradient was steepest ca. 22-23 ka, which coincided with the maximum extent of the Laurentide Ice Sheet (LIS) (Fig. 16). After ca. 22 ka, the meridional gradient in winter insolation declined rapidly, reaching a minimum ca. 12 ka. As the winter insolation gradient declined, the meridional gradient in summer insolation steepened. Many glaciers in the Cordilleran Glacier Complex expanded to their maximum extents after the trajectories in these changing gradients crossed ca. 19 ka (Fig. 32). The ideal conditions for glacier growth around the Gulf of Alaska margin probably occurred ca. 19 ka when the insolation gradients between the tropics and the subarctic were steep during both winter and summer, which caused both abundant winter snowfall and persistent summer cloudiness. At the same time, the orographic effects of the LIS that diverted storm tracks away from the Northwest Coast were waning, and the Asian Summer Monsoon was experiencing a short-lived peak (Fig. 35).

4.2.3. Deglaciation begins

By 21 ka, the Northern Hemisphere ice sheets had undergone net growth for ~ 100 kyrs, and had accumulated most of the total eustatic drawdown (Denton et al. 2010). Sufficient time had passed for maximum isostatic depression to occur. Thus, a maximum amount of "excess ice" had accumulated (Raymo 1997), and this ice was flowing seaward across isostatically depressed continental shelves to terminate along marine-based margins. In this situation, outlet glaciers and ice sheets were vulnerable to catastrophic calving retreats triggered by a combination of rising eustatic sea level, and warming ocean temperatures. Meanwhile, starting ca. 21 ka, summer insolation started to increase at high northern latitudes, and the gradient between low- and high-latitude summer insolation steepened (Fig. 32). Strong baroclinicity implies vigorous cyclogenesis along the Subarctic Front in the North Pacific (Section 7.1.2.2), which entails large amounts of latent heat arriving at high latitudes within extratropical cyclones. At the intersection of these events, a grand ice-age termination was probably inevitable.

Deglaciation caused an influx of meltwater and ice bergs into the boreal oceans. In response, eustatic sea level rose and sea surface temperatures (SSTs) cooled in the subarctic

Pacific and North Atlantic. This caused a major expansion in winter sea ice (Denton et al., 2010; 2022), even as waters at intermediate depths warmed and caused further retreat of marine-based glaciers (Fig. 43). Freshening surface waters and cooling SSTs suppressed overturning circulation, which declined in both boreal oceans. This change shows up in the Gulf of Alaska ca. 19-17 ka as an increase in (Benthic - Planktonic) ^{14}C ages (Fig. 35). Meanwhile in the Southern Ocean, the circum-Antarctic belt of winter sea ice shrank, and the Austral Westerlies strengthened (Denton et al. 2010), which enhanced the release of CO_2 from the ocean to the atmosphere (Fig. 45). From this point onward, the continued rise of CO_2 contributed increasingly to global deglaciation (Shakun et al. 2012).

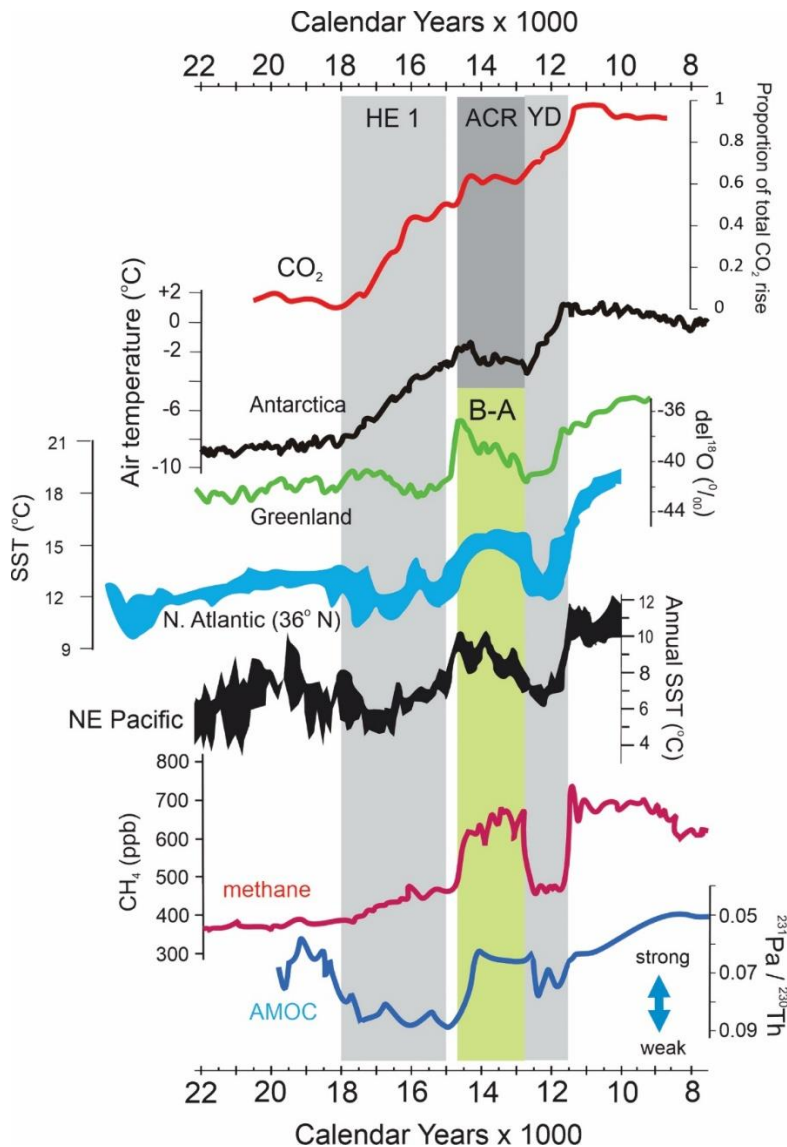


Figure 45. Global events during the last deglaciation. **A.** Atmospheric CO_2 concentrations are from Marcott et al. (2014). **B.** Antarctic surface temperatures are from Parrenin et al. (2013) and Bereiter et al. (2018). **C.** Greenland surface temperatures are from the NGRIP Ice Core

plotted on the GICC05 age scale (Svensson et al. 2008). **D.** North Atlantic sea surface temperatures (SSTs) at 36° N are from Martrat et al. (2014). **E.** Northeast Pacific SSTs are from Praetorius et al. (2023). **F.** Atmospheric methane (CH₄) data are from the WAIS Divide Ice Core (Rhodes et al. 2015; Bereiter et al. 2018). **G.** The record of Atlantic Meridional Overturning Circulation (AMOC) is from Bereiter et al. (2018). "HE 1" = Heinrich Event 1. "ACR" = Antarctic Cold Reversal. "YD" = Younger Dryas. "B-A" = Bølling-Allerød interstadial.

4.2.4. Henrich Event 1

The global, fine structure of Heinrich Event 1 (HE 1) provides a type example of ice-age modes of climate change and highlights key processes involved. HE 1 lasted from ~ 18 to ~ 15 ka and interrupted the CO₂-enhanced progression of global deglaciation. According to the canonical, Atlantic-centric interpretation, HE 1 began with a cooling of sea surface temperatures (SSTs) caused by the discharge of massive amounts of meltwater and icebergs into the North Atlantic in response to increasing summer insolation at high northern latitudes (Denton et al. 2005; Denton et al. 2010; Denton et al. 2022). Another possibility is that for reasons unknown, the cooling trend in the North Atlantic in which HE 1 was embedded began 10²-10³ yrs prior to the onset of intense iceberg calving (Max et al. 2022). Whatever its proximate cause, cooling SSTs slowed Atlantic Meridional Overturning Circulation (AMOC) and initiated the Marcott Mechanism of ice-sheet retreat (Fig. 43). The retreat of marine-based glaciers was further enhanced by a combination of rising eustatic sea level, increasing summer insolation at high northern latitudes, and enhanced heat transport in response to a steepening Equator to Subarctic gradient in summer insolation (Section 4.1.1). As the influx of icebergs and meltwater increased, SST cooled further in the North Atlantic and Gulf of Alaska.

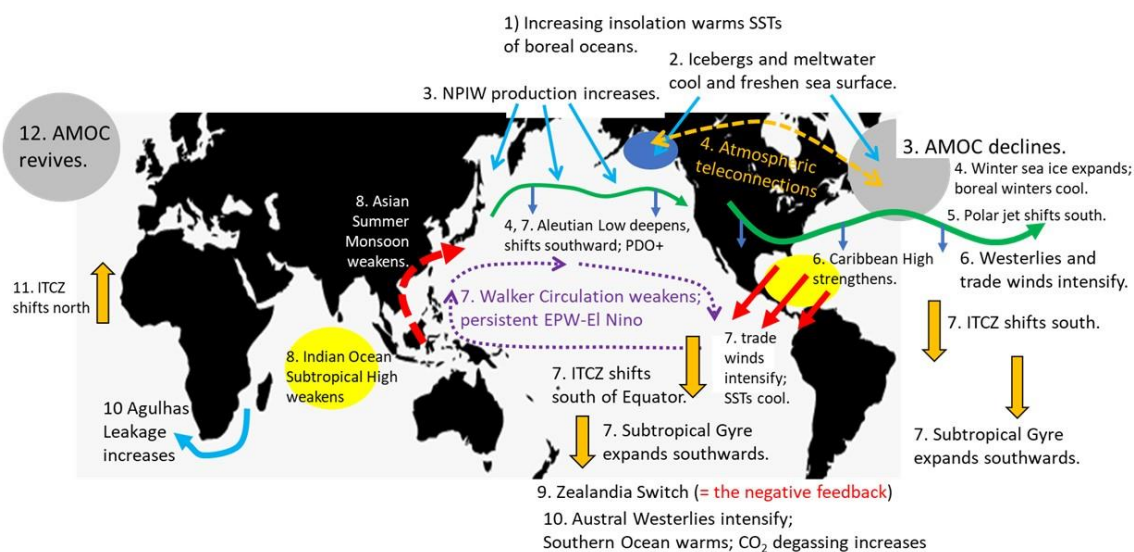


Figure 46. A possible sequence of events during Heinrich Event 1. A similar, but less pronounced cycle of cryosphere-atmosphere-ocean interactions may have occurred during the Younger Dryas. The Walczak Hypothesis asserts that the initial step was a strengthening of the Asian Summer Monsoon, which set off the retreat of glaciers along the Northwest Coast, which then caused the cooling of both boreal oceans. The negative feedback on global cooling triggered by the Zealandia Switch is described in detail by Denton et al. (2021). "AMOC" = Atlantic Meridional Overturning Circulation. "ITCZ" = Intertropical Convergence Zone. "SST" = sea surface temperature. "NPIW" = North Pacific Intermediate Water. "PDO+" = positive phase of Pacific Decadal Oscillation. "EPW-El Niño" = Eastern Pacific Warm-El Niño.

If the alternate, Walczak hypothesis is correct, the ultimate cause for ocean cooling at high northern latitudes at the onset of Heinrich Event 1 lay in the tropics, not at high latitudes (Section 4.1.10). Strengthening of the Asian Summer Monsoon (ASM) starting ca. 21 ka may have triggered glacial retreat along the Gulf of Alaska margin. An expansion of sea ice followed, which caused further sea-surface cooling and further glacier retreat, again through the Marcott Mechanism. This influx of freshwater into the Gulf of Alaska would have revved-up the Alaska Coastal Current (Royer and Finney, 2020), particularly between ca. 22 and 16.4 ka (Praetorius et al., 2023). Along the Northwest Coast, isostatic rebound accentuated the destabilizing effects that rising sea level had on marine-based glaciers by displacing meltwater seaward (Pan et al. 2021). Cooling in the subarctic Pacific was then teleconnected via the atmosphere (Petee et al., 1997) to the North Atlantic, where it initiated the shutting down of Atlantic Meridional Overturning Circulation, which then triggered the full, global impacts of Heinrich Event 1 (Fig. 46).

Regardless of whether the North Atlantic or the Northeast Pacific was the trigger point for Heinrich Event 1, meridional heat transport declined in the Northern Hemisphere as Atlantic Meridional Overturning Circulation (AMOC) slowed. In response, sea ice expanded across the North Atlantic in winter (Denton et al. 2005), and the Intertropical Convergence Zone shifted southward (Chiang and Bitz 2005; Bradley and Diaz 2021) (Fig. 46). Once AMOC had weakened significantly, the entire Northern Hemisphere cooled (Wu et al. 2008; Maier et al. 2018). The expansion of sea ice in winter was probably key in promulgating what started in the North Atlantic (alternatively, in the Gulf of Alaska) to the rest of the planet (Denton et al. 2005; Denton et al. 2010; Denton et al. 2022).

In response to the southward shift of the Intertropical Convergence Zone (ITCZ) over the Equatorial Atlantic, trade winds intensified north of the Equator, which displaced the Pacific ITCZ southwards and weakened both the Hadley Circulation (Chiang et al. 2014) and the Walker Circulation (Koutavas et al. 2002) (Fig. 46). This probably strengthened the already persistent Eastern Pacific Warm-El Niño phase of ENSO in the Equatorial Pacific (Section 4.1.5). It probably also have weakened the Asian Summer Monsoon (ASM) (Section 4.1.3), which then reduced cyclogenesis, which in turn reduced heat and moisture export to the high-latitude North Pacific.

Another effect of a reduced ASM would have been weakening of the Indian Ocean Subtropical High, which would have caused a decline in the Agulhas Leakage, which then further suppressed Atlantic Meridional Overturning Circulation by reducing the amount of salty, tropical water entering the North Atlantic from the Indian Ocean (Beck et al. 2018). Eventually, the poleward displacement of the subtropical gyres in the Southern Ocean caused the belt of Austral Westerlies to narrow and intensify. Once the Austral Westerlies shifted south of Aotearoa-New Zealand, a negative feedback (the "Zealandia Switch") was activated (Denton et al., 2021), which then enhanced overturning circulation in the Southern Ocean, warmed sea surface temperatures there, and triggered the release of enormous amounts of CO₂ into the atmosphere (Fig. 45).

Floods issuing from the Columbia River basin and from the Copper River basin in southern Alaska entered the North Pacific intermittently during the deglacial period (Section 4.1.9). Some of these floods cooled the North Pacific, possibly to the extent of triggering responses in the North Atlantic via atmospheric teleconnections. However, direct effects of this Columbia basin freshwater on Atlantic Overturning Circulation were limited because flow through Bering Strait remained minor until sometime after 11 ka (Section 4.1.6).

4.2.5. Aftermath of Heinrich Event 1

Heinrich Event 1 (HE 1) ended as marine-based glaciers retreated onto land, reducing the supply of icebergs and meltwater, which reduced sea ice cover in winter, at the same time that increasing amounts of CO₂ and CH₄ were being released into the atmosphere (Fig. 45), and solar insolation was steadily increasing (Fig. 31, 41). As HE 1 ended, sea surface temperatures (SSTs) warmed across the North Atlantic and North Pacific, Atlantic Meridional Overturning Circulation revived (Fig. 45), and the production of North Pacific Intermediate Water decreased (Section 4.1.8). Because the gradient in latitudinal insolation continued to steepen over the North Pacific (Fig. 32), more frequent cyclonic storms probably arrived over the Northwest Coast. Together with the reinvigoration of the Asian Summer Monsoon (Section 4.1.3), this increased the advection of moisture over the subarctic Pacific, which freshened the Gulf of Alaska and further strengthened the halocline there.

After Atlantic Meridional Overturning Circulation (AMOC) resumed abruptly ca. 14.7 ka at the outset of the Bølling-Allerød interstadial, CH₄ concentrations rose rapidly in the atmosphere (Fig. 45), probably mainly in response to the reinvigoration of the Asian Summer Monsoon, which tracked the rise of summer insolation and peaked ca. 10 ka (Fig. 33). The establishment of an ENSO regime similar to today's saw a reduction in the occurrence of Eastern Pacific Warm-El Niños and removed the persistent dipole pattern of winter precipitation over the western USA. This caused pluvial lakes in the Southwest USA to dessicate.

Air temperatures rose dramatically throughout the Arctic as CO₂ levels progressively rose (Fig. 45). Holocene-like temperature were reached in the northern hemisphere between

14.6 and 12.9 ka at a time when the Southern Hemisphere was experiencing gradual cooling during the Antarctic Cold Reversal. Estimates of sea surface temperatures in the Gulf of Alaska suggest they peaked ca. 14 ka and then gradually cooled to near full-glacial conditions ca. 12 ka during the Younger Dryas chronozone.

It seems increasingly likely that the Younger Dryas (YD) was a winter phenomenon (Fig. 27). Cooler, drier winters during the YD in southern Alaska would explain the apparent lack of advances by coastal glaciers as well the subtlety and geographical variability of the paleobotanical signal (Section 3.3). Cooler, drier conditions in the Gulf of Alaska imply a southward-shifted Aleutian Low (AL), which is consistent with advances and standstills of alpine glaciers in the western USA during the YD (Marcott et al. 2019; Barth et al. 2022). Southward diversion of the AL is also consistent with the partial re-wetting of the western USA during the YD (Section 3.5) (Pigati and Springer 2022).

5. RESEARCH NEEDS

5.1. Testing the Extreme Winter Hypothesis

The Extreme Winter hypothesis (Fig. 27) was proposed by Denton et al. (2005, 2010, 2021, 2022) to resolve the Mercer Paradox, the observation that during Marine Isotope Stage 2, mountain glaciers in the two polar hemispheres fluctuated in synchrony even though Milankovitch orbital forcing was asynchronous there. Extreme winters and mild, steadily ameliorating summers may explain the enigmatic records of climate during the Younger Dryas chronozone along the Northwest Coast (Section 3.3).

Testing the extreme winter hypothesis at sites along the Northwest Coast requires proxy data that specify winter climate. Oceanographic proxies for sea surface temperature (Fig. 24) do not resolve summer conditions well, nor do the glacial geological records, nor do many climate-models. Possibilities for winter-climate proxies include pollen and plant macrofossil records from coastal tundra and high alpine sites where plants were strongly affected by winter winds and/or snow depth. Another possibility is reconstructing the growth rates of ice wedges during, before, and after the Younger Dryas (YD). Other possibilities include reconstructing the changing duration of ice-cover in lakes and ponds and constructing time series of ice-push ridges on lake shores (e.g., Berg et al. 2022). The ideal data set would be a record of sea ice cover in an embayment like Prince William Sound where winter cooling might have caused varying amounts of sea ice to form over the course of the YD.

6.2. North Pacific Sea Ice

The extent and timing of sea ice cover in the North Pacific during the Last Glacial Maximum and last deglaciation remain uncertain. This information is crucial for reconstructing

oceanic and atmospheric circulations. Because sea ice can impact the dynamics of overturning circulation, these data are also needed to understand the time course of CO₂ release from North Pacific deepwater during deglaciation.

The main change in sea ice dynamics in the North Pacific involved seasonal (winter) ice. Given the relatively sensitive nature of the subarctic Pacific's halocline and thermocline today (Section 7.1.1.3), did changes in sea-ice cover affect overturning circulation? In the Southern Ocean today, the formation / melting of sea ice affects the surface buoyancy flux (Watson et al. 2015). Perennially ice-covered areas have a negative buoyancy flux conducive to overturning circulation, while areas covered by seasonal ice have a positive flux, which (other factors like wind-stirring being equal) tends to resist overturning circulation. What impacts, if any, did changing sea-ice coverage have on overturning circulation during Marine Isotope Stage 2 in the high-latitude North Pacific?

6.3. Testing the Walczak Hypothesis

It is a compelling idea that the 3500-km long, marine-based margin of the Cordilleran Glacier Complex served as the hair trigger for global deglaciation; however, the dating control upon which Walczak et al.'s (2020) hypothesis rests needs careful scrutiny. Specifically, we need to know how the marine-reservoir effect varied between 30 and 15 ka. One approach to do this would be to use chemically fingerprinted tephra layers (e.g., Austin et al. (1995)) that can be precisely ¹⁴C-dated onshore using plant macrofossils and then be traced offshore, where they can serve as chronological markers in marine cores. Ideally, such paired dates would document marine reservoir ages over the entire span of Marine Isotope Stage 2 (MIS 2). This approach requires ice-free areas that accumulated tephras throughout MIS 2. Sites containing multiple tephras preserved in organic-rich pond sediment dating back to 17-18 ka exist at Low Cape on southwestern Kodiak Island (Mann and Peteet (1994) (Fig. 12), and possibly on Sanak Island (Misarti et al., 2016) (Fig. 14). Deglaciation probably occurred even earlier on Chirikof Island at the seaward end of the Shelikof Trough (Fig. 13).

6.4. Ice-free Areas; Glacial Refugia

Ice-free areas undoubtedly existed along the Northwest Coast during Marine Isotope Stage 2; however, being ice-free did not equate to being a biological refugium. Changing glacier extent and fluctuating sea level meant that ice-free areas were often small, transient, and widely separated. Many were probably too small, too transient, and had too harsh a climate to support organisms. Evidence for the existence of small refugia that shifted their locations over time has proved elusive, even in Scandinavia where the topic of glacial refugia has been researched for more than a century (Kullman 2004; Birks and Willis 2008; Alsos et al. 2020). Even if organisms did survive in an ice-free area, species diversity was probably low and restricted to arctic-alpine taxa that were unimportant in colonizing post-glacial landscapes. This does not mean that refugia are not of interest. The point is that identifying them will require a

higher level of research effort. This challenge is made clear by the fact that despite decades of state-of-the-art, interdisciplinary investigation, it remains unclear if, when, and exactly where a biological refugium existed on Haida Gwaii (Section 2.1.3.4).

The Alexander Archipelago is another area of the Northwest Coast where biological refugia have long been sought. Despite a much-improved understanding of the deglaciation chronology of Southeast Alaska (Lesnek et al., 2020; Baichtal et al., 2021; Walcott et al. 2022), it remains uncertain whether the outer coastline of the archipelago and adjacent continental shelf were totally covered by glacial ice during the local Last Glacial Maximum. The limited number geomorphic surfaces that have been dated, combined with the mountainous topography, makes it possible that some locations did in fact remain ice free and subaerial. The reconstructions of Carrera et al. (2007) and Lesnek et al. (2020) continue to seem reasonable in concept if not detail. Between the ice streams issuing from the major fjord systems, high coastal topography would have created “ice shadows” in their lee, particularly where a narrow shelf and/or deepwater prevented the accumulation of thick glacial ice (e.g., (Vorren et al. 2015; Barrie et al. 2021) (Fig. 47). It seems likely that scattered ice-free areas flickered in and out of existence along the outer coast of the Alexander Archipelago and on the adjacent continental shelf. A first step in testing this idea is to reconstruct how relative sea levels and equilibrium-line altitudes changed along this coastline over the course of the Last Glacial Maximum and deglaciation.

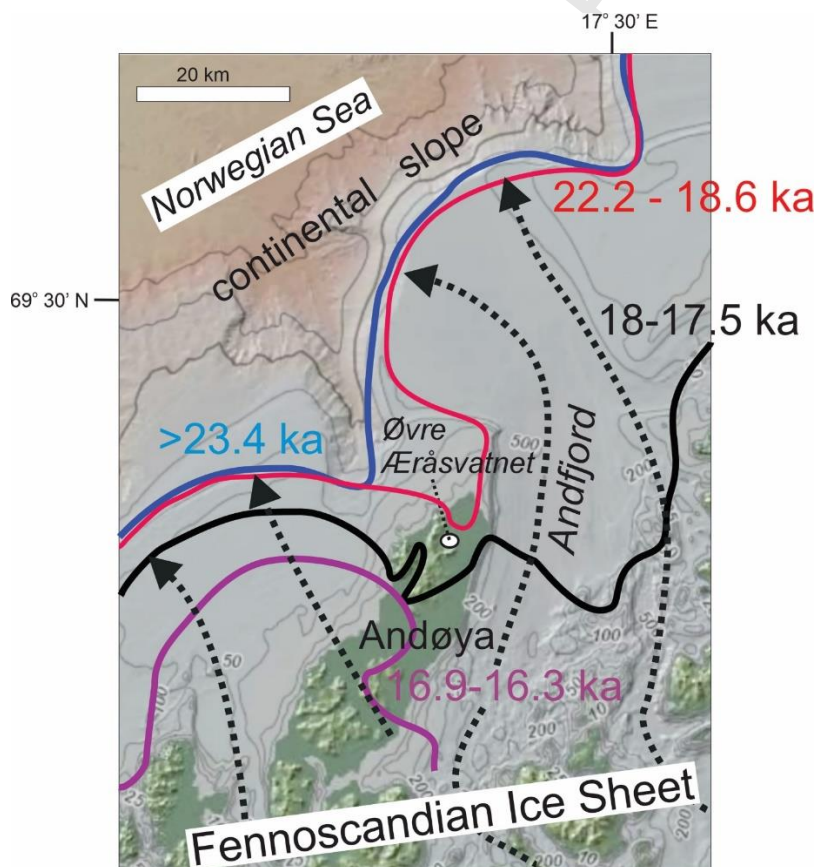


Figure 47. An iconic outer coast refugium: Andøya in northwest Norway during Marine Isotope Stage 2 (Vorren et al. 2015). Areas with similar geography existed along the Northwest Coast and may have experienced similar glacial and refugial histories. The northern end of Andøya is located < 10 km from the outer edge of the continental shelf. Calving of icebergs into the Norwegian Sea limited the buildup of grounded ice there, and low mountains partially shielded the northern end of Andøya from glaciers flowing from the interior. The area around Øvre Æråsvatnet was possibly deglaciated as early as 26.7 ka (Alsos et al. 2020), and it probably served as a biological refugium through the remainder of the ice age (Birks et al. 2014). Glacial limits and their ages are from Vorren and Plassen (2002) and Vorren et al. (2015). The base map is from the National Centers for Environmental Information, Bathymetric Data Viewer, <https://www.ncei.noaa.gov/maps/bathymetry/>.

6.5. Reconstructing Paleo-Teleconnections

Today, tropical phenomena like ENSO strongly influence the climate of the Northwest Coast (Section 7.1.3). Throughout this review, we have assumed that tropical teleconnections also operated along the Northwest Coast during the ice age, but how they functioned remains unclear because critical boundary conditions like sea ice extent and the topography of North American ice masses were fundamentally different then. The Pacific Decadal Oscillation (PDO) (Section 7.1.3.2) is probably of most interest because of its importance today in the weather and climate of downwind North America and because of its teleconnections to Eastern Pacific Warm-El Niños (EPW- El Niños), which are thought to have been frequent during the coldest periods of Marine Isotope Stage 2 (Section 4.1.5). In conjunction with EPW-El Niños, the PDO probably spent long intervals in its positive phase; however, because of the expansion of winter sea ice in the Gulf of Alaska, the PDO's associated sea surface temperature and winter-precipitation patterns may have shifted southwards along the western coast of North America. Testing this hypothesis would involve reconstructing proxy records of winter storminess along the coastline between Washington and California. During recent centuries, the PDO has left a winter signature in the form of storm-damaged trees along the Northwest Coast (Gaglioti et al. 2019). Similar records of winter damage could be reconstructed from subfossil wood recovered from sites along the unglaciated, western coast of the USA. Varying amounts of winter precipitation caused by shifts in the location and vigor of the Aleutian Low (e.g., Gaglioti et al. 2017) under the influence of the PDO probably also left isotopic records in plant material deposited in lakes and bogs along the Northwest Coast (Anderson et al. 2016).

6.6. Global Impacts of CO₂ Degassing from the Abyssal North Pacific during Deglaciation

When and how much CO₂ was released from the North Pacific's deepwater after ca. 20 ka? Addressing these questions requires first resolving the ongoing controversy over the extent and timing of deep, overturning circulation in the subarctic Pacific during Marine Isotope Stage

2. To do this, more time series of (Benthic - Planktonic) foraminifera ^{14}C ages are needed in order to reconstruct the history of changes in deep, overturning circulation. As described in Section 6.3, obtaining age control for these time series requires paired, terrestrial-marine ^{14}C dates. To minimize complications arising from glacial meltwater and icebergs, the core sites need to be far offshore, perhaps in places like the Patton Sea Mount.

7. REFERENCES CITED

- Abdul, N., Mortlock, R., Wright, J., and Fairbanks, R. 2016. Younger Dryas sea level and meltwater pulse 1B recorded in Barbados reef crest coral *Acropora palmata*. *Paleoceanography* 31(2): 330-344. doi:<https://doi.org/10.1002/2015PA002847>.
- Ager, T.A., and Phillips, R.L. 2008. Pollen evidence for late Pleistocene Bering land bridge environments from Norton Sound, northeastern Bering Sea, Alaska. *Arctic, Antarctic, and Alpine Research* 40(3): 451-461. doi:[https://doi.org/10.1657/1523-0430\(07-076\)\[AGER\]2.0.CO;2](https://doi.org/10.1657/1523-0430(07-076)[AGER]2.0.CO;2).
- Ager, T.A., and Rosenbaum, J.G. 2009. Late glacial-Holocene pollen-based vegetation history from Pass Lake, Prince of Wales Island, southeastern Alaska. *In Studies by the U.S. Geological Survey in Alaska, 2007. Edited by P.J. Haeussler and J.P. Galloway. US Geological Survey. pp. 1-19.*
- Ager, T.A., Carrara, P.E., Smith, J.L., Anne, V., and Johnson, J. 2010. Postglacial vegetation history of Mitkof Island, Alexander Archipelago, southeastern Alaska. *Quaternary Research* 73(2): 259-268. doi:<https://doi.org/10.1016/j.yqres.2009.12.005>.
- Ager, T.A. 2019. Late Quaternary vegetation development following deglaciation of northwestern Alexander Archipelago, Alaska. *Frontiers in Earth Science* 7: 104. doi:<https://doi.org/10.3389/feart.2019.00104>.
- Al-Suwaidi, M., Ward, B., Wilson, M., Hebda, R.J., Nagorsen, D.W., Marshall, D., Ghaleb, B., Wigen, R., and Enkin, R. 2006. Late Wisconsinan Port Eliza Cave deposits and their implications for human coastal migration, Vancouver Island, Canada. *Geoarchaeology: an International Journal* 21(4): 307-332. doi:<https://doi.org/10.1002/gea.20106>.
- Alaska, F.S.C. 2023. AFSC/RACE/GAP/Zimmermann: Aleutians Bathymetry Grid from 2010-06-15 to 2010-08-15. NOAA National Centers for Environmental Information. doi:<https://www.fisheries.noaa.gov/inport/item/22164>.
- Alexander, M.A., Bladé, I., Newman, M., Lanzante, J.R., Lau, N.-C., and Scott, J.D. 2002. The atmospheric bridge: The influence of ENSO teleconnections on air-sea interaction over the global oceans. *Journal of climate* 15(16): 2205-2231. doi:[https://doi.org/10.1175/1520-0442\(2002\)015%3C2205:TABTIO%3E2.0.CO;2](https://doi.org/10.1175/1520-0442(2002)015%3C2205:TABTIO%3E2.0.CO;2).

Alexander, M.A., Bhatt, U.S., Walsh, J.E., Timlin, M.S., Miller, J.S., and Scott, J.D. 2004. The atmospheric response to realistic Arctic sea ice anomalies in an AGCM during winter. *Journal of Climate* 17(5): 890-905. doi:[https://doi.org/10.1175/1520-0442\(2004\)017%3C0890:TARTRA%3E2.0.CO;2](https://doi.org/10.1175/1520-0442(2004)017%3C0890:TARTRA%3E2.0.CO;2).

Allen, B.D., and Anderson, R.Y. 2000. A continuous, high-resolution record of late Pleistocene climate variability from the Estancia basin, New Mexico. *Geological Society of America Bulletin* 112(9): 1444-1458. doi:[https://doi.org/10.1130/0016-7606\(2000\)112%3C1444:ACHRRO%3E2.0.CO;2](https://doi.org/10.1130/0016-7606(2000)112%3C1444:ACHRRO%3E2.0.CO;2).

Alsos, I.G., Sjögren, P., Brown, A.G., Gielly, L., Merkel, M.K.F., Paus, A., Lammers, Y., Edwards, M.E., Alm, T., and Leng, M. 2020. Last Glacial Maximum environmental conditions at Andøya, northern Norway; evidence for a northern ice-edge ecological “hotspot”. *Quaternary Science Reviews* 239: 106364. doi:<https://doi.org/10.1016/j.quascirev.2020.106364>.

Alvarez-Solas, J., Robinson, A., Montoya, M., and Ritz, C. 2013. Iceberg discharges of the last glacial period driven by oceanic circulation changes. *Proceedings of the National Academy of Sciences* 110(41): 16350-16354. doi:<https://doi.org/10.1073/pnas.1306622110>.

Alves, E.Q., Macario, K., Ascough, P., and Bronk Ramsey, C. 2018. The worldwide marine radiocarbon reservoir effect: definitions, mechanisms, and prospects. *Reviews of Geophysics* 56(1): 278-305. doi:<https://doi.org/10.1002/2017RG000588>.

Amaya, D.J. 2019. The Pacific meridional mode and ENSO: A review. *Current Climate Change Reports* 5: 296-307. doi:<https://doi.org/10.1007/s40641-019-00142-x>.

Anderson, B., and Mackintosh, A. 2012. Controls on mass balance sensitivity of maritime glaciers in the Southern Alps, New Zealand: The role of debris cover. *Journal of Geophysical Research: Earth Surface* 117(F1). doi:<https://doi.org/10.1029/2011JF002064>.

Anderson, L., Berkelhammer, M., Barron, J.A., Steinman, B.A., Finney, B.P. and Abbott, M.B., 2016. Lake oxygen isotopes as recorders of North American Rocky Mountain hydroclimate: Holocene patterns and variability at multi-decadal to millennial time scales. *Global and Planetary Change*, 137, pp.131-148.

Angelopoulos, M., Overduin, P.P., Miesner, F., Grigoriev, M.N., and Vasiliev, A.A. 2020. Recent advances in the study of Arctic submarine permafrost. *Permafrost and Periglacial Processes* 31(3): 442-453. doi:<https://doi.org/10.1002/ppp.2061>.

Antevs, E. 1945. Correlation of Wisconsin glacial maxima. *American Journal of Science* 243-A: 1-39.

Antevs, E. 1948. Climatic changes and pre-white man. *University of Utah Bulletin* 38(20): 168-191.

Atwater, B.F. 1986. Pleistocene glacial-lake deposits of the Sanpoil River valley, northeastern Washington. US geological Survey Bulletin 1661.

Atwater, B.F. 1987. Status of glacial Lake Columbia during the last floods from glacial Lake Missoula. *Quaternary Research* 27(2): 182-201. doi:[https://doi.org/10.1016/0033-5894\(87\)90076-7](https://doi.org/10.1016/0033-5894(87)90076-7).

Austermann, J. and Forte, A.M., 2019. The importance of dynamic topography for understanding past sea level changes. *Past Glob Changes Mag*, 27, pp.18-19.

Austin, W.E., Bard, E., Hunt, J.B., Kroon, D., and Peacock, J.D. 1995. The ^{14}C age of the Icelandic Vedde Ash: implications for Younger Dryas marine reservoir age corrections. *Radiocarbon* 37(1): 53-62. doi:<https://doi.org/10.1017/S0033822200014788>.

Aylmer, J., Ferreira, D., and Feltham, D. 2022. Different mechanisms of Arctic and Antarctic sea ice response to ocean heat transport. *Climate Dynamics* 59(1-2): 315-329. doi:<https://doi.org/10.1007/s00382-021-06131-x>.

Baichtal, J.F., Lesnek, A.J., Carlson, R.J., Schmuck, N.S., Smith, J.L., Landwehr, D.J., and Briner, J.P. 2021. Late Pleistocene and early Holocene sea-level history and glacial retreat interpreted from shell-bearing marine deposits of southeastern Alaska, USA. *Geosphere* 17(6): 1590-1615. doi:<https://doi.org/10.1130/GES02359.1>.

Balbas, A.M., Barth, A.M., Clark, P.U., Clark, J., Caffee, M., O'Connor, J., Baker, V.R., Konrad, K., and Bjornstad, B. 2017. ^{10}Be dating of late Pleistocene megafloods and Cordilleran Ice Sheet retreat in the northwestern United States. *Geology* 45(7): 583-586. doi:<https://doi.org/10.1130/G38956.1>.

Balco, G., and Rovey, C.W. 2010. Absolute chronology for major Pleistocene advances of the Laurentide Ice Sheet. *Geology* 38(9): 795-798. doi:<https://doi.org/10.1130/G30946.1>.

Bard, E. 2002. Climate shock: abrupt changes over millennial time scales. *Physics Today* 55(12): 32-38.

Barr, I.D., and Clark, C.D. 2012. Late Quaternary glaciations in Far NE Russia; combining moraines, topography and chronology to assess regional and global glaciation synchrony. *Quaternary Science Reviews* 53: 72-87. doi:<https://doi.org/10.1016/j.quascirev.2012.08.004>.

Barrie, J.V., and Conway, K.W. 1999. Late Quaternary glaciation and postglacial stratigraphy of the northern Pacific margin of Canada. *Quaternary Research* 51(2): 113-123. doi:<https://doi.org/10.1006/qres.1998.2021>.

Barrie, J.V., and Conway, K.W. 2002. Rapid sea-level change and coastal evolution on the Pacific margin of Canada. *Sedimentary Geology* 150(1-2): 171-183. doi:[https://doi.org/10.1016/S0037-0738\(01\)00274-3](https://doi.org/10.1016/S0037-0738(01)00274-3).

Barrie, J.V., Conway, K.W., Picard, K., and Greene, H.G. 2009. Large-scale sedimentary bedforms and sediment dynamics on a glaciated tectonic continental shelf: Examples from the Pacific margin of Canada. *Continental Shelf Research* 29(5-6): 796-806.

doi:<https://doi.org/10.1016/j.csr.2008.12.007>.

Barrie, J.V., Greene, H.G., Conway, K.W., and Brothers, D.S. 2021. Late Quaternary sea level, isostatic response, and sediment dispersal along the Queen Charlotte fault. *Geosphere* 17(2): 375-388. doi:<https://doi.org/10.1130/GES02311.1>.

Barron, J.A., Bukry, D., Dean, W.E., Addison, J.A., and Finney, B. 2009. Paleooceanography of the Gulf of Alaska during the past 15,000 years: results from diatoms, silicoflagellates, and geochemistry. *Marine Micropaleontology* 72(3-4): 176-195.

doi:<https://doi.org/10.1016/j.marmicro.2009.04.006>.

Barth, A.M., Ceperley, E.G., Vavrus, C., Marcott, S.A., Shakun, J.D., and Caffee, M.W. 2022. ¹⁰Be age control of glaciation in the Beartooth Mountains, USA, from the latest Pleistocene through the Holocene. *Geochronology* 4(2): 731-743. doi:<https://doi.org/10.5194/gchron-4-731-2022>.

Bartlein, P., Edwards, M., Hostetler, S.W., Shafer, S., Anderson, P., Brubaker, L., and Lozhkin, A. 2015. Early-Holocene warming in Beringia and its mediation by sea-level and vegetation changes. *Climate of the Past* 11(9): 1197-1222. doi:<https://doi.org/10.5194/cp-11-1197-2015>.

Bartlein, P.J., Anderson, K.H., Anderson, P., Edwards, M., Mock, C., Thompson, R.S., Webb, R.S., Webb III, T., and Whitlock, C. 1998. Paleoclimate simulations for North America over the past 21,000 years: features of the simulated climate and comparisons with paleoenvironmental data. *Quaternary Science Reviews* 17(6-7): 549-585. doi:[https://doi.org/10.1016/S0277-3791\(98\)00012-2](https://doi.org/10.1016/S0277-3791(98)00012-2).

Bassis, J.N., Petersen, S.V., and Mac Cathles, L. 2017. Heinrich events triggered by ocean forcing and modulated by isostatic adjustment. *Nature* 542(7641): 332-334.

doi:<https://doi.org/10.1038/nature21069>.

Batchelor, C., and Dowdeswell, J. 2014. The physiography of High Arctic cross-shelf troughs. *Quaternary Science Reviews* 92: 68-96. doi:<https://doi.org/10.1016/j.quascirev.2013.05.025>.

Batchelor, C.L., Margold, M., Krapp, M., Murton, D.K., Dalton, A.S., Gibbard, P.L., Stokes, C.R., Murton, J.B., and Manica, A. 2019. The configuration of Northern Hemisphere ice sheets through the Quaternary. *Nature Communications* 10(1): 3713.

doi:<https://doi.org/10.1038/s41467-019-11601-2>.

Bates, R.L., and Jackson, J.A. 1987. *Glossary of geology, USA*.

Beck, J.W., Zhou, W., Li, C., Wu, Z., White, L., Xian, F., Kong, X., and An, Z. 2018. A 550,000-year record of East Asian monsoon rainfall from ¹⁰Be in loess. *Science* 360(6391): 877-881.

doi:<https://doi.org/10.1126/science.aam5825>.

Benn, D.I., Warren, C.R., and Mottram, R.H. 2007. Calving processes and the dynamics of calving glaciers. *Earth-Science Reviews* 82(3-4): 143-179.

doi:<https://doi.org/10.1016/j.quascirev.2016.11.026>.

Benson, L., Kashgarian, M., and Rubin, M. 1995. Carbonate deposition, Pyramid Lake subbasin, Nevada: 2. Lake levels and polar jet stream positions reconstructed from radiocarbon ages and elevations of carbonates (tufas) deposited in the Lahontan basin. *Palaeogeography, Palaeoclimatology, Palaeoecology* 117(1-2): 1-30. doi:[https://doi.org/10.1016/0031-0182\(94\)00103-F](https://doi.org/10.1016/0031-0182(94)00103-F).

Bereiter, B., Shackleton, S., Baggenstos, D., Kawamura, K., and Severinghaus, J. 2018. Mean global ocean temperatures during the last glacial transition. *Nature* 553(7686): 39-44.

doi:<https://doi.org/10.1038/nature25152>.

Berg, E.E., Kaufman, D.S., Anderson, R.S., Wiles, G.C., Lowell, T.V., Mitchell, E.A., Hu, F.S., and Werner, A. 2022. Late-Glacial and Holocene lake-level fluctuations on the Kenai Lowland, reconstructed from satellite-fen peat deposits and ice-shoved ramparts, Kenai Peninsula, Alaska. *Quaternary* 5(2): 23. doi:<https://doi.org/10.3390/quat5020023>.

Berger, A., and Loutre, M.-F. 1991. Insolation values for the climate of the last 10 million years. *Quaternary Science Reviews* 10(4): 297-317. doi:[https://doi.org/10.1016/0277-3791\(91\)90033-Q](https://doi.org/10.1016/0277-3791(91)90033-Q).

Berger, A., Loutre, M.-F., and Mélice, J. 2006. Equatorial insolation: from precession harmonics to eccentricity frequencies. *Climate of the Past* 2(2): 131-136. doi:<https://doi.org/10.5194/cp-2-131-2006>.

Beszczyńska-Möller, A., Woodgate, R.A., Lee, C., Melling, H., and Karcher, M. 2011. A synthesis of exchanges through the main oceanic gateways to the Arctic Ocean. *Oceanography* 24(3): 82-99. doi:<http://dx.doi.org/10.5670/oceanog.2011.59>.

Bhatt, U.S., Walker, D.A., Walsh, J.E., Carmack, E.C., Frey, K.E., Meier, W.N., Moore, S.E., Parmentier, F.-J.W., Post, E., and Romanovsky, V.E. 2014. Implications of Arctic sea ice decline for the Earth system. *Annual Review of Environment and Resources* 39: 57-89.

doi:<https://doi.org/10.1146/annurev-environ-122012-094357>.

Birks, H.H., Aarnes, I., Bjune, A.E., Brooks, S.J., Bakke, J., Kühl, N., and Birks, H.J.B. 2014. Lateglacial and early-Holocene climate variability reconstructed from multi-proxy records on Andøya, northern Norway. *Quaternary Science Reviews* 89: 108-122.

doi:<https://doi.org/10.1016/j.quascirev.2014.01.018>.

Birks, H.J.B., and Willis, K.J. 2008. Alpines, trees, and refugia in Europe. *Plant Ecology & Diversity* 1(2): 147-160. doi:<https://doi.org/10.1080/17550870802349146>.

- Bitz, C., and Battisti, D. 1999. Interannual to decadal variability in climate and the glacier mass balance in Washington, western Canada, and Alaska. *Journal of Climate* 12(11): 3181-3196. doi:[https://doi.org/10.1175/1520-0442\(1999\)012%3C3181:ITDVIC%3E2.0.CO;2](https://doi.org/10.1175/1520-0442(1999)012%3C3181:ITDVIC%3E2.0.CO;2).
- Bjerknes, J. 1969. Atmospheric teleconnections from the equatorial Pacific. *Monthly weather review* 97(3): 163-172. doi:[https://doi.org/10.1175/1520-0493\(1969\)097%3C0163:ATFTEP%3E2.3.CO;2](https://doi.org/10.1175/1520-0493(1969)097%3C0163:ATFTEP%3E2.3.CO;2).
- Blais-Stevens, A., Clague, J., Mathewes, R., Hebda, R., and Bornhold, B. 2003. Record of large, late Pleistocene outburst floods preserved in Saanich Inlet sediments, Vancouver Island, Canada. *Quaternary Science Reviews* 22(21-22): 2327-2334. doi:[https://doi.org/10.1016/S0277-3791\(03\)00212-9](https://doi.org/10.1016/S0277-3791(03)00212-9).
- Blaise, B., Clague, J.J., and Mathewes, R.W. 1990. Time of maximum Late Wisconsin glaciation, west coast of Canada. *Quaternary Research* 34(3): 282-295. doi:[https://doi.org/10.1016/0033-5894\(90\)90041-I](https://doi.org/10.1016/0033-5894(90)90041-I).
- Bond, N., Overland, J., Spillane, M., and Stabeno, P. 2003. Recent shifts in the state of the North Pacific. *Geophysical Research Letters* 30(23). doi:<https://doi.org/10.1029/2003GL018597>.
- Bond, N., and Harrison, D. 2006. ENSO's effect on Alaska during opposite phases of the Arctic Oscillation. *International Journal of Climatology* 26(13): 1821-1841. doi:<https://doi.org/10.1002/joc.1339>.
- Booth, D.B., and Hallet, B. 1993. Channel networks carved by subglacial water: Observations and reconstruction in the eastern Puget Lowland of Washington. *Geological Society of America Bulletin* 105(5): 671-683. doi:[https://doi.org/10.1130/0016-7606\(1993\)105%3C0671:CNCBSW%3E2.3.CO;2](https://doi.org/10.1130/0016-7606(1993)105%3C0671:CNCBSW%3E2.3.CO;2).
- Booth, D.B., Troost, K.G., Clague, J.J., and Waitt, R.B. 2003. The Cordilleran ice sheet. *Developments in Quaternary Sciences* 1: 17-43. doi:[https://doi.org/10.1016/S1571-0866\(03\)01002-9](https://doi.org/10.1016/S1571-0866(03)01002-9).
- Bostock, H.C., Opdyke, B.N., and Williams, M.J. 2010. Characterising the intermediate depth waters of the Pacific Ocean using $\delta^{13}\text{C}$ and other geochemical tracers. *Deep Sea Research Part I: Oceanographic Research Papers* 57(7): 847-859. doi:<https://doi.org/10.1016/j.dsr.2010.04.005>.
- Boulton, G., and Clark, C. 1990. The Laurentide ice sheet through the last glacial cycle: the topology of drift lineations as a key to the dynamic behaviour of former ice sheets. *Earth and Environmental Science Transactions of The Royal Society of Edinburgh* 81(4): 327-347. doi:<https://doi.org/10.1017/S0263593300020836>.
- Bradley, R.S., and England, J.H. 2008. The Younger Dryas and the sea of ancient ice. *Quaternary Research* 70(1): 1-10. doi:<https://doi.org/10.1016/j.yqres.2008.03.002>.

Bradley, R.S., and Diaz, H.F. 2021. Late Quaternary Abrupt Climate Change in the Tropics and Sub-Tropics: The Continental Signal of Tropical Hydroclimatic Events (THEs). *Reviews of Geophysics* 59(4): e2020RG000732. doi:<https://doi.org/10.1029/2020RG000732>.

Brigham-Grette, J., 2001. New perspectives on Beringian Quaternary paleogeography, stratigraphy, and glacial history. *Quaternary Science Reviews*, 20(1-3), pp.15-24. doi: [https://doi.org/10.1016/S0277-3791\(00\)00134-7](https://doi.org/10.1016/S0277-3791(00)00134-7)

Briner, J.P., and Kaufman, D.S. 2008. Late Pleistocene mountain glaciation in Alaska: key chronologies. *Journal of Quaternary Science: Published for the Quaternary Research Association* 23(6-7): 659-670. doi:<https://doi.org/10.1002/jqs.1196>.

Briner, J.P., Tulenko, J., Kaufman, D.S., Young, N.E., Baichtal, J., and Lesnek, A. 2017. The last deglaciation of Alaska. *Cuadernos de investigación geográfica: Geographical Research Letters*(43): 429-448. doi:<http://doi.org.10.18172/cig.3229>.

Broadman, E., Kaufman, D.S., Anderson, R.S., Bogle, S., Ford, M., Fortin, D., Henderson, A.C., Lacey, J.H., Leng, M.J., and McKay, N.P. 2022. Reconstructing postglacial hydrologic and environmental change in the eastern Kenai Peninsula lowlands using proxy data and mass balance modeling. *Quaternary Research* 107: 1-26. doi:<https://doi.org/10.1017/qua.2021.75>.

Broccoli, A., and Manabe, S. 1987. The influence of continental ice, atmospheric CO₂, and land albedo on the climate of the Last Glacial Maximum. *Climate Dynamics* 1: 87-99. doi:<https://doi.org/10.1007/BF01054478>.

Broecker, W., and Denton, G. 1989. The role of ocean-atmosphere reorganizations in glacial cycles. *Geochimica et Cosmochimica Acta* 53(10): 2465-2501. doi:[https://doi.org/10.1016/0016-7037\(89\)90123-3](https://doi.org/10.1016/0016-7037(89)90123-3).

Broecker, W.S., and Putnam, A.E. 2013. Hydrologic impacts of past shifts of Earth's thermal equator offer insight into those to be produced by fossil fuel CO₂. *Proceedings of the National Academy of Sciences* 110(42): 16710-16715. doi:<https://doi.org/10.1073/pnas.1301855110>.

Bromley, G., Putnam, A., Hall, B., Rademaker, K., Thomas, H., Balter-Kennedy, A., Barker, S., and Rice, D. 2023. Lateglacial shifts in seasonality reconcile conflicting North Atlantic temperature signals. *Journal of Geophysical Research. Earth Surface* 128(1). doi:<http://dx.doi.org/10.1029/2022JF006951>.

Bromwich, D.H., Toracinta, E.R., Wei, H., Oglesby, R.J., Fastook, J.L., and Hughes, T.J. 2004. Polar MM5 simulations of the winter climate of the Laurentide Ice Sheet at the LGM. *Journal of Climate* 17(17): 3415-3433. doi:[https://doi.org/10.1175/1520-0442\(2004\)017%3C3415:PMSOTW%3E2.0.CO;2](https://doi.org/10.1175/1520-0442(2004)017%3C3415:PMSOTW%3E2.0.CO;2).

Bruns, T.R. 1982. Structure and petroleum potential of the continental margin between Cross Sound and Icy Bay, northern Gulf of Alaska. US Geological Survey 82-929, Menlo Park, CA.

Buckley, M.W., and Marshall, J. 2016. Observations, inferences, and mechanisms of the Atlantic Meridional Overturning Circulation: A review. *Reviews of Geophysics* 54(1): 5-63. doi:<https://doi.org/10.1002/2015RG000493>.

Budikova, D. 2005. Impact of the Pacific Decadal Oscillation on relationships between temperature and the Arctic Oscillation in the USA in winter. *Climate Research* 29(3): 199-208. doi:<https://doi.org/10.3354/cr029199>.

Buizert, C., and Schmittner, A. 2015. Southern Ocean control of glacial AMOC stability and Dansgaard-Oeschger interstadial duration. *Paleoceanography* 30(12): 1595-1612. doi:<https://doi.org/10.1002/2015PA002795>.

Butzin, M., Köhler, P., and Lohmann, G. 2017. Marine radiocarbon reservoir age simulations for the past 50,000 years. *Geophysical Research Letters* 44(16): 8473-8480. doi:<https://doi.org/10.1002/2017GL074688>.

Cahill, J.A., Heintzman, P.D., Harris, K., Teasdale, M.D., Kapp, J., Soares, A.E., Stirling, I., Bradley, D., Edwards, C.J., and Graim, K. 2018. Genomic evidence of widespread admixture from polar bears into brown bears during the last ice age. *Molecular Biology and Evolution* 35(5): 1120-1129. doi:<https://doi.org/10.1093/molbev/msy018>.

Caissie, B.E., Brigham-Grette, J., Lawrence, K.T., Herbert, T.D., and Cook, M.S. 2010. Last Glacial Maximum to Holocene sea surface conditions at Umnak Plateau, Bering Sea, as inferred from diatom, alkenone, and stable isotope records. *Paleoceanography* 25(1). doi:<https://doi.org/10.1029/2008PA001671>.

Capps, S.R. 1931. Glaciation in Alaska. US Geological Survey Professional Paper 170-A.

Carlson, P.R., Bruns, T.R., Molnia, B.F., and Schwab, W.C. 1982. Submarine valleys in the northeastern Gulf of Alaska: characteristics and probable origin. *Marine Geology* 47(3-4): 217-242. doi:[https://doi.org/10.1016/0025-3227\(82\)90070-6](https://doi.org/10.1016/0025-3227(82)90070-6).

Carrara, P., Ager, T., and Baichtal, J. 2007. Possible refugia in the Alexander Archipelago of southeastern Alaska during the late Wisconsin glaciation. *Canadian Journal of Earth Sciences* 44(2): 229-244. doi:<https://doi.org/10.1139/e06-081>.

Castro, C.L., McKee, T.B., and Pielke Sr, R.A. 2001. The relationship of the North American monsoon to tropical and North Pacific sea surface temperatures as revealed by observational analyses. *Journal of Climate* 14(24): 4449-4473. doi:[https://doi.org/10.1175/1520-0442\(2001\)014%3C4449:TROTNA%3E2.0.CO;2](https://doi.org/10.1175/1520-0442(2001)014%3C4449:TROTNA%3E2.0.CO;2).

Cessi, P. 2020. Control of Bering Strait transport by the meridional overturning circulation. *Journal of Physical Oceanography* 50(7): 1853-1870. doi:<https://doi.org/10.1175/JPO-D-20-0026.1>.

- Chamberlin, T.C. 1895. The classification of American glacial deposits. *The Journal of Geology* 3(3): 270-277.
- Chang, E.K., Lee, S., and Swanson, K.L. 2002. Storm track dynamics. *Journal of climate* 15(16): 2163-2183. doi:[https://doi.org/10.1175/1520-0442\(2002\)015%3C02163:STD%3E2.0.CO;2](https://doi.org/10.1175/1520-0442(2002)015%3C02163:STD%3E2.0.CO;2).
- Chapman, J.B., Haeussler, P.J., and Pavlis, T.L. 2009. Quaternary uplift history of Wingham Island, south-central Alaska. *US Geological Survey* 1760-B 2330-7102.
- Chappell, J., Omura, A., Esat, T., McCulloch, M., Pandolfi, J., Ota, Y., and Pillans, B. 1996. Reconciliation of late Quaternary sea levels derived from coral terraces at Huon Peninsula with deep sea oxygen isotope records. *Earth and Planetary Science Letters* 141(1-4): 227-236. doi:[https://doi.org/10.1016/0012-821X\(96\)00062-3](https://doi.org/10.1016/0012-821X(96)00062-3).
- Cheng, H., Edwards, R.L., Sinha, A., Spötl, C., Yi, L., Chen, S., Kelly, M., Kathayat, G., Wang, X., and Li, X. 2016. The Asian monsoon over the past 640,000 years and ice age terminations. *Nature* 534(7609): 640-646. doi:<https://doi.org/10.1038/nature18591>.
- Chiang, J.C., and Bitz, C.M. 2005. Influence of high latitude ice cover on the marine Intertropical Convergence Zone. *Climate Dynamics* 25(5): 477-496. doi:<https://doi.org/10.1007/s00382-005-0040-5>.
- Chiang, J.C. 2009. The tropics in paleoclimate. *Annual Review of Earth and Planetary Sciences* 37: 263-297. doi:<https://doi.org/10.1146/annurev.earth.031208.100217>.
- Chiang, J.C., Lee, S.-Y., Putnam, A.E., and Wang, X. 2014. South Pacific Split Jet, ITCZ shifts, and atmospheric North–South linkages during abrupt climate changes of the last glacial period. *Earth and Planetary Science Letters* 406: 233-246. doi:<https://doi.org/10.1016/j.epsl.2014.09.012>.
- Clague, J., Ward, B., Ehlers, J., Gibbard, P., and Hughes, P. 2011. Quaternary Glaciations—Extent and Chronology: A Closer Look. Chapter 44—Pleistocene Glaciation of British Columbia: 563-573.
- Clague, J.J. 1981. Late Quaternary Geology and Geochronology of British Columbia Part 2. *Geological Survey of Canada Paper* 80(35): 1-14.
- Clague, J.J. 1989. Cordilleran ice sheet. *In* *Quaternary Geology of Canada and Greenland*. Edited by R.J. Fulton. Geological Society of America, Boulder, CO. pp. 40-42.
- Clague, J.J., and James, T.S. 2002. History and isostatic effects of the last ice sheet in southern British Columbia. *Quaternary Science Reviews* 21(1-3): 71-87. doi:[https://doi.org/10.1016/S0277-3791\(01\)00070-1](https://doi.org/10.1016/S0277-3791(01)00070-1).
- Clague, J.J., and Ward, B. 2011. Pleistocene glaciation of British Columbia. *Developments in Quaternary Sciences* 15: 563-573. doi:<https://doi.org/10.1016/B978-0-444-53447-7.00044-1>.

- Clark, P.U., Dyke, A.S., Shakun, J.D., Carlson, A.E., Clark, J., Wohlfarth, B., Mitrovica, J.X., Hostetler, S.W., and McCabe, A.M. 2009. The Last Glacial Maximum. *Science* 325(5941): 710-714. doi:<https://doi.org/10.1126/science.1172873>.
- Clark, P.U., Shakun, J.D., Baker, P.A., Bartlein, P.J., Brewer, S., Brook, E., Carlson, A.E., Cheng, H., Kaufman, D.S., and Liu, Z. 2012. Global climate evolution during the last deglaciation. *Proceedings of the National Academy of Sciences* 109(19): E1134-E1142. doi:<https://doi.org/10.1073/pnas.1116619109/-/DCSupplemental>.
- Clary, W., Worthington, L., Scuderi, L., Gulick, S.P., and Scudiero, E. 2021. Quantifying the relative influence of ice sheets, faults, and instability on channel and gully cross-profile shapes in the Gulf of Alaska. *Marine Geology* 435: 106416. doi:<https://doi.org/10.1016/j.margeo.2020.106416>.
- Clemens, S.C., Yamamoto, M., Thirumalai, K., Giosan, L., Richey, J.N., Nilsson-Kerr, K., Rosenthal, Y., Anand, P., and McGrath, S.M. 2021. Remote and local drivers of Pleistocene South Asian summer monsoon precipitation: A test for future predictions. *Science Advances* 7(23): eabg3848. doi:<https://doi.org/10.1126/sciadv.abg3848>.
- Clement Kinney, J., Assmann, K.M., Maslowski, W., Björk, G., Jakobsson, M., Jutterström, S., Lee, Y.J., Osinski, R., Semiletov, I., and Ulfsbo, A. 2022. On the circulation, water mass distribution, and nutrient concentrations of the western Chukchi Sea. *Ocean Science* 18(1): 29-49. doi:<https://doi.org/10.5194/os-18-29-2022>.
- COHMAP Members. 1988. Climatic changes of the last 18,000 years: observations and model simulations. *Science* 241(4869): 1043-1052. doi:<https://doi.org/10.1126/science.241.4869.1043>.
- Cook, A.J., Holland, P., Meredith, M., Murray, T., Luckman, A., and Vaughan, D.G. 2016. Ocean forcing of glacier retreat in the western Antarctic Peninsula. *Science* 353(6296): 283-286. doi:<https://doi.org/10.1126/science.aae0017>.
- Cook, J., Bidlack, A., Conroy, C.J., Demboski, J., Fleming, M., Runck, A., Stone, K., and MacDonald, S. 2001. A phylogeographic perspective on endemism in the Alexander Archipelago of southeast Alaska. *Biological Conservation* 97(2): 215-227. doi:[https://doi.org/10.1016/S0006-3207\(00\)00114-2](https://doi.org/10.1016/S0006-3207(00)00114-2).
- Cosma, T., and Hendy, I. 2008. Pleistocene glacimarine sedimentation on the continental slope off Vancouver Island, British Columbia. *Marine Geology* 255(1-2): 45-54. doi:<https://doi.org/10.1016/j.margeo.2008.07.001>.
- Coulter, H., Hopkins, D., Karlstrom, T., Péwé, T., Wahrhaftig, C., and Williams, J.R. 1965. Map showing extent of glaciations in Alaska. Geologic Survey Map.
- Cowan, E.A., Zellers, S.D., Müller, J., Walczak, M.H., Worthington, L.L., Caissie, B.E., Clary, W.A., Jaeger, J.M., Gulick, S.P., and Pratt, J.W. 2020. Sediment controls dynamic behavior of a

Cordilleran Ice Stream at the Last Glacial Maximum. *Nature Communications* 11(1): 1826.
doi:<https://doi.org/10.1038/s41467-020-15579-0>.

Cowan, E.A. 2022. Unraveling the Deep-Sea Sedimentary Record of Ice Sheet History. *Paleoceanography and Paleoclimatology* 37(8): e2022PA004488.
doi:<https://doi.org/10.1029/2022PA004488>.

Curry, B.B., Lowell, T.V., Wang, H., and Anderson, A.C. 2018. Revised time-distance diagram for the Lake Michigan Lobe, Michigan subepisode, Wisconsin episode, Illinois, USA. *In Quaternary Glaciation of the Great Lakes Region: Process, Landforms, Sediments, and Chronology Edited by A.E. Kehew and B.B. Curry*. Geological society of America.

Dalton, A.S., Margold, M., Stokes, C.R., Tarasov, L., Dyke, A.S., Adams, R.S., Allard, S., Arends, H.E., Atkinson, N., and Attig, J.W. 2020. An updated radiocarbon-based ice margin chronology for the last deglaciation of the North American Ice Sheet Complex. *Quaternary Science Reviews* 234: 106223. doi:<https://doi.org/10.1016/j.quascirev.2020.106223>.

Danielson, S.L., Hennon, T.D., Monson, D.H., Suryan, R.M., Campbell, R.W., Baird, S.J., Holderied, K., and Weingartner, T.J. 2022. Temperature variations in the northern Gulf of Alaska across synoptic to century-long time scales. *Deep Sea Research Part II: Topical Studies in Oceanography* 203: 105155. doi:<https://doi.org/10.1016/j.dsr2.2022.105155>.

Darvill, C., Menounos, B., Goehring, B., Lian, O.B., and Caffee, M. 2018. Retreat of the western Cordilleran ice sheet margin during the last deglaciation. *Geophysical Research Letters* 45(18): 9710-9720. doi:<https://doi.org/10.1029/2018GL079419>.

Darvill, C., Menounos, B., Goehring, B., and Lesnek, A. 2022. Cordilleran Ice Sheet stability during the last deglaciation. *Geophysical Research Letters* 49(10): e2021GL097191.
doi:<https://doi.org/10.1029/2021GL097191>.

Davies-Walczak, M., Mix, A.C., Stoner, J.S., Southon, J., Cheseby, M., and Xuan, C. 2014. Late Glacial to Holocene radiocarbon constraints on North Pacific Intermediate Water ventilation and deglacial atmospheric CO₂ sources. *Earth and Planetary Science Letters* 397: 57-66.
doi:<http://dx.doi.org/10.1016/j.epsl.2014.04.004>.

Davies, B., Carrivick, J., Glasser, N., Hambrey, M., and Smellie, J.L. 2012. Variable glacier response to atmospheric warming, northern Antarctic Peninsula, 1988–2009. *The Cryosphere* 6(5): 1031-1048. doi:<https://doi.org/10.5194/tc-6-1031-2012>.

Davies, M.H., Mix, A.C., Stoner, J.S., Addison, J.A., Jaeger, J., Finney, B., and Wiest, J. 2011. The deglacial transition on the southeastern Alaska Margin: Meltwater input, sea level rise, marine productivity, and sedimentary anoxia. *Paleoceanography* 26(2).
doi:<https://doi.org/10.1029/2010PA002051>.

De Deckker, P. 2016. The Indo-Pacific Warm Pool: critical to world oceanography and world climate. *Geoscience Letters* 3(1): 1-12. doi:<https://doi.org/10.1186/s40562-016-0054-3>.

de La Fuente, M., Skinner, L., Calvo, E., Pelejero, C., and Cacho, I. 2015. Increased reservoir ages and poorly ventilated deepwaters inferred in the glacial Eastern Equatorial Pacific. *Nature Communications* 6(1): 7420. doi:<https://doi.org/10.1038/ncomms8420>.

de Vernal, A., and Pedersen, T.F. 1997. Micropaleontology and palynology of core PAR87A-10: A 23,000 year record of paleoenvironmental changes in the Gulf of Alaska, northeast North Pacific. *Paleoceanography* 12(6): 821-830. doi:<https://doi.org/10.1029/97PA02167>.

Deininger, M., McDermott, F., Cruz, F.W., Bernal, J.P., Mudelsee, M., Vonhof, H., Millo, C., Spötl, C., Treble, P.C., and Pickering, R. 2020. Inter-hemispheric synchronicity of Holocene precipitation anomalies controlled by Earth's latitudinal insolation gradients. *Nature communications* 11(1): 5447. doi:<https://doi.org/10.1038/s41467-020-19021-3>.

Denton, G.H., Alley, R.B., Comer, G.C., and Broecker, W.S. 2005. The role of seasonality in abrupt climate change. *Quaternary Science Reviews* 24(10-11): 1159-1182. doi:<https://doi.org/10.1016/j.quascirev.2004.12.002>.

Denton, G.H., Anderson, R.F., Toggweiler, J., Edwards, R., Schaefer, J., and Putnam, A. 2010. The last glacial termination. *Science* 328(5986): 1652-1656. doi:<https://doi.org/10.1126/science.1184119>.

Denton, G.H., Putnam, A.E., Russell, J.L., Barrell, D.J., Schaefer, J.M., Kaplan, M.R., and Strand, P.D. 2021. The Zealandia Switch: Ice age climate shifts viewed from Southern Hemisphere moraines. *Quaternary Science Reviews* 257: 106771. doi:<https://doi.org/10.1016/j.quascirev.2020.106771>.

Denton, G.H., Toucanne, S., Putnam, A.E., Barrell, D.J., and Russell, J.L. 2022. Heinrich summers. *Quaternary Science Reviews* 295: 107750. doi:<https://doi.org/10.1016/j.quascirev.2022.107750>.

Deser, C., Alexander, M.A., Xie, S.-P., and Phillips, A.S. 2010. Sea surface temperature variability: Patterns and mechanisms. *Annual Review of Marine Science* 2: 115-143. doi:<https://doi.org/10.1146/annurev-marine-120408-151453>.

Dethier, D.P., Pessl Jr, F., Keuler, R., Balzarini, M., and Pevear, D. 1995. Late Wisconsinan glaciomarine deposition and isostatic rebound, northern Puget Lowland, Washington. *Geological Society of America Bulletin* 107(11): 1288-1303. doi:[https://doi.org/10.1130/0016-7606\(1995\)107%3C1288:LWGDAI%3E2.3.CO;2](https://doi.org/10.1130/0016-7606(1995)107%3C1288:LWGDAI%3E2.3.CO;2).

Detterman, R.L. 1986. Glaciation of the Alaska Peninsula. *In* *Glaciation in Alaska: The Geologic Record*. Alaska Geological Society. pp. 151-170.

Dey, D., and Döös, K. 2020. Atmospheric freshwater transport from the Atlantic to the Pacific Ocean: A Lagrangian analysis. *Geophysical Research Letters* 47(6): e2019GL086176. doi:<https://doi.org/10.1029/2019GL086176>.

- Di Lorenzo, E., Schneider, N., Cobb, K.M., Franks, P., Chhak, K., Miller, A.J., McWilliams, J.C., Bograd, S.J., Arango, H., and Curchitser, E. 2008. North Pacific Gyre Oscillation links ocean climate and ecosystem change. *Geophysical Research Letters* 35(8). doi:<https://doi.org/10.1029/2007GL032838>.
- Di Lorenzo, E., and Schneider, N. 2010. An overview of Pacific climate variability. Recuperado de: <http://www.offices.us/npggo/docs/Decadal-Intro.pdf>. Última visita 28.
- Di Lorenzo, E., Combes, V., Keister, J.E., Strub, P.T., Thomas, A.C., Franks, P.J., Ohman, M.D., Furtado, J.C., Bracco, A., and Bograd, S.J. 2013. Synthesis of Pacific Ocean climate and ecosystem dynamics. *Oceanography* 26(4): 68-81. doi:<https://doi.org/10.5670/oceanog.2013.76>.
- Di Lorenzo, E., Liguori, G., Schneider, N., Furtado, J., Anderson, B., and Alexander, M. 2015. ENSO and meridional modes: A null hypothesis for Pacific climate variability. *Geophysical Research Letters* 42(21): 9440-9448. doi:<https://doi.org/10.1002/2015GL066281>.
- Di Lorenzo, E., Xu, T., Zhao, Y., Newman, M., Capotondi, A., Stevenson, S., Amaya, D., Anderson, B., Ding, R., and Furtado, J. 2023. Modes and mechanisms of pacific decadal-scale variability. *Annual Review of Marine Science* 15: 249-275. doi:<https://doi.org/10.1146/annurev-marine-040422-084555>.
- Di Nezio, P.N., Timmermann, A., Tierney, J.E., Jin, F.F., Otto-Bliesner, B., Rosenbloom, N., Mapes, B., Neale, R., Ivanovic, R.F., and Montenegro, A. 2016. The climate response of the Indo-Pacific warm pool to glacial sea level. *Paleoceanography* 31(6): 866-894. doi:<https://doi.org/10.1002/2015PA002890>.
- Docquier, D., Koenigk, T., Fuentes-Franco, R., Karami, M.P., and Ruprich-Robert, Y. 2021. Impact of ocean heat transport on the Arctic sea ice decline: a model study with EC-Earth3. *Climate Dynamics* 56: 1407-1432. doi:<https://doi.org/10.1007/s00382-020-05540-8>.
- Dredge, L.A., and Thorleifson, L.H. 1987. The Middle Wisconsinan history of the Laurentide ice sheet. *Géographie Physique et Quaternaire* 41(2): 215-235. doi:<https://doi.org/10.7202/032680ar>.
- Du, J., Haley, B.A., Mix, A.C., Walczak, M.H., and Praetorius, S.K. 2018. Flushing of the deep Pacific Ocean and the deglacial rise of atmospheric CO₂ concentrations. *Nature Geoscience* 11(10): 749-755. doi:<https://doi.org/10.1038/s41561-018-0205-6>.
- Duk-Rodkin, A., Barendregt, R.W., Froese, D.G., Weber, F., Enkin, R., Smith, I.R., Zazula, G.D., Waters, P., and Klassen, R. 2004. Timing and extent of Plio-Pleistocene glaciations in north-western Canada and east-central Alaska. *In* *Developments in Quaternary Sciences*. Edited by J. Ehlers and P.L. Gibbard. Elsevier. pp. 313-345.
- Duk-Rodkin, A., and Barendregt, R.W. 2011. Stratigraphical record of glacials/interglacials in northwest Canada. *In* *Developments in Quaternary Sciences*. Elsevier. pp. 661-698.

- Dyke, A., Andrews, J., Clark, P., England, J., Miller, G., Shaw, J., and Veillette, J. 2002. The Laurentide and Innuitian ice sheets during the Last Glacial Maximum. *Quaternary Science Reviews* 21(1-3): 9-31. doi:[https://doi.org/10.1016/S0277-3791\(01\)00095-6](https://doi.org/10.1016/S0277-3791(01)00095-6).
- Dyke, A.S., Dale, J.E., and McNeely, R.N. 1996. Marine molluscs as indicators of environmental change in glaciated North America and Greenland during the last 18 000 years. *Géographie physique et Quaternaire* 50(2): 125-184. doi:<https://doi.org/10.7202/033087ar>.
- Dyke, A.S., and Savelle, J.M. 2001. Holocene History of the Bering Sea Bowhead Whale (*Balaena mysticetus*) in Its Beaufort Sea Summer Grounds off Southwestern Victoria Island, Western Canadian Arctic. *Quaternary Research* 55(3): 371-379. doi:<https://doi.org/10.1006/qres.2001.2228>.
- Dyke, A.S. 2004. An outline of North American deglaciation with emphasis on central and northern Canada. *Developments in quaternary sciences* 2: 373-424. doi:[https://doi.org/10.1016/S1571-0866\(04\)80209-4](https://doi.org/10.1016/S1571-0866(04)80209-4).
- Eamer, J.B., Shugar, D.H., Walker, I.J., Lian, O.B., Neudorf, C.M., and Telka, A.M. 2017. A glacial readvance during retreat of the Cordilleran Ice Sheet, British Columbia central coast. *Quaternary Research* 87(3): 468-481. doi:<https://doi.org/10.1017/qua.2017.16>.
- Ehlers, J., Grube, A., Stephan, H.-J., and Wansa, S. 2011. Pleistocene glaciations of North Germany—new results. *Developments in Quaternary Sciences* 15: 149-162. doi:<https://doi.org/10.1016/B978-0-444-53447-7.00013-1>.
- Elias, S.A., Short, S.K., and Phillips, R.L. 1992. Paleoecology of late-glacial peats from the Bering Land Bridge, Chukchi Sea shelf region, northwestern Alaska. *Quaternary Research* 38(3): 371-378. doi:[https://doi.org/10.1016/0033-5894\(92\)90045-K](https://doi.org/10.1016/0033-5894(92)90045-K).
- Elias, S.A., Short, S.K., Nelson, C.H., and Birks, H.H. 1996. Life and times of the Bering Land Bridge. *Nature* 382(6586): 60-63. doi:<https://doi.org/10.1038/382060a0>.
- Emile-Geay, J., Cane, M.A., Naik, N., Seager, R., Clement, A.C., and van Geen, A. 2003. Warren revisited: Atmospheric freshwater fluxes and “Why is no deepwater formed in the North Pacific”. *Journal of Geophysical Research: Oceans* 108(C6). doi:<https://doi.org/10.1029/2001JC001058>, 2003.
- England, J.H., and Furze, M.F. 2008. New evidence from the western Canadian Arctic Archipelago for the resubmergence of Bering Strait. *Quaternary research* 70(1): 60-67. doi:<https://doi.org/10.1016/j.yqres.2008.03.001>.
- Engstrom, D.R., Fritz, S.C., Milner, A., and Wood, J. 1990. Early lake ontogeny following neoglacial ice recession at Glacier Bay, Alaska. *In Proceedings of the Second Glacier Bay Science Symposium*. National Park Service, Anchorage, Alaska, USA. pp. 127-132.

- Enkelmann, E., Zeitler, P., Pavlis, T., Garver, J., and Ridgway, K. 2009. Intense localized rock uplift and erosion in the St Elias orogen of Alaska. *Nature Geoscience* 2(5): 360-363. doi:<https://doi.org/10.1038/ngeo502>.
- Enkelmann, E., Koons, P.O., Pavlis, T.L., Hallet, B., Barker, A., Elliott, J., Garver, J.I., Gulick, S.P., Headley, R.M., and Pavlis, G.L. 2015. Cooperation among tectonic and surface processes in the St. Elias Range, Earth's highest coastal mountains. *Geophysical Research Letters* 42(14): 5838-5846. doi:<https://doi.org/10.1002/2015GL064727>.
- Epstein, S. 1995. The isotopic climatic records in the Allerød-Bølling-Younger Dryas and post-Younger Dryas events. *Global Biogeochemical Cycles* 9(4): 557-563. doi:<https://doi.org/10.1002/jqs.1279>.
- Eyles, C.H., and Lagoe, M.B. 1990. Sedimentation patterns and facies geometries on a temperate glacially-influenced continental shelf: the Yakataga Formation, Middleton Island, Alaska. *Geological Society, London, Special Publications* 53(1): 363-386. doi:<https://doi.org/10.1144/GSL.SP.1990.053.01.21>.
- Eyles, N., Moreno, L.A., and Sookhan, S. 2018. Ice streams of the Late Wisconsin Cordilleran Ice Sheet in western North America. *Quaternary Science Reviews* 179: 87-122. doi:<https://doi.org/10.1016/j.quascirev.2017.10.027>.
- Fan, W., Jian, Z., Bassinot, F., and Chu, Z. 2013. Holocene centennial-scale changes of the Indonesian and South China Sea throughflows: Evidences from the Makassar Strait. *Global and Planetary Change* 111: 111-117. doi:<https://doi.org/10.1016/j.gloplacha.2013.08.017>.
- Fan, W., Jian, Z., Chu, Z., Dang, H., Wang, Y., Bassinot, F., Han, X., and Bian, Y. 2018. Variability of the Indonesian throughflow in the Makassar Strait over the last 30 ka. *Scientific Reports* 8(1): 5678. doi:<https://doi.org/10.1038/s41598-018-24055-1>.
- Farmer, J.R., Hertzberg, J., Cardinal, D., Fietz, S., Hendry, K., Jaccard, S., Paytan, A., Rafter, P., Ren, H., and Somes, C.J. 2021. Assessment of C, N, and Si isotopes as tracers of past ocean nutrient and carbon cycling. *Global Biogeochemical Cycles* 35(7): e2020GB006775. doi:<https://doi.org/10.1029/2020GB006775>.
- Farmer, J.R., Pico, T., Underwood, O.M., Cleveland Stout, R., Granger, J., Cronin, T.M., Fripiat, F., Martínez-García, A., Haug, G.H., and Sigman, D.M. 2023. The Bering Strait was flooded 10,000 years before the Last Glacial Maximum. *Proceedings of the National Academy of Sciences* 120(1): e2206742119. doi:<https://doi.org/10.1073/pnas.2206742119>.
- Farquharson, L., Mann, D., Rittenour, T., Groves, P., Grosse, G., and Jones, B. 2018. Alaskan marine transgressions record out-of-phase Arctic Ocean glaciation during the last interglacial. *Geology* 46(9): 783-786. doi:<https://doi.org/10.1130/G40345.1>.

- Fedje, D., Mackie, Q., Lacourse, T., and McLaren, D. 2011. Younger Dryas environments and archaeology on the Northwest Coast of North America. *Quaternary International* 242(2): 452-462. doi:<https://doi.org/10.1016/j.quaint.2011.03.042>.
- Fedje, D., Mackie, Q., McLaren, D., Wigen, B., and Southon, J. 2021. Karst caves in Haida Gwaii: Archaeology and paleontology at the Pleistocene-Holocene transition. *Quaternary Science Reviews* 272: 107221. doi:<https://doi.org/10.1016/j.quascirev.2021.107221>.
- Fedje, D.W., and Josenhans, H. 2000. Drowned forests and archaeology on the continental shelf of British Columbia, Canada. *Geology* 28(2): 99-102. doi:[https://doi.org/10.1130/0091-7613\(2000\)28%3C99:DFAAOT%3E2.0.CO;2](https://doi.org/10.1130/0091-7613(2000)28%3C99:DFAAOT%3E2.0.CO;2).
- Fedje, D.W., Josenhans, H., Clague, J.J., Barrie, J.V., Archer, D.J., Southon, J.R., and Mathewes, R. 2005. Hecate strait paleoshorelines. *In* Haida Gwaii: Human History and Environment from the Time of Loon to the Time of the Iron People. *Edited by* D. Fedje and R. Mathewes. UBC Press, Vancouver, BC. pp. 21-37.
- Fedorov, A.V., Hu, S., Wittenberg, A.T., Levine, A.F., and Deser, C. 2020. ENSO low-frequency modulation and mean state interactions. *In* El Niño southern oscillation in a changing climate. *Edited by* M.J. McPhaden and A. Santoso and W. Cai. pp. 173-198.
- Feely, R.A., Sabine, C.L., Takahashi, T., and Wanninkhof, R. 2001. Uptake and storage of carbon dioxide in the ocean: The global CO_2 survey. *Oceanography* 14(4): 18-32.
- Feng, M., Zhang, N., Liu, Q., and Wijffels, S. 2018. The Indonesian throughflow, its variability and centennial change. *Geoscience Letters* 5(1): 1-10. doi:<https://doi.org/10.1186/s40562-018-0102-2>.
- Ferrari, R., Jansen, M.F., Adkins, J.F., Burke, A., Stewart, A.L., and Thompson, A.F. Antarctic sea ice control on ocean circulation in present and glacial climates. *Proceedings of the National Academy of Sciences of the U S A*. 2014. 111 (24): 8753-8. doi: 10.1073/pnas.1323922111.
- Ferreira, D., Marshall, J., and Campin, J.-M. 2010. Localization of deepwater formation: Role of atmospheric moisture transport and geometrical constraints on ocean circulation. *Journal of Climate* 23(6): 1456-1476. doi:<https://doi.org/10.1175/2009JCLI3197.1>.
- Ferrians, O., Carter, L., Hamilton, T., and Galloway, J. 1989. Glacial Lake Atna, Copper River Basin, Alaska. *US Geological Survey Circular* 1026: 85-88.
- Ferrigno, J.G., Williams, R.S., and Thomson, J.W. 2002. Coastal-change and glaciological maps of the Antarctic Peninsula. *US Geological Survey Reston, VA*. U.S. Geological Survey Fact Sheet 017-02.
- Fladmark, K.R. 1979. Routes: Alternate migration corridors for early man in North America. *American Antiquity* 44(1): 55-69. doi:<https://doi.org/10.2307/279189>.

- Ford, H., McChesney, C., Hertzberg, J., and McManus, J. 2018. A deep eastern equatorial Pacific thermocline during the Last Glacial Maximum. *Geophysical Research Letters* 45(21): 11,806-811,816. doi:<https://doi.org/10.1029/2018GL079710>.
- Forget, G., and Ferreira, D. 2019. Global ocean heat transport dominated by heat export from the tropical Pacific. *Nature Geoscience* 12(5): 351-354. doi:<https://doi.org/10.1038/s41561-019-0333-7>.
- Friele, P.A., and Clague, J.J. 2002. Younger Dryas readvance in Squamish river valley, southern Coast mountains, British Columbia. *Quaternary Science Reviews* 21(18-19): 1925-1933. doi:[https://doi.org/10.1016/S0277-3791\(02\)00081-1](https://doi.org/10.1016/S0277-3791(02)00081-1).
- Froese, D., Barendregt, R., Enkin, R., and Baker, J. 2000. Paleomagnetic evidence for multiple late Pliocene-early Pleistocene glaciations in the Klondike area, Yukon Territory. *Canadian Journal of Earth Sciences* 37(6): 863-877. doi:<https://doi.org/10.1139/e00-014>.
- Fulton, R.J. 1991. A conceptual model for growth and decay of the Cordilleran Ice Sheet. *Géographie Physique et Quaternaire* 45(3): 281-286. doi:<https://doi.org/10.7202/032875ar>.
- Funder, S., Sørensen, A.H., Larsen, N.K., Bjørk, A.A., Briner, J.P., Olsen, J., Schomacker, A., Levy, L.B., and Kjær, K.H. 2021. Younger Dryas ice margin retreat in Greenland: new evidence from southwestern Greenland. *Climate of the Past* 17(2): 587-601. doi:<https://doi.org/10.5194/cp-17-587-2021>.
- Furtado, J.C., Di Lorenzo, E., Anderson, B.T., and Schneider, N. 2012. Linkages between the North Pacific Oscillation and central tropical Pacific SSTs at low frequencies. *Climate Dynamics* 39: 2833-2846. doi:<https://doi.org/10.1007/s00382-011-1245-4>.
- Gaglioti, B.V., Mann, D.H., Wooller, M.J., Jones, B.M., Wiles, G.C., Groves, P., Kunz, M.L., Baughman, C.A., and Reanier, R.E. 2017. Younger-Dryas cooling and sea ice feedbacks were prominent features of the Pleistocene-Holocene transition in Arctic Alaska. *Quaternary Science Reviews* 169: 330-343. doi:<https://doi.org/10.1016/j.quascirev.2017.05.012>.
- Gaglioti, B.V., Mann, D.H., Groves, P., Kunz, M.L., Farquharson, L.M., Reanier, R.E., Jones, B.M., and Wooller, M.J. 2018. Aeolian stratigraphy describes ice-age paleoenvironments in unglaciated Arctic Alaska. *Quaternary Science Reviews* 182: 175-190. [<https://doi.org/10.1016/j.quascirev.2018.01.002>].
- Gaglioti, B.V., Mann, D.H., Williams, A.P., Wiles, G.C., Stoffel, M., Oelkers, R., Jones, B.M., and Andreu-Hayles, L. 2019. Traumatic resin ducts in Alaska mountain hemlock trees provide a new proxy for winter storminess. *Journal of Geophysical Research*
- Gallagher, S.J., Kitamura, A., Iryu, Y., Itaki, T., Koizumi, I., and Hoiles, P.W. 2015. The Pliocene to recent history of the Kuroshio and Tsushima Currents: a multi-proxy approach. *Progress in Earth and Planetary Science* 2: 1-23. doi:<https://DOI.org/10.1186/s40645-015-0045-6>.

Garrett, E., Barlow, N.L., Cool, H., Kaufman, D.S., Shennan, I., and Zander, P.D. 2015. Constraints on regional drivers of relative sea-level change around Cordova, Alaska. *Quaternary Science Reviews* 113: 48-59. doi:<https://doi.org/10.1016/j.quascirev.2014.12.002>.

Geen, R., Bordoni, S., Battisti, D.S., and Hui, K. 2020. Monsoons, ITCZs, and the concept of the global monsoon. *Reviews of Geophysics* 58(4): e2020RG000700. doi:<https://doi.org/10.1029/2020RG000700>.

Geirsdóttir, Á., Miller, G.H., and Andrews, J.T. 2007. Glaciation, erosion, and landscape evolution of Iceland. *Journal of Geodynamics* 43(1): 170-186. doi:<https://doi.org/10.1016/j.jog.2006.09.017>.

Geirsdóttir, Á., Miller, G.H., Axford, Y., and Ólafsdóttir, S. 2009. Holocene and latest Pleistocene climate and glacier fluctuations in Iceland. *Quaternary Science Reviews* 28(21-22): 2107-2118. doi:<https://doi.org/10.1016/j.quascirev.2009.03.013>.

Godbout, J., Fazekas, A., Newton, C.H., Yeh, F.C., and Bousquet, J. 2008. Glacial vicariance in the Pacific Northwest: evidence from a lodgepole pine mitochondrial DNA minisatellite for multiple genetically distinct and widely separated refugia. *Molecular Ecology* 17(10): 2463-2475. doi:<https://doi.org/10.1111/j.1365-294X.2008.03761.x>.

Gombiner, J.H., Hemming, S.R., Hendy, I.L., Bryce, J.G., and Blichert-Toft, J. 2016. Isotopic and elemental evidence for Scabland Flood sediments offshore Vancouver Island. *Quaternary Science Reviews* 139: 129-137. doi:<https://doi.org/10.1016/j.quascirev.2016.02.026>.

Gong, X., Lembke-Jene, L., Lohmann, G., Knorr, G., Tiedemann, R., Zou, J., and Shi, X. 2019. Enhanced North Pacific deep-ocean stratification by stronger intermediate water formation during Heinrich Stadial 1. *Nature Communications* 10(1): 656. doi:<https://doi.org/10.1038/s41467-019-08606-2>.

Gordon, A.L., Weiss, R.F., Smethie Jr, W.M., and Warner, M.J. 1992. Thermocline and intermediate water communication between the South Atlantic and Indian Oceans. *Journal of Geophysical Research: Oceans* 97(C5): 7223-7240. doi:<https://doi.org/10.1029/92JC00485>.

Gordon, A.L., and Fine, R.A. 1996. Pathways of water between the Pacific and Indian oceans in the Indonesian seas. *Nature* 379(6561): 146-149. doi:<https://doi.org/10.1038/379146a0>.

Gordon, J.E., and Harkness, D.D. 1992. Magnitude and geographic variation of the radiocarbon content in Antarctic marine life: implications for reservoir corrections in radiocarbon dating. *Quaternary Science Reviews* 11(7-8): 697-708. doi:[https://doi.org/10.1016/0277-3791\(92\)90078-M](https://doi.org/10.1016/0277-3791(92)90078-M).

Gowan, E.J., Zhang, X., Khosravi, S., Rovere, A., Stocchi, P., Hughes, A.L., Gyllencreutz, R., Mangerud, J., Svendsen, J.-I., and Lohmann, G. 2021. A new global ice sheet reconstruction for the past 80 000 years. *Nature Communications* 12(1): 1199. doi:<https://doi.org/10.1038/s41467-021-21469-w>.

- Gray, W.R., Rae, J.W., Wills, R.C., Shevenell, A.E., Taylor, B., Burke, A., Foster, G.L., and Lear, C.H. 2018. Deglacial upwelling, productivity and CO₂ outgassing in the North Pacific Ocean. *Nature Geoscience* 11(5): 340-344. doi:<https://doi.org/10.1038/s41561-018-0108-6>.
- Greene, H., Reynolds, J., and Todd, B. 2016. Ice-sheet related landforms at the continental shelf edge, Albatross Bank, Alaska. *In Atlas of Submarine Glacial Landforms: Modern, Quaternary and Ancient. Edited by J.A. Dowdeswell and M. Canals and M. Jakobsson and B.J. Todd and E.K. Dowdeswell and K.A. Hogan. Geological society, London. pp. 379-380.*
- Greene, H.G., Bizzarro, J.J., O'Connell, V.M., and Brylinsky, C.K. 2007. Construction of digital potential marine benthic habitat maps using a coded classification scheme and its application. *Mapping the seafloor for habitat characterization: Geological Association of Canada Special Paper 47: 141-155.*
- Greene, H.G., O'Connell, V.M., and Brylinsky, C.K. 2011. Tectonic and glacial related seafloor geomorphology as possible demersal shelf rockfish habitat surrogates—Examples along the Alaskan convergent transform plate boundary. *Continental Shelf Research* 31(2): S39-S53. doi:<https://doi.org/10.1016/j.csr.2010.11.004>.
- Gu, D., and Philander, S.G. 1997. Interdecadal climate fluctuations that depend on exchanges between the tropics and extratropics. *Science* 275(5301): 805-807. doi:<https://doi.org/10.1126/science.275.5301.805>.
- Gulick, S.P., Jaeger, J.M., Mix, A.C., Asahi, H., Bahlburg, H., Belanger, C.L., Berbel, G.B., Childress, L., Cowan, E., and Drab, L. 2015. Mid-Pleistocene climate transition drives net mass loss from rapidly uplifting St. Elias Mountains, Alaska. *Proceedings of the National Academy of Sciences* 112(49): 15042-15047. doi:<https://doi.org/10.1073/pnas.1512549112>.
- Guthrie, R.D. 2001. Origin and causes of the mammoth steppe: a story of cloud cover, woolly mammal tooth pits, buckles, and inside-out Beringia. *Quaternary Science Reviews* 20: 549-574.
- Ha, K.-J., Seo, Y.-W., Lee, J.-Y., Kripalani, R., and Yun, K.-S. 2018. Linkages between the South and East Asian summer monsoons: a review and revisit. *Climate dynamics* 51: 4207-4227. doi:<https://doi.org/10.1007/s00382-017-3773-z>.
- Ha, K.J., Heo, K.Y., Lee, S.S., Yun, K.S., and Jhun, J.G. 2012. Variability in the East Asian monsoon: A review. *Meteorological Applications* 19(2): 200-215. doi:<https://doi.org/10.1002/met.1320>.
- Haeussler, P.J., Armstrong, P.A., Liberty, L.M., Ferguson, K.M., Finn, S.P., Arkle, J.C., and Pratt, T.L. 2015. Focused exhumation along megathrust splay faults in Prince William Sound, Alaska. *Quaternary Science Reviews* 113: 8-22. doi:<https://doi.org/10.1016/j.quascirev.2014.10.013>.
- Haeussler, P.J., Matmon, A., Arnold, M., Aumaître, G., Bourles, D., and Keddadouche, K. 2022. Late Quaternary deglaciation of Prince William Sound, Alaska. *Quaternary Research* 105: 115-134. doi:<https://doi.org/10.1017/qua.2021.33>.

- Hajdas, I., Bonani, G., Bodén, P., Peteet, D.M., and Mann, D.H. 1998. Cold reversal on Kodiak Island, Alaska, correlated with the European Younger Dryas by using variations of atmospheric ^{14}C content. *Geology* 26(11): 1047-1050. doi:[https://doi.org/10.1130/0091-7613\(1998\)026%3C1047:CROKIA%3E2.3.CO;2](https://doi.org/10.1130/0091-7613(1998)026%3C1047:CROKIA%3E2.3.CO;2).
- Hamilton, T.D., and Thorson, R.M. 1983. The Cordilleran ice sheet in Alaska. *In* Late Quaternary Environments of the United States. *Edited by* H.E. Wright. University of Minnesota, Minneapolis. pp. 38-52.
- Hamilton, T.D. 1994. Late Cenozoic glaciation of Alaska. *In* The Geology of Alaska. *Edited by* G. Plafker and H.C. Berg. Geological Society of America.
- Hamilton, T.D. 2010. Surficial geologic map of the Noatak National Preserve, Alaska. US Geological Survey Map 3036.
- Han, Z., Zhang, Q., Wen, Q., Lu, Z., Feng, G., Su, T., Li, Q., and Zhang, Q. 2020. The changes in ENSO-induced tropical Pacific precipitation variability in the past warm and cold climates from the EC-Earth simulations. *Climate Dynamics* 55: 503-519. doi:<https://doi.org/10.1007/s00382-020-05280-9>.
- Hansen, B.C., and Engstrom, D.R. 1996. Vegetation history of Pleasant Island, southeastern Alaska, since 13,000 yr BP. *Quaternary Research* 46(2): 161-175. doi:<https://doi.org/10.1006/qres.1996.0056>.
- Hanslik, D., Jakobsson, M., Backman, J., Björck, S., Sellén, E., O'Regan, M., Fornaciari, E., and Skog, G. 2010. Quaternary Arctic Ocean sea ice variations and radiocarbon reservoir age corrections. *Quaternary Science Reviews* 29(25-26): 3430-3441. doi:<https://doi.org/10.1016/j.quascirev.2010.06.011>.
- Harris, H.M., French, J.A., Heginbottom, G.H., Johnston, G.H., Ladanyi, B., Sego, D.C., and van Everdingen, R.O. 1988. Glossary of permafrost and related ground-ice terms. National Research Council of Canada, Ottawa Technical Memorandum No. 142 156, Ottawa, Ontario.
- Hartmann, B., and Wendler, G. 2005. The significance of the 1976 Pacific climate shift in the climatology of Alaska. *Journal of Climate* 18(22): 4824-4839. doi:<https://doi.org/10.1175/JCLI3532.1>.
- Haug, G.H., Ganopolski, A., Sigman, D.M., Rosell-Mele, A., Swann, G.E., Tiedemann, R., Jaccard, S.L., Bollmann, J., Maslin, M.A., and Leng, M.J. 2005. North Pacific seasonality and the glaciation of North America 2.7 million years ago. *Nature* 433(7028): 821-825. doi:<https://doi.org/10.1038/nature03332>.
- He, C., Zhou, T., Lin, A., Wu, B., Gu, D., Li, C., and Zheng, B. 2015. Enhanced or weakened western North Pacific subtropical high under global warming? *Scientific reports* 5(1): 16771.

- Heath, S.L., Loope, H.M., Curry, B.B., and Lowell, T.V. 2018. Pattern of southern Laurentide Ice Sheet margin position changes during Heinrich Stadials 2 and 1. *Quaternary Science Reviews* 201: 362-379. doi:<https://doi.org/10.1016/j.quascirev.2018.10.019>.
- Heaton, T.H., Talbot, S.L., and Shields, G.F. 1996. An ice age refugium for large mammals in the Alexander Archipelago, southeastern Alaska. *Quaternary Research* 46(2): 186-192. doi:<https://doi.org/10.1006/qres.1996.0058>.
- Heaton, T.H., and Grady, F. 2003. The late Wisconsin vertebrate history of Prince of Wales Island, southeast Alaska. *In* Ice age cave faunas of North America. *Edited by* B.W. Schubert and J.I. Mead and R.W. Graham. Indiana University Press, Bloomington, IN. pp. 17-53.
- Heaton, T.J., Köhler, P., Butzin, M., Bard, E., Reimer, R.W., Austin, W.E., Ramsey, C.B., Grootes, P.M., Hughen, K.A., and Kromer, B. 2020. Marine20—the marine radiocarbon age calibration curve (0–55,000 cal BP). *Radiocarbon* 62(4): 779-820. doi:<https://doi.org/10.1017/RDC.2020.68>.
- Hebda, C.F., McLaren, D., Mackie, Q., Fedje, D., Pedersen, M.W., Willerslev, E., Brown, K.J., and Hebda, R.J. 2022. Late Pleistocene palaeoenvironments and a possible glacial refugium on northern Vancouver Island, Canada: Evidence for the viability of early human settlement on the northwest coast of North America. *Quaternary Science Reviews* 279: 107388. doi:<https://doi.org/10.1016/j.quascirev.2022.107388>.
- Hebda, R.J. 1997. Late quaternary paleoecology of Brooks Peninsula. *In* Brooks Peninsula: An Ice Age Refugium on Vancouver Island. *Edited by* R.J. Hebda and J.C. Haggarty. BC Parks, Victoria, BC. pp. 9.1-9.48.
- Hebda, R.J., Howes, D., and Maxwell, B. 1997. Brooks Peninsula as an ice age refugium. *In* Brooks Peninsula: An Ice Age Refugium on Vancouver Island. *Edited by* R.J. Hebda and J.C. Haggarty. BC Parks, Victoria, BC. pp. 15.11-15.17.
- Hendy, I. 2009. A fresh perspective on the Cordilleran Ice Sheet. *Geology* 37(1): 95-96. doi:<https://doi.org/10.1130/focus012009.1>.
- Hendy, I.L., and Cosma, T. 2008. Vulnerability of the Cordilleran Ice Sheet to iceberg calving during late Quaternary rapid climate change events. *Paleoceanography* 23(2). doi:<https://doi.org/10.1029/2008PA001606>.
- Hetherington, R., Barrie, J.V., Reid, R.G., MacLeod, R., and Smith, D.J. 2004. Paleogeography, glacially induced crustal displacement, and Late Quaternary coastlines on the continental shelf of British Columbia, Canada. *Quaternary Science Reviews* 23(3-4): 295-318. doi:<https://doi.org/10.1016/j.quascirev.2003.04.001>.
- Heusser, C., Heusser, L., and Peteet, D. 1999. Humptulips revisited: a revised interpretation of Quaternary vegetation and climate of western Washington, USA. *Palaeogeography, Palaeoclimatology, Palaeoecology* 150(3-4): 191-221. doi:[https://doi.org/10.1016/S0031-0182\(98\)00225-9](https://doi.org/10.1016/S0031-0182(98)00225-9).

Heusser, C.J. 1960. Late-Pleistocene environments of north Pacific North America: an elaboration of late-glacial and postglacial climatic, physiographic, and biotic changes. American Geographical Society Special Publication No.35.

Heusser, C.J. 1989. North Pacific coastal refugia: the Queen Charlotte Islands in perspective. *In* The Outer Shores. *Edited by* G.G.E. Scudder and N. Gessler. University of British Columbia, Vancouver, BC. pp. 91-106.

Hidy, A.J., Gosse, J.C., Froese, D.G., Bond, J.D., and Rood, D.H. 2013. A latest Pliocene age for the earliest and most extensive Cordilleran Ice Sheet in northwestern Canada. *Quaternary Science Reviews* 61: 77-84. doi:<https://doi.org/10.1016/j.quascirev.2012.11.009>.

Higgins, R.W., Silva, V., Shi, W., and Larson, J. 2007. Relationships between climate variability and fluctuations in daily precipitation over the United States. *Journal of Climate* 20(14): 3561-3579. doi:<https://doi.org/10.1175/JCLI4196.1>.

Hill, D., Bruhis, N., Calos, S., Arendt, A., and Beamer, J. 2015. Spatial and temporal variability of freshwater discharge into the Gulf of Alaska. *Journal of Geophysical Research: Oceans* 120(2): 634-646. doi:<https://doi.org/10.1002/2014JC010395>.

Hill, J.C., and Driscoll, N.W. 2008. Paleodrainage on the Chukchi shelf reveals sea level history and meltwater discharge. *Marine Geology* 254(3-4): 129-151. doi:<https://doi.org/10.1016/j.margeo.2008.05.018>.

Hodell, D.A., Nicholl, J.A., Bontognali, T.R., Danino, S., Dorador, J., Dowdeswell, J.A., Einsle, J., Kuhlmann, H., Martrat, B., and Mlenek-Vautravers, M.J. 2017. Anatomy of Heinrich Layer 1 and its role in the last deglaciation. *Paleoceanography* 32(3): 284-303. doi:<https://doi.org/10.1002/2016PA003028>.

Hoffecker, J.F., Elias, S.A., Scott, G.R., O'Rourke, D.H., Hlusko, L.J., Potapova, O., Pitulko, V., Pavlova, E., Bourgeon, L., and Vachula, R.S. 2023. Beringia and the peopling of the Western Hemisphere. *Proceedings of the Royal Society B* 290(1990): 20222246. doi:<https://doi.org/10.1098/rspb.2022.2246>.

Hogg, A., Southon, J., Turney, C., Palmer, J., Bronk Ramsey, C., Fenwick, P., Boswijk, G., Friedrich, M., Helle, G., and Hughen, K. 2016. Punctuated shutdown of Atlantic meridional overturning circulation during Greenland Stadial 1. *Scientific Reports* 6(1): 25902. doi:<https://doi.org/10.1038/srep25902>.

Holloway, M.D., Sime, L.C., Singarayer, J.S., Tindall, J.C., Bunch, P., and Valdes, P.J. 2016. Antarctic last interglacial isotope peak in response to sea ice retreat not ice-sheet collapse. *Nature Communications* 7(1): 12293. doi:<https://doi.org/10.1038/ncomms12293>.

Holtedahl, H. 1958. Some remarks on geomorphology of continental shelves off Norway, Labrador, and southeast Alaska. *The Journal of Geology* 66(4): 461-467. doi:<https://doi.org/10.1086/626528>.

Hopkins, D.M. 1967. *The Bering Land Bridge*. Stanford University Press, Stanford.

Horikawa, K., Asahara, Y., Yamamoto, K., and Okazaki, Y. 2010. Intermediate water formation in the Bering Sea during glacial periods: Evidence from neodymium isotope ratios. *Geology* 38(5): 435-438. doi:<https://doi.org/10.1130/G30225.1>.

Hoskins, B.J., and Valdes, P.J. 1990. On the existence of storm-tracks. *Journal of Atmospheric Sciences* 47(15): 1854-1864. doi:[https://doi.org/10.1175/1520-0469\(1990\)047%3C1854:OTEOST%3E2.0.CO;2](https://doi.org/10.1175/1520-0469(1990)047%3C1854:OTEOST%3E2.0.CO;2).

Hoskins, B.J., and Hodges, K.I. 2002. New perspectives on the Northern Hemisphere winter storm tracks. *Journal of the Atmospheric Sciences* 59(6): 1041-1061. doi:[https://doi.org/10.1175/1520-0469\(2002\)059%3C1041:NPOTNH%3E2.0.CO;2](https://doi.org/10.1175/1520-0469(2002)059%3C1041:NPOTNH%3E2.0.CO;2).

Hostetler, S.W., and Clark, P.U. 1997. Climatic controls of western US glaciers at the Last Glacial Maximum. *Quaternary Science Reviews* 16(6): 505-511. doi:[https://doi.org/10.1016/S0277-3791\(96\)00116-3](https://doi.org/10.1016/S0277-3791(96)00116-3).

Hu, A., Meehl, G.A., and Han, W. 2007. Role of the Bering Strait in the thermohaline circulation and abrupt climate change. *Geophysical Research Letters* 34(5). doi:<https://doi.org/10.1029/2006GL028906>.

Hu, A., Meehl, G.A., Otto-Bliesner, B.L., Waelbroeck, C., Han, W., Loutre, M.-F., Lambeck, K., Mitrovica, J.X., and Rosenbloom, N. 2010. Influence of Bering Strait flow and North Atlantic circulation on glacial sea-level changes. *Nature Geoscience* 3(2): 118-121. doi:<https://doi.org/10.1038/ngeo729>.

Hu, A., Meehl, G.A., Han, W., Timmermann, A., Otto-Bliesner, B., Liu, Z., Washington, W.M., Large, W., Abe-Ouchi, A., and Kimoto, M. 2012. Role of the Bering Strait on the hysteresis of the ocean conveyor belt circulation and glacial climate stability. *Proceedings of the National Academy of Sciences* 109(17): 6417-6422. doi:<https://doi.org/10.1073/pnas.1116014109>.

Hu, D., Wu, L., Cai, W., Gupta, A.S., Ganachaud, A., Qiu, B., Gordon, A.L., Lin, X., Chen, Z., and Hu, S. 2015. Pacific western boundary currents and their roles in climate. *Nature* 522(7556): 299-308. doi:<https://doi.org/10.1038/nature14504>.

Hu, F.S., Brubaker, L.B., and Anderson, P.M. 1995. Postglacial vegetation and climate change in the northern Bristol Bay region, southwestern Alaska. *Quaternary Research* 43(3): 382-392. doi:<https://doi.org/10.1006/qres.1995.1044>.

Hu, Y., and Freymueller, J.T. 2019. Geodetic observations of time-variable glacial isostatic adjustment in Southeast Alaska and its implications for Earth rheology. *Journal of Geophysical Research: Solid Earth* 124(9): 9870-9889. doi:<https://doi.org/10.1029/2018JB017028>.

Hudson, A.M., Hatchett, B.J., Quade, J., Boyle, D.P., Bassett, S.D., Ali, G., and De los Santos, M.G. 2019. North-south dipole in winter hydroclimate in the western United States during the last deglaciation. *Scientific Reports* 9(1): 4826. doi:<https://doi.org/10.1038/s41598-019-41197-y>.

Hughes, A.L., Gyllencreutz, R., Lohne, Ø.S., Mangerud, J., and Svendsen, J.I. 2016. The last Eurasian ice sheets—a chronological database and time-slice reconstruction, DATED-1. *Boreas* 45(1): 1-45. doi:<https://doi.org/10.1111/bor.12142>.

Hughes, P.D., and Gibbard, P.L. 2018. Global glacier dynamics during 100 ka Pleistocene glacial cycles. *Quaternary Research* 90(1): 222-243. doi:<https://doi.org/10.1017/qua.2018.37>.

Hultén, E. 1937. Outline of the history of arctic and boreal biota during the Quaternary period. (No Title). Bokforlags Aktiebolaget Thule, Stockholm, Sweden.

Hutchinson, I., James, T.S., Reimer, P.J., Bornhold, B.D., and Clague, J.J. 2004. Marine and limnic radiocarbon reservoir corrections for studies of late- and postglacial environments in Georgia Basin and Puget Lowland, British Columbia, Canada and Washington, USA☆. *Quaternary Research* 61(2): 193-203. doi:<https://doi.org/10.1016/j.yqres.2003.10.004>.

Hutchinson, I. 2020. Spatiotemporal variation in ΔR on the West Coast of North America in the late Holocene: implications for dating the shells of marine mollusks. *American Antiquity* 85(4): 676-693. doi:<https://doi.org/10.1017/aaq.2020.47>.

Imbrie, J., Boyle, E., Clemens, S., Duffy, A., Howard, W., Kukla, G., Kutzbach, J., Martinson, D., McIntyre, A., and Mix, A. 1992. On the structure and origin of major glaciation cycles 1. Linear responses to Milankovitch forcing. *Paleoceanography* 7(6): 701-738. doi:<https://doi.org/10.1029/92PA02253>.

Jaccard, S., Galbraith, E., Sigman, D., Haug, G., Francois, R., Pedersen, T., Dulski, P., and Thierstein, H. 2009. Subarctic Pacific evidence for a glacial deepening of the oceanic respired carbon pool. *Earth and Planetary Science Letters* 277(1-2): 156-165. doi:<https://doi.org/10.1016/j.epsl.2008.10.017>.

Jakobsson, M., Pearce, C., Cronin, T.M., Backman, J., Anderson, L.G., Barrientos, N., Björk, G., Coxall, H., de Boer, A., and Mayer, L.A. 2017. Post-glacial flooding of the Bering Land Bridge dated to 11 cal ka BP based on new geophysical and sediment records. *Climate of the Past* 13(8): 991-1005. doi:<https://doi.org/10.5194/cp-13-991-2017>.

James, N.P., Eyles, C.H., Eyles, N., Hiatt, E.E., and Kurtis Kyser, T. 2009a. Carbonates within a Pleistocene glaciomarine succession, Yakataga Formation, Middleton Island, Alaska. *Sedimentology* 56(2): 367-397. doi:<https://doi.org/10.1111/j.1365-3091.2008.00973.x>.

James, T.S., Gowan, E.J., Wada, I., and Wang, K. 2009b. Viscosity of the asthenosphere from glacial isostatic adjustment and subduction dynamics at the northern Cascadia subduction zone,

- British Columbia, Canada. *Journal of Geophysical Research: Solid Earth* 114(B4). doi:<https://doi.org/10.1029/2008JB006077>.
- Joh, Y., Di Lorenzo, E., Siqueira, L., and Kirtman, B.P. 2021. Enhanced interactions of Kuroshio Extension with tropical Pacific in a changing climate. *Scientific reports* 11(1): 6247. doi:<https://doi.org/10.1038/s41598-021-85582-y>.
- Joh, Y., Delworth, T.L., Wittenberg, A.T., Cooke, W.F., Rosati, A.J., and Zhang, L. 2022. Stronger decadal variability of the Kuroshio Extension under simulated future climate change. *npj Climate and Atmospheric Science* 5(1): 63. doi:<https://doi.org/10.1038/s41612-022-00285-z>.
- Jóhannesson, T., Raymond, C., and Waddington, E. 1989. Time-scale for adjustment of glaciers to changes in mass balance. *Journal of Glaciology* 35(121): 355-369. doi:<https://doi.org/10.3189/S002214300000928X>.
- Jones, M.C., Peteet, D.M., Kurdyla, D., and Guilderson, T. 2009. Climate and vegetation history from a 14,000-year peatland record, Kenai Peninsula, Alaska. *Quaternary Research* 72(2): 207-217. doi:<https://doi.org/10.1016/j.yqres.2009.04.002>.
- Josberger, E.G., Bidlake, W.R., March, R.S., and Kennedy, B.W. 2007. Glacier mass-balance fluctuations in the Pacific Northwest and Alaska, USA. *Annals of Glaciology* 46: 291-296. doi:<https://doi.org/10.3189/172756407782871314>.
- Josenhans, H. 1994. Surficial geology, Quaternary stratigraphy and paleoenvironments of Queen Charlotte Basin. Geological Survey of Canada.
- Josenhans, H., Fedje, D., Pienitz, R., and Southon, J. 1997. Early humans and rapidly changing holocene sea levels in the queen Charlotte islands-Hecate strait, british Columbia, Canada. *Science* 277(5322): 71-74. doi:DOI: 10.1126/science.277.5322.71.
- Kaboth-Bahr, S., Bahr, A., Zeeden, C., Yamoah, K.A., Lone, M.A., Chuang, C.-K., Löwemark, L., and Wei, K.-Y. 2021. A tale of shifting relations: East Asian summer and winter monsoon variability during the Holocene. *Scientific Reports* 11(1): 6938. doi:<https://doi.org/10.1038/s41598-021-85444-7>.
- Kanevskiy, M. 2003. Cryogenic structure of mountain slope deposits, northeast Russia. *In* Proceedings of the Eighth International Conference on Permafrost, Zurich, Switzerland. Switzerland. Swets & Zeitlinger. pp. 513-518.
- Kanevskiy, M., Shur, Y., Fortier, D., Jorgenson, M., and Stephani, E. 2011. Cryostratigraphy of late Pleistocene syngenetic permafrost (yedoma) in northern Alaska, Ikillik River exposure. *Quaternary research* 75(3): 584-596. doi:<https://doi.org/10.1016/j.yqres.2010.12.003>.
- Kari, J. 2019. The Resilience of Dene Generative Geography, Considering" the Nen'Yese'Ensemble.". *Alaska Journal of Anthropology* 17(1-2)). doi:<https://doi.org/10.1038/s41598-022-20571-3>.

- Karlstrom, T.N. 1964. Quaternary geology of the Kenai Lowland and glacial history of the Cook Inlet region, Alaska. US Government Printing Office 443 2330-7102, Washington DC.
- Karlstrom, T.N. 1969. Regional setting and geology. *In* The Kodiak Island refugium: its geology, flora, fauna and history. *Edited by* T.N.V. Karlstrom and G.E. Ball. University of Alberta Press. pp. 20-54.
- Kathayat, G., Cheng, H., Sinha, A., Spötl, C., Edwards, R.L., Zhang, H., Li, X., Yi, L., Ning, Y., and Cai, Y. 2016. Indian monsoon variability on millennial-orbital timescales. *Scientific reports* 6(1): 24374. doi:<https://doi.org/10.1038/srep24374>.
- Kaufman, D.S., Anderson, R.S., Hu, F.S., Berg, E., and Werner, A. 2010. Evidence for a variable and wet Younger Dryas in southern Alaska. *Quaternary Science Reviews* 29(11-12): 1445-1452. doi:<https://doi.org/10.1016/j.quascirev.2010.02.025>.
- Kaufman, D.S., Young, N.E., Briner, J.P., and Manley, W.F. 2011. Alaska palaeo-glacier atlas (version 2). *Developments in Quaternary Sciences* 15: 427-445. doi:<https://doi.org/10.1016/B978-0-444-53447-7.00033-7>.
- Keigwin, L.D. 1998. Glacial-age hydrography of the far northwest Pacific Ocean. *Paleoceanography* 13(4): 323-339. doi:<https://doi.org/10.1029/98PA00874>.
- Keigwin, L.D., Donnelly, J.P., Cook, M.S., Driscoll, N.W., and Brigham-Grette, J. 2006. Rapid sea-level rise and Holocene climate in the Chukchi Sea. *Geology* 34(10): 861-864. doi:<https://doi.org/10.1130/G22712.1>.
- Keigwin, L.D., and Cook, M.S. 2007. A role for North Pacific salinity in stabilizing North Atlantic climate. *Paleoceanography* 22(3). doi:<https://doi.org/10.1029/2007PA001420>.
- Kerr, F.A. 1934. Glaciation in northern British Columbia. *Royal Society of Canada Transactions* 3(4): 17-31.
- Kim, H., Yeh, S.-W., An, S.-I., and Song, S.-Y. 2020. Changes in the role of Pacific decadal oscillation on sea ice extent variability across the mid-1990s. *Scientific reports* 10(1): 17564. doi:<https://doi.org/10.1038/s41598-020-74260-0>.
- Klein, D.R. 1965. Postglacial distribution patterns of mammals in the southern coastal regions of Alaska. *Arctic* 18(1): 7-20. doi:<https://www.jstor.org/stable/40507335>.
- Kleman, J., Fastook, J., Ebert, K., Nilsson, J., and Caballero, R. 2013. Pre-LGM Northern Hemisphere ice sheet topography. *Climate of the Past* 9(5): 2365-2378. doi:<https://doi.org/10.5194/cp-9-2365-2013>.
- Knippertz, P., Wernli, H., and Gläser, G. 2013. A global climatology of tropical moisture exports. *Journal of Climate* 26(10): 3031-3045. doi:<https://doi.org/10.1175/JCLI-D-12-00401.1>.

Knudson, K.P., and Ravelo, A.C. 2015. North Pacific Intermediate Water circulation enhanced by the closure of the Bering Strait. *Paleoceanography* 30(10): 1287-1304. doi:<https://doi.org/10.1002/2015PA002840>.

Kokorowski, H.D., Anderson, P.M., Mock, C.J., and Lozhkin, A.V. 2008. A re-evaluation and spatial analysis of evidence for a Younger Dryas climatic reversal in Beringia. *Quaternary Science Reviews* 27(17-18): 1710-1722. doi:<https://doi.org/10.1016/j.quascirev.2008.06.010>.

Kopczynski, S.E., Kelley, S.E., Lowell, T.V., Evenson, E.B., and Applegate, P.J. 2017. Latest Pleistocene advance and collapse of the Matanuska–Knik glacier system, Anchorage Lowland, southern Alaska. *Quaternary Science Reviews* 156: 121-134. doi:<https://doi.org/10.1016/j.quascirev.2016.11.026>.

Kotilainen, A., and Shackleton, N. 1995. Rapid climate variability in the North Pacific Ocean during the past 95,000 years. *Nature* 377(6547): 323-326. doi:<https://doi.org/10.1038/377323a0>.

Koutavas, A., Lynch-Stieglitz, J., Marchitto Jr, T.M., and Sachs, J.P. 2002. El Niño-like pattern in ice age tropical Pacific sea surface temperature. *Science* 297(5579): 226-230. doi:<https://doi.org/10.1126/science.1072376>.

Kovanen, D.J. 2002. Morphologic and stratigraphic evidence for Allerød and Younger Dryas age glacier fluctuations of the Cordilleran Ice Sheet, British Columbia, Canada and northwest Washington, USA. *Boreas* 31(2): 163-184. doi:<https://doi.org/10.1111/j.1502-3885.2002.tb01064.x>.

Kovanen, D.J., and Easterbrook, D.J. 2002. Paleodeviations of radiocarbon marine reservoir values for the northeast Pacific. *Geology* 30(3): 243-246. doi:[https://doi.org/10.1130/0091-7613\(2002\)030%3C0243:PORMRV%3E2.0.CO;2](https://doi.org/10.1130/0091-7613(2002)030%3C0243:PORMRV%3E2.0.CO;2).

Kubota, Y., Haneda, Y., Kameo, K., Itaki, T., Hayashi, H., Shikoku, K., Izumi, K., Head, M.J., Suganuma, Y., and Okada, M. 2021. Paleoceanography of the northwestern Pacific across the early–middle Pleistocene boundary (marine isotope stages 20–18). *Progress in Earth and Planetary Science* 8(1): 1-24. doi:<https://doi.org/10.1186/s40645-020-00395-3>.

Küehn, H., Lembke-Jene, L., Gersonde, R., Esper, O., Lamy, F., Arz, H., Kuhn, G., and Tiedemann, R. 2014. Laminated sediments in the Bering Sea reveal atmospheric teleconnections to Greenland climate on millennial to decadal timescales during the last deglaciation. *Climate of the Past* 10(6): 2215-2236. doi:<https://doi.org/10.5194/cp-10-2215-2014>.

Kuhnt, W., Holbourn, A., Hall, R., Zuvela, M., and Käse, R. 2004. Neogene history of the Indonesian throughflow. *Continent-Ocean Interactions within East Asian Marginal Seas. Geophysical Monograph* 149: 299-320. doi:<https://doi.org/10.1029/149GM16>.

- Kuhnt, W., Holbourn, A., Xu, J., Opdyke, B., De Deckker, P., Röhl, U., and Mudelsee, M. 2015. Southern Hemisphere control on Australian monsoon variability during the late deglaciation and Holocene. *Nature Communications* 6(1): 5916. doi:<https://doi.org/10.1038/ncomms6916>.
- Kullman, L. 2004. The changing flora of the alpine world. *IGBP Global Change Newsletter* 57.
- Kurek, J., Cwynar, L.C., Ager, T.A., Abbott, M.B., and Edwards, M.E. 2009. Late Quaternary paleoclimate of western Alaska inferred from fossil chironomids and its relation to vegetation histories. *Quaternary Science Reviews* 28(9-10): 799-811. doi:<https://doi.org/10.1016/j.quascirev.2008.12.001>.
- Kutzbach, J.E., and Guetter, P.J. 1986. The influence of changing orbital parameters and surface boundary conditions on climate simulations for the past 18 000 years. *Journal of Atmospheric Sciences* 43(16): 1726-1759. doi:[https://doi.org/10.1175/1520-0469\(1986\)043%3C1726:TIOCOP%3E2.0.CO;2](https://doi.org/10.1175/1520-0469(1986)043%3C1726:TIOCOP%3E2.0.CO;2).
- Laabs, B.J., Licciardi, J.M., Leonard, E.M., Munroe, J.S., and Marchetti, D.W. 2020. Updated cosmogenic chronologies of Pleistocene mountain glaciation in the western United States and associated paleoclimate inferences. *Quaternary Science Reviews* 242: 106427. doi:<https://doi.org/10.1016/j.quascirev.2020.106427>.
- Laberg, J., Vorren, T., Dowdeswell, J., Kenyon, N., and Taylor, J. 2000. The Andøya Slide and the Andøya Canyon, north-eastern Norwegian–Greenland Sea. *Marine Geology* 162(2-4): 259-275. doi:[https://doi.org/10.1016/S0025-3227\(99\)00087-0](https://doi.org/10.1016/S0025-3227(99)00087-0).
- Lachniet, M., Asmerom, Y., Polyak, V., and Denniston, R. 2017. Arctic cryosphere and Milankovitch forcing of Great Basin paleoclimate. *Scientific Reports* 7(1): 12955. doi:<https://doi.org/10.1038/s41598-017-13279-2>.
- Lagoe, M.B., Eyles, C.H., Eyles, N., and Hale, C. 1993. Timing of late Cenozoic tidewater glaciation in the far North Pacific. *Geological Society of America Bulletin* 105(12): 1542-1560. doi:[https://doi.org/10.1130/0016-7606\(1993\)105%3C1542:TOLCTG%3E2.3.CO;2](https://doi.org/10.1130/0016-7606(1993)105%3C1542:TOLCTG%3E2.3.CO;2).
- Laidre, K.L., Supple, M.A., Born, E.W., Regehr, E.V., Wiig, Ø., Ugarte, F., Aars, J., Dietz, R., Sonne, C., and Hegelund, P. 2022. Glacial ice supports a distinct and undocumented polar bear subpopulation persisting in late 21st-century sea ice conditions. *Science* 376(6599): 1333-1338. doi:<https://doi.org/10.1126/science.abk2793>.
- Lakeman, T.R., Clague, J.J., and Menounos, B. 2008. Advance of alpine glaciers during final retreat of the Cordilleran ice sheet in the Finlay River area, northern British Columbia, Canada. *Quaternary Research* 69(2): 188-200. doi:<https://doi.org/10.1016/j.yqres.2008.01.002>.
- Lam, A.R., MacLeod, K.G., Schilling, S.H., Leckie, R.M., Fraass, A.J., Patterson, M.O., and Venti, N.L. 2021. Pliocene to earliest Pleistocene (5–2.5 Ma) reconstruction of the Kuroshio Current Extension reveals a dynamic current. *Paleoceanography and Paleoclimatology* 36(9): e2021PA004318. doi:<https://doi.org/10.1029/2021PA004318>.

- Lambeck, K., and Chappell, J. 2001. Sea level change through the last glacial cycle. *Science* 292(5517): 679-686. doi:<https://doi.org/10.1126/science.1059549>.
- Lambeck, K., Rouby, H., Purcell, A., Sun, Y., and Sambridge, M. 2014. Sea level and global ice volumes from the Last Glacial Maximum to the Holocene. *Proceedings of the National Academy of Sciences* 111(43): 15296-15303. doi:<https://doi.org/10.1073/pnas.1411762111>.
- Landrum, L.L., and Holland, M.M. 2022. Influences of changing sea ice and snow thicknesses on simulated Arctic winter heat fluxes. *The Cryosphere* 16(4): 1483-1495. doi:<https://doi.org/10.5194/tc-16-1483-2022>.
- Lapointe, F., Francus, P., Lamoureux, S.F., Vuille, M., Jenny, J.-P., Bradley, R.S., and Massa, C. 2017. Influence of North Pacific decadal variability on the western Canadian Arctic over the past 700 years. *Climate of the Past* 13(4): 411-420. doi:<https://doi.org/10.5194/cp-13-411-2017>.
- Larsen, C.F., Motyka, R.J., Freymueller, J.T., Echelmeyer, K.A., and Ivins, E.R. 2005. Rapid viscoelastic uplift in southeast Alaska caused by post-Little Ice Age glacial retreat. *Earth and Planetary Science Letters* 237(3-4): 548-560. doi:<https://doi.org/10.1016/j.epsl.2005.06.032>.
- Laskar, J., Fienga, A., Gastineau, M., and Manche, H. 2011. La2010: a new orbital solution for the long-term motion of the Earth. *Astronomy & Astrophysics* 532: A89. doi:<https://DOI.org/10.1051/0004-6361/201116836>.
- Lease, R.O., Haeussler, P.J., Witter, R.C., Stockli, D.F., Bender, A.M., Kelsey, H.M., and O'Sullivan, P.B. 2021. Extreme Quaternary plate boundary exhumation and strike slip localized along the southern Fairweather fault, Alaska, USA. *Geology* 49(5): 602-606. doi:<https://doi.org/10.1130/G48464.1>.
- Leathers, D.J., Yarnal, B., and Palecki, M.A. 1991. The Pacific/North American teleconnection pattern and United States climate. Part I: Regional temperature and precipitation associations. *Journal of Climate* 4(5): 517-528. doi:[https://doi.org/10.1175/1520-0442\(1991\)004%3C0517:TPATPA%3E2.0.CO;2](https://doi.org/10.1175/1520-0442(1991)004%3C0517:TPATPA%3E2.0.CO;2).
- Leduc, G., Vidal, L., Tachikawa, K., Rostek, F., Sonzogni, C., Beaufort, L., and Bard, E. 2007. Moisture transport across Central America as a positive feedback on abrupt climatic changes. *Nature* 445(7130): 908-911. doi:<https://doi:10.1038/nature05578>.
- Lee, S.Y., and Poulsen, C. 2005. Tropical Pacific climate response to obliquity forcing in the Pleistocene. *Paleoceanography* 20(4). doi:<https://doi.org/10.1029/2005PA001161>.
- Lembke-Jene, L., Tiedemann, R., Nürnberg, D., Kokfelt, U., Kozdon, R., Max, L., Röhl, U., and Gorbarenko, S.A. 2017. Deglacial variability in Okhotsk Sea Intermediate Water ventilation and biogeochemistry: Implications for North Pacific nutrient supply and productivity. *Quaternary Science Reviews* 160: 116-137. doi:<https://doi.org/10.1016/j.quascirev.2017.01.016>.

- Lesnek, A.J., Briner, J.P., Lindqvist, C., Baichtal, J.F., and Heaton, T.H. 2018. Deglaciation of the Pacific coastal corridor directly preceded the human colonization of the Americas. *Science Advances* 4(5): eaar5040. doi:doi:10.1126/sciadv.aar5040.
- Lesnek, A.J., Briner, J.P., Baichtal, J.F., and Lyles, A.S. 2020. New constraints on the last deglaciation of the Cordilleran Ice Sheet in coastal Southeast Alaska. *Quaternary Research* 96: 140-160. doi:https://doi.org/10.1017/qua.2020.32.
- Letham, B., Martindale, A., Macdonald, R., Guiry, E., Jones, J., and Ames, K.M. 2016. Postglacial relative sea-level history of the Prince Rupert area, British Columbia, Canada. *Quaternary Science Reviews* 153: 156-191. doi:https://doi.org/10.1016/j.quascirev.2016.10.004.
- Levy, L.B., Kelly, M.A., Lowell, T.V., Hall, B.L., Howley, J.A., and Smith, C.A. 2016. Coeval fluctuations of the Greenland ice sheet and a local glacier, central East Greenland, during late glacial and early Holocene time. *Geophysical Research Letters* 43(4): 1623-1631. doi:https://doi.org/10.1002/2015GL067108.
- Lewis, D., and Smith, D. 2004. Dendrochronological mass balance reconstruction, Strathcona Provincial Park, Vancouver Island, British Columbia, Canada. *Arctic, Antarctic, and Alpine Research* 36(4): 598-606. doi:https://DOI.org/10.1657/1523-0430(2004)036[0598:DMBRSP]2.0.CO;2.
- Li, T., Wang, B., Wu, B., Zhou, T., Chang, C.-P., and Zhang, R. 2017. Theories on formation of an anomalous anticyclone in western North Pacific during El Niño: A review. *Journal of Meteorological Research* 31(6): 987-1006. doi:https://doi.org/10.1007/s13351-017-7147-6.
- Liakka, J., and Löfverström, M. 2018. Arctic warming induced by the Laurentide Ice Sheet topography. *Climate of the Past* 14(6): 887-900. doi:https://doi.org/10.5194/cp-14-887-2018.
- Liang, X., Zhao, D., Hua, Y., & Xu, Y.-G. (2024). Big mantle wedge and intraplate volcanism in Alaska: Insight from anisotropic tomography. *Journal of Geophysical Research: Solid Earth*, 129, e2023JB027617. https://doi.org/10.1029/2023JB027617
- Linkin, M.E., and Nigam, S. 2008. The North Pacific Oscillation–west Pacific teleconnection pattern: Mature-phase structure and winter impacts. *Journal of Climate* 21(9): 1979-1997. doi:https://doi.org/10.1175/2007JCLI2048.1.
- Linsley, B.K., Rosenthal, Y., and Oppo, D.W. 2010. Holocene evolution of the Indonesian throughflow and the western Pacific warm pool. *Nature Geoscience* 3(8): 578-583. doi:https://doi.org/10.1038/ngeo920.
- Liu, Q., Li, T., and Zhou, W. 2021. Impacts of multi-timescale circulations on meridional moisture transport. *Journal of Climate* 34(19): 8065-8085. doi:https://doi.org/10.1175/JCLI-D-20-0126.s1.

- Liu, W., and Fedorov, A.V. 2019. Global impacts of Arctic sea ice loss mediated by the Atlantic meridional overturning circulation. *Geophysical Research Letters* 46(2): 944-952. doi:<https://doi.org/10.1029/2018GL080602>.
- Liu, Z., and Alexander, M. 2007. Atmospheric bridge, oceanic tunnel, and global climatic teleconnections. *Reviews of Geophysics* 45(2). doi:<https://DOI.org/10.1029/2005RG000172>.
- Liu, Z., Lu, Z., Wen, X., Otto-Bliesner, B.L., Timmermann, A., and Cobb, K.M. 2014. Evolution and forcing mechanisms of El Niño over the past 21,000 years. *Nature* 515(7528): 550-553. doi:<https://doi.org/10.1038/nature13963>.
- Liu, Z., Tang, Y., Jian, Z., Poulsen, C.J., Welker, J.M., and Bowen, G.J. 2017. Pacific North American circulation pattern links external forcing and North American hydroclimatic change over the past millennium. *Proceedings of the National Academy of Sciences* 114(13): 3340-3345. doi:<https://doi.org/10.1073/pnas.1618201114>.
- Löfverström, M., Caballero, R., Nilsson, J., and Kleman, J. 2014. Evolution of the large-scale atmospheric circulation in response to changing ice sheets over the last glacial cycle. *Climate of the Past* 10(4): 1453-1471. doi:<https://doi.org/10.5194/cp-10-1453-2014>.
- Löfverström, M. 2020. A dynamic link between high-intensity precipitation events in southwestern North America and Europe at the Last Glacial Maximum. *Earth and Planetary Science Letters* 534: 116081. doi:<https://doi.org/10.1016/j.epsl.2020.116081>.
- Long, S.-M., Xie, S.-P., Zheng, X.-T., and Liu, Q. 2014. Fast and slow responses to global warming: Sea surface temperature and precipitation patterns. *Journal of Climate* 27(1): 285-299. doi:<https://doi.org/10.1175/JCLI-D-13-00297.1>.
- Lopes, C., and Mix, A. 2009. Pleistocene megafloods in the northeast Pacific. *Geology* 37(1): 79-82. doi:<https://doi.org/10.1130/G25025A.1>.
- Lopez-Maldonado, R., Bateman, J.B., Ellis, A., Bader, N.E., Ramirez, P., Arnold, A., Ajoku, O., Lee, H.I., Jesmok, G., and Upadhyay, D. 2023. Paleoclimate Changes in the Pacific Northwest Over the Past 36,000 Years From Clumped Isotope Measurements and Model Analysis. *Paleoceanography and Paleoclimatology* 38(2): e2021PA004266. doi:<https://doi.org/10.1029/2021PA004266>.
- Lopez, H., and Kirtman, B.P. 2019. ENSO influence over the Pacific North American sector: Uncertainty due to atmospheric internal variability. *Climate dynamics* 52(9-10): 6149-6172. doi:<https://doi.org/10.1007/s00382-018-4500-0>.
- Lora, J.M., Mitchell, J.L., Risi, C., and Tripathi, A.E. 2017. North Pacific atmospheric rivers and their influence on western North America at the Last Glacial Maximum. *Geophysical Research Letters* 44(2): 1051-1059. doi:<https://doi.org/10.1002/2017GL074274>.

Lund, D.C., Lynch-Stieglitz, J., and Curry, W.B. 2006. Gulf Stream density structure and transport during the past millennium. *Nature* 444(7119): 601-604. doi:<https://doi.org/10.1038/nature05277>.

Lund, D.C., Mix, A.C., and Southon, J. 2011. Increased ventilation age of the deep northeast Pacific Ocean during the last deglaciation. *Nature Geoscience* 4(11): 771-774. doi:<https://doi.org/10.1038/ngeo1272>.

Lutsko, N.J., and Popp, M. 2018. The influence of meridional gradients in insolation and longwave optical depth on the climate of a gray radiation GCM. *Journal of Climate* 31(19): 7803-7822. doi:<https://doi.org/10.1175/JCLI-D-18-0103.1>.

Lyle, M., Barron, J., Bralower, T.J., Huber, M., Olivarez Lyle, A., Ravelo, A.C., Rea, D.K., and Wilson, P.A. 2008. Pacific Ocean and Cenozoic evolution of climate. *Reviews of Geophysics* 46(2). doi:<https://doi.org/10.1029/2005RG000190>.

Lyle, M., Heusser, L., Ravelo, C., Yamamoto, M., Barron, J., Diffenbaugh, N.S., Herbert, T., and Andreasen, D. 2012. Out of the tropics: the Pacific, Great Basin Lakes, and Late Pleistocene water cycle in the western United States. *science* 337(6102): 1629-1633. doi:<https://doi.org/10.1126/science.1218390>.

Lynch-Stieglitz, J. 2017. The Atlantic meridional overturning circulation and abrupt climate change. *Annual Review of Marine Science* 9: 83-104. doi:<https://doi.org/10.1146/annurev-marine-010816-060415>.

Mackinnon, J.A., Simmons, H.L., Hargrove, J., Thomson, J., Peacock, T., Alford, M.H., Barton, B.I., Boury, S., Brenner, S.D., and Couto, N. 2021. A warm jet in a cold ocean. *Nature communications* 12(1): 2418. doi:<https://doi.org/10.1038/s41467-021-22505-5>.

Mackintosh, A.N., Anderson, B.M., and Pierrehumbert, R.T. 2017. Reconstructing climate from glaciers. *Annual Review of Earth and Planetary Sciences* 45: 649-680. doi:<https://doi.org/10.1146/annurev-earth-063016-020643>.

Maier, E., Méheust, M., Abelman, A., Gersonde, R., Chaplign, B., Ren, J., Stein, R., Meyer, H., and Tiedemann, R. 2015. Deglacial subarctic Pacific surface water hydrography and nutrient dynamics and links to North Atlantic climate variability and atmospheric CO₂. *Paleoceanography* 30(7): 949-968. doi:<https://doi.org/10.1002/2014PA002763>.

Maier, E., Zhang, X., Abelman, A., Gersonde, R., Mulitza, S., Werner, M., Méheust, M., Ren, J., Chaplign, B., and Meyer, H. 2018. North Pacific freshwater events linked to changes in glacial ocean circulation. *Nature* 559(7713): 241-245. doi:<https://doi.org/10.1038/s41586-018-0276-y>.

Maksym, T. 2019. Arctic and Antarctic Sea ice change: contrasts, commonalities, and causes. *Annual Review of Marine Science* 11: 187-213. doi:<https://doi.org/10.1146/annurev-marine-010816-060610>.

Malcomb, N.L., and Wiles, G.C. 2013. Tree-ring-based reconstructions of North American glacier mass balance through the Little Ice Age—Contemporary warming transition. *Quaternary Research* 79(2): 123-137. doi:<https://doi.org/10.1016/j.yqres.2012.11.005>.

Mangerud, J., Dokken, T., Hebbeln, D., Heggen, B., Ingólfsson, Ó., Landvik, J.Y., Mejdahl, V., Svendsen, J.I., and Vorren, T.O. 1998. Fluctuations of the Svalbard–Barents Sea Ice Sheet during the last 150 000 years. *Quaternary Science Reviews* 17(1-3): 11-42. doi:[https://doi.org/10.1016/S0277-3791\(97\)00069-3](https://doi.org/10.1016/S0277-3791(97)00069-3).

Manley, W., and Kaufman, D. 2002. *Alaska PaleoGlacier Atlas*. Institute of Arctic and Alpine Research (INSTAAR).

Mann, D.H., and Peteet, D.M. 1994. Extent and timing of the Last Glacial Maximum in southwestern Alaska. *Quaternary Research* 42(2): 136-148. doi:<https://doi.org/10.1006/qres.1994.1063>.

Mann, D.H., and Hamilton, T.D. 1995. Late Pleistocene and Holocene paleoenvironments of the North Pacific coast. *Quaternary Science Reviews* 14(5): 449-471.

Mann, D.H., and Crowell, A.L. 1996. A large earthquake occurring 700–800 years ago in Aialik Bay, southern coastal Alaska. *Canadian Journal of Earth Sciences* 33(1): 117-126. doi:<https://doi.org/10.1139/e96-012>.

Mann, D.H., Reanier, R.E., Peteet, D.M., Kunz, M.L., and Johnson, M. 2001. Environmental change and arctic paleoindians. *Arctic Anthropology*: 119-138. doi:<https://www.jstor.org/stable/40316726>.

Mann, D.H., Peteet, D.M., Reanier, R.E., and Kunz, M.L. 2002. Responses of an arctic landscape to Lateglacial and early Holocene climatic changes: the importance of moisture. *Quaternary Science Reviews* 21(8-9): 997-1021. doi:[https://doi.org/10.1016/S0277-3791\(01\)00116-0](https://doi.org/10.1016/S0277-3791(01)00116-0).

Mann, D.H., and Streveler, G.P. 2008. Post-glacial relative sea level, isostasy, and glacial history in Icy Strait, Southeast Alaska, USA. *Quaternary Research* 69(2): 201-216. doi:<https://doi.org/10.1016/j.yqres.2007.12.005>.

Mann, D.H., Groves, P., Reanier, R.E., and Kunz, M.L. 2010. Floodplains, permafrost, cottonwood trees, and peat: What happened the last time climate warmed suddenly in arctic Alaska? *Quaternary Science Reviews* 29(27-28): 3812-3830. doi:<https://doi.org/10.1016/j.quascirev.2010.09.002>.

Mantua, N.J., Hare, S.R., Zhang, Y., Wallace, J.M., and Francis, R.C. 1997. A Pacific interdecadal climate oscillation with impacts on salmon production. *Bulletin of the American Meteorological Society* 78(6): 1069-1080. doi:[https://doi.org/10.1175/1520-0477\(1997\)078%3C1069:APICOW%3E2.0.CO;2](https://doi.org/10.1175/1520-0477(1997)078%3C1069:APICOW%3E2.0.CO;2).

- Mantua, N.J., and Hare, S.R. 2002. The Pacific decadal oscillation. *Journal of oceanography* 58: 35-44. doi:<https://doi.org/10.1023/A:1015820616384>.
- Marcinkowski, K., and Peterson, D.L. 2015. A 350-year reconstruction of the response of South Cascade Glacier to interannual and interdecadal climatic variability. *Northwest Science* 89(1): 14-33. doi:<https://doi.org/10.3955/046.089.0102>.
- Marcott, S.A., Clark, P.U., Padman, L., Klinkhammer, G.P., Springer, S.R., Liu, Z., Otto-Bliesner, B.L., Carlson, A.E., Ungerer, A., and Padman, J. 2011. Ice-shelf collapse from subsurface warming as a trigger for Heinrich events. *Proceedings of the National Academy of Sciences* 108(33): 13415-13419. doi:<https://doi.org/10.1073/pnas.1104772108>.
- Marcott, S.A., Bauska, T.K., Buizert, C., Steig, E.J., Rosen, J.L., Cuffey, K.M., Fudge, T., Severinghaus, J.P., Ahn, J., and Kalk, M.L. 2014. Centennial-scale changes in the global carbon cycle during the last deglaciation. *Nature* 514(7524): 616-619. doi:<https://doi.org/10.1038/nature13799>.
- Marcott, S.A., Clark, P.U., Shakun, J.D., Brook, E.J., Davis, P.T., and Caffee, M.W. 2019. ^{10}Be age constraints on latest Pleistocene and Holocene cirque glaciation across the western United States. *npj Climate and Atmospheric Science* 2(1): 5. doi:<https://doi.org/10.1038/s41612-019-0062-z>.
- MARGO Project Members. 2009. Constraints on the magnitude and patterns of ocean cooling at the Last Glacial Maximum. *Nature Geoscience* 2(2): 127-132. doi:<https://doi.org/10.1038/ngeo411>.
- Margold, M., Jansson, K.N., Kleman, J., Stroeven, A.P., and Clague, J.J. 2013. Retreat pattern of the Cordilleran Ice Sheet in central British Columbia at the end of the last glaciation reconstructed from glacial meltwater landforms. *Boreas* 42(4): 830-847. doi:<https://doi.org/10.1111/bor.12007>.
- Marlow, M.S., Cooper, A.K. and Fisher, M.A., 1994. Geology of the eastern Bering Sea continental shelf. In Plafker, G. et al., *The Geology of Alaska*. <https://doi.org/10.1130/DNAG-GNA-G1>
- Marshall, S.J., Tarasov, L., Clarke, G.K., and Peltier, W.R. 2000. Glaciological reconstruction of the Laurentide Ice Sheet: physical processes and modelling challenges. *Canadian Journal of Earth Sciences* 37(5): 769-793. doi:<https://doi.org/10.1139/e99-113>.
- Marshall, S.J., and Clark, P.U. 2002. Basal temperature evolution of North American ice sheets and implications for the 100-kyr cycle. *Geophysical Research Letters* 29(24): 67-61-67-64. doi:<https://doi.org/10.1029/2002GL015192>.
- Martrat, B., Jimenez-Amat, P., Zahn, R., and Gimalt, J.O. 2014. Similarities and dissimilarities between the last two deglaciations and interglaciations in the North Atlantic region. *Quaternary Science Reviews* 99: 122-134. doi:<https://doi.org/10.1016/j.quascirev.2014.06.016>.

- Maslin, M. 2020. Tying celestial mechanics to Earth's ice ages. *Physics Today* 73(5): 48-53. doi:<https://doi.org/10.1063/PT.3.4474>.
- Mason, O.K., and Jordan, J.W. 2001. Minimal late Holocene sea level rise in the Chukchi Sea: arctic insensitivity to global change? *Global and Planetary Change* 32(1): 13-23. doi:[https://doi.org/10.1016/S0921-8181\(01\)00146-1](https://doi.org/10.1016/S0921-8181(01)00146-1).
- Mathewes, R.W., Heusser, L.E., and Patterson, R.T. 1993. Evidence for a Younger Dryas-like cooling event on the British Columbia coast. *Geology* 21(2): 101-104. doi:[https://doi.org/10.1130/0091-7613\(1993\)021%3C0101:EFAYDL%3E2.3.CO;2](https://doi.org/10.1130/0091-7613(1993)021%3C0101:EFAYDL%3E2.3.CO;2).
- Mathewes, R.W., Lian, O.B., Clague, J.J., and Huntley, M.J. 2015. Early Wisconsinan (MIS 4) glaciation on Haida Gwaii, British Columbia, and implications for biological refugia. *Canadian Journal of Earth Sciences* 52(11): 939-951. doi:<https://doi.org/10.1139/cjes-2015-0041>.
- Mathewes, R.W., and Clague, J.J. 2017. Paleoecology and ice limits of the early Fraser glaciation (marine isotope stage 2) on Haida Gwaii, British Columbia, Canada. *Quaternary Research* 88(2): 277-292. doi:v.
- Matmon, A., Briner, J.P., Carver, G., Bierman, P., and Finkel, R.C. 2010. Moraine chronosequence of the Donnelly Dome region, Alaska. *Quaternary Research* 74(1): 63-72. doi:<https://doi.org/10.1016/j.yqres.2010.04.007>.
- Matsumoto, K., Oba, T., Lynch-Stieglitz, J., and Yamamoto, H. 2002. Interior hydrography and circulation of the glacial Pacific Ocean. *Quaternary Science Reviews* 21(14-15): 1693-1704. doi:[https://doi.org/10.1016/S0277-3791\(01\)00142-1](https://doi.org/10.1016/S0277-3791(01)00142-1).
- Matsumoto, K. 2007. Radiocarbon-based circulation age of the world oceans. *Journal of Geophysical Research: Oceans* 112(C9). doi:<https://doi.org/10.1029/2007JC004095>.
- Max, L., Riethdorf, J.R., Tiedemann, R., Smirnova, M., Lembke-Jene, L., Fahl, K., Nürnberg, D., Matul, A., and Mollenhauer, G. 2012. Sea surface temperature variability and sea-ice extent in the subarctic northwest Pacific during the past 15,000 years. *Paleoceanography* 27(3). doi:<https://doi.org/10.1029/2012PA002292>.
- Max, L., Lembke-Jene, L., Riethdorf, J.-R., Tiedemann, R., Nürnberg, D., Kühn, H., and Mackensen, A. 2014. Pulses of enhanced North Pacific Intermediate Water ventilation from the Okhotsk Sea and Bering Sea during the last deglaciation. *Climate of the Past* 10(2): 591-605. doi:<https://doi.org/10.5194/cpd-9-6221-2013>.
- Max, L., Rippert, N., Lembke-Jene, L., Mackensen, A., Nürnberg, D., and Tiedemann, R. 2017. Evidence for enhanced convection of North Pacific Intermediate Water to the low-latitude Pacific under glacial conditions. *Paleoceanography* 32(1): 41-55. doi:<https://doi.org/10.1002/2016PA002994>.

- Max, L., Nürnberg, D., Chiessi, C.M., Lenz, M.M., and Mulitza, S. 2022. Subsurface ocean warming preceded Heinrich Events. *Nature Communications* 13(1): 4217. doi:<https://doi.org/10.1038/s41467-022-31754-x>.
- McCabe, G.J., Fountain, A.G., and Dyurgerov, M. 2000. Variability in winter mass balance of Northern Hemisphere glaciers and relations with atmospheric circulation. *Arctic, Antarctic, and Alpine Research* 32(1): 64-72. doi:<https://doi.org/10.1080/15230430.2000.12003340>.
- McCabe, G.J., Palecki, M.A., and Betancourt, J.L. 2004. Pacific and Atlantic Ocean influences on multidecadal drought frequency in the United States. *Proceedings of the National Academy of Sciences* 101(12): 4136-4141. doi:<https://doi.org/10.1073/pnas.0306738101>.
- McLaren, D., Fedje, D., Hay, M.B., Mackie, Q., Walker, I.J., Shugar, D.H., Eamer, J.B., Lian, O.B., and Neudorf, C. 2014. A post-glacial sea level hinge on the central Pacific coast of Canada. *Quaternary Science Reviews* 97: 148-169. doi:<https://doi.org/10.1016/j.quascirev.2014.05.023>.
- McManus, D., Creager, J., Echols, R., Holmes, M., Masters, P., and Flemming, N. 1983. The Holocene transgression on the Arctic flank of Beringia: Chukchi valley to Chukchi estuary to Chukchi Sea. *In Quaternary Coastlines and Marine Archaeology: Towards a Prehistory of Land Bridges and Continents. Edited by P.M. Masters and N.C. Fleming. Pergamon London, London.* pp. 365-388.
- McManus, D.A., and Creager, J.S. 1984. Sea-level Data for Parts of the Bering-Chukchi Shelves of Beringia from 19,000 to 10,000 14C yr BP 1. *Quaternary Research* 21(3): 317-325. doi:[https://doi.org/10.1016/0033-5894\(84\)90071-1](https://doi.org/10.1016/0033-5894(84)90071-1).
- McPhaden, M.J., Zebiak, S.E., and Glantz, M.H. 2006. ENSO as an integrating concept in earth science. *Science* 314(5806): 1740-1745. doi:<https://doi.org/10.1126/science.1132588>.
- Méheust, M., Stein, R., Fahl, K., and Gersonde, R. 2018. Sea ice variability in the subarctic North Pacific and adjacent Bering Sea during the past 25 ka: new insights from IP 25 and U k' 37 proxy records. *arktos* 4: 1-19. doi:<https://doi.org/10.1007/s41063-018-0043-1>.
- Meier, M.F., Dyurgerov, M.B., and McCabe, G.J. 2003. The health of glaciers: Recent changes in glacier regime. *Climatic Change* 59(1-2): 123-135. doi:<https://doi.org/10.1023/A:1024410528427>.
- Menounos, B., Osborn, G., Clague, J.J., and Luckman, B.H. 2009. Latest Pleistocene and Holocene glacier fluctuations in western Canada. *Quaternary Science Reviews* 28(21-22): 2049-2074.
- Menounos, B., Goehring, B.M., Osborn, G., Margold, M., Ward, B., Bond, J., Clarke, G.K., Clague, J.J., Lakeman, T., and Koch, J. 2017. Cordilleran Ice Sheet mass loss preceded climate reversals near the Pleistocene Termination. *Science* 358(6364): 781-784. doi:<https://doi.org/10.1126/science.aan3001>.

Menviel, L., Timmermann, A., Timm, O.E., Mouchet, A., Abe-Ouchi, A., Chikamoto, M., Harada, N., Ohgaito, R., and Okazaki, Y. 2012. Removing the North Pacific halocline: Effects on global climate, ocean circulation and the carbon cycle. *Deep Sea Research Part II: Topical Studies in Oceanography* 61: 106-113. doi:<https://doi.org/10.1016/j.dsr2.2011.03.005>.

Mercer, J.H. 1984. Simultaneous climatic change in both hemispheres and similar bipolar interglacial warming: Evidence and implications. *In Climate Processes and Climate Sensitivity. Edited by J.E. Hansen and T. Takahashi. American Geophysical Union, Washington D.C.* pp. 307-313.

Merrand, Y., and Hallet, B. 2001. Glacier Erosion and Convergent Tectonics in Southern Alaska. *In AGU Fall Meeting Abstracts.* pp. IP51B-12.

Mesquita, M.S., Atkinson, D.E., and Hodges, K.I. 2010. Characteristics and variability of storm tracks in the North Pacific, Bering Sea, and Alaska. *Journal of Climate* 23(2): 294-311. doi:<https://doi.org/10.1175/2009JCLI3019.1>.

Miller, R.D. 1972. Surficial geology of the Juneau urban area and vicinity, Alaska, with emphasis on earthquake and other geologic hazards. US Geological Survey] 2331-1258.

Miller, R.D. 1973. Gastineau channel formation: a composite glaciomarine deposit near Juneau, Alaska. US Geological Survey Bulletin 1394(C): C1-C20. doi:<https://doi.org/10.3133/b1394C>.

Miller, R.D. 1975. Surficial geologic map of the Juneau urban area and vicinity, Alaska. *In US Geological Survey Misc. Investigations Series.* p. Map 855.

Misarti, N., Finney, B.P., Jordan, J.W., Maschner, H.D., Addison, J.A., Shapley, M.D., Krumhardt, A., and Beget, J.E. 2012. Early retreat of the Alaska Peninsula Glacier Complex and the implications for coastal migrations of First Americans. *Quaternary Science Reviews* 48: 1-6. doi:<https://doi.org/10.1016/j.quascirev.2012.05.014>.

Molnia, B.F. 1986. Glacial history of the northeastern Gulf of Alaska—a synthesis. *In Glaciation in Alaska: The Geologic Record, 1986. Edited by T.D. Hamilton and K.M. Reed and R.M. Thorson. Alaska Geological Society.*

Molnia, B.F., and Post, A. 1995. Holocene history of Bering Glacier, Alaska: a prelude to the 1993–1994 surge. *Physical Geography* 16(2): 87-117. doi:<https://doi.org/10.1080/02723646.1995.10642545>.

Molnos, S., Petri, S., Lehmann, J., Peukert, E., and Coumou, D. 2017. The sensitivity of the large-scale atmosphere circulation to changes in surface temperature gradients in the Northern Hemisphere. *Earth System Dynamics Discussions*: 1-17. doi:<https://doi.org/10.5194/esd-2017-65>.

- Montelli, A., Gulick, S.P., Worthington, L.L., Mix, A., Davies-Walczak, M., Zellers, S.D., and Jaeger, J.M. 2017. Late Quaternary glacial dynamics and sedimentation variability in the Bering Trough, Gulf of Alaska. *Geology* 45(3): 251-254. doi:<https://doi.org/10.1130/G38836.1>.
- Montelli, A., Dowdeswell, J.A., Ottesen, D., and Johansen, S.E. 2022. Three-dimensional architecture and evolution of Quaternary contourite drifts on the Vøring Plateau, Norwegian Sea. *Marine Geology* 453: 106882. doi:<https://doi.org/10.1016/j.margeo.2022.106882>.
- Moore, J.C. 1974. Geologic and structural map of the Sanak Islands, southwestern Alaska.
- Moore Jr, T., Burckle, L., Geitzenauer, K., Luz, B., Molina-Cruz, A., Robertson, J., Sachs, H., Sancetta, C., Thiede, J., and Thompson, P. 1980. The reconstruction of sea surface temperatures in the Pacific Ocean of 18,000 BP. *Marine Micropaleontology* 5: 215-247. doi:[https://doi.org/10.1016/0377-8398\(80\)90012-2](https://doi.org/10.1016/0377-8398(80)90012-2).
- Morée, A.L., and Schwinger, J. 2020. A Last Glacial Maximum forcing dataset for ocean modelling. *Earth System Science Data* 12(4): 2971-2985. doi:<https://doi.org/10.5194/essd-12-2971-2020>.
- Morley, J.J., Hays, J.D., and Robertson, J.H. 1982. Stratigraphic framework for the late Pleistocene in the northwest Pacific Ocean. *Deep Sea Research Part A. Oceanographic Research Papers* 29(12): 1485-1499. doi:[https://doi.org/10.1016/0198-0149\(82\)90038-3](https://doi.org/10.1016/0198-0149(82)90038-3).
- Morrill, C., Lowry, D.P., and Hoell, A. 2018. Thermodynamic and dynamic causes of pluvial conditions during the Last Glacial Maximum in western North America. *Geophysical Research Letters* 45(1): 335-345. doi:<https://doi.org/10.1002/2017GL075807>.
- Mosher, D.C., and Hewitt, A.T. 2004. Late Quaternary deglaciation and sea-level history of eastern Juan de Fuca Strait, Cascadia. *Quaternary International* 121(1): 23-39. doi:<https://doi.org/10.1016/j.quaint.2004.01.021>.
- Motyka, R.J., Truffer, M., Fahnestock, M., Mortensen, J., Rysgaard, S., and Howat, I. 2011. Submarine melting of the 1985 Jakobshavn Isbræ floating tongue and the triggering of the current retreat. *Journal of Geophysical Research: Earth Surface* 116(F1). doi:<https://doi.org/10.1029/2009JF001632>.
- Moucha, R., Forte, A.M., Mitrovica, J.X., Rowley, D.B., Quéré, S., Simmons, N.A. and Grand, S.P., 2008. Dynamic topography and long-term sea-level variations: There is no such thing as a stable continental platform. *Earth and Planetary Science Letters*, 271(1-4), pp.101-108. doi:<https://doi.org/10.1016/j.epsl.2008.03.056>.
- Muhs, D.R., Ager, T.A., Been, J., Bradbury, J.P., and Dean, W.E. 2003. A late Quaternary record of eolian silt deposition in a maar lake, St. Michael Island, western Alaska. *Quaternary Research* 60(1): 110-122. doi:[https://doi.org/10.1016/S0033-5894\(03\)00062-0](https://doi.org/10.1016/S0033-5894(03)00062-0).

Muhs, D.R., Budahn, J.R., McGeehin, J.P., Bettis III, E.A., Skipp, G., Paces, J.B., and Wheeler, E.A. 2013. Loess origin, transport, and deposition over the past 10,000 years, Wrangell-St. Elias National Park, Alaska. *Aeolian Research* 11: 85-99.
doi:<https://doi.org/10.1016/j.aeolia.2013.06.001>.

Muller, E.H. 1952. The glacial geology of the Naknek district, the Bristol Bay region, Alaska. Earth Science, University of Illinois at Urbana-Champaign, Ann Arbor MI.

Mundhenk, B.D., Barnes, E.A., and Maloney, E.D. 2016. All-season climatology and variability of atmospheric river frequencies over the North Pacific. *Journal of Climate* 29(13): 4885-4903.
doi:<https://doi.org/10.1175/JCLI-D-15-0655.1>.

Munroe, J.S., and Laabs, B.J. 2013. Temporal correspondence between pluvial lake highstands in the southwestern US and Heinrich Event 1. *Journal of Quaternary Science* 28(1): 49-58.
doi:<https://doi.org/10.1002/jqs.2586>.

Munroe, J.S., Walcott, C.K., Amidon, W.H., and Landis, J.D. 2020. A top-to-bottom luminescence-based chronology for the post-LGM regression of a Great Basin pluvial Lake. *Quaternary* 3(2): 11. doi:<https://doi.org/10.3390/quat3020011>.

Murton, J.B., Goslar, T., Edwards, M.E., Bateman, M.D., Danilov, P.P., Savvinov, G.N., Gubin, S.V., Ghaleb, B., Haile, J., and Kanevskiy, M. 2015. Palaeoenvironmental interpretation of yedoma silt (ice complex) deposition as cold-climate Loess, Duvanny Yar, Northeast Siberia. *Permafrost and Periglacial Processes* 26(3): 208-288. doi:<https://doi.org/10.1002/ppp.1843>.

Namias, J., Yuan, X., and Cayan, D.R. 1988. Persistence of North Pacific sea surface temperature and atmospheric flow patterns. *Journal of Climate* 1(7): 682-703.
doi:[https://doi.org/10.1175/1520-0442\(1988\)001%3C0682:PONPSS%3E2.0.CO;2](https://doi.org/10.1175/1520-0442(1988)001%3C0682:PONPSS%3E2.0.CO;2).

National, W.S. 2023. What Does El Niño Mean for Northern California? [accessed 15 July 2023 2023].

Neal, E.G., Hood, E., and Smikrud, K. 2010. Contribution of glacier runoff to freshwater discharge into the Gulf of Alaska. *Geophysical Research Letters* 37(6).
doi:<https://doi.org/10.1029/2010GL042385>.

Nelson, D.B., Abbott, M.B., Steinman, B., Polissar, P.J., Stansell, N.D., Ortiz, J.D., Rosenmeier, M.F., Finney, B.P., and Riedel, J. 2011. Drought variability in the Pacific Northwest from a 6,000-yr lake sediment record. *Proceedings of the National Academy of Sciences* 108(10): 3870-3875.
doi:<https://doi.org/10.1073/pnas.1009194108>.

Newman, M., Kiladis, G.N., Weickmann, K.M., Ralph, F.M., and Sardeshmukh, P.D. 2012. Relative contributions of synoptic and low-frequency eddies to time-mean atmospheric moisture transport, including the role of atmospheric rivers. *Journal of climate* 25(21): 7341-7361. doi:<https://DOI.org/10.1175/JCLI-D-11-00665.1>.

- Newman, M., Alexander, M.A., Ault, T.R., Cobb, K.M., Deser, C., Di Lorenzo, E., Mantua, N.J., Miller, A.J., Minobe, S., and Nakamura, H. 2016. The Pacific decadal oscillation, revisited. *Journal of Climate* 29(12): 4399-4427. doi:<https://doi.org/10.1175/JCLI-D-15-0508.1>.
- NGRIP Members. 2004. High-resolution record of Northern Hemisphere climate extending into the last interglacial period. *Nature* 431(7005): 147-151. doi:<https://doi.org/10.1038/nature02805>.
- Nichols, D.R., and Yehle, L.A. 1969. Engineering geologic map of the southeastern Copper River basin, Alaska. *In* USGS Misc Investigations. USGS.
- Nielsen, T., De Santis, L., Dahlgren, K., Kuijpers, A., Laberg, J., Nygård, A., Praeg, D., and Stoker, M. 2005. A comparison of the NW European glaciated margin with other glaciated margins. *Marine and Petroleum Geology* 22(9-10): 1149-1183. doi:<https://doi.org/10.1016/j.marpetgeo.2004.12.007>.
- Norel, M., Kałczyński, M., Pińskwar, I., Krawiec, K., and Kundzewicz, Z.W. 2021. Climate variability indices—a guided tour. *Geosciences* 11(3): 128. doi:<https://doi.org/10.3390/geosciences11030128>.
- Norris, S., Garcia-Castellanos, D., Jansen, J., Carling, P., Margold, M., Woywitka, R., and Froese, D. 2021. Catastrophic drainage from the northwestern outlet of glacial Lake Agassiz during the Younger Dryas. *Geophysical Research Letters* 48(15): e2021GL093919. doi:<https://doi.org/10.1029/2021GL093919>.
- O’Conner, J., and Costa, J. 2004. *The World’s Largest Floods Past and Present: Their Causes and Magnitudes*. US Geological Survey Circular 1254, Reston, VA, USA.
- Oerlemans, J. 1992. Climate sensitivity of glaciers in southern Norway: application of an energy-balance model to Nigardsbreen, Hellstugubreen and Alfotbreen. *Journal of Glaciology* 38(129): 223-232. doi:<https://doi.org/10.3189/S0022143000003634>.
- Oerlemans, J. 2005. Extracting a climate signal from 169 glacier records. *Science* 308(5722): 675-677. doi:<https://doi.org/10.1126/science.1107046>.
- Ohmura, A., Kasser, P., and Funk, M. 1992. Climate at the equilibrium line of glaciers. *Journal of Glaciology* 38(130): 397-411.
- Okazaki, Y., Timmermann, A., Menviel, L., Harada, N., Abe-Ouchi, A., Chikamoto, M., Mouchet, A., and Asahi, H. 2010. Deepwater formation in the North Pacific during the last glacial termination. *Science* 329(5988): 200-204. doi:<https://doi.org/10.1126/science.1190612>.
- Okazaki, Y., Sagawa, T., Asahi, H., Horikawa, K., and Onodera, J. 2012. Ventilation changes in the western North Pacific since the last glacial period. *Climate of the Past* 8(1): 17-24. doi:<https://doi.org/10.5194/cp-8-17-2012>.

- Okazaki, Y., Kimoto, K., Asahi, H., Sato, M., Nakamura, Y., and Harada, N. 2014. Glacial to deglacial ventilation and productivity changes in the southern Okhotsk Sea. *Palaeogeography, Palaeoclimatology, Palaeoecology* 395: 53-66. doi:<https://doi.org/10.1016/j.palaeo.2013.12.013>.
- Osman, M.B., Tierney, J.E., Zhu, J., Tardif, R., Hakim, G.J., King, J., and Poulsen, C.J. 2021. Globally resolved surface temperatures since the Last Glacial Maximum. *Nature* 599(7884): 239-244. doi:<https://doi.org/10.1038/s41586-021-03984-4>.
- Oster, J.L., Ibarra, D.E., Winnick, M.J., and Maher, K. 2015. Steering of westerly storms over western North America at the Last Glacial Maximum. *Nature Geoscience* 8(3): 201-205. doi:<https://doi.org/10.1038/ngeo2365>.
- Ottesen, D., Dowdeswell, J., and Rise, L. 2005. Submarine landforms and the reconstruction of fast-flowing ice streams within a large Quaternary ice sheet: The 2500-km-long Norwegian-Svalbard margin (57–80 N). *Geological Society of America Bulletin* 117(7-8): 1033-1050. doi:<https://doi.org/10.1130/B25577.1>.
- Otto-Bliesner, B.L., Brady, E.C., Clauzet, G., Tomas, R., Levis, S., and Kothavala, Z. 2006. Last Glacial Maximum and Holocene climate in CCSM3. *Journal of Climate* 19(11): 2526-2544. doi:<https://doi.org/10.1175/JCLI3748.1>.
- Overland, J.E., Adams, J.M., and Bond, N.A. 1999. Decadal variability of the Aleutian low and its relation to high-latitude circulation. *Journal of Climate* 12(5): 1542-1548. doi:[https://doi.org/10.1175/1520-0442\(1999\)012%3C1542:DVOTAL%3E2.0.CO;2](https://doi.org/10.1175/1520-0442(1999)012%3C1542:DVOTAL%3E2.0.CO;2).
- Oviatt, C.G. 2015. Chronology of Lake Bonneville, 30,000 to 10,000 yr BP. *Quaternary Science Reviews* 110: 166-171. doi:<https://doi.org/10.1016/j.quascirev.2014.12.016>.
- Pan, L., Powell, E.M., Latychev, K., Mitrovica, J.X., Creveling, J.R., Gomez, N., Hoggard, M.J., and Clark, P.U. 2021. Rapid postglacial rebound amplifies global sea level rise following West Antarctic Ice Sheet collapse. *Science Advances* 7(18): eabf7787. doi:<https://doi.org/10.1126/sciadv.abf7787>.
- Papineau, J.M. 2001. Winter temperature anomalies in Alaska correlated with ENSO and PDO. *International Journal of Climatology: A Journal of the Royal Meteorological Society* 21(13): 1577-1592. doi:<https://doi.org/10.1002/joc.686>.
- Parrenin, F., Masson-Delmotte, V., Köhler, P., Raynaud, D., Paillard, D., Schwander, J., Barbante, C., Landais, A., Wegner, A., and Jouzel, J. 2013. Synchronous change of atmospheric CO₂ and Antarctic temperature during the last deglacial warming. *Science* 339(6123): 1060-1063. doi:<https://doi.org/10.1126/science.1226368>.
- Paul, A., Mulitza, S., Stein, R., and Werner, M. 2021. A global climatology of the ocean surface during the Last Glacial Maximum mapped on a regular grid (GLOMAP). *Climate of the Past* 17(2): 805-824. doi:<https://doi.org/10.5194/cp-17-805-2021>.

Pederson, G.T., Betancourt, J.L., and McCabe, G.J. 2013. Regional patterns and proximal causes of the recent snowpack decline in the Rocky Mountains, US. *Geophysical Research Letters* 40(9): 1811-1816. doi:<https://doi.org/10.1002/grl.50424>.

Peltier, W.R., Argus, D., and Drummond, R. 2015. Space geodesy constrains ice age terminal deglaciation: The global ICE-6G_C (VM5a) model. *Journal of Geophysical Research: Solid Earth* 120(1): 450-487. doi:<https://doi.org/10.1002/2014JB011176>.

Pelto, B.M., Caissie, B.E., Petsch, S.T., and Brigham-Grette, J. 2018. Oceanographic and climatic change in the Bering Sea, Last Glacial Maximum to Holocene. *Paleoceanography and Paleoclimatology* 33(1): 93-111. doi:<https://doi.org/10.1002/2017PA003265>.

Perkins, A.J., and Brennand, T.A. 2015. Refining the pattern and style of Cordilleran Ice Sheet retreat: palaeogeography, evolution and implications of lateglacial ice-dammed lake systems on the southern Fraser Plateau, British Columbia, Canada. *Boreas* 44(2): 319-342. doi:<https://doi.org/10.1111/bor.12100>.

Peteet, D.M., and Mann, D.H. 1994. Late-glacial vegetational, tephra, and climatic history of southwestern Kodiak Island, Alaska. *Ecoscience* 1(3): 255-267. doi:<https://doi.org/10.1080/11956860.1994.11682250>.

Peteet, D., Del Genio, A., and Lo, K.K.W. 1997. Sensitivity of northern hemisphere air temperatures and snow expansion to North Pacific sea surface temperatures in the Goddard Institute for Space Studies general circulation model. *Journal of Geophysical Research: Atmospheres* 102(D20): 23781-23791. doi:<https://doi.org/10.1029/97JD01573>.

Peteet, D.M. 2007. Muskeg archives of vegetation, migration, and climate history in the Gulf of Alaska arc. *In* Geological Society of America, Cordilleran Section - 103rd Annual Meeting, Bellingham.

Petrick, B., Martínez-García, A., Auer, G., Reuning, L., Auderset, A., Deik, H., Takayanagi, H., De Vleeschouwer, D., Iryu, Y., and Haug, G.H. 2019. Glacial Indonesian Throughflow weakening across the mid-Pleistocene climatic transition. *Scientific reports* 9(1): 16995. doi:<https://doi.org/10.1038/s41598-019-53382-0>.

Péwé, T., and Reger, R. 1983. Delta river area, Alaska range. *In* Guidebook to Permafrost and Quaternary Geology Along the Richardson and Glenn Highways Between Fairbanks and Anchorage, Alaska. University of Alaska, Fairbanks. *Edited by* T. Péwé and R.D. Reger. pp. 47-135.

Péwé, T.L. 1975. Quaternary Geology of Alaska. US Government Printing Office. pp. 1-144.

Pickart, R.S., Moore, G., Macdonald, A.M., Renfrew, I.A., Walsh, J.E., and Kessler, W.S. 2009. Seasonal evolution of Aleutian low-pressure systems: Implications for the North Pacific sub-polar circulation. *Journal of Physical Oceanography* 38: 1. doi:<https://DOI.org/10.1175/2008JPO3891.1>.

- Pico, T., Mitrovica, J., and Mix, A. 2020. Sea level fingerprinting of the Bering Strait flooding history detects the source of the Younger Dryas climate event. *Science Advances* 6(9): eaay2935. doi:<https://doi.org/10.1126/sciadv.aay2935>.
- Pierrehumbert, R.T. 2000. Climate change and the tropical Pacific: The sleeping dragon wakes. *Proceedings of the National Academy of Sciences* 97(4): 1355-1358. doi:<https://doi.org/10.1073/pnas.97.4.1355>.
- Pigati, J.S., and Springer, K.B. 2022. Hydroclimate response of spring ecosystems to a two-stage Younger Dryas event in western North America. *Scientific Reports* 12(1): 7323. doi:<https://doi.org/10.1038/s41598-022-11377-4>.
- Pinho, T.M., Chiessi, C.M., Portilho-Ramos, R.C., Campos, M.C., Crivellari, S., Nascimento, R.A., Albuquerque, A.L., Bahr, A., and Mulitza, S. 2021. Meridional changes in the South Atlantic Subtropical Gyre during Heinrich Stadials. *Scientific Reports* 11(1): 9419. doi:<https://doi.org/10.1038/s41598-021-88817-0>.
- Porter, S.C. 1976. Pleistocene glaciation in the southern part of the North Cascade Range, Washington. *Geological Society of America Bulletin* 87(1): 61-75. doi:[https://doi.org/10.1130/0016-7606\(1976\)87%3C61:PGITSP%3E2.0.CO;2](https://doi.org/10.1130/0016-7606(1976)87%3C61:PGITSP%3E2.0.CO;2).
- Porter, S.C. 1983. Late Wisconsin mountain glaciation in the western United States. *In* *The Late Pleistocene*. Edited by S.C. Porter. University of Minnesota Press, Minneapolis. pp. 71-111.
- Porter, S.C., and Zhisheng, A. 1995. Correlation between climate events in the North Atlantic and China during the last glaciation. *Nature* 375(6529): 305-308. doi:<https://doi.org/10.1038/375305a0>.
- Porter, S.C., and Swanson, T.W. 1998. Radiocarbon age constraints on rates of advance and retreat of the Puget lobe of the Cordilleran ice sheet during the last glaciation. *Quaternary Research* 50(3): 205-213. doi:<https://doi.org/10.1006/qres.1998.2004>.
- Porter, S.C. 2000. Snowline depression in the tropics during the Last Glaciation. *Quaternary Science Reviews* 20(10): 1067-1091. doi:[https://doi.org/10.1016/S0277-3791\(00\)00178-5](https://doi.org/10.1016/S0277-3791(00)00178-5).
- Porter, S.C., and Swanson, T.W. 2008. ³⁶Cl dating of the classic Pleistocene glacial record in the northeastern Cascade Range, Washington. *American Journal of Science* 308(2): 130-166. doi:<https://doi.org/10.2475/02.2008.02>.
- Praetorius, S.K., and Mix, A.C. 2014. Synchronization of North Pacific and Greenland climates preceded abrupt deglacial warming. *Science* 345(6195): 444-448. doi:<https://doi.org/10.1126/science.1252000>.
- Praetorius, S.K., Condron, A., Mix, A.C., Walczak, M.H., McKay, J.L., and Du, J. 2020. The role of Northeast Pacific meltwater events in deglacial climate change. *Science Advances* 6(9): eaay2915. doi:<https://doi.org/10.1126/sciadv.aay2915>.

- Praetorius, S.K., Alder, J.R., Condrón, A., Mix, A.C., Walczak, M.H., Caissie, B.E., and Erlandson, J.M. 2023. Ice and ocean constraints on early human migrations into North America along the Pacific coast. *Proceedings of the National Academy of Sciences* 120(7): e2208738120. doi:doi.org/10.1073/pnas.2208738120.
- Pruett, C.L., Topp, C.M., Maley, J.M., McCracken, K.G., Rohwer, S., Birks, S., Sealy, S.G., and Winker, K. 2013. Evidence from the genetics of landbirds for a forested Pleistocene glacial refugium in the Haida Gwaii area. *The Condor* 115(4): 725-737. doi:<https://doi.org/10.1525/cond.2013.120123>.
- Putnam, A.E., Denton, G.H., and Schaefer, J.M. 2023. A ^{10}Be chronology of the Esmark Moraine and Lysefjorden region, southwestern Norway: Evidence for coeval glacier resurgence in both polar hemispheres during the Antarctic Cold Reversal. *Quaternary Science Reviews* 316: 108259. doi:<https://doi.org/10.1016/j.quascirev.2023.108259>.
- Qian, Q., Liang, P., Qi, L., Ding, Y., and He, J. 2020. Sub-seasonal variability of meridional activity of western pacific subtropical high in boreal late summer. *Frontiers in Earth Science* 8: 597969. doi:<https://doi.org/10.3389/feart.2020.597969>.
- Qiu, B., and Chen, S. 2005. Variability of the Kuroshio Extension jet, recirculation gyre, and mesoscale eddies on decadal time scales. *Journal of Physical Oceanography* 35(11): 2090-2103. doi:<https://doi.org/10.1175/JPO2807.1>.
- Qiu, B. 2019. Kuroshio and Oyashio currents. *Encyclopedia of ocean sciences* 3: 384-394.
- Quirk, B.J., Huss, E., Leonard, E., Licciardi, J., Plummer, M.A., and Caffee, M.W. 2022. Late Pleistocene glacial chronologies and paleoclimate in the northern Rocky Mountains. *Climate of the Past* 18(2): 293-312. doi:<https://doi.org/10.5194/cp-18-293-2022>.
- Rae, J.W., Sarnthein, M., Foster, G.L., Ridgwell, A., Grootes, P.M., and Elliott, T. 2014. Deepwater formation in the North Pacific and deglacial CO₂ rise. *Paleoceanography* 29(6): 645-667. doi:<https://doi.org/10.1002/2013PA002570>.
- Rae, J.W., Gray, W., Wills, R., Eisenman, I., Fitzhugh, B., Fotheringham, M., Littley, E., Rafter, P., Rees-Owen, R., and Ridgwell, A. 2020. Overturning circulation, nutrient limitation, and warming in the Glacial North Pacific. *Science advances* 6(50): eabd1654. doi:<https://doi.org/10.1126/sciadv.abd1654>.
- Raymo, M. 1997. The timing of major climate terminations. *Paleoceanography* 12(4): 577-585. doi:<https://doi.org/10.1029/97PA01169>.
- Raymo, M.E., and Nisancioglu, K.H. 2003. The 41 kyr world: Milankovitch's other unsolved mystery. *Paleoceanography* 18(1). doi:<https://doi.org/10.1029/2002PA000791>.

- Raymo, M.E., Lisiecki, L., and Nisancioglu, K.H. 2006. Plio-Pleistocene ice volume, Antarctic climate, and the global $\delta^{18}\text{O}$ record. *Science* 313(5786): 492-495. doi:<https://doi.org/10.1126/science.1123296>.
- Rea, B.R., Pellitero, R., Spagnolo, M., Hughes, P., Ivy-Ochs, S., Renssen, H., Ribolini, A., Bakke, J., Lukas, S., and Braithwaite, R.J. 2020. Atmospheric circulation over Europe during the Younger Dryas. *Science Advances* 6(50): eaba4844. doi:<https://doi.org/10.1126/sciadv.aba4844>.
- Reger, R.D. 1991. Deglaciation of the Allison-Sawmill Creeks area, south shore of Port Valdez, Alaska. Alaska Division of Geological and Geophysical Surveys Fairbanks, Alaska. pp. 55-62.
- Reger, R.D., Combellick, R.A., and Brigham-Grette, J. 1995. Late-Wisconsin events in the upper Cook Inlet region, southcentral Alaska. *In Short Notes on Alaska Geology. Edited by R.A. Combellick and F. Tannian.* pp. 33-45.
- Reger, R.D., and Pinney, D.S. 1997. Last major glaciation of Kenai Lowland. 1997 Guide to the geology of the Kenai Peninsula, Alaska, 1997: 54-67.
- Reger, R.D., De Anne, S., and Solie, D.N. 2008a. Surficial geology of the Alaska Highway corridor, Delta Junction to Dot Lake, Alaska. State of Alaska, Department of Natural Resources, Division of Geological and Geophysical Surveys.
- Reger, R.D., Sturmman, A., Berg, E.E., and Burns, P. 2008b. A guide to the late Quaternary history of northern and western Kenai Peninsula, Alaska. State of Alaska, Department of Natural Resources Guidebook, Fairbanks, AK.
- Reger, R.D., Lowell, T., and Evenson, E.B. 2011. Discussion of "Late Quaternary megafloods from Glacial Lake Atna, Southcentral Alaska, USA". *Quaternary Research* 75(1): 301-302. doi:<https://doi.org/10.1016/j.yqres.2010.09.006>.
- Regnéll, C., Blomdin, R., Goodfellow, B.W., Greenwood, S.L., Gyllencreutz, R., Mangerud, J., Mikko, H., Peterson Becher, G., Regnéll, J., and Svendsen, J.I. 2021. Ice-dammed lakes of Scandinavia—a key to the pattern and chronology of the final decay of the Scandinavian Ice Sheet. *In EGU General Assembly Conference Abstracts.* pp. EGU21-3827.
- Reheis, M.C., Adams, K.D., Oviatt, C.G., and Bacon, S.N. 2014. Pluvial lakes in the Great Basin of the western United States—a view from the outcrop. *Quaternary Science Reviews* 97: 33-57. doi:<https://doi.org/10.1016/j.quascirev.2014.04.012>.
- Reimer, P.J. 2012. Refining the radiocarbon time scale. *Science* 338(6105): 337-338. doi:<https://doi.org/10.1126/science.1228653>.
- Reimer, R.W., and Reimer, P.J. 2017. An online application for ΔR calculation. *Radiocarbon* 59(5): 1623-1627. doi:<https://doi.org/10.1017/RDC.2016.117>.

- Rhodes, R.H., Brook, E.J., Chiang, J.C., Blunier, T., Maselli, O.J., McConnell, J.R., Romanini, D., and Severinghaus, J.P. 2015. Enhanced tropical methane production in response to iceberg discharge in the North Atlantic. *Science* 348(6238): 1016-1019. doi:<https://doi.org/10.1126/science.1262005>.
- Riedel, J.L., Clague, J.J., and Ward, B.C. 2010. Timing and extent of early marine oxygen isotope stage 2 alpine glaciation in Skagit Valley, Washington. *Quaternary Research* 73(2): 313-323. doi:<https://doi.org/10.1016/j.yqres.2009.10.004>.
- Rippert, N., Max, L., Mackensen, A., Cacho, I., Povea, P., and Tiedemann, R. 2017. Alternating influence of northern versus southern-sourced water masses on the equatorial Pacific subthermocline during the past 240 ka. *Paleoceanography* 32(11): 1256-1274. doi:<https://doi.org/10.1002/2017PA003133>.
- Rodgers, K.B., Cane, M.A., Naik, N.H., and Schrag, D.P. 1999. The role of the Indonesian Throughflow in equatorial Pacific thermocline ventilation. *Journal of Geophysical Research: Oceans* 104(C9): 20551-20570. doi:<https://doi.org/10.1029/1998JC900094>.
- Rodgers, K.B., Lohmann, G., Lorenz, S., Schneider, R., and Henderson, G.M. 2003. A tropical mechanism for Northern Hemisphere deglaciation. *Geochemistry, Geophysics, Geosystems* 4(5). doi:<https://doi.org/10.1029/2003GC000508>.
- Rodionov, S., Bond, N., and Overland, J. 2007. The Aleutian Low, storm tracks, and winter climate variability in the Bering Sea. *Deep Sea Research Part II: Topical Studies in Oceanography* 54(23-26): 2560-2577. doi:<https://doi.org/10.1016/j.dsr2.2007.08.002>.
- Roe, H.M., Doherty, C.T., Patterson, R.T., and Milne, G.A. 2013. Isolation basin records of late Quaternary sea-level change, central mainland British Columbia, Canada. *Quaternary International* 310: 181-198. doi:<https://doi.org/10.1016/j.quaint.2013.01.026>.
- Royer, T.C., Grosch, C.E., and Mysak, L.A. 2001. Interdecadal variability of Northeast Pacific coastal freshwater and its implications on biological productivity. *Progress in Oceanography* 49(1-4): 95-111. doi:[https://doi.org/10.1016/S0079-6611\(01\)00017-9](https://doi.org/10.1016/S0079-6611(01)00017-9).
- Royer, T.C., and Grosch, C.E. 2006. Ocean warming and freshening in the northern Gulf of Alaska. *Geophysical Research Letters* 33(16). doi:<https://doi.org/10.1029/2006GL026767>.
- Royer, T.C., and Finney, B. 2020. An oceanographic perspective on early human migrations to the Americas. *Oceanography* 33(1): 32-41.
- Ruddiman, W.F. 2003. Orbital insolation, ice volume, and greenhouse gases. *Quaternary Science Reviews* 22(15-17): 1597-1629. doi:[https://doi.org/10.1016/S0277-3791\(03\)00087-8](https://doi.org/10.1016/S0277-3791(03)00087-8).
- Rutz, J.J., Steenburgh, W.J., and Ralph, F.M. 2014. Climatological characteristics of atmospheric rivers and their inland penetration over the western United States. *Monthly Weather Review* 142(2): 905-921. doi:<https://doi.org/10.1175/MWR-D-13-00168.1>.

- Sancetta, C. 1983. Effect of Pleistocene glaciation upon oceanographic characteristics of the North Pacific Ocean and Bering Sea. *Deep Sea Research Part A. Oceanographic Research Papers* 30(8): 851-869. doi:[https://doi.org/10.1016/0198-0149\(83\)90004-3](https://doi.org/10.1016/0198-0149(83)90004-3).
- Sancetta, C., Heusser, L., Labeyrie, L., Naidu, A.S., and Robinson, S.W. 1984. Wisconsin—Holocene paleoenvironment of the Bering Sea: Evidence from diatoms, pollen, oxygen isotopes and clay minerals. *Marine Geology* 62(1-2): 55-68. doi:[https://doi.org/10.1016/0025-3227\(84\)90054-9](https://doi.org/10.1016/0025-3227(84)90054-9).
- Santoso, A., Cai, W., England, M., and Phipps, S. 2011. The role of the Indonesian Throughflow on ENSO dynamics in a coupled climate model. *Journal of Climate* 24(3): 585-601. doi:<https://doi.org/10.1175/2010JCLI3745.1>.
- Schenk, F., Välranta, M., Muschitiello, F., Tarasov, L., Heikkilä, M., Björck, S., Brandefelt, J., Johansson, A.V., Näslund, J.-O., and Wohlfarth, B. 2018. Warm summers during the Younger Dryas cold reversal. *Nature Communications* 9(1): 1634. doi:<https://doi.org/10.1038/s41467-018-04071-5>.
- Shcherbina, A. Y., L. D. Talley, and D. L. Rudnick (2004), Dense water formation on the northwestern shelf of the Okhotsk Sea: 1. Direct observations of brine rejection. *Journal of Geophysical Research* 109, C09S08, doi:10.1029/2003JC002196.
- Schmoll, H.R., and Yehle, L.A. 1986. Pleistocene glaciation of the upper Cook Inlet basin. *In* *Glaciation in Alaska. Edited by T.D. Hamilton and K.M. Reed and R.M. Thorson.* Alaska Geological Society, Anchorage, AK. pp. 193-218.
- Schmuck, N., Reuther, J., Baichtal, J.F., and Carlson, R.J. 2021. Quantifying marine reservoir effect variability along the Northwest Coast of North America. *Quaternary Research* 103: 160-181. doi:<https://doi.org/10.1017/qua.2020.131>.
- Schultz, D.M., Bosart, L.F., Colle, B.A., Davies, H.C., Dearden, C., Keyser, D., Martius, O., Roebber, P.J., Steenburgh, W.J., and Volkert, H. 2019. Extratropical cyclones: A century of research on meteorology's centerpiece. *Meteorological monographs* 59: 16.11-16.56. doi:<https://DOI.org/10.1175/AMSMONOGRAPHS-D-18-0015.1>.
- Seguinot, J., Rogozhina, I., Stroeven, A.P., Margold, M., and Kleman, J. 2016. Numerical simulations of the Cordilleran ice sheet through the last glacial cycle. *The Cryosphere* 10(2): 639-664. doi:<https://doi.org/10.5194/tc-10-639-2016>.
- Serreze, M.C., and Barry, R.G. 2011. Processes and impacts of Arctic amplification: A research synthesis. *Global and Planetary Change* 77(1-2): 85-96. doi:<https://doi.org/10.1016/j.gloplacha.2011.03.004>.
- Shackleton, N., Duplessy, J.-C., Arnold, M., Maurice, P., Hall, M., and Cartlidge, J. 1988. Radiocarbon age of last glacial Pacific deepwater. *Nature* 335(6192): 708-711. doi:<https://doi.org/10.1038/335708a0>.

- Shafer, A.B., Cullingham, C.I., Côté, S.D., and Coltman, D.W. 2010. Of glaciers and refugia: a decade of study sheds new light on the phylogeography of northwestern North America. *Molecular ecology* 19(21): 4589-4621. doi:<https://doi.org/10.1111/j.1365-294X.2010.04828.x>.
- Shakhova, N., Semiletov, I., Gustafsson, O., Sergienko, V., Lobkovsky, L., Dudarev, O., Tumskey, V., Grigoriev, M., Mazurov, A., and Salyuk, A. 2017. Current rates and mechanisms of subsea permafrost degradation in the East Siberian Arctic Shelf. *Nature Communications* 8(1): 15872. doi:<https://doi.org/10.1038/ncomms15872>.
- Shakhova, N., Semiletov, I., and Chuvilin, E. 2019. Understanding the permafrost–hydrate system and associated methane releases in the East Siberian Arctic Shelf. *Geosciences* 9(6): 251. doi:<https://doi.org/10.3390/geosciences9060251>.
- Shakun, J.D., and Carlson, A.E. 2010. A global perspective on Last Glacial Maximum to Holocene climate change. *Quaternary Science Reviews* 29(15-16): 1801-1816. doi:<https://doi.org/10.1016/j.quascirev.2010.03.016>.
- Shakun, J.D., Clark, P.U., He, F., Marcott, S.A., Mix, A.C., Liu, Z., Otto-Bliesner, B., Schmittner, A., and Bard, E. 2012. Global warming preceded by increasing carbon dioxide concentrations during the last deglaciation. *Nature* 484(7392): 49-54. doi:<https://doi.org/10.1038/nature10915>.
- Shakun, J.D., Raymo, M.E., and Lea, D.W. 2016. An early Pleistocene Mg/Ca- $\delta^{18}O$ record from the Gulf of Mexico: Evaluating ice sheet size and pacing in the 41-kyr world. *Paleoceanography* 31(7): 1011-1027. doi:<https://doi.org/10.1002/2016PA002956>.
- Shaw, J., Barrie, J.V., Conway, K.W., Lintern, D.G., and Kung, R. 2020. Glaciation of the northern British Columbia continental shelf: the geomorphic evidence derived from multibeam bathymetric data. *Boreas* 49(1): 17-37. doi:<https://doi.org/10.1111/bor.12411>.
- Shaw, T., Baldwin, M., Barnes, E.A., Caballero, R., Garfinkel, C., Hwang, Y.-T., Li, C., O'gorman, P., Rivière, G., and Simpson, I. 2016. Storm track processes and the opposing influences of climate change. *Nature Geoscience* 9(9): 656-664. doi:<https://doi.org/10.1038/ngeo2783>.
- Shennan, I., Bradley, S., Milne, G., Brooks, A., Bassett, S., and Hamilton, S. 2006. Relative sea-level changes, glacial isostatic modelling and ice-sheet reconstructions from the British Isles since the Last Glacial Maximum. *Journal of Quaternary Science: Published for the Quaternary Research Association* 21(6): 585-599. doi:<https://doi.org/10.1002/jqs.1049>.
- Shennan, I., Bruhn, R., Barlow, N., Good, K., and Hocking, E. 2014. Late Holocene great earthquakes in the eastern part of the Aleutian megathrust. *Quaternary Science Reviews* 84: 86-97. doi:<https://doi.org/10.1016/j.quascirev.2013.11.010>.
- Shestakova, A.A., Fedorov, A.N., Torgovkin, Y.I., Konstantinov, P.Y., Vasylyev, N.F., Kalinicheva, S.V., Samsonova, V.V., Hiyama, T., Iijima, Y., and Park, H. 2021. Mapping the main

characteristics of permafrost on the basis of a permafrost-landscape map of Yakutia using GIS. *Land* 10(5): 462. doi:<https://doi.org/10.3390/land10050462>.

Shimizu, Y., Iwao, T., Yasuda, I., Ito, S.-I., Watanabe, T., Uehara, K., Shikama, N., and Nakano, T. 2004. Formation process of North Pacific Intermediate Water revealed by profiling floats set to drift on 26.7 σ_{θ} isopycnal surface. *Journal of Oceanography* 60: 453-462. doi:<https://DOI.org/10.1023/B:JOCE.0000038061.55914.eb>.

Shugar, D.H., Walker, I.J., Lian, O.B., Eamer, J.B., Neudorf, C., McLaren, D., and Fedje, D. 2014. Post-glacial sea-level change along the Pacific coast of North America. *Quaternary Science Reviews* 97: 170-192. doi:<https://doi.org/10.1016/j.quascirev.2014.05.022>.

Siddall, M., Rohling, E.J., Almogi-Labin, A., Hemleben, C., Meischner, D., Schmelzer, I., and Smeed, D. 2003. Sea-level fluctuations during the last glacial cycle. *Nature* 423(6942): 853-858. doi:<https://doi.org/10.1038/nature01690>.

Simms, A.R., Lisiecki, L., Gebbie, G., Whitehouse, P.L., and Clark, J.F. 2019. Balancing the Last Glacial Maximum (LGM) sea-level budget. *Quaternary Science Reviews* 205: 143-153. doi:<https://doi.org/10.1016/j.quascirev.2018.12.018>.

Sirkin, L., and Tuthill, S.J. 1987. Late Pleistocene and Holocene deglaciation and environments of the southern Chugach Mountains, Alaska. *Geological Society of America Bulletin* 99(3): 376-384. doi:[https://doi.org/10.1130/0016-7606\(1987\)99%3C376:LPAHDA%3E2.0.CO;2](https://doi.org/10.1130/0016-7606(1987)99%3C376:LPAHDA%3E2.0.CO;2).

Skinner, C.B., Lora, J.M., Tabor, C., and Zhu, J. 2023. Atmospheric river contributions to ice sheet hydroclimate at the Last Glacial Maximum. *Geophysical Research Letters* 50(1): e2022GL101750. doi:<https://doi.org/10.1029/2022GL101750>.

Skinner, L., Primeau, F., Freeman, E., de la Fuente, M., Goodwin, P., Gottschalk, J., Huang, E., McCave, I., Noble, T., and Scrivner, A. 2017. Radiocarbon constraints on the glacial ocean circulation and its impact on atmospheric CO₂. *Nature Communications* 8(1): 16010. doi:<https://doi.org/10.1038/ncomms16010>.

Skinner, L., Muschitiello, F., and Scrivner, A. 2019. Marine reservoir age variability over the last deglaciation: implications for marine carbon cycling and prospects for regional radiocarbon calibrations. *Paleoceanography and Paleoclimatology* 34(11): 1807-1815. doi:<https://doi.org/10.1029/2019PA003667>.

Small, D., Smedley, R.K., Chiverrell, R.C., Scourse, J.D., Cofaigh, C.Ó., Duller, G.A., McCarron, S., Burke, M.J., Evans, D.J., and Fabel, D. 2018. Trough geometry was a greater influence than climate-ocean forcing in regulating retreat of the marine-based Irish-Sea Ice Stream. *GSA Bulletin* 130(11-12): 1981-1999. doi:<https://doi.org/10.1130/B31852.1>.

Smith, G.M. 2019. Geoarchaeology of glacial lakes Susitna and Atna Alaska *Journal of Anthropology* 17.

Song, Q., Gordon, A.L., and Visbeck, M. 2004. Spreading of the Indonesian throughflow in the Indian Ocean. *Journal of Physical Oceanography* 34(4): 772-792.

doi:[https://doi.org/10.1175/1520-0485\(2004\)034%3C0772:SOTITI%3E2.0.CO;2](https://doi.org/10.1175/1520-0485(2004)034%3C0772:SOTITI%3E2.0.CO;2).

Song, Q., Vecchi, G.A., and Rosati, A.J. 2007. The role of the Indonesian Throughflow in the Indo-Pacific climate variability in the GFDL Coupled Climate Model. *Journal of Climate* 20(11): 2434-2451. doi:<https://doi.org/10.1175/JCLI4133.1>.

Sprintall, J., Gordon, A.L., Koch-Larrouy, A., Lee, T., Potemra, J.T., Pujiana, K., and Wijffels, S.E. 2014. The Indonesian seas and their role in the coupled ocean-climate system. *Nature Geoscience* 7(7): 487-492. doi:<https://doi.org/10.1038/ngeo2188>.

Stilwell, K.B., and Kaufman, D.S. 1996. Late Wisconsin glacial history of the northern Alaska Peninsula, southwestern Alaska, USA. *Arctic and Alpine Research* 28(4): 475-487.

doi:<https://www.tandfonline.com/loi/uaar19>.

Stokes, C., Margold, M., Clark, C., and Tarasov, L. 2016. Ice stream activity scaled to ice sheet volume during Laurentide Ice Sheet deglaciation. *Nature* 530(7590): 322-326.

doi:<https://doi.org/10.1038/nature16947>.

Stokes, C.R., Tarasov, L., and Dyke, A.S. 2012. Dynamics of the North American Ice Sheet Complex during its inception and build-up to the Last Glacial Maximum. *Quaternary Science Reviews* 50: 86-104. doi:<https://doi.org/10.1016/j.quascirev.2012.07.009>.

Stokes, C.R., Corner, G.D., Winsborrow, M.C., Husum, K., and Andreassen, K. 2014. Asynchronous response of marine-terminating outlet glaciers during deglaciation of the Fennoscandian Ice Sheet. *Geology* 42(5): 455-458. doi:<https://doi.org/10.1130/G35299.1>.

Stroeven, A.P., Hättestrand, C., Kleman, J., Heyman, J., Fabel, D., Fredin, O., Goodfellow, B.W., Harbor, J.M., Jansen, J.D., and Olsen, L. 2016. Deglaciation of Fennoscandia. *Quaternary Science Reviews* 147: 91-121. doi:<https://doi.org/10.1016/j.quascirev.2015.09.016>.

Stuiver, M., and Braziunas, T.F. 1993. Modeling atmospheric ^{14}C influences and ^{14}C ages of marine samples to 10,000 BC. *Radiocarbon* 35(1): 137-189.

doi:<https://doi.org/10.1017/S0033822200013874>.

Stuiver, M., Reimer, P.J., and Reimer, R.W. 1993. CALIB 8.2. *Radiocarbon* 35: 215-230.

doi:<http://calib.org/calib/>.

Stumpf, A.J., Broster, B.E., and Levson, V.M. 2000. Multiphase flow of the late Wisconsinan Cordilleran ice sheet in western Canada. *Geological Society of America Bulletin* 112(12): 1850-1863. doi:[https://doi.org/10.1130/0016-7606\(2000\)112%3C1850:MFOTLW%3E2.0.CO;2](https://doi.org/10.1130/0016-7606(2000)112%3C1850:MFOTLW%3E2.0.CO;2).

Sun, J., and Wang, H. 2006. Relationship between Arctic oscillation and Pacific decadal oscillation on decadal timescale. *Chinese Science Bulletin* 51: 75-79.

doi:<https://doi.org/10.1007/s11434-004-0221-3>.

- Svensson, A., Andersen, K.K., Bigler, M., Clausen, H.B., Dahl-Jensen, D., Davies, S., Johnsen, S.J., Muscheler, R., Parrenin, F., and Rasmussen, S.O. 2008. A 60 000 year Greenland stratigraphic ice core chronology. *Climate of the Past* 4(1): 47-57. doi:<https://doi.org/10.5194/cp-4-47-2008>.
- Swartz, J.M., Gulick, S.P., and Goff, J.A. 2015. Gulf of Alaska continental slope morphology: evidence for recent trough mouth fan formation. *Geochemistry, Geophysics, Geosystems* 16(1): 165-177. doi:<https://doi.org/10.1002/2014GC005594>.
- Tabor, C., Poulsen, C., and Pollard, D. 2014. Mending Milankovitch's theory: obliquity amplification by surface feedbacks. *Climate of the Past* 10(1): 41-50. doi:<https://doi.org/10.5194/cp-10-41-2014>.
- Takahashi, T., Broecker, W.S., and Bainbridge, A.E. 1981. The alkalinity and total carbon dioxide concentration in the world oceans. *Carbon cycle modelling, SCOPE* 16(3078): 271-286.
- Talley, L.D. 2013. Closure of the global overturning circulation through the Indian, Pacific, and Southern Oceans: Schematics and transports. *Oceanography* 26(1): 80-97. doi:<http://dx.doi.org/10.5670/oceanog.2013.07>.
- Taylor, M., Hendy, I., and Pak, D. 2014. Deglacial ocean warming and marine margin retreat of the Cordilleran Ice Sheet in the North Pacific Ocean. *Earth and Planetary Science Letters* 403: 89-98. doi:<https://doi.org/10.1016/j.epsl.2014.06.026>.
- Ten Brink, N.W., and Waythomas, C.F. 1985. Late Wisconsin glacial chronology of the north-central Alaska Range: a regional synthesis and its implications for early human settlements. *Nat. Geog. Soc. Res. Repts.* 19: 15-32.
- Thorson, R.M. 1986. Late Cenozoic glaciation of the northern Nenana Valley. *In* *Glaciation in Alaska - The Geologic Record. Edited by* T.D. Hamilton and K.M. Reed and R.M. Thorson. Alaska Geological Society, Anchorage, AK.
- Thorson, R.M. 1989. Glacio-isostatic response of the Puget Sound area, Washington. *Geological Society of America Bulletin* 101(9): 1163-1174. doi:[https://doi.org/10.1130/0016-7606\(1989\)101%3C1163:GIROTP%3E2.3.CO;2](https://doi.org/10.1130/0016-7606(1989)101%3C1163:GIROTP%3E2.3.CO;2).
- Tierney, J.E., Zhu, J., King, J., Malevich, S.B., Hakim, G.J., and Poulsen, C.J. 2020. Glacial cooling and climate sensitivity revisited. *Nature* 584(7822): 569-573. doi:<https://doi.org/10.1038/s41586-020-2617-x>.
- Trenberth, K. 2022. *The Changing Flow of Energy Through the Climate System*. Cambridge University Press, Cambridge.
- Trenberth, K.E., and Hurrell, J.W. 1994. Decadal atmosphere-ocean variations in the Pacific. *Climate Dynamics* 9: 303-319. doi:<https://doi.org/10.1007/BF00204745>.

- Trenberth, K.E., and Solomon, A. 1994. The global heat balance: Heat transports in the atmosphere and ocean. *Climate Dynamics* 10: 107-134.
doi:<https://doi.org/10.1007/BF00210625>.
- Trenberth, K.E., and Fasullo, J.T. 2017. Atlantic meridional heat transports computed from balancing Earth's energy locally. *Geophysical Research Letters* 44(4): 1919-1927.
doi:<https://doi.org/10.1002/2016GL072475>.
- Trenberth, K.E., and Zhang, Y. 2019. Observed interhemispheric meridional heat transports and the role of the Indonesian throughflow in the Pacific Ocean. *Journal of Climate* 32(24): 8523-8536. doi:<https://DOI.org/10.1175/JCLI-D-19-0465.1>.
- Trenberth, K.E., Zhang, Y., Fasullo, J.T., and Cheng, L. 2019. Observation-based estimates of global and basin ocean meridional heat transport time series. *Journal of Climate* 32(14): 4567-4583. doi:<https://doi.org/10.1175/JCLI-D-18-0872.s1>.
- Tseng, Y.-h., Ding, R., Zhao, S., Kuo, Y.-c., and Liang, Y.-c. 2020. Could the North Pacific oscillation be modified by the initiation of the East Asian winter monsoon? *Journal of Climate* 33(6): 2389-2406. doi:<https://doi.org/10.1175/JCLI-D-19-0112.1>.
- Tulenko, J.P., Briner, J.P., Young, N.E., and Schaefer, J.M. 2018. Beryllium-10 chronology of early and late Wisconsinan moraines in the Revelation Mountains, Alaska: insights into the forcing of Wisconsinan glaciation in Beringia. *Quaternary Science Reviews* 197: 129-141.
doi:<https://doi.org/10.1016/j.quascirev.2018.08.009>.
- Tulenko, J.P., Löfverström, M., and Briner, J.P. 2020. Ice sheet influence on atmospheric circulation explains the patterns of Pleistocene alpine glacier records in North America. *Earth and Planetary Science Letters* 534: 116115. doi:<https://doi.org/10.1016/j.epsl.2020.116115>.
- Tulenko, J.P., Briner, J.P., Young, N.E., and Schaefer, J.M. 2022. The last deglaciation of Alaska and a new benchmark ^{10}Be moraine chronology from the western Alaska Range. *Quaternary Science Reviews* 287: 107549. doi:<https://doi.org/10.1016/j.quascirev.2022.107549>.
- Tulenko, J.P., Briner, J.P., Young, N.E., and Schaefer, J.M. 2023. Abrupt warming and alpine glacial retreat through the last deglaciation in Alaska interrupted by modest Northern Hemisphere cooling. *Climate of the Past Discussions* 2023: 1-22.
- Turner, D.G., Ward, B.C., Bond, J.D., Jensen, B.J., Froese, D.G., Telka, A.M., Zazula, G.D., and Bigelow, N.H. 2013. Middle to Late Pleistocene ice extents, tephrochronology and paleoenvironments of the White River area, southwest Yukon. *Quaternary Science Reviews* 75: 59-77. doi:<https://doi.org/10.1016/j.quascirev.2013.05.011>.
- Ujiié, Y., Ujiié, H., Taira, A., Nakamura, T., and Oguri, K. 2003. Spatial and temporal variability of surface water in the Kuroshio source region, Pacific Ocean, over the past 21,000 years: evidence from planktonic foraminifera. *Marine Micropaleontology* 49(4): 335-364.
doi:[https://doi.org/10.1016/S0377-8398\(03\)00062-8](https://doi.org/10.1016/S0377-8398(03)00062-8).

Ullman, D., LeGrande, A., Carlson, A.E., Anslow, F., and Licciardi, J. 2014. Assessing the impact of Laurentide Ice Sheet topography on glacial climate. *Climate of the Past* 10(2): 487-507. doi:<https://doi.org/10.5194/cp-10-487-2014>.

Viaggi, P. 2021. Quantitative impact of astronomical and sun-related cycles on the Pleistocene climate system from Antarctica records. *Quaternary Science Advances* 4: 100037. doi:<https://doi.org/10.1016/j.qsa.2021.100037>.

Vincent, J.-S., and Prest, V.K. 1987. The early Wisconsinan history of the Laurentide ice sheet. *Géographie Physique et Quaternaire* 41(2): 199-213. doi:<https://doi.org/10.7202/032679ar>.

Voris, H.K. 2000. Maps of Pleistocene sea levels in Southeast Asia: shorelines, river systems and time durations. *Journal of Biogeography* 27(5): 1153-1167. doi:<https://doi.org/10.1046/j.1365-2699.2000.00489.x>.

Vorren, T.O., and Plassen, L. 2002. Deglaciation and palaeoclimate of the Andfjord-Vågsfjord area, North Norway. *Boreas* 31(2): 97-125. doi:<https://doi.org/10.1111/j.1502-3885.2002.tb01060.x>.

Vorren, T.O., Rydningen, T.A., Baeten, N.J., and Laberg, J.S. 2015. Chronology and extent of the Lofoten–Vesterålen sector of the Scandinavian Ice Sheet from 26 to 16 cal. ka BP. *Boreas* 44(3): 445-458. doi:<https://doi.org/10.1111/bor.12118>.

WAIS Divide Project Members. 2015. Precise inter-polar phasing of abrupt climate change during the last ice age. *Nature* 520(7549): 661-665. doi:<https://doi.org/10.1038/nature14401>.

Walcott, C.K., Briner, J.P., Baichtal, J.F., Lesnek, A.J., and Licciardi, J.M. 2022. Cosmogenic ages indicate no MIS 2 refugia in the Alexander Archipelago, Alaska. *Geochronology* 4: 191-211. doi:<https://doi.org/10.5194/gchron-4-191-2022>.

Walczak, M.H., Mix, A.C., Cowan, E.A., Fallon, S., Fifield, L.K., Alder, J.R., Du, J., Haley, B., Hobern, T., and Padman, J. 2020. Phasing of millennial-scale climate variability in the Pacific and Atlantic Oceans. *Science* 370(6517): 716-720. doi:<https://doi.org/10.1126/science.aba7096>.

Walker, J.M., Bordoni, S., and Schneider, T. 2015. Interannual variability in the large-scale dynamics of the South Asian summer monsoon. *Journal of Climate* 28(9): 3731-3750. doi:<https://doi.org/10.1175/JCLI-D-14-00612.1>.

Wallace, J.M., and Gutzler, D.S. 1981. Teleconnections in the geopotential height field during the Northern Hemisphere winter. *Monthly Weather Review* 109(4): 784-812. doi:[https://doi.org/10.1175/1520-0493\(1981\)109%3C0784:TITGHF%3E2.0.CO;2](https://doi.org/10.1175/1520-0493(1981)109%3C0784:TITGHF%3E2.0.CO;2).

Walsh, J.E. 1983. The role of sea ice in climatic variability: Theories and evidence. *Atmosphere-Ocean* 21(3): 229-242. doi:<https://doi.org/10.1080/07055900.1983.9649166>.

- Walters, R.A., and Meier, M.F. 1989. Variability of glacier mass balances in western North America. *Aspects of Climate Variability in the Pacific and the Western Americas* 55: 365-374. doi:<https://doi.org/10.1029/GM055p0365>.
- Wang, B., Liu, J., Kim, H.-J., Webster, P.J., Yim, S.-Y., and Xiang, B. 2013. Northern Hemisphere summer monsoon intensified by mega-El Niño/southern oscillation and Atlantic multidecadal oscillation. *Proceedings of the National Academy of Sciences* 110(14): 5347-5352. doi:<https://doi.org/10.1073/pnas.1219405110>.
- Wang, R., Kuhn, G., Gong, X., Biskaborn, B.K., Gersonde, R., Lembke-Jene, L., Lohmann, G., Tiedemann, R. and Diekmann, B. 2021. Deglacial land-ocean linkages at the Alaskan continental margin in the Bering Sea. *Frontiers in Earth Science*, 9: 712415. doi: <https://doi.org/10.3389/feart.2021.712415>
- Wang, S., Huang, J., He, Y., and Guan, Y. 2014. Combined effects of the Pacific decadal oscillation and El Niño-southern oscillation on global land dry–wet changes. *Scientific reports* 4(1): 6651. doi:<https://doi.org/10.1038/srep06651>.
- Ward, B.C., Bond, J.D., and Gosse, J.C. 2007. Evidence for a 55–50 ka (early Wisconsin) glaciation of the Cordilleran ice sheet, Yukon Territory, Canada. *Quaternary Research* 68(1): 141-150. doi:<https://doi.org/10.1016/j.yqres.2007.04.002>.
- Ward, B.C., Bond, J.D., Froese, D., and Jensen, B. 2008. Old Crow tephra (140±10 ka) constrains penultimate Reid glaciation in central Yukon Territory. *Quaternary Science Reviews* 27(19-20): 1909-1915. doi:<https://doi.org/10.1016/j.quascirev.2008.07.012>.
- Warner, B.G., Clague, J.J., and Mathewes, R.W. 1984. Geology and paleoecology of a mid-Wisconsin peat from the Queen Charlotte Islands, British Columbia, Canada. *Quaternary Research* 21(3): 337-350. doi:[https://doi.org/10.1016/0033-5894\(84\)90073-5](https://doi.org/10.1016/0033-5894(84)90073-5).
- Warren, B.A. 1983. Why is no deepwater formed in the North Pacific? *Journal of Marine Research* 41(2): 327-347.
- Waters, M.R. 1989. Late Quaternary lacustrine history and paleoclimatic significance of pluvial Lake Cochise, southeastern Arizona. *Quaternary Research* 32(1): 1-11. doi:[https://doi.org/10.1016/0033-5894\(89\)90027-6](https://doi.org/10.1016/0033-5894(89)90027-6).
- Watson, A., Vallis, G., and Nikurashin, M. 2015. Southern Ocean buoyancy forcing of ocean ventilation and glacial atmospheric CO₂. *Nature Geoscience* 8. 10.1038/ngeo2538.
- Weeks, W. 2010. *On Sea Ice*. University of Alaska Press. pp. 664.
- Weijer, W., Cheng, W., Drijfhout, S.S., Fedorov, A.V., Hu, A., Jackson, L.C., Liu, W., McDonagh, E., Mecking, J., and Zhang, J. 2019. Stability of the Atlantic Meridional Overturning Circulation: A review and synthesis. *Journal of Geophysical Research: Oceans* 124(8): 5336-5375. doi:<https://doi.org/10.1029/2019JC015083>.

- Weingartner, T.J., Danielson, S., Sasaki, Y., Pavlov, V., and Kulakov, M. 1999. The Siberian Coastal Current: A wind-and buoyancy-forced Arctic coastal current. *Journal of Geophysical Research: Oceans* 104(C12): 29697-29713. doi:<https://doi.org/10.1029/1999JC900161>.
- Weingartner, T.J., Danielson, S.L., and Royer, T.C. 2005. Freshwater variability and predictability in the Alaska Coastal Current. *Deep Sea Research Part II: Topical Studies in Oceanography* 52(1-2): 169-191. doi:<https://doi.org/10.1016/j.dsr2.2004.09.030>.
- Wellner, J., Lowe, A., Shipp, S., and Anderson, J. 2001. Distribution of glacial geomorphic features on the Antarctic continental shelf and correlation with substrate: implications for ice behavior. *Journal of Glaciology* 47(158): 397-411. doi:<https://doi.org/10.3189/172756501781832043>.
- Wendler, G., Galloway, K., and Stuefer, M. 2016. On the climate and climate change of Sitka, Southeast Alaska. *Theoretical and Applied Climatology* 126: 27-34. doi:<https://doi.org/10.1007/s00704-015-1542-7>.
- White, J.T., Henry, A., Kuehn, S., Loso, M.G., and Rasic, J.T. 2022. Terminal Pleistocene human occupation of the upper Copper River basin, southern Alaska: Results of test excavations at *Natael Na'*. *Quaternary International* 640: 23-43. doi:<https://doi.org/10.1016/j.quaint.2022.08.012>.
- Whitlock, C., and Bartlein, P.J. 1997. Vegetation and climate change in northwest America during the past 125 kyr. *Nature* 388(6637): 57-61. doi:<https://doi.org/10.1038/40380>.
- Wiedmer, M., Montgomery, D.R., Gillespie, A.R., and Greenberg, H. 2010. Late Quaternary megafloods from Glacial Lake Atna, Southcentral Alaska, USA. *Quaternary Research* 73(3): 413-424. doi:<https://doi.org/10.1016/j.yqres.2010.02.005>.
- Wiedmer, M., Montgomery, D.R., Gillespie, A.R., and Greenberg, H. 2011. Reply to the comments of Reger, Lowell, and Evenson on "Late Quaternary megafloods from Glacial Lake Atna, Southcentral Alaska, USA". *Quaternary Research* 75(1): 303-304. doi:<https://doi.org/10.1016/j.yqres.2010.09.003>.
- Wiles, G., Devereux, K., Gaglioti, B., and D'Arrigo, R. 2023. A 420-Year Perspective on Winter Lake Erie Levels. *Geophysical Research Letters* 50(1): e2022GL099911. doi:<https://doi.org/10.1029/2022GL099911>.
- Willerslev, E., and Meltzer, D.J. 2021. Peopling of the Americas as inferred from ancient genomics. *Nature* 594(7863): 356-364. doi:<https://doi.org/10.1038/s41586-021-03499-y>.
- Williams, J.R., Carter, L., Hamilton, T., and Galloway, J. 1989. A working glacial chronology for the western Copper River Basin, Alaska. *In* *Late Cenozoic History of the Interior Basins of Alaska and the Yukon.: Circular. Edited by* L.D. Carter and T.D. Hamilton and J.P. Galloway. USGS. pp. 81-85.

- Winsborrow, M.C., Clark, C.D., and Stokes, C.R. 2004. Ice streams of the Laurentide ice sheet. *Géographie Physique et Quaternaire* 58(2): 269-280. doi:<https://doi.org/10.7202/013142ar>.
- Wise, E.K. 2010. Spatiotemporal variability of the precipitation dipole transition zone in the western United States. *Geophysical Research Letters* 37(7). doi:<https://doi.org/10.1029/2009GL042193>.
- Wittmeier, H.E., Schaefer, J.M., Bakke, J., Rupper, S., Paasche, Ø., Schwartz, R., and Finkel, R.C. 2020. Late Glacial mountain glacier culmination in Arctic Norway prior to the Younger Dryas. *Quaternary Science Reviews* 245: 106461. doi:<https://doi.org/10.1016/j.quascirev.2020.106461>.
- Woodgate, R.A., and Aagaard, K. 2005. Revising the Bering Strait freshwater flux into the Arctic Ocean. *Geophysical Research Letters* 32(2). doi:<https://doi.org/10.1029/2004GL021747>.
- Woodgate, R.A., Aagaard, K., and Weingartner, T.J. 2005. Monthly temperature, salinity, and transport variability of the Bering Strait through flow. *Geophysical Research Letters* 32(4). doi:<https://doi.org/10.1029/2004GL021880>.
- Woodgate, R.A., Weingartner, T., and Lindsay, R. 2010. The 2007 Bering Strait oceanic heat flux and anomalous Arctic sea-ice retreat. *Geophysical Research Letters* 37(1). doi:<https://doi.org/10.1029/2009GL041621>.
- Woodgate, R.A. 2018. Increases in the Pacific inflow to the Arctic from 1990 to 2015, and insights into seasonal trends and driving mechanisms from year-round Bering Strait mooring data. *Progress in Oceanography* 160: 124-154. doi:<https://doi.org/10.1016/j.pcean.2017.12.007>.
- Woodgate, R.A., and Peralta-Ferriz, C. 2021. Warming and Freshening of the Pacific Inflow to the Arctic from 1990-2019 implying dramatic shoaling in Pacific Winter Water ventilation of the Arctic water column. *Geophysical Research Letters* 48(9): e2021GL092528. doi:<https://doi.org/10.1029/2021GL092528>.
- Wu, L., Li, C., Yang, C., and Xie, S.-P. 2008. Global teleconnections in response to a shutdown of the Atlantic meridional overturning circulation. *Journal of Climate* 21(12): 3002-3019. doi:<https://doi.org/10.1175/2007JCLI1858.1>.
- Wunderling, N., Willeit, M., Donges, J.F., and Winkelmann, R. 2020. Global warming due to loss of large ice masses and Arctic summer sea ice. *Nature Communications* 11(1): 5177. doi:<https://doi.org/10.1038/s41467-020-18934-3>.
- Xian, T., Xia, J., Wei, W., Zhang, Z., Wang, R., Wang, L.-P., and Ma, Y.-F. 2021. Is Hadley cell expanding? *Atmosphere* 12(12): 1699. doi:<https://doi.org/10.3390/atmos12121699>.

- Xie, N., Sun, Y., and Gao, M. 2020. The influence of five teleconnection patterns on winter extratropical cyclones over northwest Pacific. *Atmosphere* 11(11): 1248. doi:<https://doi.org/10.3390/atmos11111248>.
- Xu, J., Kuhnt, W., Holbourn, A., Regenber, M., and Andersen, N. 2010. Indo-Pacific warm pool variability during the Holocene and Last Glacial Maximum. *Paleoceanography* 25(4). doi:<https://doi.org/10.1029/2010PA001934>.
- Yang, S., Li, Z., Yu, J-Y., Hu, X., Dong, W., and He, S. 2018. El Niño–Southern Oscillation and its impact in the changing climate. *National Science Review* 5: 840–857, 2018 doi: 10.1093/nsr/nwy046
- You, Y., N. Sugino, M. Fukasawa, I. Yasuda, I. Kaneko, H. Yoritaka, and M. Kawamiya (2000), Roles of the Okhotsk Sea and Gulf of Alaska in forming the North Pacific Intermediate Water, *J. Geophys. Res.*, 105(C2), 3253–3280, doi:10.1029/1999JC900304.
- Young, N.E., Briner, J.P., and Kaufman, D.S. 2009. Late Pleistocene and Holocene glaciation of the Fish Lake valley, northeastern Alaska Range, Alaska. *Journal of Quaternary Science*: 24(7): 677-689. doi:<https://doi.org/10.1002/jqs.1279>.
- Young, N.E., Briner, J.P., Schaefer, J., Zimmerman, S., and Finkel, R.C. 2019. Early Younger Dryas glacier culmination in southern Alaska: Implications for North Atlantic climate change during the last deglaciation. *Geology* 47(6): 550-554. doi:<https://doi.org/10.1130/G46058.1>.
- Yuan, X., and Talley, L.D. 1996. The subarctic frontal zone in the North Pacific: Characteristics of frontal structure from climatological data and synoptic surveys. *Journal of Geophysical Research: Oceans* 101(C7): 16491-16508. doi:<https://doi.org/10.1029/96JC01249>.
- Zabihi, K., Huettmann, F., and Young, B. 2021. Predicting multi-species bark beetle (Coleoptera: Curculionidae: Scolytinae) occurrence in Alaska: First use of open access big data mining and open source GIS to provide robust inference and a role model for progress in forest conservation. *Biodiversity Informatics* 16(1): 1-19. doi:<https://doi.org/10.17161/bi.v16i1.14758>.
- Zaucker, F., and Broecker, W.S. 1992. The influence of atmospheric moisture transport on the fresh water balance of the Atlantic drainage basin: General circulation model simulations and observations. *Journal of Geophysical Research: Atmospheres* 97(D3): 2765-2773. doi:<https://doi.org/10.1029/91JD01699>.
- Zemp, M., Frey, H., Gärtner-Roer, I., Nussbaumer, S.U., Hoelzle, M., Paul, F., Haeberli, W., Denzinger, F., Ahlstrøm, A.P., and Anderson, B. 2015. Historically unprecedented global glacier decline in the early 21st century. *Journal of Glaciology* 61(228): 745-762. doi:<https://doi.org/10.3189/2015JoG15J017>.
- Zhang, H., Griffiths, M.L., Chiang, J.C., Kong, W., Wu, S., Atwood, A., Huang, J., Cheng, H., Ning, Y., and Xie, S. 2018. East Asian hydroclimate modulated by the position of the westerlies during Termination I. *Science* 362(6414): 580-583. doi:<https://doi.org/10.1126/science.aat9393>.

Zhang, L., Ren, X., Wang, C.-Y., Gan, B., Wu, L., and Cai, W. 2023. An observational study on the interactions between storm tracks and sea ice in the Southern Hemisphere. *Climate Dynamics*: 1-20. doi:<https://doi.org/10.1007/s00382-023-06894-5>.

Zhang, W., and Villarini, G. 2018. Uncovering the role of the East Asian jet stream and heterogeneities in atmospheric rivers affecting the western United States. *Proceedings of the National Academy of Sciences* 115(5): 891-896. doi:<https://doi.org/10.1073/pnas.1717883115>.

Zhang, W., Zhou, X., Hsu, P.-C., and Liu, F. 2020. Diversity of east China summer rainfall change in post-El Niño summers. *Frontiers in Earth Science* 8: 595548. doi:<https://doi.org/10.3389/feart.2020.595548>.

Zhang, Y.G., Pagani, M., and Liu, Z. 2014. Response to Comment on “A 12-million-year temperature history of the tropical Pacific Ocean”. *Science* 346(6216): 1467-1467. doi:<https://doi.org/10.1126/science.1257930>.

Zhang, Z., Ralph, F.M., and Zheng, M. 2019. The relationship between extratropical cyclone strength and atmospheric river intensity and position. *Geophysical Research Letters* 46(3): 1814-1823. doi:<https://doi.org/10.1029/2018GL079071>.

Zhang, Z., Li, G., Cai, Y., Cheng, X., Sun, Y., Zhao, J., Shu, P., Ma, L., and An, Z. 2022. Millennial-scale monsoon variability modulated by low-latitude insolation during the last glaciation. *Geophysical Research Letters* 49(1): e2021GL096773. doi:<https://doi.org/10.1029/2021GL096773>.

Zhong, Y., Lu, Z., Wilson, D.J., Zhao, D., Liu, Y., Chen, T., Gai, C., Gong, X., Jiang, Z., and Liu, J. 2023. Paleoclimate evolution of the North Pacific Ocean during the late Quaternary: Progress and challenges. *Geosystems and Geoenvironment* 2: 100124. doi:<https://doi.org/10.1016/j.geogeo.2022.100124>.

Zhu, Y., and Newell, R.E. 1998. A proposed algorithm for moisture fluxes from atmospheric rivers. *Monthly weather review* 126(3): 725-735. doi:[https://doi.org/10.1175/1520-0493\(1998\)126%3C0725:APAFMF%3E2.0.CO;2](https://doi.org/10.1175/1520-0493(1998)126%3C0725:APAFMF%3E2.0.CO;2).

Zimmermann, M., and Prescott, M.M. 2015. AFSC/RACE/GAP/Zimmermann: Central Gulf of Alaska Grid raster digital data Available from http://www.afsc.noaa.gov/RACE/groundfish/bathymetry/CGOA_bathymetry_grid.zip [accessed June, 2023 2023].

Zimmermann, M., Prescott, M.M., and Haeussler, P.J. 2019. Bathymetry and geomorphology of Shelikof Strait and the Western Gulf of Alaska. *Geosciences* 9(10): 409. doi:<https://doi.org/10.3390/geosciences9100409>.

Zuffa, G., Normark, W., Serra, F., and Brunner, C.A. 2000. Turbidite megabeds in an oceanic rift valley recording jökulhlaups of late Pleistocene glacial lakes of the western United States. *The Journal of Geology* 108(3): 253-274. doi:<https://doi.org/10.1086/314404>.

7. SUPPLEMENTARY MATERIAL

7.1. The Northeast Pacific's ocean-atmosphere system today

The Pacific is remarkable among oceans in terms of its size, the relative freshness of its surface waters, the isolation of its deepwater, the large amount of dissolved carbon it stores, and for the vast amount of heat it traps from the sun (Lyle et al. 2008). During the Quaternary, changes in these characteristics affected climates along the Northwest Coast and across the entire planet (Chiang 2009). Our understanding of how the North Pacific's ocean-atmosphere system functions has advanced rapidly, but many of these advances are segregated from one another within specialist literature. The knowledge threads involved are complicated because many of the systems they describe are complex, non-linear, and still poorly understood. Nevertheless, understanding how the North Pacific's ocean-atmosphere system functions today is prerequisite for deciphering its behavior during prehistory.

8.1.1. Oceanography

8.1.1.1. *Surface Currents*

The subtropical and subpolar gyres occupy much of the North Pacific. They are separated by the Subarctic Front between 40° N and 44° N in the central and western Pacific (Yuan and Talley 1996) (Fig. 48). Along this thermohaline boundary, colder and fresher water to the north is separated from warmer, saltier water to the south (Talley 2013). The subtropical gyre is maintained by trade winds in the tropics and by the Westerlies poleward of 20°-25° N (Hu et al. 2015). The subarctic gyre is maintained by the Westerlies and, like the subtropical gyre, its vigor varies with that of the Aleutian Low (Section 8.1.2.3). Trade winds associated with the Subtropical Gyre push warm, tropical water into the Western Pacific Warm Pool (Section 7.1.1.4) (De Deckker 2016).

The Kuroshio Current (Qiu 2019) is the North Pacific's western boundary current (Talley 2013). It carries large amounts of heat from the Western Pacific Warm Pool into mid-latitudes of the North Pacific where it nourishes extratropical cyclones (Hu et al. 2015). The Kuroshio Current carries up to 55 Sv ($10^6 \text{ m}^3\text{s}^{-1}$) of warm, salty, subtropical water from east of the Philippines northward towards Japan (Qiu 2019; Joh et al. 2021). Turning eastward from Japan, the Kuroshio becomes the Kuroshio Extension, which reaches flows as high as 130 Sv (Lam et al. 2021). Together the Kuroshio and Kuroshio Extension carry large amounts of heat into the high-latitude North Pacific, where it is released to the atmosphere as latent and sensible heat, which then fuels cyclogenesis along the Subarctic Front (Joh et al. 2022) (Section 7.1.2.2). Flow in the Kuroshio Current increases in summer during the Asian Summer Monsoon and declines in

winter, when its flow varies inversely with the strength of the East Asian Winter Monsoon (Hu et al. 2015).

Where the Kuroshio veers east it meets the cold Oyashio Current, the western boundary current of the subpolar gyre. In response to seasonal changes in the vigor of the subpolar gyre, which is modulated by the strength of the Aleutian Low, the amount of water carried by the Oyashio Current varies widely, reaching 20-30 Sv in winter and spring, before declining to 3-4 Sv in summer and fall (Qiu 2019).

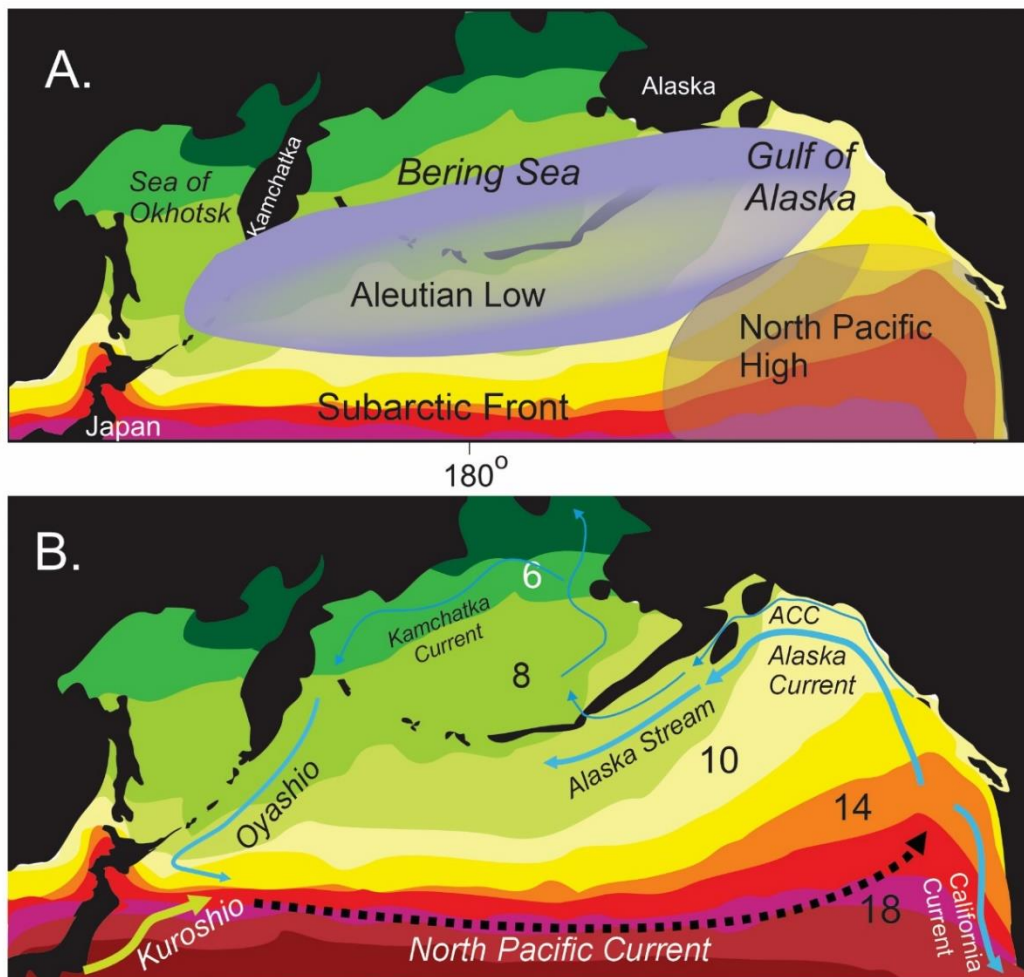


Figure 48. **A.** Generalized positions of the Aleutian Low, North Pacific High, and Subarctic Front. **B.** Major current systems in the North Pacific today (after Talley (2013), along with sea surface temperatures (°C) during the autumn of 2002 (Pickart et al., 2009).

The latitude where the Oyashio and Kuroshio currents converge varies markedly over seasonal and decadal time scales, accompanying north-south shifts in the Subarctic Front (Kubota et al., 2021). The position and steepness of the Subarctic Front respond sensitively to variations in the Aleutian Low (AL), which in turn responds to the phases of the El Niño-Southern Oscillation (ENSO) and the Pacific Decadal Oscillation (PDO) (Section 7.1.3) (Hu et al. 2015). Modulation of the mid-latitude Westerlies and trade winds by ENSO in turn influence decadal variability in the Kuroshio Extension (Joh et al. 2022). In recent decades, the Kuroshio Extension has experienced reduced flow and shifted southward during positive phases of the PDO (Section 4.1.4.2), while negative phases of the PDO have accompanied a northward-shifted and strengthened Kuroshio Extension (Qiu and Chen 2005; Lam et al. 2021).

The eastward flowing Kuroshio Extension becomes the North Pacific Current, which bifurcates off the western coast of North America at $\sim 50^\circ$ N latitude (Fig. 48). Its southern branch forms the California Current, and its northern branch forms the eastern limb of the Subpolar Gyre in the Gulf of Alaska. Flowing southwestward along the Aleutian Island chain, the Alaska Stream connects the two sub-gyres that comprising the North Pacific Subpolar Gyre. The counter-clockwise motion of this gyre is driven by the winds of cyclonic storms, whose repeated passage across the North Pacific creates the Aleutian Low (Pickart et al. 2009).

In the Gulf of Alaska today, the narrow and rapidly flowing Alaska Coastal Current (ACC) lies inshore of the Alaska Current (Royer et al. 2001) (Fig. 48). Prevailing alongshore winds entrained by the Aleutian Low generate downwelling on the Gulf of Alaska continental shelf and upwelling offshore (Weingartner et al. 2005; Danielson et al. 2022). Both the Alaska Current and the ACC transport large amounts of heat, which results in a prominent east-west gradient in sea surface temperature spanning the North Pacific above 50° N latitude (Fig. 48).

The Alaska Coastal Current (ACC) is a buoyancy-driven, geostrophic current fed by freshwater originating as precipitation and glacier melt along the seaward flank of the Coast Mountains and St. Elias Mountains (Royer and Grosch 2006). The ACC transports $750\text{--}870 \text{ km}^3 \text{ yr}^{-1}$ of freshwater (Neal et al. 2010; Hill et al. 2015), which is roughly 50% more than the Mississippi River's annual discharge and accounts for some 40% of all freshwater entering the northeastern North Pacific today (Royer and Finney 2020). The ultimate sources for the freshwater feeding the ACC are extratropical cyclonic storms developing along the coast of northeast Asia and along the Subarctic Front. Both the Alaska Current and the ACC are subject to positive feedbacks involving the Aleutian Low (AL). When the AL deepens, counter-clockwise winds become more prevalent, which increases the transport of warm water northward, which enhances cyclogenesis in the region and deepens the AL (Royer et al. 2001). Warmer ocean and air temperatures further strengthen the ACC by increasing glacier melt (Royer et al. 2001).

The Alaska Stream and the Alaska Coastal Current supply most of the water entering the Bering Sea. Near-surface circulation in the Bering Sea loops northwestward along the coast of western Alaska and then divides, one branch exiting southward through Kamchatka Strait and the other northward through Bering Strait. Bering Strait is both narrow (85 km) and shallow

(~ 50 m), which restricts northerly flow through the strait to around 1 Sv, which equates roughly to the combined flow of all the planet's rivers (Woodgate et al. 2005; Woodgate 2018). That said, flow through Bering Strait is trivial compared to the Kuroshio Extension (up to 130 Sv) (Gallagher et al. 2015), the Indonesian Throughflow (ITF) (~ 15 Sv) (Sprintall et al. 2014), the Gulf Stream (~ 31 Sv) (Lund et al. 2006), and the Benguela Current (~ 25 Sv) (Gordon et al. 1992).

The predominately northward flow through Bering Strait is driven by a combination of southerly winds and, most importantly, by the difference in sea level between the North Pacific and North Atlantic/Arctic Oceans, which is caused by density differences relating to salinity. Ultimately, these salinity differences between the North Pacific and North Atlantic are the result of the meridional overturning circulation that occurs in the North Atlantic today, but not in the North Pacific (Woodgate 2018; Cessi 2020).

Although its throughflow is relatively small, Bering Strait plays important roles in the present-day oceanography and climate of the Arctic Ocean and the North Atlantic (Lyle et al. 2008). Pacific water flowing northwards through the strait accounts for roughly one third of all the freshwater entering the Arctic Basin, which, when it exits the Arctic Basin through Fram Strait, affects the vigor of Atlantic Meridional Overturning Circulation (AMOC) (Woodgate and Aagaard 2005; Hu et al. 2007; Hu et al. 2010; Hu et al. 2012; Praetorius et al. 2020). In fact, the opening of Bering Strait ca. 5 Mya may have been key in initiating AMOC (Keigwin and Cook 2007). Northward flow through Bering Strait is also an important source of nutrients for Arctic Ocean ecosystems (Woodgate and Peralta-Ferriz 2021), and it accounts for most oceanic heat transport into the western Arctic Basin (~ 14 TW yr⁻¹) (Woodgate et al. 2010; Beszczynska-Möller et al. 2011; MacKinnon et al. 2021). That said, Bering Strait's contribution to oceanic heat transport into the Arctic Basin is dwarfed by the what enters from the North Atlantic via the Barents Sea (~ 73 TW yr⁻¹) (Docquier et al. 2021).

7.1.1.2. North Pacific Intermediate Water (NPIW)

Bering Strait also plays a role in the production of North Pacific Intermediate Water (NPIW) (Fig. 49), which is the only significant, overturning circulation occurring in the North Pacific today (Talley 2013). In the North Atlantic, vertical gradients in salinity and temperature collaborate with the wind regime to facilitate overturning circulation amounting to approximately 15 Sv. This Atlantic Meridional Overturning Circulation (AMOC) descends to several thousand meters and strongly affects both regional and global climate (Weijer et al. 2019). In contrast, in the North Pacific, the overturning circulation involved in NPIW formation amounts to only about 2 Sv and descends to only 300-800 m (Emile-Geay et al. 2003; Rae et al. 2020).

Today, the precursor of North Pacific Intermediate Water (NPIW) forms mainly in polynyas (ice-free areas within an otherwise frozen sea) in the Sea of Okhotsk during winter

(Shcherbina et al., 2004), with some additional input from the westernmost Gulf of Alaska (You et al., 2000). NPIW forms when this cold, relatively low-salinity water reaches the Oyashio - Kuroshio convergence where it is overrun by the warmer and saltier Kuroshio water (Shimizu et al. 2004; Max et al. 2017). The presence of NPIW stratification in the North Pacific today (Fig. 50) limits the upwelling of deep, nutrient-rich water, which in turn restricts the exchange of ^{14}C -depleted, deepwater with the atmosphere; it also limits primary productivity in surface waters (Maier et al. 2015). As explored in Section 4.1.8, fluctuations in NPIW production may have played a key role in modulating CO_2 concentrations in the atmosphere during MIS 2 (Jaccard et al. 2009; Rae et al. 2020; Zhong et al. 2023).

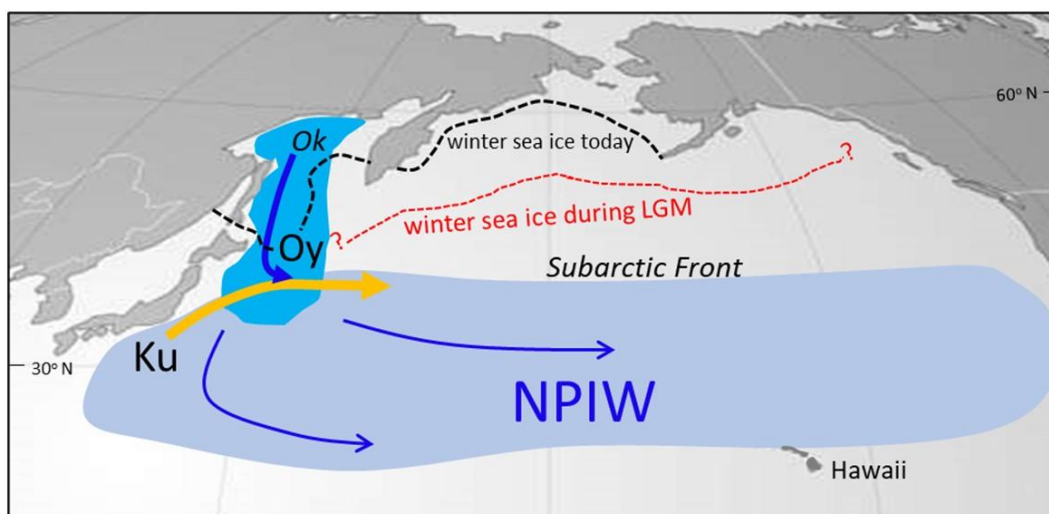


Figure 49. Today, North Pacific Intermediate Water (NPIW) forms where cold, relatively low-salinity water in the Sea of Okhotsk (Ok) is carried southward by the Oyashio Current (Oy) to mix with the warmer, saltier Kuroshio Current (Ku) east of Japan. Entrained by the North Pacific Current, NPIW forms a layer that extends nearly to the coast of California at depths of 300-800 m. Redrawn from Max et al. (2017) and Bostock et al. (2010). Sea ice extents are from Meheust et al. (2018).

7.1.1.3. Why no deepwater forms in the North Pacific today

Today, deepwater forms in the North Atlantic but not in the North Pacific because the North Pacific lacks deep, overturning circulation analogous to Atlantic Meridional Overturning Circulation (AMOC) (Ferreira et al. 2010; Rae et al. 2014). This is because the surface salinity in

the North Pacific is relatively low (~ 32.8 psu) compared to the underlying deepwater (~ 34.6 psu) (Warren, 1983). Surface salinities are relatively low in the North Pacific for several reasons. First, the North Pacific's relatively cool sea surface temperatures (SSTs) limit evaporation rates, which are roughly half those at similar latitudes in the North Atlantic (Emile-Geay et al. 2003). Second, wind-stress curl patterns over the North Pacific, which are partly controlled by the configuration and topography of the bordering continents, restrict the mixing of saltier waters from the subtropical gyre into the subpolar gyre (Warren 1983). Third, large amounts of freshwater are carried into the high-latitude North Pacific from the tropical, western Pacific by the Asian Summer Monsoon and from the Caribbean Sea across the Isthmus of Panama by the trade winds (Emile-Geay, 2003; Menviel et al. 2012). One consequence of the lack of significant overturning circulation is that the North Pacific responds comparatively quickly to solar forcing (Viaggi 2021). Its relatively shallow mixed layer causes rapid responses of surface temperatures to radiative forcing compared to the North Atlantic and Southern Oceans where overturning circulation is more vigorous (Long et al. 2014).

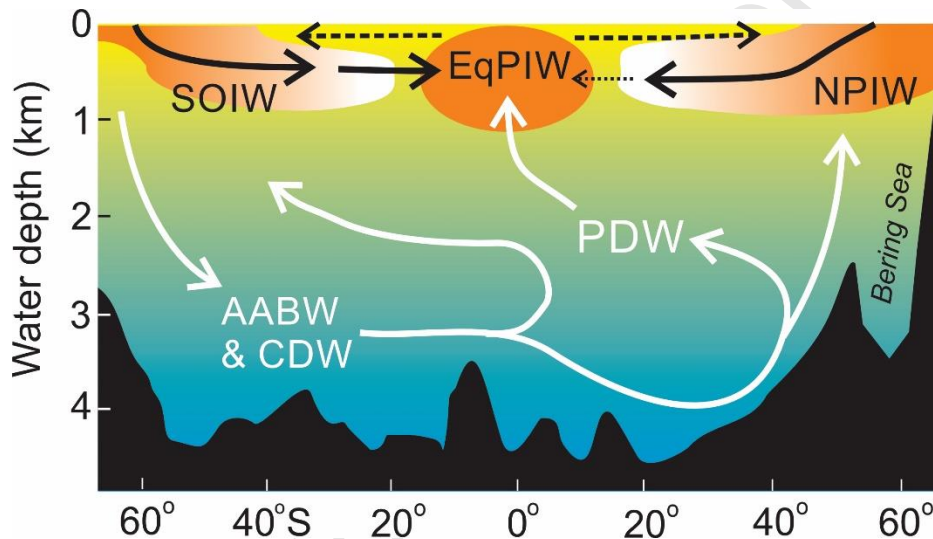


Figure 50. Cross section of the Pacific Basin today along the 170th meridian showing major ocean currents. "NPIW" = North Pacific Intermediate Water. "EqPIW" = Equatorial Pacific Intermediate Water. "SOIW" = Southern Ocean Intermediate Water. "NADW" = North Atlantic Deepwater. "AABW" = Antarctic Bottom Water. "CDW" = Circumpolar Deepwater. "PDW" = Pacific Deepwater. Redrawn from Bostock et al. (2010), Talley (2013), and Rippert et al. (2017).

In the absence of widespread overturning circulation in the North Pacific today, surface waters off the coast of Antarctica sink, mix with recirculated North Atlantic deepwater, and then flow northward across the Equator, eventually spreading at depth beneath the Gulf of Alaska (Max et al. 2017; Du et al. 2018; Walczak et al. 2020) (Fig. 50). Because it lies at a terminus for deep-water circulation, North Pacific deepwater becomes enriched in CO₂ and

dissolved nutrients compared to other oceans (Jaccard et al. 2009). For example, North Pacific deepwater contains ~ 10% more dissolved CO₂ than North Atlantic deepwater (Takahashi et al. 1981). As a result, Pacific deepwater in the Gulf of Alaska is among 'oldest' and most carbon-rich water masses in the global ocean (Denton et al. 2005; Matsumoto 2007; Du et al. 2018). At depths above 700 m on the continental slope of the northeastern Gulf of Alaska, differences in the ¹⁴C ages of contemporaneous benthic and planktonic foraminifera (B-P ages) have varied between 200 years and 2000 years over the last 40 kyr (Davies-Walczak et al. 2014; Schmuck et al. 2021). Today in the western North Pacific, a similar range in B-P age differences occurs between abyssal and surface waters (0-5000 m depth), and these offsets were probably even greater during the last ice age (Rae et al. 2020). Today's gradients in B-P ages are maintained by thermal and haline stratification that resists deep mixing in combination with an influx of Antarctic Bottom Water that brings ¹⁴C-depleted water into the abyssal North Pacific (Du et al. 2018; Rae et al. 2020) (Fig. 50).

The situation is markedly different in the North Atlantic where the northward course of warm, western boundary current is less constrained by the geography of the continents and by the predominant winds (Emile-Geay et al. 2003) (Fig. 51). Warm, deep-running currents penetrate to high latitudes across a broad front, and relatively warm surface waters become saltier through evaporation, with overturning circulation the eventual result. If Bering Strait were capable of carrying 70 Sv or even 10 Sv rather than the paltry 1 Sv it now carries, both the Arctic Ocean and the North Pacific would possess markedly different ocean circulations and regional climates than today. The most basic implication of weak meridional overturning circulation in the high-latitude North Pacific is that the ocean-atmosphere system there resides relatively securely in a single attractor state. In contrast, the high-latitude North Atlantic teeters between two attractor basins, one in which Atlantic Meridional Overturning Circulation (AMOC) operates in its present-day, "on" configuration, and the other where AMOC is either switched off or greatly reduced (Bard 2002).

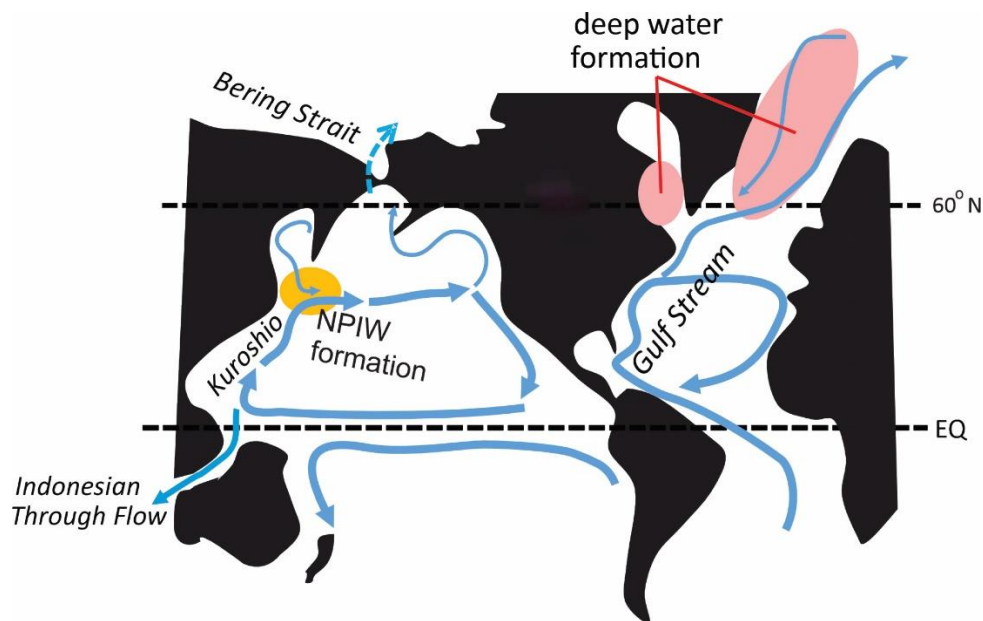


Figure 51. The North Pacific has only restricted communication with the Arctic Basin through the narrow and shallow Bering Strait. This is one reason why overturning circulation in the North Pacific is limited to the production of North Pacific Intermediate Water (NPIW). In contrast, the Atlantic Ocean has broad access to the Arctic, which facilitates vigorous meridional overturning circulation.

Today, the precipitation that freshens the high-latitude North Pacific and suppresses overturning circulation there comes from four sources. Changes in any one of these sources might have triggered changes in the vigor of overturning circulation in the subarctic Pacific during prehistory (Rae et al., 2020). The first source is the moisture carried across the Isthmus of Panama by trade winds converging into the Intertropical Convergence Zone (ITCZ) off the western coast of South America (Zaucker and Broecker 1992). Today, the ITCZ in the eastern Pacific remains north of the Equator year-round, which means that large amounts of the precipitation falling there are advected westward by the North Equatorial Current and eventually carried into the North Pacific by the Kuroshio Current. The second, major source of North Pacific freshening comes from water vapor carried from the Atlantic Ocean across Eurasia in the Westerlies (Dey and Döös 2020). The third and largest source is the Asian Summer Monsoon, which transports water vapor northeastwards from the low-latitude western Pacific (Liu et al. 2021) (Fig. 52).

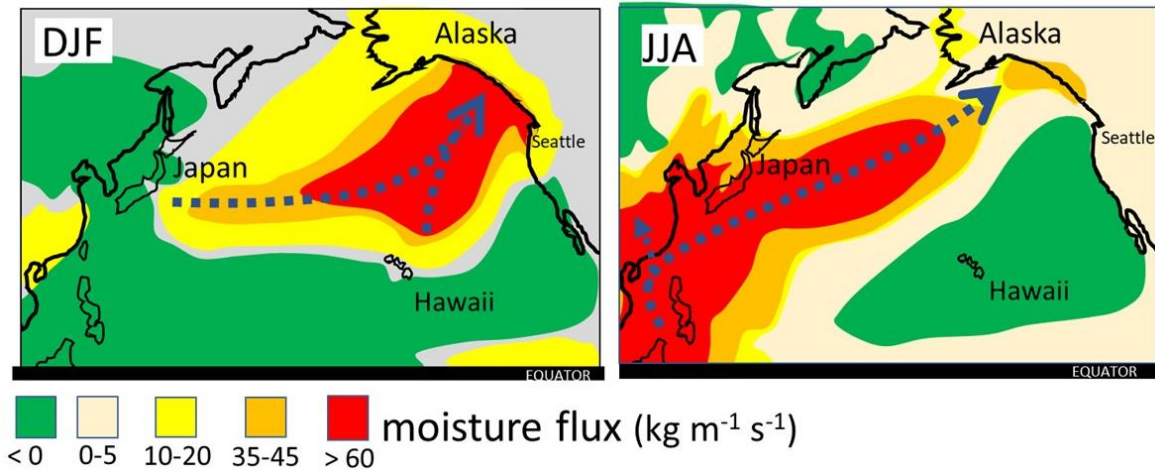


Figure 52. Vertically integrated, seasonal mean, meridional moisture transport over the North Pacific. In winter, most of this moisture is carried by extratropical cyclonic storms forming along the Subarctic Front. In summer, large amounts of water vapor are carried into the North Pacific by the Asian Summer Monsoon. Redrawn from Liu et al. (2021). "DJF" = December, January, February. "JJA" = June, July, August.

A fourth source of the freshwater that maintains the relative freshness of the subarctic Pacific's surface waters is moisture evaporated from the surface of the Kuroshio Current by dry air masses originating in the Eurasian interior (Newman et al. 2012). Extratropical cyclonic storms forming along the northern margin of the Kuroshio-Oyashio Extension and the North Pacific Current track northeastward and release this freshwater over the Gulf of Alaska (Schultz et al. 2019) (Section 8.1.2.2). Once rained into the high-latitude North Pacific, this freshwater tends to remain because there is limited cross-gyre mixing with subtropical waters (Emile-Geay et al. 2003).

7.1.1.4. Western Pacific Warm Pool (WPWP)

The Western Pacific Warm Pool (WPWP) (alternatively, the Indo-Pacific Warm Pool) is a region of the western, tropical Pacific approximately the size of the conterminous United States where SSTs are perennially $> 28^\circ \text{C}$. During the boreal winter, the WPWP extends between 10°N and 20°S ; during the boreal summer, it expands to 30°N . Year-round it is centered northeast of the Maritime Continent and Sahul. Because of the large amounts of heat it contains, the WPWP plays key roles in Earth's energy budget (De Deckker 2016). Warm water from the WPWP is transferred to other oceans by two main routes. Some 700 Tw ($700 \times 10^{12} \text{ W}$) of heat is exported into the high-latitude North Pacific via the Kuroshio Current, while some 1000 Tw of heat is transferred into the Indian Ocean via the Indonesian Throughflow.

The Western Pacific Warm Pool (WPWP) links ENSO to the monsoons (Yang et al. 2018). Because of its position beneath the western end of Walker Circulation, sea surface temperature (SST) and precipitation in the WPWP region are strongly affected by the state of ENSO (Hu et al. 2015). La Niña events accompany especially warm SSTs in the WPWP, which revs-up Hadley Circulation and causes the East Asian Summer Monsoon (EASM) to begin earlier and proceed more intensely (Zhang et al. 2021). When Walker Circulation is most active during La Niña events, abundant rainfall freshens surface waters in the WPWP, and some of this fresh, warm water reaches the Northeast Pacific via the Kuroshio and its tributary currents (Hu et al., 2015). In contrast, strong El Niño events bring cooler SSTs to the WPWP, which tends to delay and weaken the EASM (Zhang et al., 2021).

7.1.1.5. Indonesian Throughflow (ITF)

The Indonesian Throughflow (ITF) is the only low-latitude, inter-ocean current on the planet today, and it carries large amounts of oceanic heat from the Western Pacific Warm Pool (WPWP) into the Indian Ocean through channels traversing the Maritime Continent (Gordon and Fine 1996). By transporting warm, relatively fresh water from the WPWP to the Indian Ocean, the ITF plays an important role in global thermohaline circulation (Hu et al. 2015). Some 40% of WPWP water entering the Indian Ocean via the ITF eventually enters the South Atlantic by way of the Agulhas Current (Song et al. 2004) where it affects Atlantic Meridional Overturning Circulation (Beck et al. 2018).

Today, the ITF responds sensitively to the phases of ENSO (Xu et al. 2010). While annual ITF averages 15 Sv, interannual variations of 5 Sv can occur in response to perturbations relating to ENSO (Feng et al. 2018). The ITF tends to slow during El Niño events in response to weakening in the Indian-Pacific pressure gradient (Sprintall et al. 2014; Hu et al. 2015). The ITF is most vigorous during La Niña conditions in response to strengthening trade winds that increase the Pacific-Indian Ocean pressure gradient. In recent decades, reductions in the ITF accompanied cooling in the eastern Indian Ocean, which then reduced the vigor of South Asian Summer Monsoon (Petrick et al. 2019).

At glacial/interglacial time scales, the Indonesian Throughflow (ITF) is sensitive to changes in relative sea level (De Deckker, 2016; Fan et al. 2018) (Section 4.1.4). Modeling suggests that complete closure of the ITF would contribute to a semi-permanent El Niño state in the Pacific (Song et al. 2007; Santoso et al. 2011).

7.1.1.6. Global patterns of oceanic heat transport (OHT)

By virtue of its large size (47% of the global ocean; 3x > Atlantic), the Pacific Ocean receives most of the solar energy reaching the Earth's oceans (Fig. 53). Heat transport is asymmetrical about the Equator; northward oceanic heat transport (OHT) is ~ 2x that of

southward OHT (Trenberth and Fasullo 2017; Forget and Ferreira 2019). Much of this asymmetry is due to Atlantic Overturning Circulation (AMOC) (Weijer et al. 2019), which draws warm, salty surface waters northward from everywhere north of 30° S in the Atlantic basin (Trenberth and Fasullo 2017). Warm surface water carried to high latitudes in the North Atlantic returns to the Southern Ocean as cold, salty, deepwater, and from there flows back into the North Pacific at depth (Talley 2013; Buckley and Marshall 2016). Because of its broad connections with the Arctic Basin, Atlantic waters transport roughly 10x more heat into the Arctic Ocean than what is transported through Bering Strait (Trenberth and Zhang 2019). As a result, the North Atlantic is the northern hemisphere's most important conduit for OHT from equatorial seas to polar seas, and for the eventual dissipation of this energy back to space (Docquier et al. 2021). The conjunction of this large amount of Arctic-bound OHT with the instability of AMOC meant that during MIS 2, AMOC functioned as a crucial, flickering switch in the planet's atmosphere-ocean system (Lynch-Stieglitz 2017).

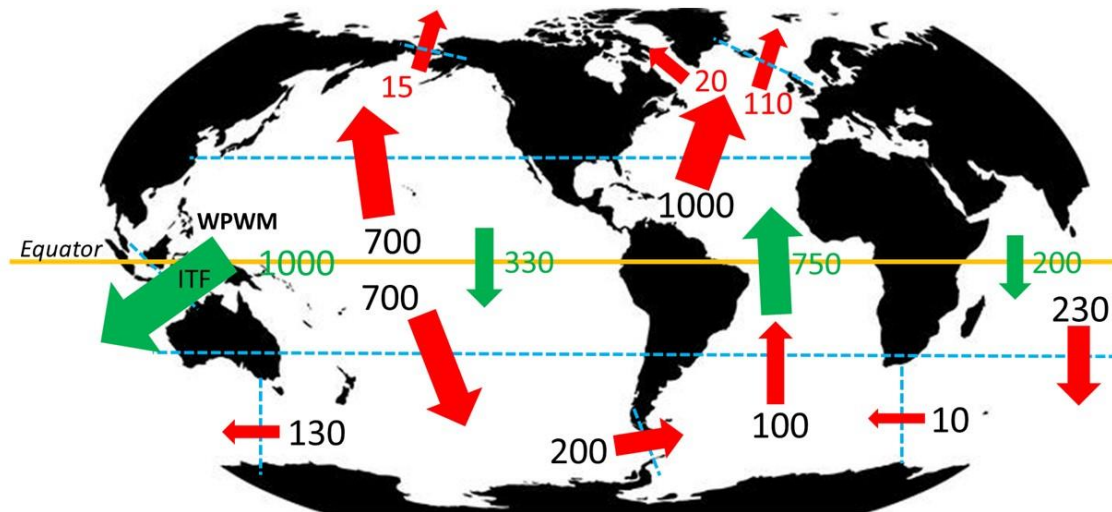


Figure 53. Ocean heat transport (OHT) today in units of TW (1 TW = 10^{12} W, or PW^{-3}). Green arrows depict cross-Equator transfers. Redrawn from Forget and Ferreira (2019) with modifications based on Trenberth and Fasullo (2017), Trenberth and Zhang (2019), and Docquier et al. (2021).

7.1.1.7. Summary: Oceanography today

The tropical Pacific is the Earth's great heat engine. Factors important in determining the amounts and routes of oceanic heat transport (OHT) in and out of the North Pacific include the phases of ENSO and fluctuations in the flows of the Kuroshio Current, the Indonesian

Throughflow (ITF), and the Alaskan Stream. The vigor of the Aleutian Low (AL), and consequently the amount and routing of moisture carried into downwind North America where it can contribute to glacier growth, are intimately tied to the gradients in sea surface temperature (SST) setup by OHT. Because the North Pacific is relatively fresh, and because the cooling of its surface waters is restricted by its limited ingress to the Arctic Basin, the amount of deep, overturning circulation is presently trivial in the high-latitude North Pacific compared to the North Atlantic and Southern Ocean. The relative freshness of the North Pacific is maintained by interactions between the trade winds, the Asian Summer Monsoon, the westerlies carrying storms across Eurasia, and the vigor of the Kuroshio Current. The dynamics of all these processes varied markedly over the course of Marine Isotope Stage 2. When overturning circulation was restricted, North Pacific deepwater accumulated large amounts of CO₂, which was released when the dynamics of overturning circulation changed over the course of the last deglaciation (Section 4.1.8).

7.1.2. Climate today

7.1.2.1. *Atmospheric heat transport*

Maintenance of the current, steady-state latitudinal temperature gradient in the atmosphere requires a poleward heat transport by the combined atmosphere and ocean of ~ 5 PW (1 PW = 10¹⁵ W) annually (Trenberth and Zhang 2019) (Fig. 54). It is because of this net flow of heat energy that the climates of high and low latitudes are inseparably linked. The North Pacific surpasses the North Atlantic in the amount of poleward heat transport occurring through the atmosphere (Trenberth and Solomon 1994), but the situation is reversed in terms of oceanic heat transport (Fig. 54). In winter, the western North Pacific is a large heat source region for the global atmosphere. This uploading of heat occurs when / where cold, continental air masses gain sensible and latent heat from the subtropical waters flowing northward in the Kuroshio Current (Trenberth and Solomon 1994). In summer, the Asian Summer Monsoon transfers large amounts of heat into the Northeast Pacific (Liu et al. 2021).

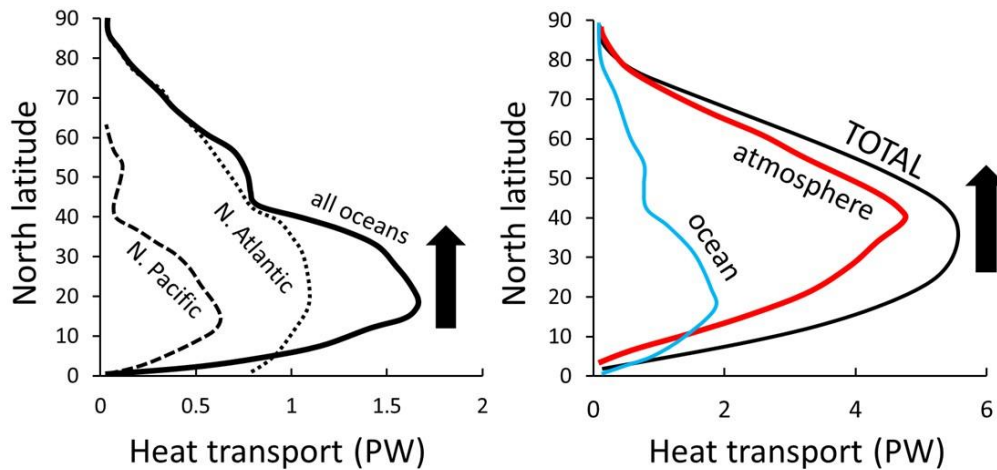


Figure 54. Solar energy received at low latitudes is redistributed poleward by the ocean and atmosphere, with the atmosphere playing the larger role. **LEFT** Oceanic heat transport in northern oceans between 2000 and 2016 expressed as annual, meridional heat transport. A Petawatt (PW) equals 10^{15} watts. Redrawn from Trenberth et al. (2019). **RIGHT** Combined oceanic and atmospheric heat transport. Redrawn from Trenberth et al. (2019).

Most of the energy transported poleward in the atmosphere from low latitudes is in the form of sensible heat, latent heat, and the kinetic energy contained in extratropical cyclones (Trenberth et al. 2019; Xie et al. 2020) (Fig. 55). An important subset of these cyclones are atmospheric rivers, transient tendrils of heat and moisture transport that develop near the cold fronts of extratropical cyclones over the sea and extend from the subtropics to high latitudes (Zhu and Newell 1998; Zhang et al. 2019). Today, atmospheric rivers provide up to half of all winter precipitation in the western USA (Rutz et al. 2014), which includes the snow nourishing glaciers and the runoff supplying pluvial lakes (Hudson et al. 2019) (Section 3.5). Along the western coast of North America, atmospheric rivers occur most frequently in fall and winter when the weather is dominated by strong onshore flow of Pacific air masses.

7.1.2.2. Cyclogenesis

Extratropical cyclones develop from eddies formed where steep, meridional gradients in temperature create high baroclinicity in the atmosphere (Chang et al. 2002). In the northwestern Pacific, contrasting surface temperatures between the interior of Asia and the warm Kuroshio Current create a region of particularly strong baroclinicity (Hu et al. 2015),

particularly in winter when the subtropical jet is strongest (Hoskins and Hodges 2002). Cyclogenesis is enhanced when and where abundant latent heat is abundant, as from evaporation from warm ocean water like what is carried in the Kuroshio and the North Pacific currents (Schultz et al. 2019). In turn, the wind fields created by the repeated passage of extratropical cyclones help maintain western boundary currents like the Kuroshio that transport warm water poleward (Hoskins and Valdes 1990).

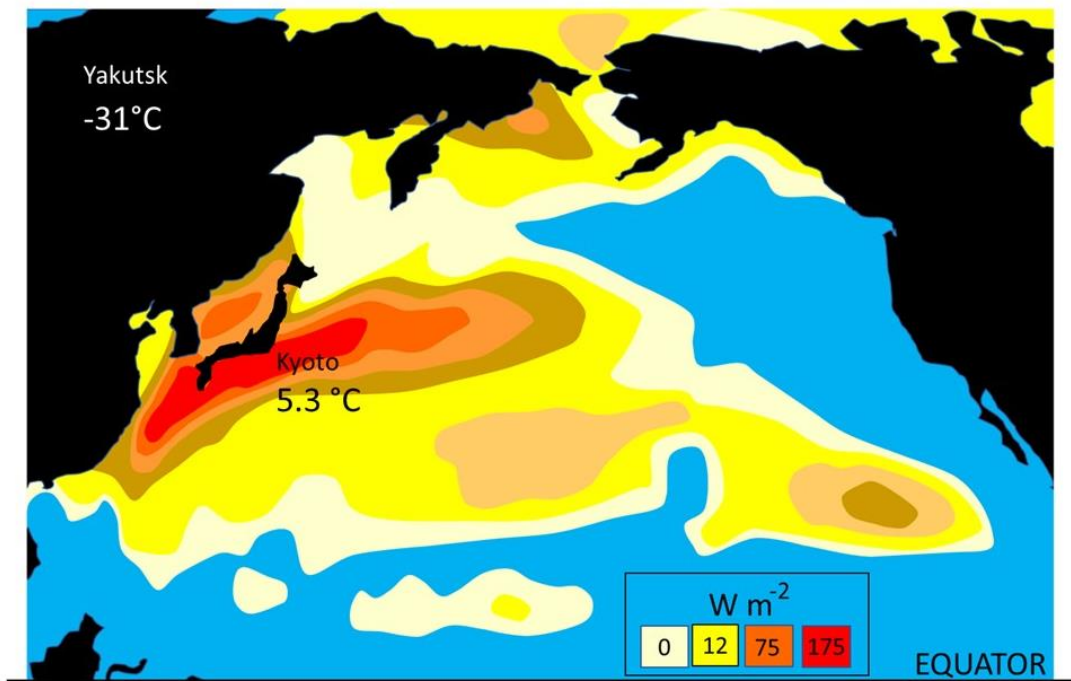


Figure 55. Annual average, net surface energy flux from ocean to atmosphere between the years of 2000 and 2016. The Kuroshio and North Pacific Currents supply much of the sensible and latent heat that maintains the baroclinicity responsible for generating extratropical cyclonic storms. Note the 25° C difference in average January temperatures between Yakutsk and Kyoto. Redrawn from Trenberth et al. (2019).

Much of water vapor feeding the extratropical cyclones that track into the Northeast Pacific and nourish glaciers along the Northwest Coast originates in the tropical and subtropical Pacific. During the boreal summer, the Intertropical Convergence Zone (ITCZ) shifts northward over southern Asia, triggering the Asian Summer Monsoon (ASM) (Fig. 56) (Walker et al. 2015; Ha et al. 2018; Liu et al. 2021). One of the main controls over how far north the ITCZ moves and for how long is northern, low-latitude, summer insolation, which affects the strength of the ASM by modulating the land-sea thermal contrast over southern Asia (Beck et al. 2018; Zhang et al. 2022) (Section 4.1.1). Also important is the steepness of the meridional temperature gradient between the tropics and the high latitude North Pacific (Chiang and Bitz 2005).

Different combinations of cooling/warming at high and low latitudes can cause the Westerlies to strengthen and shift southward, accompanied by a southward-shift in the ITCZ, which then limits the northward extent of the ASM (Zhang et al. 2018).

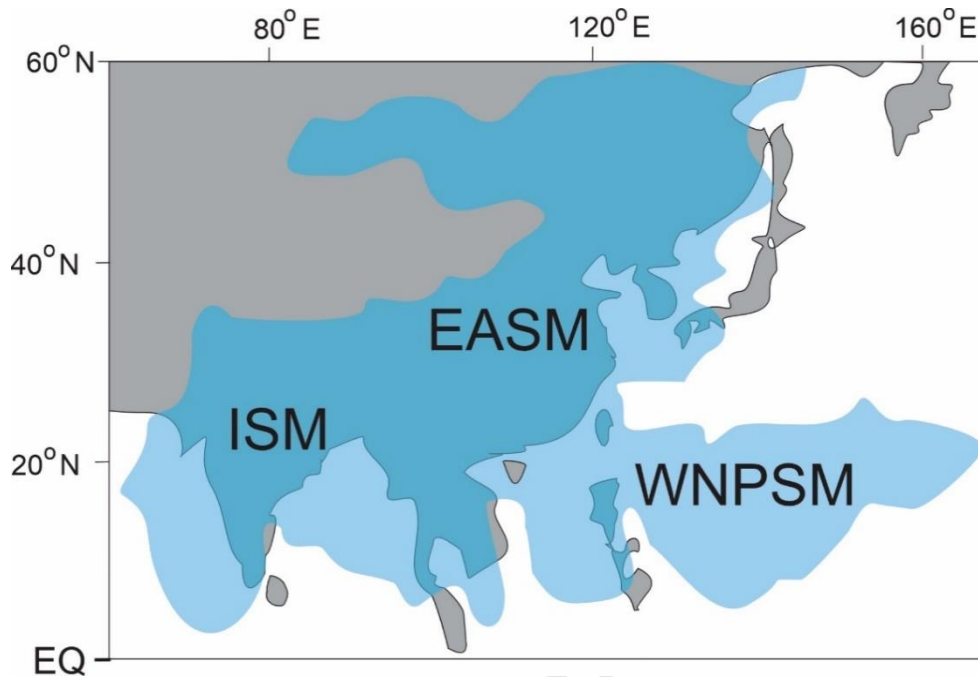


Figure 56. Typical geographic extents of the three components of the Asian Summer Monsoon during recent times. "ISM"= Indian Summer Monsoon, "EASM" = East Asian Summer Monsoon, "WNPSM" = Western North Pacific Summer Monsoon. (after Ha et al. 2018).

Today, most cyclogenesis in the North Pacific occurs in the central North Pacific in the region bounded by 35° N and 45° N and 150°W to 160°E (Fig. 57) (Hoskins and Hodges 2002; Rodionov et al. 2007; Knippertz et al. 2013). The storms generated here, together with those originating off the eastern coast of Japan, travel northeastward in the Westerlies towards North America. The Gulf of Alaska is the graveyard of North Pacific storms because many become trapped there by the high coastal mountain ranges (Mesquita et al. 2010). The repeated passage of storms over the Northwest Coast contributes to the high precipitation there. Seasonally, most storms occur in autumn, and in the present day, most of these storms cross into North America over northern British Columbia and Southeastern Alaska.

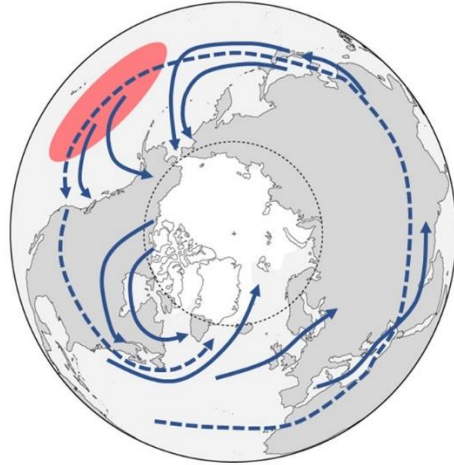


Figure 57. Schematic of northern hemisphere storm tracks during recent decades. In winter, when the Aleutian Low is strongest, cyclones generated off the eastern coast of Japan can reach the Gulf of Alaska; however, most storms originate along the Subarctic Front in the central North Pacific north of Hawaii (pink oval). Redrawn from Chang (2002), Hoskins and Hodges (2002), Rodionov et al. (2007) and Mesquita et al. (2010).

7.1.2.3. *The Aleutian Low*

The Aleutian Low (AL) is generated by the repeated passage of extratropical cyclonic storms over the North Pacific. It is one of the largest circulation patterns in the northern hemisphere and one of the main centers of action within Earth's atmospheric (Rodionov et al. 2007). The AL has an ever-shifting intensity, seasonality, and geographical position, and these dynamics modulate climate throughout the North Pacific region (Lyle et al., 2008). The AL also serves as a key linkage in teleconnections between low and high latitudes (Zhong et al. 2023).

The Aleutian Low (AL) is most strongly developed in winter when it is centered over the Aleutian Islands. In summer, when cyclogenesis declines to a minimum off northeastern Asia and along the Subpolar Front, the AL is least active and is displaced northwestward by the expanding North Pacific High (Fig. 51, 58). This high pressure system is persistent over the coastlines of southern British Columbia and Washington during late summer and early autumn, and what storms do occur tend to be shunted into the Bering Sea and southern Alaska. In winter, when cyclogenesis revs-up again, the North Pacific High shrinks and withdraws southeastward, while the AL deepens and expands. By late winter, most cyclonic storms track into southern British Columbia and Washington, Oregon, and northern California, leaving southern Alaska under the frequent influence of the expanded Polar High. As discussed below, the AL is strongly affected by ENSO and is a key player in various teleconnections, including the Pacific Decadal Oscillation (PDO), the Pacific North American Pattern (PNA), and the Arctic Oscillation (AO).

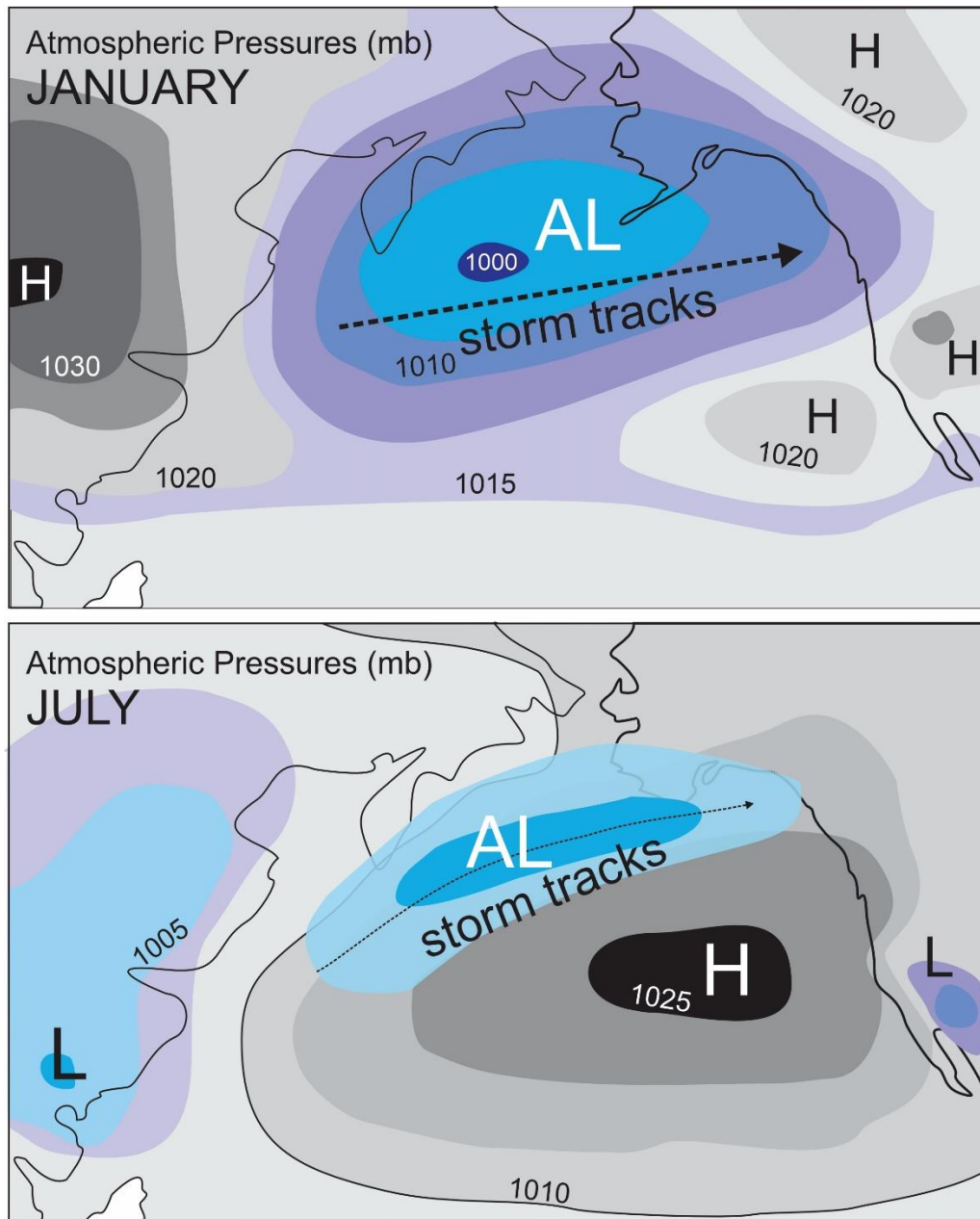


Figure 58. Seasonal changes in atmospheric pressure over the North Pacific. Redrawn from Lyle et al. (2008).

7.1.3. Atmosphere-Ocean Teleconnections in the North Pacific

"...chaos (weather noise) is a prominent factor in the extratropics, but the climate is molded by the tropical influences with the ocean selectively bringing out the long time scales."

Trenberth and Hurrell (1994).

The poleward flow of Sun-derived energy links the climate and weather of widely separated locations through teleconnections taking the form of atmospheric bridges and oceanic tunnels (Alexander et al. 2002; Liu and Alexander 2007). Understanding how the ocean-atmosphere system of the North Pacific operated during prehistory requires at least a summary understanding of the teleconnections that influence climate today. With the ice-age Northwest Coast in mind, we review five of the most prominent ocean-climate teleconnections now operating in the Northeast Pacific region.

7.1.3.1. *El Niño-Southern Oscillation*

Today ENSO is the planet's main source of interannual variability in climate (Liu et al. 2014; Norel et al. 2021). ENSO's timing is both irregular (6-18 months) and quasi-periodic (2-8 years). It involves shifts in the longitudinal positions of warm equatorial waters and attendant changes in the intensity and location of the trade winds and Hadley Circulation (McPhaden et al. 2006). In addition to controlling much of the variability in rainfall associated with monsoon systems (Wang et al. 2013), ENSO is an important driver of annual- and decadal-scale variability in the present-day ocean-atmosphere system of the subarctic Pacific (Newman et al. 2016).

ENSO operates within a complex web of teleconnections (Kaboth-Bahr et al. 2021), some of which extend into the Northeast Pacific and from there into downwind North America (Wiles et al. 2023). Many of these teleconnections operate either directly or indirectly via changes in the position, vigor, and seasonality of the Aleutian Low (AL). The same atmospheric changes affecting the AL also trigger shifts in upwelling, current strength, and sea surface temperatures (SSTs) throughout the North Pacific. For example, during El Niño phases warm waters surge eastward along the Equator and eventually spread poleward along the western coast of North America, sometimes as far as the Gulf of Alaska (Wendler et al. 2016).

Today, the state of ENSO strongly influences the climate of the Northwest Coast (Fig. 59). During warm El Niño phases (negative Southern Oscillation Index, SOI-), the Aleutian Low (AL) deepens, leading to ridging over western North America and a southward-shift in storm tracks. This often results in relatively dry conditions in the Pacific Northwest (Oregon, Washington, and southern British Columbia) and relatively wet conditions in the Southwest USA (Nevada, Utah, Arizona). At the same time, warmer than average conditions tend to occur over western Canada and southern Alaska, and sea surface temperatures tend to be warmer than average in coastal waters between the Bering Sea and Mexico but cooler in the central North Pacific. Atmospheric rivers (Zhu and Newell 1998) originating in the central Pacific tend to become more frequent above 30° N in the eastern Pacific during El Niño events (Mundhenk et al. 2016).

Contrasting patterns occur during La Niñas, when sea surface temperatures tend to be warmer than usual over the tropical, western Pacific and cooler in the Gulf of Alaska. These Southern Oscillation Index positive (SOI+) phases are often accompanied by more northerly storm tracks, cooler/wetter conditions in Interior Alaska, warmer/wetter conditions around the Gulf of Alaska margin, a relatively wet Pacific Northwest, and a relatively dry Southwest USA (Wise 2010). Atmospheric rivers tend to penetrate further north during La Niña conditions (Liu et al. 2021). Differences in precipitation between the Pacific Northwest and the Southwest USA are most pronounced when the Pacific Decadal Oscillation (PDO) and the SOI are in reinforcing states (SOI+, PDO-) or, alternatively (SOI-, PDO+) (Hudson et al. 2019).

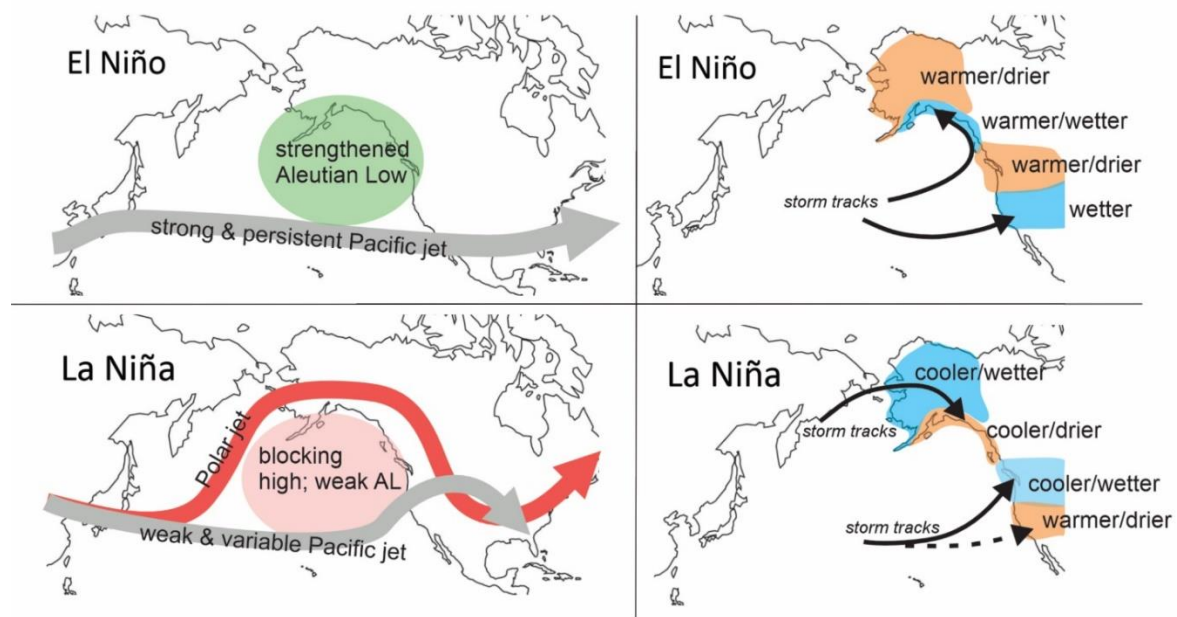


Figure 59. **LEFT PANELS.** Generalized atmospheric circulation and winter climate during strong El Niño and La Niña events. During El Niño winters, the Aleutian Low (AL) deepens in response to more frequent cyclonic storms. These storms bring abundant snow to coastal mountains bordering the Gulf of Alaska. During strong La Niña events, the AL weakens and shifts westward, and blocking highs occur more frequently over the eastern Gulf of Alaska.

RIGHT PANELS. Winter temperature and precipitation vary across relatively short distances along the Northwest Coast according to the phases of ENSO. Wetter conditions correspond to increased snowfall at high elevations. Summarized from various sources including Papineau (2001), Rodionov et al. (2007), Mesquita et al. (2010), Wise (2010), and National Weather Service (2023).

ENSO's teleconnections with the high latitude North Pacific vary according to whether it is in an El Niño or La Niña phase, and according to the specific type of El Niño that is occurring.

When El Niño warming is centered in the eastern tropical Pacific (Eastern Pacific Warm-El Niño, EPW- El Niño), convection deepens over the anomalously warm sea surface there, causing more heat to be transferred to the troposphere. The exact mechanisms linking an EPW-El Niño to the Aleutian Low (AL) are complex and still unclear (Li et al. 2017; Zhang and Villarini 2018; Qian et al. 2020; Zhang et al. 2020) (Fig. 60). In general terms, enhanced convection over the eastern tropical Pacific during EPW-El Niños alters Hadley Circulation, which then triggers a chain reaction of changes in atmospheric circulation and poleward energy transport (Newman et al. 2012). Atmospheric Rossby waves are shifted and amplified, which affects the dynamics of the Western Pacific Subtropical High, which in turn causes changes in the Asian Summer Monsoon (ASM) (Ha et al. 2012) that affect extra-tropical cyclogenesis (He et al. 2015), which increases the amount of moisture and heat transported to high latitudes (Liu et al. 2021). The end result is the deepening of the AL as cyclonic storms increase in frequency and intensity.

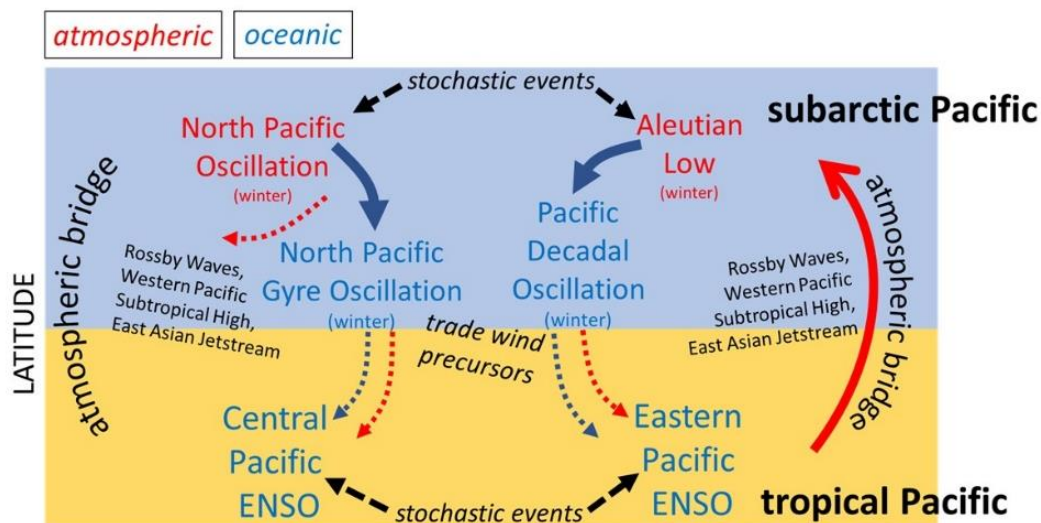


Figure 60. The oceanography and climatology of the subarctic Pacific are strongly linked to the tropical Pacific. Teleconnections link the El Niño-Southern Oscillation (ENSO) to the Aleutian Low (AL), the North Pacific Decadal Oscillation (PDO), the North Pacific Oscillation (NPO), and the (North Pacific Gyre Oscillation (NPGO). In turn, conditions in the North Pacific affect ENSO through feedbacking effects on the trade winds. These tropical-extratropical linkages operate over time scales of months to decades. Simplified somewhat from Di Lorenzo et al. (2013; 2015; 2023) and Newman et al. (2016).

When surface warming during El Niño events is centered in the central tropical Pacific (CPW-El Niño), Hadley Circulation teleconnects to the North Pacific system in different ways (Fig. 60). In this case, Hadley Circulation modulates the phase and intensity of the North Pacific

Oscillation (NPO), a decadal-scale see-sawing of sea-level pressure between the central North Pacific and Interior Alaska whose oceanic counterpart is the North Pacific Gyre Oscillation (NPGO) (Section 7.1.3.3).

In summary, the monthly and annual changes in ENSO teleconnect to the Aleutian Low (AL), whose responses then modify ocean circulation, salinity, and sea surface temperatures throughout the North Pacific. The resultant oceanic processes have greater inertia than do ENSO-induced changes in the tropical atmosphere. This means that ENSO teleconnections to the boreal ocean can resonate there for decades (Gu and Philander 1997) as low-frequency modes of variability taking the form of the Pacific Decadal Oscillation (PDO), the North Pacific Oscillation (NPO), and the North Pacific Gyre Oscillation (NPGO). We turn to these teleconnections next.

7.1.3.2. *Pacific Decadal Oscillation*

The Pacific Decadal Oscillation (PDO) involves decadal shifts in temperature and pressure over the North Pacific (Fig. 61). Poleward of 20° N, it is the dominant year-round pattern of monthly sea surface temperature (SST) and sea-level pressure variability within the North Pacific basin (Mantua and Hare 2002). The PDO is closely associated with changes in the intensity, position, and orientation of the Aleutian Low (Newman et al. 2016; Di Lorenzo et al. 2023). During positive, “warm” phases of the PDO, patterns of SST and sea-level pressure resemble those occurring during Eastern Pacific Warm-El Niños. Namely, SSTs cool and sea level pressures decrease over the North Pacific north of Hawaii, while SSTs warm and pressures rise along the western coast of North America. During negative, “cold” phases, the opposite occurs, with cooler than normal SSTs and lower pressures along the western coast of North America. Shifts in predominant winds accompany changes in PDO phases. During positive phases, southwesterly winds dominate; during negative phases, northerly winds are prevalent over the Northeast Pacific, which cause the upwelling of cold water offshore.

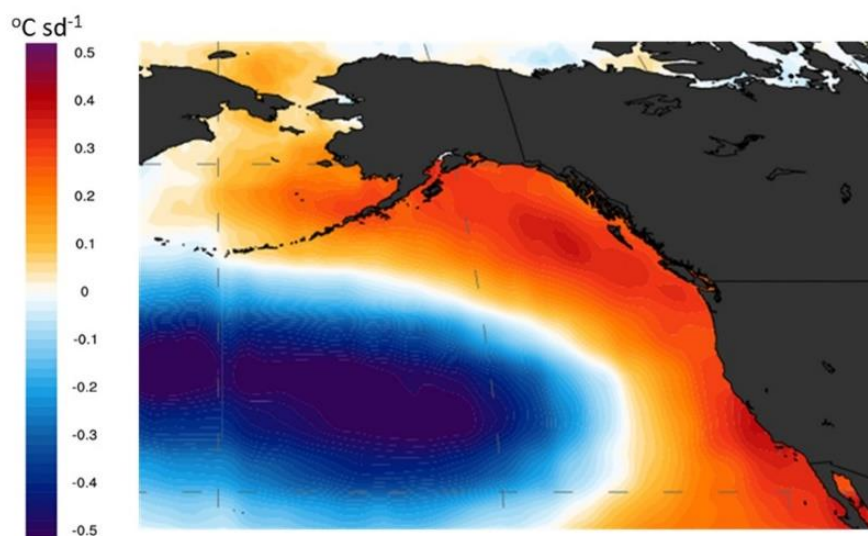


Figure 61. Positive phases of the Pacific Decadal Oscillation (PDO+) are associated with warmer than average sea surface temperatures (SSTs) along the Northwest Coast and cooler than average SSTs in the central North Pacific. Units are °C per standard deviation of the PDO index. (diagram borrowed from Wikipedia Commons: <http://www.cgd.ucar.edu/cas/cdeser/Docs/deser.sstvariability.annrevmarsci10.pdf>. (Accessed 7/8/2023)).

Teleconnections linking ENSO and the Pacific Decadal Oscillation (PDO) operate in both directions (Trenberth and Hurrell 1994; Alexander et al. 2002). For example, the Pacific Meridional Mode (PMM) is an interannual oscillation in pressure and wind fields (Bond et al. 2003) that connects the PDO to ENSO through wind-evaporation-sea surface temperature (SST) feedbacks in the subtropical Pacific (Di Lorenzo et al. 2015) (Fig. 60). During positive phases of the PMM, trade winds between Baja California and Hawaii weaken, allowing SSTs to warm, which draws the Intertropical Convergence Zone (ITCZ) northwards and modulates ENSO (Amaya 2019). These teleconnections may reach into the temperate zone via the Asian Winter Monsoon and by this means influence the state of the PDO (Tseng et al. 2020). The phase of the PDO also affects the poleward extent of Hadley Circulation, which tends to expand into both polar hemispheres during PDO- phases, and contract during PDO+ phases (Xian et al. 2021).

The decadal time scale of the Pacific Decadal Oscillation (PDO) emerges from the thermal inertia of the upper ocean as it integrates short-term forcing from ENSO and the Aleutian Low (AL). In doing so it accentuates and maintains these conditions for decades at a time (Namias et al. 1988; Di Lorenzo et al. 2023). Additional decadal-scale inputs come from changes in the vigor and routing of the Kuroshio-Oyashio Currents (Di Lorenzo et al. 2013; Di

Lorenzo et al. 2015) (Section 4.1.4). Together, these slower, oceanographic processes maintain the AL in configurations that maintain a given phase of the PDO for several decades at a time (Newman et al. 2016). Put another way, the two phases of the PDO represent long-term memories of ENSO preserved in a fuzzy manner by the inertia present in two, preferred attractor states shared by the Aleutian Low and the oceanography of the North Pacific Ocean.

The Pacific Decadal Oscillation (PDO) strongly affects downstream weather and climate conditions in North America, where its effects vary markedly by region (Linkin and Nigam 2008; Wiles et al. 2023) (Fig. 62). Approximately half of the variability in the frequency of measurable daily precipitation in the western, conterminous USA is explained by the phase of the PDO (Higgins et al. 2007). During PDO+ (warm) phases, the Aleutian Low (AL) tends to deepen and shift southward over the central Pacific, which causes storm tracks to be diverted away from the Pacific Northwest towards southern and Southeastern Alaska, which leads to above-average snowpacks and positive glacier mass balances there (Hartmann and Wendler 2005; Wendler et al. 2016) and to the opposite conditions in the Pacific Northwest (Walters and Meier 1989; Bitz and Battisti 1999; Lewis and Smith 2004; Marcinkowski and Peterson 2015). During PDO- (cold) phases, the AL tends to be centered over the northwestern Pacific, and winter storms tend to track more to the southeast, which brings cooler, snowier conditions to the Pacific Northwest and drier, less glaciogenic conditions to southern Alaska (Josberger et al. 2007; Malcomb and Wiles 2013).

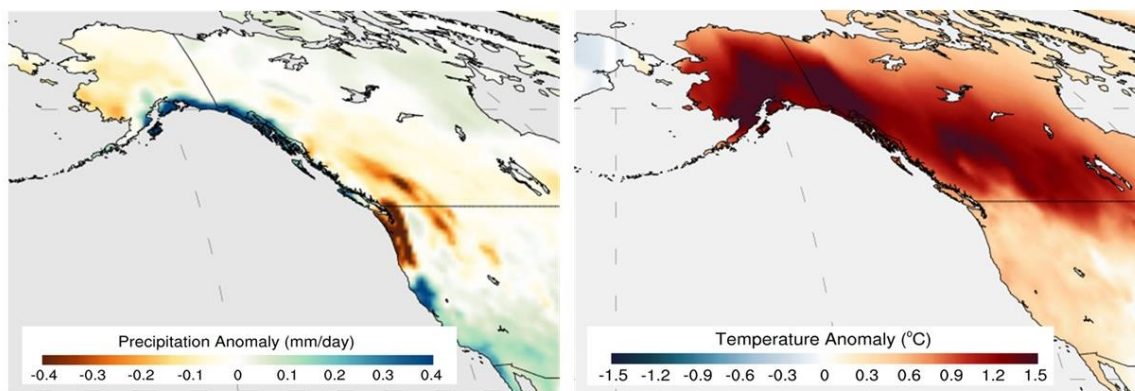


Figure 62. **LEFT** During positive phases of the Pacific Decadal Oscillation (PDO+), winter precipitation tends to increase in Southeast Alaska and decrease in the Pacific Northwest. Shown here is December through March precipitation regressed on the PDO index. Units are mm/day per standard deviation of the PDO index. **RIGHT** Near-surface temperatures tend to be slightly warmer in winter during positive phases of the PDO over northwestern North America and the Northwest Coast. These warmer temperatures tend to enhance snowfall in high mountains and at high latitudes. Shown here is the regression of CRU TS 3.1 2m temperature data on the PDO index. Units are °C per standard deviation of the PDO index. Graphic borrowed

from WIKIPEDIA Commons.

http://badc.nerc.ac.uk/view/badc.nerc.ac.uk_ATOM_dataent_125622377

<http://jisao.washington.edu/pdo/PDO.latest3328276>. Accessed 7/10/2023.

A striking feature of the Pacific Decadal Oscillation (PDO) is the geographical complexity of climate it engenders (Fig. 62). Summer droughts in the Pacific Northwest are more frequent during positive phases of the PDO (Nelson et al. 2011). In Interior Alaska north of the Alaska Range, positive phases of the PDO also tend to accompany droughts, while at the same time anomalously warm and wet conditions tend to occur along the Gulf of Alaska coastline (Mantua and Hare 2002; Hartmann and Wendler 2005). The opposite trends occur during negative phases of the PDO (Wendler et al. 2016) when warmer, more moist conditions extend northward into the western Arctic Basin accompanied by a decline in sea ice cover there (Lapointe et al. 2017).

Interactions between ENSO and Pacific Decadal Oscillation (PDO) have far-reaching effects, both in western North America (McCabe et al. 2004) and globally (Wang et al. 2014). When the PDO is in a positive/warm phase, La Niña conditions tend to be weaker, while El Niño conditions tend to be weaker when the PDO is in a negative/cool phase. During warm (positive) phases of the PDO, El Niños tend to trigger more widespread and to cause more severe droughts western North America than when they accompany cold (negative) PDO phases. La Niña winters tend to be wetter over land during negative phases of the PDO (Wang et al. 2014). The North American Monsoon is stronger over the Southwest USA when El Niño conditions coincide with positive PDO phases, while monsoonal flow tends to weaken when La Niña conditions coincide with negative PDO phases (Castro et al. 2001).

In summary, sea surface temperatures (SSTs) and pressure fields during positive (warm) phases of the Pacific Decadal Oscillation (PDO+) often resemble a multi-decadal version of conditions during strong Eastern Pacific Warm-El Niño events (Deser et al. 2010). The PDO affects the climates of the Northwest Coast in geographically complex ways. Positive PDOs often accompany summer droughts in the Pacific Northwest, wetter summers in the Southwest USA, and drier summers in Interior Alaska. During winter, PDO+ conditions accompany anomalously warm and wet conditions along the Gulf of Alaska coast, which nourish glaciers there. The opposite trends occur during PDO- conditions.

7.1.3.3. *North Pacific Oscillation (NPO) and North Pacific Gyre Oscillation (NPGO)*

The North Pacific Oscillation (NPO) is a north-south seesaw involving wintertime, sea-level pressure between Interior Alaska and the central North Pacific operating over annual and decadal time scales (Furtado et al. 2012). It is defined as the second dominant mode of sea-level pressure in the North Pacific (the Pacific Decadal Oscillation is the dominant mode).

During positive phases of the NPO, the Aleutian Low (AL) tends to deepen and shift eastward. The accompanying diversion of storm tracks brings higher precipitation to Southeast Alaska and coastal British Columbia, along with milder winter temperatures there (Linkin and Nigam, 2008). The opposite occurs during negative phases of the NPO when the AL weakens and shifts westward. Positive phases of the NPO tend to be accompanied by an increase in sea ice in the Sea of Okhotsk and the western Bering Sea (Linkin and Nigam 2008). The effects of the NPO teleconnect to the subtropics and tropics through the Pacific Meridional Mode, which involves fluctuations in the strength of the trade winds, which can cause sea surface temperatures to warm and influence the timing, position, and magnitude of the next El Niño event (Di Lorenzo et al. 2013; Di Lorenzo et al. 2023) (Fig. 60).

The North Pacific Gyre Oscillation (NPGO) is the oceanic expression of the North Pacific Oscillation (NPO) and is the second dominant mode of sea-surface height variability in the Northeast Pacific. It tracks the second empirical orthogonal function of North Pacific sea surface temperature, the Victoria Mode, with the Pacific Decadal Oscillation (PDO) being the dominant mode in both cases (Furtado et al. 2012; Di Lorenzo et al. 2013). The NPGO reflects changes in the intensity of circulation and upwelling in the North Pacific subtropical and subpolar gyres caused by variations in wind direction and speed. It has complex interactions with the Aleutian Low (AL), the Pacific Decadal Oscillation (PDO), the NPO, and ENSO (Di Lorenzo et al. 2013; Di Lorenzo et al. 2023) (Fig. 60). Unlike the PDO, which is closely connected with the AL and Eastern Pacific Warm-El Niño events, the NPGO is closely connected to the NPO and most responsive to Central Pacific Warm-El Niño Events (Di Lorenzo et al. 2008; Di Lorenzo and Schneider 2010). The effects of the NPO and NPGO are basin-wide and involve changes in both the North Pacific Current and the Kuroshio-Oyashio Extension.

7.1.3.4 Arctic Oscillation (AO)

The Arctic Oscillation (AO) involves changes in sea level pressure between high and middle latitudes occurring over timescales of days to months. It reflects the strength of the polar vortex and is the dominant pattern of non-seasonal variation of sea level pressure at middle and high latitudes throughout the Northern Hemisphere. When atmospheric pressure is high over the North American Arctic (AO-), pressure tends to be lower over the mid-latitude North Pacific, and vice versa (Fig. 63). During these AO- phases, atmospheric circulation is more meridional, with outbreaks of polar air reaching the Gulf of Mexico. During AO+ phases, circulation is more zonal, and the Polar Jet usually remains farther north, which means the Aleutian Low also remains farther north (Overland et al. 1999). This brings increased snowfall to the mountains of southern Alaska and drier conditions to the Southwest USA, while northern Alaska is colder than usual. The opposite trends occur when the AO is in a negative phase.

The phase of the Arctic Oscillation (AO) modifies the effects that ENSO has on winter weather in Pacific Northwest (Bond and Harrison 2006). The AO also plays an important role in

the low-frequency variability of the Pacific Decadal Oscillation (PDO) (Budikova 2005; Sun and Wang 2006). Changes in the position, intensity, and orientation of storm tracks associated with the Aleutian Low provide the basis for these AO-ENSO and AO-PDO interactions (Overland et al. 1999).

Today, the phases of the Arctic Oscillation (AO) affect glacier mass balances in the North Atlantic region but do so only weakly in Pacific Northwest, where its influence is minor compared to the PDO and ENSO (McCabe et al. 2000). Persistent high pressure over the North American ice sheets during the Last Glacial Maximum (LGM) (Löffverström et al., 2014) created conditions similar to those during AO- phases today (Fig. 63). This suggests that during the coldest intervals of the LGM, winter precipitation was relatively low in southern Alaska and relatively high in the western USA (Section 3.6).

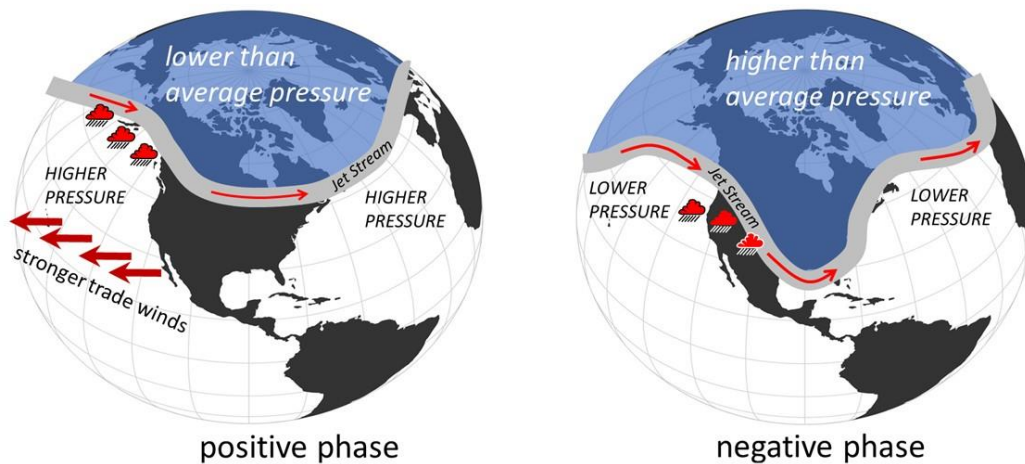


Figure 63. The Arctic Oscillation (AO) involves short-term shifts in atmospheric pressure between the High Arctic and middle latitudes. Through its effects on the trade winds, the AO forms a meridional link between high latitudes and the tropics.

7.1.3.5. Pacific-North American Pattern (PNA)

The Pacific-North American Pattern (PNA) is the second leading pattern of variation in atmospheric pressure over the Northern Hemisphere (Wallace and Gutzler 1981; Leathers et al. 1991; Liu et al. 2017). Its phases shift every few days to a week. Like the Pacific Decadal Oscillation (PDO), the Arctic Oscillation (AO), and the North Pacific Oscillation (NPO), the phase of the PNA involves changes in the strength, location, and orientation of the Aleutian Low (AL). Positive

phases of the PNA are accompanied by a higher-than-average pressure (often a blocking high) extending from Hawaii over the mountains of western North America, and lower-than-average pressure in the subarctic Pacific south of Alaska (Figure 64). This pressure pattern accompanies a stronger mid-latitude (East Asian) jet stream over the Pacific Ocean and increases the likelihood of above-average temperatures in the Pacific Northwest. In winter, the positive phase of the PNA is tends to accompany below-average precipitation in southern British Columbia and Washington (Liu et al. 2017).

The negative phase of the Pacific North American Pattern (PNA) is roughly the mirror image of its positive phase. High pressure often extends southwestward from Alaska and frequently blocks storm tracks from entering the Gulf of Alaska, while a belt of lower-than-average pressure arcs from Hawaii, through Mexico, to Maine and delineates the path of a weaker subtropical jet stream (Wallace and Gutzler 1981). During negative PNA phases, temperature and precipitation trends are generally opposite those during positive phases. As a result, the Gulf of Alaska tends to be cooler than average.

The influence of the Pacific North American Pattern (PNA) on weather in downstream North America varies widely seasonally (Pederson et al. 2013). Moreover, the PNA's intermediate states can be accompanied by weather patterns that are quite different from the ones accompanying its extreme phases. The PNA is influenced by ENSO, with the PNA+ pattern often accompanying strong El Niños, while the PNA- pattern often accompanies La Niñas (Lopez and Kirtman 2019). A pressure pattern similar to the present-day PNA- may have been persistent during the Last Glacial Maximum (Section 4.2).

Today, interactions between the Pacific Decadal Oscillation (PDO), ENSO, and the Pacific North American Pattern (PNA) affect the mass balance of glaciers along the Northwest Coast, (McCabe et al. 2000; Meier et al. 2003; Malcomb and Wiles 2013). When a winter PNA+ coincides with the positive (warm) phase of the PDO and an El Niño, winter storms tend to track further north in the Gulf of Alaska and away from the Pacific Northwest and southern British Columbia, resulting in anomalously warm winter temperatures and diminished snowpacks in those regions. When a PNA- in winter coincides with the negative phase of the PDO and a La Niña, storms to track further south, bringing increased snowfall to the mountains of southern British Columbia and Washington (McCabe et al. 2000).

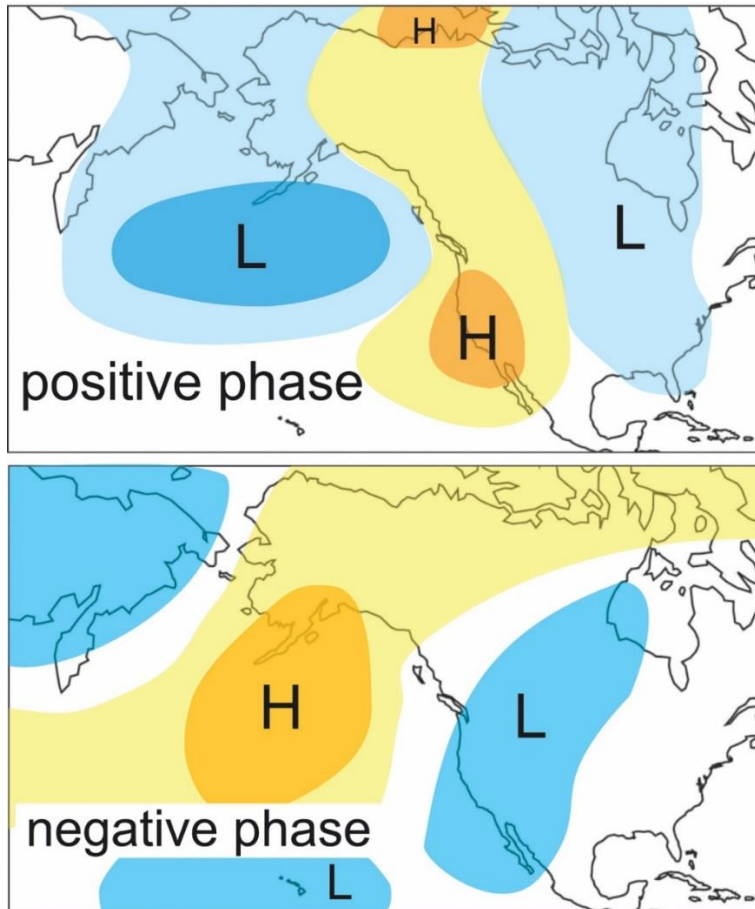


Figure 64. The Pacific North American Pattern (PNA) involves shifts in the locations of low pressure centers and blocking highs at time scales of days to weeks. Its effects are most pronounced in winter and are modified by the state of ENSO and of the Pacific Decadal Oscillation. Redrawn from NOAA Climate.gov image (<https://www.climate.gov/news-features/understanding-climate/climate-variability-pacific%E2%80%93north-american-pattern>. Accessed 2/23)

7.2 Summary: The oceanography and climatology of the Northwest Coast today

The oceanography and climatology of the Northeast Pacific and Northwest Coast are intimately connected to the tropical Pacific. ENSO is the planet's primary source of interannual climate variability, which is communicated globally through a network of ocean-atmosphere teleconnections, some of which extend to the subarctic Pacific. The two main types of El Niños affect the ocean/atmosphere of the high-latitude North Pacific differently. Eastern Pacific Warm-El Niños (EPW-El Niño) modulate the phase of the Pacific Decadal Oscillation (PDO), while Central Pacific Warm-El Niños affect the North Pacific Oscillation (NPO+) and the North Pacific Gyre Oscillation (NPGO). These teleconnection patterns differentially affect glacier mass

balances along the Northwest Coast by influencing winter snowfall and summer temperature, both of which relate closely to the dynamics of the Aleutian Low.

Today, the conditions most favorable for glacier growth in southern and Southeastern Alaska occur when a positive Pacific North American (PNA+) pattern in winter coincides with a positive Pacific Decadal Oscillation (PDO+) during an Eastern Pacific Warm-El Niño. This same conjunction tends to increase effective moisture in the Southwest USA (Hudson et al. 2019), but it accompanies less-glaciogenic conditions in southern British Columbia and the Pacific Northwest. The winter conditions most favorable for glacier growth in the Pacific Northwest (and least favorable in southern Alaska) occur when a negative Pacific North American Pattern (PNA-) occurs during a La Niña and a PDO- phase. During the last ice age, this same anti-phase relationship between southern/southeast Alaska and the Pacific Northwest may have been responsible for time-transgressive glaciations in these different sectors of the Northwest Coast (Section 2.1.5).

Ocean-atmosphere phenomena in the high-latitude North Pacific feedback to the Hadley Circulation, ENSO, and to other low-latitude, oceanographic and atmospheric processes by affecting the vigor of the trade winds and the position of Intertropical Convergence Zone (ITCZ). The summer position of the ITCZ in turn controls the strength of the Asian Summer Monsoon (ASM), which then influences the amount of water vapor and heat energy entering the high-latitude North Pacific. During winter, the position and vigor of the ITCZ modulates meridional temperature gradients in both the ocean and the atmosphere, which then influence the baroclinicity responsible for spawning the extratropical cyclonic storms whose repeated passage across the North Pacific create the Aleutian Low (AL). Shifts in the strength, location, and seasonality of the AL are key determinates of climate along the Northwest Coast and across wide swaths of downstream North America. Based on their importance in controlling climate, weather, and specifically glacier mass balances in the mountains of the Northwest Coast today, four oceanic/atmospheric phenomena were probably of paramount importance during MIS 2: ENSO, the Kuroshio current system, the South Asian Monsoon, and the Aleutian Low.

8. ACKNOWLEDGEMENTS

This review was written with four pioneers of Alaskan Quaternary science in mind: Calvin Heusser, Stephen Porter, Austin Post, and Richard Goldthwait. We thank the following people for their long-term interest and collaboration in researching paleoenvironments of the Northwest Coast: Dorothy Peteet, Greg Streveler, Cathy Whitlock, Tom Ager, David Meltzer, and Richard Reger. Rick Reanier, Pamela Groves, and Maureen Walczak provided useful discussions during preparation of this review. Our studies have been supported by grants from the U.S. National Park Service (Glacier Bay National Park in particular). Partial support came from National Science Foundation grants "Paleo-Perspectives on Climate Change 2002561" and

"Arctic Social Science 1203271". The efforts of two anonymous and patient reviewers greatly improved this manuscript.

Journal Pre-proof

Declaration of interests

The authors declare the following financial interests/personal relationships which may be considered as potential competing interests:

Daniel H. Mann reports financial support was provided by United States National Park Service.
Daniel H. Mann reports financial support was provided by National Science Foundation. If there are other authors, they declare that they have no known competing financial interests or personal relationships that could have appeared to influence the work reported in this paper.

Journal Pre-proof